Bioinspired drug delivery of interleukin-4

Dissertation zur Erlangung des naturwissenschaftlichen Doktorgrades der

Julius-Maximilians-Universität Würzburg

vorgelegt von

Valerie Spieler

aus Mainz

Würzburg 2019

Eingereicht bei der Fakultät für Chemie und Pharmazie am

Gutachter der schriftlichen Arbeit

1. Gutachter:

2. Gutachter:

Prüfer des öffentlichen Promotionskolloquiums

1. Prüfer:

2. Prüfer:

3. Prüfer:

Datum des öffentlichen Promotionskolloquiums

Doktorurkunde ausgehändigt am

Die vorliegende Arbeit wurde in der Zeit von März 2015 bis Juli 2019 am Institut für Pharmazie und Lebensmittelchemie der Bayerischen Julius-Maximilians-Universität Würzburg unter der Anleitung von Herrn Prof. Dr. Dr. Lorenz Meinel angefertigt.

Table of contents

Summary

Chronic inflammatory diseases such as rheumatoid arthritis, type 2 diabetes and cardiovascular diseases, are associated with the homeostatic imbalance of one of several physiological systems combined with the lack of spontaneous remission, which causes the disease to persevere throughout patients' lives. The inflammatory response relies mainly on tissue-resident, pro-inflammatory M1 type macrophages and, consequently, a chance for therapeutic intervention lies in driving macrophage polarization towards the anti-inflammatory M2 phenotype. Therefore, anti-inflammatory cytokines that promote M2 polarization, including interleukin-4 (IL4), have promising therapeutic potential. Unfortunately, their systemic use is hampered by a short serum half-life and dose-limiting toxicity. On the way towards cytokine therapies with superior safety and efficacy, this thesis is focused on designing bioresponsive delivery systems for the anti-inflammatory cytokine IL4.

C**hapter 1** describes how anti-inflammatory cytokines are tightly regulated in chronic, systemic inflammation as in rheumatoid arthritis but also in acute, local inflammation as in myocardial infarction. Both diseases show a characteristic progression during which anti-inflammatory cytokine delivery is of variable benefit. A conventional, passive drug delivery system is unlikely to release the cytokines such that the delivery matches the dynamic course of the (patho-)physiological progress. This chapter presents a blueprint for active drug delivery systems equipped with a 24/7 inflammation detector that continuously senses for matrix metalloproteinases (MMP) as surrogate markers of the disease progress and responds by releasing cytokines into the affected tissues at the right time and place. Because they are silent during phases of low disease activity, bioresponsive depots could be used to treat patients in asymptomatic states, as a preventive measure. The drug delivery system only gets activated during flares of inflammation, which are then immediately suppressed by the released cytokine drug and could prevent the steady damage of subclinical chronic inflammation, and therefore reduce hospitalization rates.

In a first proof of concept study on controlled cytokine delivery (**chapter 2**), we developed IL4-decorated particles aiming at sustained and localized cytokine activity. Genetic code expansion was deployed to generate muteins with the IL4's lysine 42 replaced by two different unnatural amino acids bearing a side chain suitable for click chemistry modification. The new IL4 muteins were thoroughly characterized to ensure proper folding

and full bioactivity. Both muteins showed cell-stimulating ability and binding affinity to IL4 receptor alpha similar to those of wild type IL4. Copper-catalyzed (CuAAC) and strain-promoted (SPAAC) azide–alkyne cycloadditions were used to site-selectively anchor IL4 to agarose particles. These particles had sustained IL4 activity, as demonstrated by the induction of TF-1 cell proliferation and anti-inflammatory M2 polarization of M-CSF-generated human macrophages. This approach of site-directed IL4 anchoring on particles demonstrates that cytokine-functionalized particles can provide sustained and spatially controlled immune-modulating stimuli.

The idea of a 24/7 sensing, MMP driven cytokine delivery system, as described in the introductory chapter, was applied in **chapter 3.** There, we simulated the natural process of cytokine storage in the extracellular matrix (ECM) by using an injectable solution of IL4 for depot formation by enzyme-catalyzed covalent attachment to ECM components such as fibronectin. The immobilized construct is meant to be cleaved from the ECM by matrix-metalloproteinases (MMPs) which are upregulated during flares of inflammation. These two functionalities are facilitated by a peptide containing two sequences: a protease-sensitive peptide linker (PSL) for MMP cleavage and a sequence for covalent attachment by activated human transglutaminase FXIIIa (TGase) included in the injection mix for co-administration. This peptide was site-selectively conjugated to the unnatural amino acid at IL4 position 42 allowing to preserve wild type bioactivity of IL4. In vitro experiments confirmed the anticipated MMP response towards the PSL and TGase-mediated construct attachment to fibronectin of the ECM. Furthermore, the IL4-peptide conjugates were able to reduce inflammation and protect non-load bearing cartilage along with the anterior cruciate ligament from degradation in an osteoarthritis model in rabbits. This represents the first step towards a minimally invasive treatment option using bioresponsive cytokine depots with potential clinical value for inflammatory conditions.

One of the challenges with this approach was the production of the cytokine conjugate, with incorporation of the unnatural amino acid into IL4 being the main bottleneck. Therefore, in **chapter 4**, we designed a simplified version of this depot system by genetically fusing the bifunctional peptide via a flexible peptide spacer to murine IL4. While human IL4 loses its activity upon C-terminal elongation, murine IL4 is not affected by this modification. The produced murine IL4 fusion protein could be effectively bound to in vitro grown extracellular matrix in presence of TGase. Moreover, the protease-sensitive linker was selectively recognized and cleaved by MMPs, liberating intact and active IL4, although at a slower rate than expected. Murine IL4 offers the advantage to evaluate the bioresponsive

cytokine depot in many available mouse models, which was so far not possible with human IL4 due to species selectivity.

For murine IL4, the approach was further extended to systemic delivery in **chapter 5.** To increase the half-life and specifically target disease sites, we engineered a murine IL4 variant conjugated with a folate-bearing PEG chain for targeting of activated macrophages. The bioactive IL4 conjugate had a high serum stability and the PEGylation increased the half-life to 4 h in vivo. Surprisingly, the folate moiety did not improve targeting in an antigen-induced arthritis (AIA) mouse model. IL4-PEG performed better in targeting the inflamed joint, while IL4-PEG-folate showed stronger accumulation in the liver. Fortunately, the modular nature of the IL4 conjugate facilitates convenient adaption of PEG chain length and the targeting moiety to further improve the half-life and localization of the cytokine.

In summary, this thesis describes a platform technology for the controlled release of cytokines in response to inflammation. By restricting the release of the therapeutic to the site of inflammation, the benefit-risk ratio of this potent class of biologics can be positively influenced. Future research will help to deepen our understanding of how to perfectly combine cytokine, protease-sensitive linker and immobilization tag or targeting moiety to tackle different diseases.

Zusammenfassung

Chronische Entzündungskrankheiten wie rheumatoide Arthritis, Typ-2-Diabetes oder Herz-Kreislauf-Erkrankungen werden durch das Ungleichgewicht eines von mehreren physiologischen Systemen in Verbindung mit fehlender spontaner Remission verursacht, wodurch die Krankheiten lebenslang bestehen bleiben. Die zugrunde liegenden Entzündungsreaktionen beruhen hauptsächlich auf im Gewebe vorhandenen Makrophagen und deren Polarisation in Richtung des entzündlichen M1-Phänotyps, was gleichzeitig die Möglichkeit einer therapeutischen Intervention bietet. Entzündungshemmende Zytokine, einschließlich Interleukin-4 (IL4), haben ein großes therapeutisches Potenzial, da sie Makrophagen in Richtung des entzündungshemmenden M2-Phänotyps zu polarisieren vermögen. Leider ist ihre systemische Anwendung durch eine kurze Serumhalbwertszeit und dosislimitierende Toxizität eingeschränkt. Auf dem Weg zu Zytokintherapeutika mit verbesserter Sicherheit und Wirksamkeit konzentriert sich diese Arbeit auf die Entwicklung von bioresponsiven Freisetzungssystemen für das entzündungshemmende Zytokin IL4.

Kapitel 1 beschreibt, wie entzündungshemmende Zytokine bei chronischen systemischen Entzündungen wie rheumatoider Arthritis im Vergleich zu akuten lokalen Entzündungen wie dem Myokardinfarkt reguliert werden. Beide Erkrankungen zeigen einen charakteristischen Verlauf, währenddessen die Freisetzung von entzündungshemmenden Zytokinen von unterschiedlich großem Nutzen ist. Gewöhnliche, passive Arzneimittelfreisetzungssysteme sind nicht in der Lage, Zytokine in idealer Menge zur optimalen Unterdrückung des dynamischen, (patho-)physiologischen Verlaufs der Krankheit freizusetzen. In diesem Kapitel werden deshalb aktive Arzneimittelfreisetzungssysteme vorgestellt, die mit einer Sensorik für die Entzündung ausgestattet sind, mit der sie kontinuierlich die Konzentration von Matrix-Metalloproteinasen (MMP) als Indikatoren für den Krankheitsverlauf erfassen können. Somit kann das aktive Arzneimittelfreisetzungssystem krankes Gewebe zum richtigen Zeitpunkt und am richtigen Ort mit Zytokinen behandeln. Solche bioresponsiven Depots können zur vorbeugenden Behandlung von asymptomatischen Patienten eingesetzt werden, da sie während Phasen geringer Krankheitsaktivität inaktiv sind. Das Freisetzungssystem wird erst durch Entzündungsschübe aktiviert, die dann sofort durch die freigesetzten Zytokine unterdrückt werden. Dadurch könnte die dauerhafte Schädigung

durch subklinische, chronische Entzündung verhindert und als Konsequenz die Hospitalisierungsrate gesenkt werden.

In einer ersten Machbarkeitsstudie wurden in **Kapitel 2** IL4-dekorierte Partikel mit dem Ziel entwickelt, eine langanhaltende und lokalisierte Zytokinaktivität zu gewährleisten. Dazu wurden IL4-Muteine erzeugt, bei denen das Lysin 42 mittels Erweiterung des genetischen Codes durch zwei verschiedene unnatürliche Aminosäuren ersetzt wurde, die jeweils eine für Klick-Chemie geeignete Seitenkette tragen. Die IL4-Muteine wurden ausführlich charakterisiert, um eine korrekte Faltung und volle Bioaktivität sicherzustellen. Beide Muteine zeigten zellstimulierende Fähigkeit und Bindungsaffinität an IL4-Rezeptor-alpha, die mit der von Wildtyp-IL4 vergleichbar ist. Anschließend wurde kupferkatalysierte (CuAAC) und kupferfreie (SPAAC) Azid-Alkin-Cycloaddition verwendet, um IL4 ortsspezifisch auf Agarosepartikeln zu verankern. Die Partikel waren in der Lage, die IL4-Aktivität über längere Zeit aufrecht zu erhalten, was durch TF-1-Zellproliferation und M2-Polarisation von M-CSF-generierten, humanen Makrophagen gezeigt werden konnte. Dieser Ansatz der ortsspezifischen Verankerung von IL4 auf Agarosepartikeln zeigt, dass zytokinfunktionalisierte Partikel anhaltende und räumlich kontrollierte, immunmodulierende Stimuli liefern können.

Die Idee eines MMP-gesteuerten Zytokinfreisetzungssystems mit 24/7-Sensorik, das im Einleitungskapitel vorgestellt wurde, wurde in **Kapitel 3** umgesetzt. Der natürliche Prozess der Zytokinspeicherung in der extrazellulären Matrix (EZM) wurde mithilfe einer injizierbaren IL4-Lösung zur enzymatischen Depotbildung durch kovalente Bindung an EZM-Komponenten, z. B. Fibronektin, simuliert. Nach der Bindung soll das Konstrukt durch Matrix-Metalloproteinasen (MMPs), die während Entzündungsschüben hochreguliert werden, aus der EZM freigesetzt werden können. Eine Peptidsequenz, die ein Protease-sensitives Verbindungsstück und eine Sequenz, mit der das Zytokin bei gleichzeitiger Injektion von aktivierter menschlicher Transglutaminase FXIIIa (TGase) kovalent auf der EZM immobilisiert wird enthält, wurde ortsspezifisch über eine unnatürliche Aminosäure an Position 42 von IL4 gekoppelt. Dadurch wurde die Bioaktivität von IL4 vollständig erhalten, während das Protease-sensitive Verbindungsstück auf MMPs reagierte und das Konstrukt durch TGase an das Fibronektin der EZM gebunden werden konnte. Die IL4-Peptid-Konjugate waren in einem Osteoarthritis-Modell bei Kaninchen in der Lage, die Entzündung des Kniegelenks zu verringern und den nicht-tragenden Knorpel sowie das vordere Kreuzband vor Degradation zu schützen. Dies ist der erste Schritt in Richtung einer

minimalinvasiven Behandlung durch Verwendung von bioresponsiven Zytokindepots mit potenziellem klinischem Nutzen bei Entzündungserkrankungen.

Eine der Herausforderungen bei diesem Vorgehen war die Herstellung der Zytokinkonjugate, wobei der Einbau der unnatürlichen Aminosäure in IL4 den größten Engpass darstellte. Deshalb wurde in **Kapitel 4** eine vereinfachte Version dieses Depotsystems entworfen, indem das bifunktionelle Peptid über eine flexible Verbindungssequenz mit murinem IL4 genetisch fusioniert wurde. Während humanes IL4 bei C-terminaler Verlängerung an Aktivität verliert, ist murines IL4 durch die Modifikation nicht beeinflusst. Die murinen IL4-Fusionsproteine konnten in Gegenwart von TGase wirksam an in vitro generierte extrazelluläre Matrix gebunden werden. Darüber hinaus wurde das Protease-sensitive Verbindungsstück selektiv von MMPs erkannt und gespalten, wobei intaktes und aktives IL4 freigesetzt wurde, wenn auch mit einer langsameren Rate als erwartet. Murines IL4 bietet die Möglichkeit das bioresponsive Zytokindepot in den vielen verfügbaren Mausmodellen zu testen, was mit humanem IL4 aufgrund der Speziesselektivität nicht möglich ist.

Für murines IL4 wurde die Entwicklung in **Kapitel 5** auf die systemische Applikation ausgeweitet. Um die Serumhalbwertszeit zu erhöhen und eine Wirkstofflokalisation im entzündeten Gewebe zu erreichen, wurde eine murine IL4-Variante entwickelt, die mit einer Folat-tragenden PEG-Kette konjugiert wurde, um aktivierte M1 Makrophagen zu adressieren. Das bioaktive IL4-Konjugat wies eine hohe Serumstabilität auf und die PEGylierung erhöhte die Halbwertszeit in vivo auf 4 h. Allerdings konnte durch die Konjugation der Folatgruppe an IL4 die Wirkstofflokalisation in einem Mausmodell mit Antigen-induzierter Arthritis (AIA) nicht verbessert werden. IL4-PEG akkumulierte sich stärker im entzündeten Gelenk, während IL4-PEG-Folat eine stärkere Anreicherung in der Leber zeigte. Erfreulicherweise erleichtert der modulare Aufbau des IL4-Konjugats die bequeme Anpassung der PEG-Kettenlänge und der zielorientierten Einheit, um die Halbwertszeit und Lokalisierung des Zytokins weiter zu verbessern.

Zusammenfassend beschreibt diese Arbeit eine Plattformtechnologie zur kontrollierten Freisetzung von Zytokinen als Reaktion auf Entzündungen. Durch die Beschränkung der Freisetzung des Therapeutikums auf den Ort der Entzündung kann das Nutzen-Risiko-Verhältnis dieser potenten Klasse von Biologika positiv beeinflusst werden. Zukünftige Forschungen werden dazu beitragen zu verstehen, wie Zytokin, Protease-sensitives

Verbindungsstück und Immobilisierungsanhängsel oder etwaige zielorientierte Einheiten zur Bekämpfung verschiedener Krankheiten perfekt kombiniert werden können.

Chapter 1: Cytokine drug delivery in chronic systemic and acute local inflammation

Valerie Spieler[1], Tessa Lühmann[1], Lorenz Meinel[1]

[1] Institute for Pharmacy and Food Chemistry, University of Würzburg, Würzburg, Germany

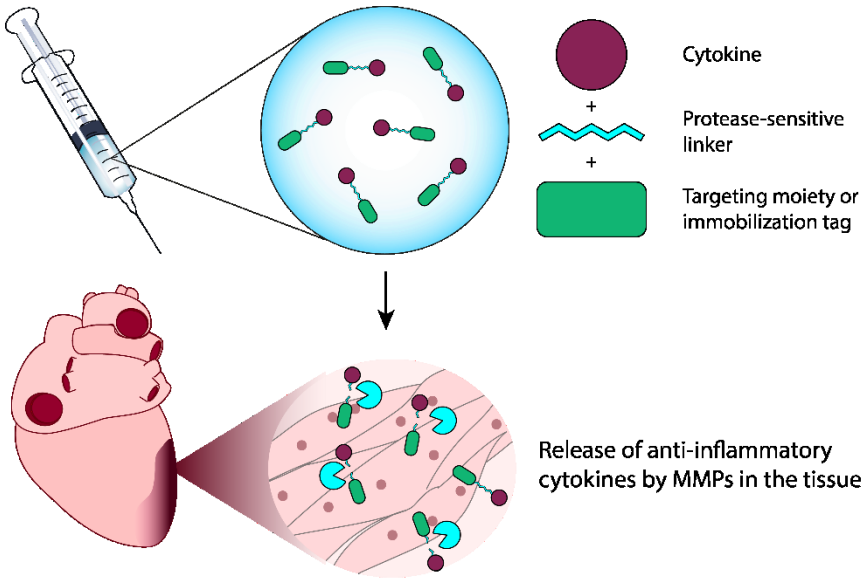

Unpublished manuscript

Abstract

Anti-inflammatory cytokines are tightly regulated in chronic systemic inflammation such as rheumatoid arthritis (RA) and in acute local inflammation such as myocardial infarction (MI). However, the range in which cytokine activity is desirable in both, RA and MI, is tempo-spatially variable, dynamic, and individually different. Therefore, passive drug delivery regimens for anti-inflammatory cytokines as therapeutics are unlikely to meet the specific requirements of treating either of these highly dynamic disorders. In this review, we discuss the therapeutic potential of engaging anti-inflammatory cytokines by using an active, disease-driven drug delivery system which utilizes matrix metalloproteinases (MMPs) - extracellular matrix degrading proteases - as a trigger for drug release. MMPs serve as surrogates of the key underlying disease mechanism, and thereby the release of anti-inflammatory cytokines is coupled to flares of inflammation. Such active delivery regimens equipped with 24/7 sensory function of the (patho-)physiologically progress continuously sense for the cue and respond by releasing the cytokines into the diseased tissues at the right time, manner, and place. Here, we focus on merging MMP profiles with cytokine concentration profiles in remission phases of RA and MI, aiming at a blueprint for future MMP-driven cytokine delivery systems.

Introduction

Cytokines – originally known as lymphokines or monokines in reference to their cellular origin - are part of a non-antigen specific protein molecule network by which cells influence each other. The different cytokines have overlapping function, or the function is unrelated to each other, sometimes mutually synergistic, sometimes antagonistic, harmful or beneficial at the same time. Therefore, the development of cytokines and inhibitors of cytokines are promising (or potentially promising once temporospatial delivery challenges are addressed, the topic this article is dedicated to). The number of cytokines is large and new cytokines are found all the time which is why we reference here to excellent available review articles summarizing their pharmacological activity, namely their key regulatory function in inflammation.[1] Acute inflammation rapidly leads to an increased permeability of the vascular endothelium through which an influx of blood cells and dissolved molecules into the compromised tissue gets facilitated. Of central importance to this process are immediate innate-immunological responses by mast cells, macrophages and leukocytes. This immediate response is modulated by adaptive immunological responses through

antibodies and lymphocytes allowing for more specific attack strategies. Once inflammatory stimuli persist, inflammation may enter chronic phases as characterized by e.g. the formation of granulomas. These orchestrated events are complex and idiosyncratic.[2] Therefore, it stands to reason how new therapeutic players such as therapeutically given cytokines can be integrated into the (idiosyncratic and unpredictable) beat of the (patho-) physiological orchestra for their optimal spatiotemporal entry into the play. Very few cytokines or growth factors that may act as therapeutics within the inflammation network have exclusively pro-inflammatory or anti-inflammatory properties, but rather have pleiotropic and diverse functions depending on disease processes, involved tissues, and their timely presence in the compromised areas. Cytokine delivery for impacting this intricate system might benefit from a bioresponsive delivery system adjusting the release of therapeutic cytokines in response to upregulated biomarkers of the disease state. Furthermore, upcoming flares could be addressed in their pre-symptomatic state by such biomarker-driven drug delivery systems.[3] Here we aim at linking **m**atrix **m**etallo**p**roteinases (**MMP**) and expression of cytokines to remission phases in RA and MI as a starting point for future cytokine **d**rug **d**elivery **sy**stems (**DDS**). These DDS aim at linking remission phases to distinct MMP concentrations with these selected MMPs triggering cytokine release from the DDS.

MMPs are a family of zinc-containing endopeptidases playing a crucial role in turnover, degradation, catabolism and destruction of the extracellular matrix.[4] Interest in MMPs sparked in the late 1960s and early 1970s following observations that MMPs are overexpressed in certain pathological conditions. Rheumatoid arthritis (RA) was the first disease to be linked to MMPs and studies have confirmed that MMPs are key enzymes in the pathological destruction of joint tissues, e.g. cartilage.[5–8] In RA, MMPs are primarily excreted by synovial lining cells after stimulation by inflammatory cytokines. Anti-inflammatory cytokines are not expressed in RA synovium or only at low levels that are not sufficient to block synovitis.[9] In addition to RA, we focus on myocardial infarction (MI), or more precisely the post-MI inflammation and tissue remodeling process. There is extensive evidence for the role of MMPs in remodeling of the heart after MI, frequently leading to myocardial necrosis, progressive ventricular dilatation, fibrosis and decreased cardiac performance.[10] In healthy tissue MMPs are present in low quantity. We selected these two model indications to compare profiles in destructive, chronic inflammation as in RA with the at least in part helpful, transient inflammation in MI. From a delivery perspective, RA arguably benefits from intercepting during flares of inflammation (when anti-inflammatory

drugs including some cytokines are highly effective). For MI, the drug delivery strategy is intercepting with inflammation when overactive to prevent chronic inflammation.

For that, we link disease progression in RA to the presence of certain MMPs. Development of small molecule drugs directly targeting MMPs has been attempted, but the MMP inhibitors failed due to insufficient selectivity.[11] Here we use MMPs as surrogates for a selected disease state. When target MMPs are upregulated, the DDS responds with cytokine release – hence, cytokine release is coupled to a disease state (Fig. 1).

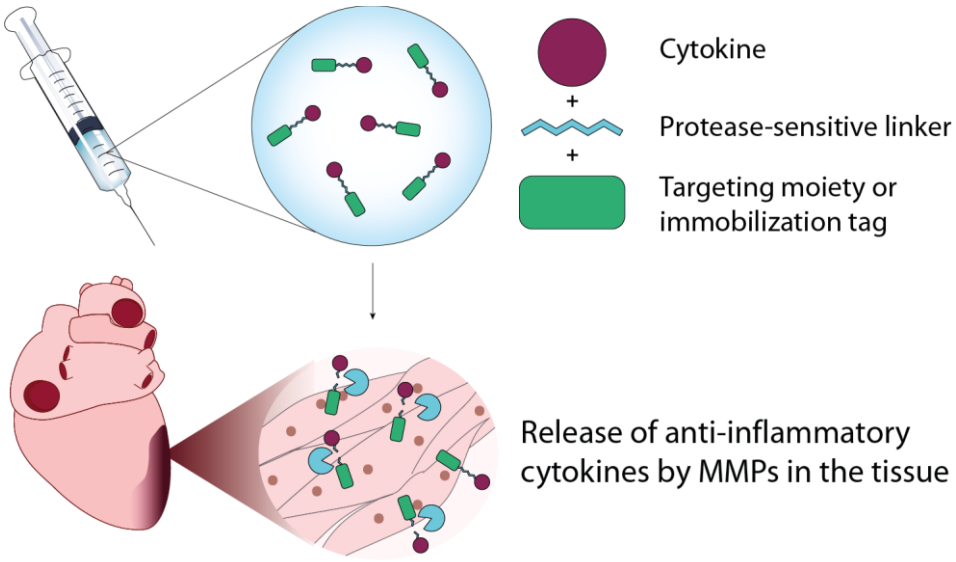

Fig. 1 Schematic depiction of MMP-mediated release of a cytokine from a bioresponsive drug delivery system. To utilize MMP targeting, a protease-sensitive linker (cyan) is attached to an anti-inflammatory cytokine (purple). Both are retained in the target tissue by being attached to a targeting moiety or an immobilization tag (green). When MMPs are present, they cleave the protease-sensitive linker, thereby releasing the active cytokine.

Temporal MMP profile in rheumatoid arthritis

RA is a chronic inflammatory disease set on an autoimmune background.[9] It leads to the destruction of articular cartilage due to the elevated activities of MMPs that degrade extracellular matrix (ECM) macromolecules and ultimately results in joint dysfunction. The main cellular sources of MMPs in RA are synovial lining cells and macrophages, which infiltrate the synovium.

It is difficult to create an early stage MMP profile for RA in humans since RA is often diagnosed late, when the disease is already in a chronic stage at which clinical symptoms

(pain, swelling) occur.[12] However, the early stage of RA in humans is dominated by increased levels of **MMP-1** and **MMP-3**.[13] Especially the level of MMP-3 is elevated compared to other MMPs. While a study in MMP-3 deficient mice suggested that joint destruction is unaltered by MMP-3[14], other studies have shown that degradation of cartilage collagen fibrils is strongly reduced in MMP-3 deficient arthritic mice.[15] Since MMP-3 levels are elevated in the early and middle stages of RA and decreased in the advanced stage, it may play a role in the initiation and progression of cartilage destruction. Serum pro-MMP-3 levels in humans are relatively stable during the first years of RA.[16] They are associated with disease activity and are also a predictive marker of joint damage progression at the onset of disease.[16] Serum levels of MMPs generally correlate with levels in synovial fluid and are therefore associated with disease activity.[17]

During RA progression, the inflamed synovium invades adjacent cartilage and promotes articular destruction, referred to as pannus formation. This process requires degradation of the collagen matrix and is mediated by the activities of osteoclasts, chondrocytes and synovial fibroblasts. **MT1-MMP** is a key collagen-degrading proteinase that promotes pannus invasion in human RA.[18] Systemic levels of **pro-MMP-8** and **-9** decrease during the first two years after disease onset[16], although synovial levels of MMP-8 and -9 are low in the early stage and increased with the progression of RA.[19] In contrast to MMP-9, other gelatinases such as **MMP-2** are constitutively expressed and not impacted by most growth factors and cytokines. The findings of an Ab-induced mouse model of RA in MMP-2 or MMP-9 knockout mice suggest that MMP-2 plays a suppressive role in RA, as the MMP-2 deficient mice exhibited severe clinical and histologic arthritis compared to wild-type mice. The MMP-9-KO mice displayed milder arthritis, indicating a pivotal role of MMP-9 in the development of RA (Fig. 2).[20]

MMPs are part of the normal biological process of tissue repair and remodeling, but in chronic inflammation, like RA, this process is probably inappropriate or unbalanced and hence leads to tissue destruction. Restoring the balance is the goal for novel therapeutic approaches like the bioresponsive release of anti-inflammatory cytokines according to MMP profiles proposed in this review.

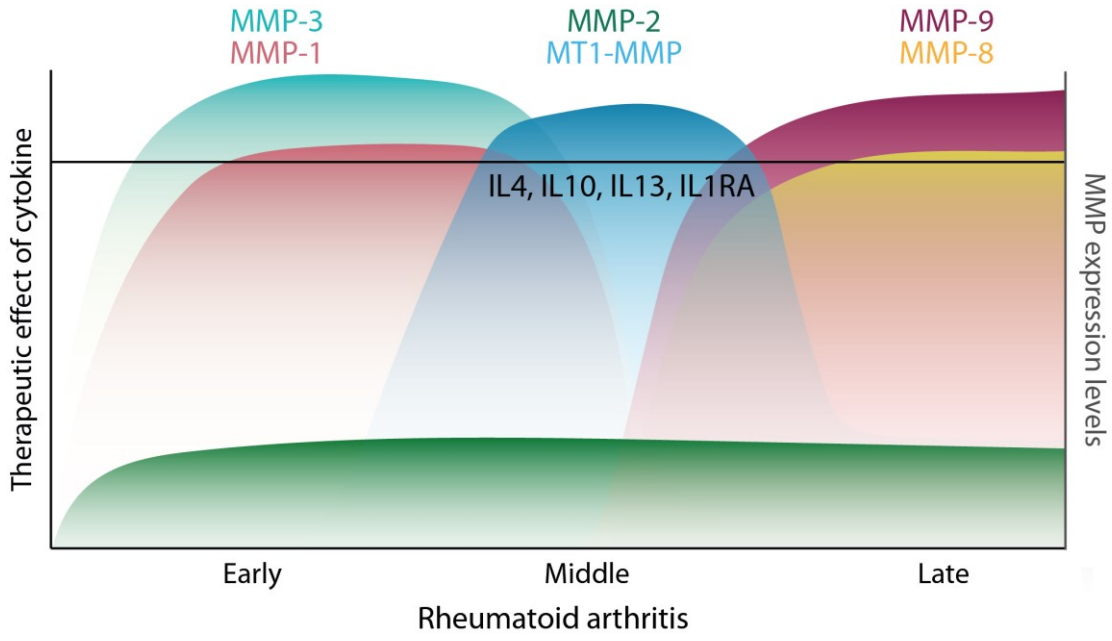

Fig. 2 Sequential changes in MMP expression levels in patients with rheumatoid arthritis

Temporal MMP profile in myocardial infarction

Myocardial infarction leads to complex remodeling events involving both the infarcted and non-infarcted myocardium. Throughout this entire process, MMPs released from inflammatory and endogenous cells degrade the matrix components of the heart, fueling myocardial matrix remodeling. The architectural alterations following MI, that continue for months and even years, can be broken down into three stages (Fig. 3).[21]

During the acute remodeling process of the early wound healing stage (0-7 days post-MI), activated MMPs degrade the ECM, allowing inflammatory cells to migrate into the infarct region to remove necrotic tissue.[22] Subsequently these inflammatory cells release more MMPs, cytokines and growth factors. In the granulation and early remodeling stage (7–21 days post-MI), the necrotic cardiac tissue is replaced by granulation tissue, consisting of inflammatory cells, newly-formed blood vessels and fibroblast-like cells depositing a collagen network to replace the granulation tissue. The result is a thin, hypocellular scar[23], actively maintained by fibroblast-like cells.[24] MMPs play an integral role in post-MI healing, but their activity may also have detrimental effects leading to destruction.

Contradictory findings concerning MMP-2 plasma levels have been obtained. It was shown that plasma **MMP-2** levels are elevated over the first 5 days post MI.[25] Conversely, levels of the pro-form of MMP-2 (proMMP-2) were shown to decrease after MI.[25] Surprisingly, one study found that low plasma MMP-2 levels correlate with increased left ventricular (LV)

volumes as a measure of ventricular dysfunction[25], while others found no significant differences in MMP-2 plasma levels in patients with large compared to moderate MI, either at admission or during the follow-up period. [26,27] Further, no relation was found to left ventricular function or volume, indicating that MMP-2 might not be critically involved in the tissue remodeling process during and after acute MI. **MMP-8** levels significantly increase post-MI, peaking at day 1 and again at day 3, and thereafter decrease to control values which they reach by day 5.[28] **MMP-9** is expressed within the first 24 h after MI and levels remain elevated for several days.[25] Depending on the study, MMP-9 plasma concentrations then normalize to baseline levels within 1 week[26] or remain significantly elevated until trending downwards by day 28.[28] A persistent or elevated MMP-9 level at day 5 could be connected to an increased end-diastolic volume at day 28.[28] Similarly, high early levels of MMP-9 associated with the LV dysfunction and remodeling in another study[27]. Moreover, levels of MMP-9 and MMP-8 were significantly higher in ruptured infarct tissue than in control MI tissue, suggesting that increased activity of these MMPs contributes to infarct rupture.[29] In contrast, increased plateau levels later after MI were associated with a relative preservation of LV function. This suggests that the temporal expression profile of MMP-9 activity controls LV remodeling, with MMP-9 playing a pathogenic role in early tissue repair but having protective function at later stages after acute MI in humans.[27] The detailed functions of MMP-9 during cardiac remodeling have been reviewed elsewhere.[30] Plasma **MMP-3** levels reach their maximum around 3 days post MI and high levels are associated with left ventricular dysfunction, adverse left ventricular remodeling and prognosis.[31] In patients who underwent successful reperfusion therapy with angioplasty after acute MI, the average serum **MMP-1** values were below control levels for the first 4 days, and thereafter increased to reach peak concentrations around day 14 to then return to middle control values.[32] The expression of other MMPs, such as **MMP-7,** remain unchanged or are even reduced compared to control levels.[28] Especially the increase of MMP-3 and MMP-9 within the first hours and days after MI thus appear as major contributing factors to the initial proteolytic degradation of the infarcted heart, by which the structural and functional integrity is compromised. Accordingly, overexpression of MMP-9 early after MI lead to adverse LV remodeling in the later post-MI periods.[28]

The late remodeling phase can last months to years and involves both the infarcted and non-infarcted LV myocardium. LV remodeling is critical for myocardial performance and residual function, as structural changes leading to LV dilatation can result in increased myocardial wall stress and ultimately congestive heart failure (CHF).[33] In this late

remodeling stage, MMP-3 and MMP-9 levels were shown to be significantly decreased. [27,31] Notably, an increase in specific MMPs was observed 8 weeks post MI in an experimental post-MI sheep model in the form of MMP-8, **MMP-13** and **MT1-MMP**.[34] This change in MMP expression pattern was discussed as the inflection point marking the transition from an acute to a chronic inflammatory response. These spatiotemporal changes in MMP expression after MI and during the remodeling phase could be harnessed to control the release of therapeutics from DDS.

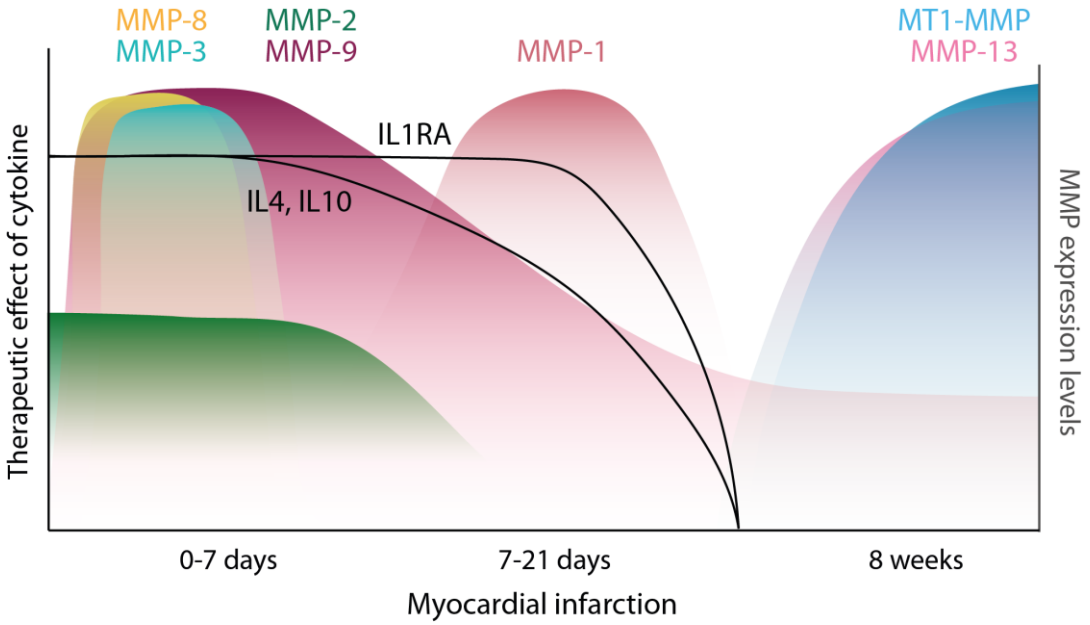

Fig. 3 Sequential changes in MMP expression levels in patients after myocardial infarction.

Inflammatory response in RA and MI

RA and MI both are associated with a strong inflammatory responses, persisting in RA, but normally resolving after MI. Inflammation can be reduced by directly targeting pro-inflammatory cytokines, or anti-inflammatory cytokines, which antagonize the impact of pro-inflammatory cytokines and modulate immune effector cells towards anti-inflammatory responses.

RA is associated with an increased production of various cytokines, playing a crucial role in the pathogenesis of the disease by maintaining chronic inflammatory synovitis and driving the destruction of joint tissue.[35] There is also an anti-inflammatory response, which includes interleukin-10 (IL10), interleukin-13 (IL13) and interleukin-1 receptor antagonist (IL1RA) but

these fail to effectively block synovitis.[35] Therefore, the cytokine profile in RA could be favorable skewed by releasing immunomodulatory cytokines into the target tissue e.g. by releasing interleukin-4 (IL4)[36] to counter-regulate the inflammatory processes.

In MI the effects of cytokines can either contribute to healing and restoration of cardiac function or, on the other hand, lead to unfavorable remodeling resulting in cardiac rupture or chronic dilatation.[22] The failure of tumor necrosis factor alpha (TNFα) inhibitors in the clinic[37,38] highlights the importance of proinflammatory cytokines in the progression to heart failure and the complexity of the healing process in the heart, contrary to the success of TNFα inhibitors in other inflammatory diseases like RA.[39] However, immune-modulatory properties of many of the current MI therapies, including angiotensin-converting enzyme inhibitors and β-blockers suggest that targeting inflammation could be beneficial.[40,41]

Cytokines as potential therapeutic targets

Since our understanding of immune-regulatory signaling pathways is improving, inducing these pathways by deploying anti-inflammatory cytokines to balance and resolve, rather than suppress inflammation, becomes an attractive therapeutic option.

Interleukin-4 (IL4) is a highly pleiotropic cytokine that leads to polarization of T helper (Th) cell differentiation toward Th2-like cells and inhibits the production of pro-inflammatory cytokines.[42] In addition to its anti-inflammatory effects in the synovium of RA it also inhibits cartilage damage and osteoclastogenesis in animal models.[43–46] In a mouse model of RA, onset of arthritis was significantly delayed and suppression of clinical symptoms was achieved by continuous administration of recombinant murine IL4[47] and the arthritis-suppressing effects were confirmed in following animal studies.[44,48] IL4 fused to the F8 antibody in the diabody format (F8–IL4 (Tetravil)) completely cured RA in a mouse model when administered in combination with dexamethasone.[49] Another interesting design is the IL4-10 fusion protein, which combines the activities of the two cytokines and suppressing experimental arthritis in mice.[50] RA could especially benefit from IL4, since it is upregulated in the synovial fluid in patients with early RA, but not established RA. IL4 therapy was tested in cancer patients, but failed due to dose-limiting effects, including vascular leakage syndrome.[51] With improved delivery systems, like local, biomarker driven MMP-mediated release, these limitations might be adequately addressed.

The outcome of MI is also improved by IL4 administration. For example, following intraperitoneal injection the number of alternatively activated macrophages in cardiac tissue following myocardial infarction in mice is increased, which protects the infarcted heart from cardiac rupture.[52] The reparative properties of macrophages through administration of IL4 were also observed after administration of a long-acting IL4-antibody complex in mice, leading to reduced infarct size and enhanced tissue repair when administered before day 28 post-MI. When injected thereafter, the IL4 complex treatment was not effective.[53] However, IL4 has a profibrotic role in the remodeling heart[54] which may be a dose limiting side effect when used for a treatment after MI.

Interleukin-10 (IL10) is an important immune-modulatory cytokine limiting and ultimately terminating inflammatory responses by inhibition of activation and effector function of T cells, monocytes, and macrophages.[55,56] Although IL10 is naturally present in RA synovial membrane and fluid, it works insufficiently in the situation of chronic activation of immune system.[35] Recombinant human IL10 (Tenovil) has been studied for treatment of RA, but disease remissions could rarely be observed.[57] IL10 in the immunocytokine format has successfully been used for treatment of RA in several preclinical studies. Fused with different antibodies (L19-IL10, F8-IL10 (Dekavil), 1-11E/vIL10) it inhibits progression of established arthritis in mice.[58–60] Dekavil is currently under investigation in a phase 2 clinical study for the treatment of RA.[61]

In MI models, deficiency in IL10 triggers an enhanced inflammatory response[62]. By inhibiting MMPs but stimulating issue inhibitor of metalloproteinases 1 (TIMP1)[63], IL10 may in addition exert protective functions after MI. IL10 was furthermore shown to induce a reparative macrophage phenotype, contributing to tissue repair by promoting fibrosis and clearance of apoptotic cells.[64] In line with these protective functions, administration of IL10 post-MI improves LV function[65], infarct wall thinning[66] and the LV microenvironment by dampening inflammation and facilitating cardiac wound healing.[67]

Interleukin-13 (IL13) functions homologous to IL4 and IL10. Like IL4 it is upregulated in the synovial fluid of early RA, but hardly detectable in established RA.[68] IL13 is a potent anti-arthritic cytokine[69,70], with anti-angiogenic effects that lead to reduction of pathologic neovascularization, an important component of the synovial tissue pannus.[71] Additionally, it inhibits cartilage damage and osteoclastogenesis.[45]

IL13 exerts protective function also after MI. IL13 knock-out mice exhibit impaired heart regeneration during early postnatal stages[72], and in adult mice deletion of IL13[73] or IL13

receptor-αl[74] resulted in impaired post-MI recovery and spontaneous heart failure, respectively. Therefore, administering recombinant ILl3 may be a therapeutic approach for activating regenerative and survival pathways in the heart.

In addition to anti-inflammatory cytokines, pro-inflammatory cytokines may also be targeted directly, and several clinical studies have shown the potential and beneficial effects of this strategy.

Interleukin-l, the prototypical inflammatory cytokine, has a naturally occurring **IL1 receptor antagonist (IL1RA)** that prevents the binding of ILlα and ILlβ to the ILl receptor, thereby stopping the release of secondary inflammatory mediators. Anakinra, a non-glycosylated recombinant form of ILRA has been approved for treatment of patients with rheumatoid arthritis who fail to respond to disease modifying agents. Anakinra therapy significantly reduced radiographic joint damage in patients with RA.[75]

Compared to the general population, RA patients exhibit a higher incidence of cardiovascular events[76] and studies in patients with rheumatoid arthritis suggest protective actions of anakinra on myocardial function, by improving vascular and left ventricular function as well as myocardial deformation.[77,78] Pilot studies have suggested that anakinra was safe when administered as a 2-week course in patients with STEMI and may favorably affect LV remodeling[79], reduce acute inflammatory response and protect from the development of post-MI heart failure.[80,8l] In general, subclinical inflammation is associated with an increased risk of myocardial dysfunction.[82] The interleukin-lβ inhibitor canakinumab given subcutaneously once every 3 months has proven to dose-dependently reduce hospitalization for heart failure in patients with a history of myocardial infarction and ongoing subclinical inflammation.[83] This shows that preventive anti-inflammatory therapy in the form of a drug depot can improve patient outcome and we suggest here a way to make drug depots responsive to the actual inflammation status of the patient.

Cytokine-targeted drug delivery strategies

In this review we linked MMP profiles to the disease phases after RA and MI. Further, the cytokine profile was linked to the disease phases. Combining both insights provides the (patho-) physiological rationale for future active, disease-driven DDS. Only when certain MMPs are naturally upregulated and expressed, these trigger the release of cytokines or inhibitors from the DDS – based on the hypothesis that the kinetic regulation profile during

the natural course of a disease is a valid template for the release profile from a DDS. What makes bioresponsive depots intriguing is that they are silent during phases of low disease activity, and only become active during flares of inflammation, which are then immediately suppressed by the cytokine drug discharged from the active DDS. This may lead to new therapies, which would treat patients in asymptomatic states, as a preventive measure. By preventing the steady damage of subclinical chronic inflammation, hospitalization rates of patients could hopefully be reduced.

Cytokines are small and typically require several daily administration or continuous infusion. Further, as of their pleiotropic actions, many of these suffer from side-effects. However, their therapeutic potential may be leveraged by bioresponsive, MMP-driven drug delivery systems as described here. We focus here on bioresponsive cytokine depots, enabling longer residence time of the cytokine in the tissue by using a targeting moiety or immobilization techniques. A protease-sensitive linker mediates release of the cytokines in response to upregulation of biomarkers, thereby reducing side effects. Since both RA and MI have characteristic temporal MMP expression patterns, MMP serve as the releasing biomarker. RA can be distinguished between early (MMP-1, MMP-3) and late RA (MMP-8, MMP-9). MI has a well characterized MMP profile with an initial ECM degradation by mainly MMP-3 and -9. In the following stage MMP activity decreases only to once again increase with MMP-1, MMP-8 and MT1-MMP, resulting in development of LV dilatation. The high substrate efficiency of MMPs can be used for the design of peptide linkers that connect cytokine and carrier and that are designed to be specifically cleaved by MMPs.[84] These peptide linkers serve as an on-switch for the cytokine depots and are activated by MMPs as biomarkers of the disease. This activation would lead to increased local drug concentrations at the site of disease, thereby circumventing dose-limiting toxicities. This on-demand anti-inflammatory cytokine release leads to down-regulation of MMP-expression in a self-regulatory system without the pitfalls of direct MMP inhibition.

For treatment of RA, the formation of a drug depot from which anti-inflammatory cytokines are released upon bursts of inflammation, which is then suppressed, seems to be the best option. This could be achieved by conjugation of the cytokine to a targeting moiety [85] or by direct immobilization within the diseased tissue. For the treatment of MI anti-inflammatory depots responding to h MMP-1 thereby modulating inflammation may form an interesting intervention as would depots responding to MMP-8 for setting stimuli by regenerative growth factors to help remodeling. Equipped with different MMP linkers, anti-inflammatory cytokines and regenerative growth factors could be applied with a single administration and

released in subsequent manner, guided by the MMP expression profile. Thereby, the initial inflammation could be dampened by anti-inflammatory cytokines to reduce tissue damage, and the remodeling process could be supported by the release of regenerative growth factors for improved cardiac repair.

Summary

Our understanding of the complex MMP and cytokine network is far from complete and successful application of MMP expression profiles for spatiotemporally controlled release of therapeutics for treatment of inflammation-related diseases will require a more thorough understanding of the underlying processes. This is not only an approach to move from empirically optimized cytokine release profiles to a hypothesis driven approach but is one way to respond to the unforeseeable and idiosyncratic differences on disease progression. MMP-driven drug delivery systems equip the DDS with the 24/7 sensory function for detecting that (patho-)physiological phase within which delivery should occur while responding to entry into this phase with therapeutic cytokine delivery.

References

1. Turner, M. D., Nedjai, B., Hurst, T. & Pennington, D. J. Cytokines and chemokines: At the crossroads of cell signalling and inflammatory disease. *Biochim. Biophys. Acta - Mol. Cell Res.* **1843**, 2563–2582 (2014).

2. Holmdahl, R., Malmström, V. & Burkhardt, H. Autoimmune priming, tissue attack and chronic inflammation - The three stages of rheumatoid arthritis. *Eur. J. Immunol.* **44**, 1593–1599 (2014).

3. Haschka, J. *et al.* Relapse rates in patients with rheumatoid arthritis in stable remission tapering or stopping antirheumatic therapy: Interim results from the prospective randomised controlled RETRO study. *Ann. Rheum. Dis.* **75**, 45–51 (2016).

4. Nagase, H., Visse, R. & Murphy, G. Structure and function of matrix metalloproteinases and TIMPs. *Cardiovasc. Res.* **69**, 562–573 (2006).

5. Harris, E. D. & Krane, S. M. An endopeptidase from rheumatoid synovial tissue culture. *BBA - Enzymol.* **258**, 566–576 (1972).

6. Martel-Pelletier, J., Welsch, D. J. & Pelletier, J. P. Metalloproteases and inhibitors in arthritic diseases. *Best Pract. Res. Clin. Rheumatol.* **15**, 805–829 (2001).

7. Mengshol, J. A., Mix, K. S. & Brinckerhoff, C. E. Matrix Metalloproteinases as Therapeutic Targets in Cancer. *Arthritis Rheum.* **546**, 13–20 (2002).

8. Burrage, P. S. Matrix Metalloproteinases: Role In Arthritis. *Front. Biosci.* **11**, 529 (2006).

9. Firestein, G. S. Evolving concepts of rheumatoid arthritis. *Nature* **423**, 356–361 (2003).

10. Lindsey, M. L., Iyer, R. P., Jung, M., DeLeon-Pennell, K. Y. & Ma, Y. Matrix metalloproteinases as input and output signals for post-myocardial infarction remodeling. *J. Mol. Cell. Cardiol.* **91**, 134–140 (2016).

11. J.M., M. & T.E., C. Matrix metalloproteinase knockout studies and the potential use of matrix metalloproteinase inhibitors in the rheumatic diseases. *Curr. Drug Targets Inflamm. Allergy* **4**, 363–375 (2005).

12. Mcinnes, I. B. & Schett, G. Pathogenetic insights from the treatment of rheumatoid arthritis. *Lancet* **389**, 2328–2337 (2017).

13. Yoshihara, Y. *et al.* Matrix metalloproteinases and tissue inhibitors of metalloproteinases in synovial fluids from patients with rheumatoid arthritis or osteoarthritis. *Ann. Rheum. Dis.* **59**, 455–61 (2000).

14. Mudgett, J. S. *et al.* Collagen-Induced Arthritis and Cartilage Destruction. *Rheumatism* **41**, 110–121 (1998).

15. van Meurs, J. *et al.* Active matrix metalloproteinases are present in cartilage during immune complex-mediated arthritis: a pivotal role for stromelysin-1 in cartilage destruction. *J. Immunol.* **163**, 5633–9 (1999).

16. Tchetverikov, I. *et al.* Matrix metalloproteinases-3, -8, -9 as markers of disease activity and joint damage progression in early rheumatoid arthritis. *Ann. Rheum. Dis.* **62**, 1094–1099 (2003).

17. Tchetverikov, I. *et al.* MMP profile in paired serum and synovial fluid samples of patients with rheumatoid arthritis. *Ann. Rheum. Dis.* **63**, 881–883 (2004).

18. Miller, M. C. *et al.* Membrane type 1 matrix metalloproteinase is a crucial promoter of synovial invasion in human rheumatoid arthritis. *Arthritis Rheum.* **60**, 686–697 (2009).

19. Yoshihara, Y. *et al.* Matrix metalloproteinases and tissue inhibitors of metalloproteinases in synovial fluids from patients with rheumatoid arthritis or osteoarthritis. *Ann. Rheum. Dis.* **59**, 455–461 (2000).

20. Itoh, T. *et al.* The Role of Matrix Metalloproteinase-2 and Matrix Metalloproteinase-9 in Antibody-Induced Arthritis. *J. Immunol.* **169**, 2643–2647 (2002).

21. Vanhoutte, D., Schellings, M., Pinto, Y. & Heymans, S. Relevance of matrix metalloproteinases and their inhibitors after myocardial infarction: A temporal and spatial window. *Cardiovasc. Res.* **69**, 604–613 (2006).

22. Frangogiannis, N. G., Smith, C. W. & Entman, M. L. The inflammatory response in myocardial infarction. **53**, 31–47 (2002).

23. Cleutjens, J. P. M., Blankesteijn, W. M., Daemen, M. J. A. P. & Smits, J. F. M. The infarcted myocardium Simply dead tissue, or a lively target for therapeutic interventions. *Cardiovasc. Res.* **44**, 232–241 (1999).

24. Brown, R. D., Ambler, S. K., Mitchell, M. D. & Long, C. S. THE CARDIAC FIBROBLAST: Therapeutic Target in Myocardial Remodeling and Failure. *Annu. Rev. Pharmacol. Toxicol.* **45**, 657–687 (2005).

25. Squire, I. B., Evans, J., Ng, L. L., Loftus, I. M. & Thompson, M. M. Plasma MMP-9 and MMP-2 following acute myocardial infarction in man: Correlation with echocardiographic and neurohumoral parameters of left ventricular dysfunction. *J. Card. Fail.* **10**, 328–333 (2004).

26. Kaden, J. J. *et al.* Time-dependent changes in the plasma concentration of matrix metalloproteinase 9 after acute myocardial infarction. *Cardiology* **99**, 140–144 (2003).

27. Kelly, D. *et al.* Plasma matrix metalloproteinase-9 and left ventricular remodelling after acute myocardial infarction in man: A prospective cohort study. *Eur. Heart J.* **28**, 711–718 (2007).

28. Webb, C. S. *et al.* Specific temporal profile of matrix metalloproteinase release occurs in patients after myocardial infarction: Relation to left ventricular remodeling. *Circulation* **114**, 1020–1027 (2006).

29. van den Borne, S. W. M. *et al.* Increased matrix metalloproteinase-8 and-9 activity in patients with infarct rupture after myocardial infarction. *Cardiovasc. Pathol.* **18**, 37–43 (2009).

30. Halade, G. V., Jin, Y. F. & Lindsey, M. L. Matrix metalloproteinase (MMP)-9: A proximal biomarker for cardiac remodeling and a distal biomarker for inflammation. *Pharmacol. Ther.* **139**, 32–40 (2013).

31. Kelly, D. *et al.* Circulating Stromelysin-1 (MMP-3): A novel predictor of LV dysfunction, remodelling and all-cause mortality after acute myocardial infarction. *Eur. J. Heart Fail.* **10**, 133–139 (2008).

32. Hirohata, S. *et al.* Time dependent alterations of serum matrix tissue inhibitor after

successful reperfusion of acute myocardial infarction. *Methods* 278–284 (1997).

33. Konstam, M. A., Kramer, D. G., Patel, A. R., Maron, M. S. & Udelson, J. E. Left ventricular remodeling in heart failure: Current concepts in clinical significance and assessment. *JACC Cardiovasc. Imaging* **4**, 98–108 (2011).

34. Wilson, E. M. *et al.* Region- and type-specific induction of matrix metalloproteinases in post-myocardial infarction remodeling. *Circulation* **107**, 2857–2863 (2003).

35. Vervoordeldonk, M. J. B. M. & Tak, P. P. Cytokines in rheumatoid arthritis. *Curr. Rheumatol. Rep.* **4**, 208–217 (2002).

36. Smeets, T. J. M., Dolhain, R. J. E. M., Breedveld, F. C. & Tak, P. P. Analysis of the cellular infiltrates and expression of cytokines in synovial tissue from patients with rheumatoid arthritis and reactive arthritis. *J. Pathol.* **186**, 75–81 (1998).

37. Hughes, S. Infliximab harmful in CHF-final results of ATTACH. HeartWire News, June 12, 2002. (2002).

38. Wood, S. RENEWAL trial: no improvement in CHF with etanercept. HeartWire News, June 11, 2002. (2002).

39. Scott, L. J. Etanercept: a review of its use in autoimmune inflammatory diseases. *Drugs* **74**, 1379–1410 (2014).

40. Butta, C. *et al.* Effects of ACE-Inhibitors and Angiotensin Receptor Blockers on Inflammation. *Curr. Pharm. Des.* **18**, 4385–4413 (2012).

41. Ohtsuka, T. *et al.* Effect of beta-blockers on circulating levels of inflammatory and anti-inflammatory cytokines in patients with dilated cardiomyopathy. *J. Am. Coll. Cardiol.* **37**, 412–417 (2002).

42. Luzina, I. G. *et al.* Regulation of inflammation by interleukin-4: a review of 'alternatives'. *J. Leukoc. Biol.* **92**, 753–764 (2012).

43. Joosten, L. A. B. *et al.* Role of interleukin-4 and interleukin-10 in murine collagen-induced arthritis: Protective effect of interleukin-4 and interleukin-10 treatment on cartilage destruction. *Arthritis Rheum.* **40**, 249–260 (1997).

44. Joosten, L. A. B. *et al.* Protection against cartilage and bone destruction by systemic interleukin-4 treatment in established murine type II collagen-induced arthritis. *Arthritis Res.* **1**, 81–91 (1999).

45. Yamada, A. *et al.* Interleukin-4 inhibition of osteoclast differentiation is stronger than that of interleukin-13 and they are equivalent for induction of osteoprotegerin production from osteoblasts. *Immunology* **120**, 573–579 (2007).

46. Fujii, T., Kitaura, H., Kimura, K., Hakami, Z. W. & Takano-Yamamoto, T. IL-4 inhibits TNF-α-mediated osteoclast formation by inhibition of RANKL expression in TNF-α-activated stromal cells and direct inhibition of TNF-α-activated osteoclast precursors via a T-cell-independent mechanism in vivo. *Bone* **51**, 771–780 (2012).

47. Horsfall, A. C. *et al.* Suppression of collagen-induced arthritis by continuous administration of IL-4. *J. Immunol.* **159**, 5687–96 (1997).

48. Ho, S. H. *et al.* Protection against collagen-induced arthritis by electrotransfer of an expression plasmid for the interleukin-4. *Biochem. Biophys. Res. Commun.* **321**, 759–766 (2004).

49. Hemmerle, T., Doll, F. & Neri, D. Antibody-based delivery of IL4 to the neovasculature cures mice with arthritis. - SI. *Proc. Natl. Acad. Sci. U. S. A.* **111**, 12008–12 (2014).

50. Steen-Louws, C. *et al.* IL4-10 fusion protein:a novel immunoregulatory drug combining activities of IL-4 & IL-10. *Clin. Exp. Immunol.* **195**, 1–9 (2018).

51. Atkins, M. B. *et al.* Phase I evaluation of thrice-daily intravenous bolus interleukin-4 in patients with refractory malignancy. *J. Clin. Oncol.* **10**, 1802–1809 (1992).

52. Shiraishi, M. *et al.* Alternatively activated macrophages determine repair of the infarcted adult murine heart. *J. Clin. Invest.* **126**, 2151–2166 (2016).

53. Shintani, Y. *et al.* IL-4 as a Repurposed Biological Drug for Myocardial Infarction through Augmentation of Reparative Cardiac Macrophages: Proof-of-Concept Data in Mice. *Sci. Rep.* **7**, 1–14 (2017).

54. Peng, H. *et al.* Profibrotic Role for Interleukin-4 in Cardiac Remodeling and Dysfunction. *Hypertension* **66**, 582–589 (2015).

55. Fiorentino, D., Bond, M. & Mosnmann, T. Two types of mouse T helper cell. IV. Th2 clones secrete a factor that inhibits cytokine production by Th1 clones. *J. Exp. Med.* **170**, 2081–2095 (1989).

56. Geginat, J. *et al.* The light and the dark sides of Interleukin-10 in immune-mediated diseases and cancer. *Cytokine Growth Factor Rev.* **30**, 87–93 (2016).

57. Asadullah, K., Sterry, W. & Volk, H. D. IL-10 therapy: Review of a new approach. *Pharmacol. Rev.* **55**, 241–269 (2003).

58. Doll, F., Schwager, K., Hemmerle, T. & Neri, D. Murine analogues of etanercept and of F8-IL10 inhibit the progression of collagen-induced arthritis in the mouse. *Arthritis Res. Ther.* **15**, (2013).

59. Trachsel, E. *et al.* Antibody-mediated delivery of IL-10 inhibits the progression of established collagen-induced arthritis. *Arthritis Res. Ther.* **9**, 1–9 (2007).

60. C., H. *et al.* Targeting of viral Interleukin-10 with an antibody fragment specific to damaged arthritic cartilage improves its therapeutic potency. *Arthritis Res. Ther.* R151 (2014). doi:10.1186/ar4613

61. Galeazzi, M. *et al.* Dekavil (F8IL10)–update on the results of clinical trials investigating the immunocytokine in patients with rheumatoid arthritis [abstract]. (2018).

62. Yang, Z., Zingarelli, B. & Szabo, C. Crucial Role of Endogenous Interleukin-10 Production in Myocardial Ischemia/Reperfusion Injury. *Circulation* **101**, 1019–1026 (2000).

63. Lacraz, S., Nicod, L. P., Chicheportiche, R., Welgus, H. G. & Dayer, J. M. IL-10 inhibits metalloproteinase and stimulates TIMP-1 production in human mononuclear phagocytes. *J. Clin. Invest.* **96**, 2304–2310 (2008).

64. Shirakawa, K. *et al.* IL (Interleukin)-10-STAT3-Galectin-3 Axis Is Essential for Osteopontin-Producing Reparative Macrophage Polarization After Myocardial Infarction. *Circulation* **138**, 2021–2035 (2018).

65. Stumpf, C. *et al.* Interleukin-10 improves left ventricular function in rats with heart

failure subsequent to myocardial infarction. *Eur. J. Heart Fail.* **10**, 733–739 (2008).

66. Krishnamurthy, P. *et al.* IL-10 inhibits inflammation and attenuates left ventricular remodeling after myocardial infarction via activation of STAT3 and suppression of HuR. *Circ. Res.* **104**, 9–18 (2009).

67. Jung, M. *et al.* IL-10 improves cardiac remodeling after myocardial infarction by stimulating M2 macrophage polarization and fibroblast activation. *Basic Res. Cardiol.* **112**, 1–14 (2017).

68. Raza, K. *et al.* Early rheumatoid arthritis is characterized by a distinct and transient synovial fluid cytokine profile of T cell and stromal cell origin. *Arthritis Res. Ther.* **7**, R784-95 (2005).

69. Bessis, N. *et al.* Attenuation of collagen-induced arthritis in mice by treatment with vector cells engineered to secrete interleukin-13. *Eur. J. Immunol.* **26**, 2399–2403 (1996).

70. Woods, J. M. *et al.* IL-13 Gene Therapy Reduces Inflammation, Vascularization, and Bony Destruction in Rat Adjuvant-Induced Arthritis. *J. Immunol.* **166**, 1214–1222 (2001).

71. Haas, C. S. *et al.* In vivo inhibition of angiogenesis by interleukin-13 gene therapy in a rat model of rheumatoid arthritis. *Arthritis Rheum.* **56**, 2535–2548 (2007).

72. Wodsedalek, D. J. *et al.* IL-13 promotes in vivo neonatal cardiomyocyte cell cycle activity and heart regeneration. 24–34 (2019). doi:10.1152/ajpheart.00521.2018

73. Hofmann, U. *et al.* Interleukin-13 deficiency aggravates healing and remodeling in male mice after experimental myocardial infarction. *Circ. Hear. Fail.* **7**, 822–830 (2014).

74. Sahu, A. *et al.* New Role for Interleukin-13 Receptor α1 in Myocardial Homeostasis and Heart Failure. *J. Am. Heart Assoc.* **6**, (2017).

75. Bresnihan, B., Newmark, R., Robbins, S. & Genant, H. K. Effects of anakinra monotherapy on joint damage in patients with rheumatoid arthritis. Extension of a 24-week randomized, placebo-controlled trial. *J. Rheumatol.* **31**, 1103–1111 (2004).

76. Primdahl, J., Clausen, J. & Hørslev-Petersen, K. Results from systematic screening for cardiovascular risk in outpatients with rheumatoid arthritis in accordance with the EULAR recommendations. *Ann. Rheum. Dis.* **72**, 1771–1776 (2013).

77. Ikonomidis, I. *et al.* Inhibition of interleukin-1 by anakinra improves vascular and left ventricular function in patients with rheumatoid arthritis. *Circulation* **117**, 2662–2669 (2008).

78. Ikonomidis, I. *et al.* Lowering interleukin-1 activity with anakinra improves myocardial deformation in rheumatoid arthritis. *Heart* **95**, 1502–1507 (2009).

79. Abbate, A. *et al.* Interleukin-1 Blockade With Anakinra to Prevent Adverse Cardiac Remodeling After Acute Myocardial Infarction (Virginia Commonwealth University Anakinra Remodeling Trial [VCU-ART] Pilot Study). *Am. J. Cardiol.* **105**, 1371-1377.e1 (2010).

80. Abbate, A. *et al.* Effects of interleukin-1 blockade with anakinra on adverse cardiac remodeling and heart failure after acute myocardial infarction [from the virginia commonwealth university-anakinra remodeling trial (2) (vcu-art2) pilot study]. *Am.*

J. Cardiol. **111**, 1394–1400 (2013).

81. Abbate, A. *et al.* Comparative safety of interleukin-1 blockade with anakinra in patients with ST-segment elevation acute myocardial infarction (from the VCU-ART and VCU-ART2 pilot studies). *Am. J. Cardiol.* **115**, 288–292 (2015).

82. Kalogeropoulos, A. *et al.* Inflammatory Markers and Incident Heart Failure Risk in Older Adults. The Health ABC (Health, Aging, and Body Composition) Study. *J. Am. Coll. Cardiol.* **55**, 2129–2137 (2010).

83. Everett, B. M. *et al.* Anti-Inflammatory Therapy With Canakinumab for the Prevention of Hospitalization for Heart Failure. *Circulation* **139**, 1289–1299 (2019).

84. Turk, B. E., Huang, L. L., Piro, E. T. & Cantley, L. C. Determination of protease cleavage site motifs using mixture-based oriented peptide libraries. *Nat. Biotechnol.* **19**, 661–667 (2001).

85. Bootz, F. & Neri, D. Immunocytokines: A novel class of products for the treatment of chronic inflammation and autoimmune conditions. *Drug Discov. Today* **21**, 180–189 (2016).

Chapter 2: Interleukin-4-clicked surfaces drive M2 macrophage polarization

Tessa Lühmann[1*], Valerie Spieler[1*], Vera Werner[1], Marie-Gabrielle Ludwig[2], Juliane Fiebig[3], Thomas D. Mueller[3], and Lorenz Meinel[1]

[1] Institute for Pharmacy and Food Chemistry, University of Würzburg, Würzburg, Germany

[2] Novartis Institutes for BioMedical Research, Novartis Pharmaceuticals AG, Basel, Switzerland

[3] Lehrstuhl für Botanik I Molekulare Pflanzenphysik und Biophysik, University of Würzburg, Würzburg, Germany

[*] These authors contributed equally to this work.

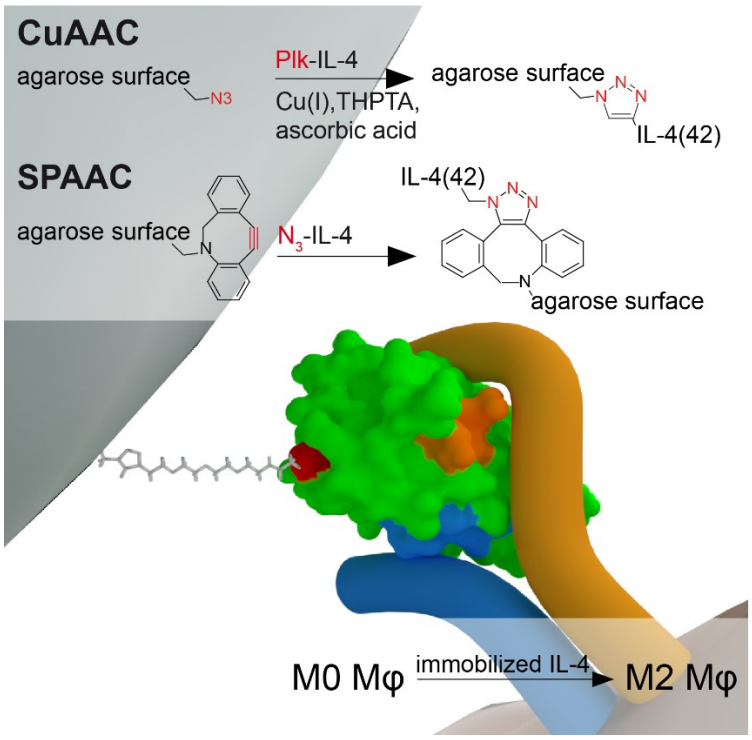

This chapter was originally published in ChemBioChem 17.22 (2016): 2123-2128. DOI: 10.1002/cbic.201600480. With permission of John Wiley and Sons, license number: 4633580642263.

Abstract

Driving macrophage (Mϕ) polarization into the M2 phenotype provides potential against inflammatory diseases. Interleukin-4 (IL-4) leverages polarization into the M2-Mϕ phenotype but its systemic use is constrained by dose-limiting toxicity. Consequently, we developed IL-4 decorated surfaces aiming at sustained and localized activity. IL-4 muteins were generated by genetic code expansion, replacing Lys 42 by unnatural amino acids (uAA). All muteins had wt-IL-4 comparable cellular performances and binding affinities to the IL4Rα. Copper catalyzed (CuAAC) and copper free strain promoted (SPAAC) 1,3-dipolar azide alkyne cycloadditions were used to site-selectively anchor IL-4 to agarose surfaces. These surfaces had sustained IL-4 activity as demonstrated by TF-1 cell proliferation and M2 but not M1 polarization of M-CSF generated human Mϕ. The approach provides a blueprint for the engineering of cytokine-activated surfaces profiled for sustained and spatially controlled activity.

Introduction

Regulation of macrophage (Mϕ) polarization and phenotypic plasticity opens exciting new treatment strategies against inflammatory diseases, including impaired wound healing, rheumatoid arthritis or arteriosclerosis.[2] By infiltrating injured tissues during the acute inflammation phase, blood-derived as well as tissue-resident Mϕ sequentially polarize towards a spectrum of different phenotypes, including a classical (pro-inflammatory = M1) and an alternative (anti-inflammatory = M2) state.[3] Interleukin-4 (IL-4) effectively triggers M2-Mϕ polarization thereby providing benefit for tissue repair and regeneration processes.[4] IL-4 has a complicated receptor usage combined with an elaborated target cell activation spectrum. IL-4 signals through two differently composed receptors, the type I receptor (subunits IL-4Rα and γc) and the type II receptor (subunits IL-4Rα and IL13Rα1). High affinity binding of IL-4 is to the IL-4Rα subunit (KD = 100 pM)[5] followed by ligand-mediated receptor heterodimerization leading to either γc (type I receptor) or IL13Rα1 (type II receptor) recruitment, respectively. The type I receptor is predominately expressed on cells of hematopoietic origin, whereas the type II receptor is mainly on non-hematopoietic cells. Mϕ express both types of IL-4 receptors (IL-4R).[4a]

Results

Translation of IL-4's therapeutic potential into clinical practice following systemic administration was constrained by dose-limiting toxicities reflecting the cytokine`s pleiotropic activities.[6] However, advancing from systemic to localized administration is expected to positively skew IL-4's risk-benefit ratio. The challenge, therefore, translated into designing IL-4 therapeutics, providing a local stimulus to tissues in need while minimizing systemic exposure. We addressed this demand by deploying genetic code expansion, thereby integrating unnatural amino acids (uAA) with either azide or alkyne functionalities into the IL-4 backbone during protein synthesis in Escherichia coli (*E. coli*). This approach provided maximal spatial control in anchoring IL-4 strictly via the inserted uAA onto surfaces. The first step was to identify IL-4 positions that serve as appropriate anchor sites and satisfy the following specifications: (i) replacement by the uAA does not impact potency; (ii) the insertion site presents the uAA such that efficient chemical immobilization is sterically favored, and (iii) introduction of the uAA will not jeopardize overall structural integrity as compared to wt-IL-4 (Figure 1).

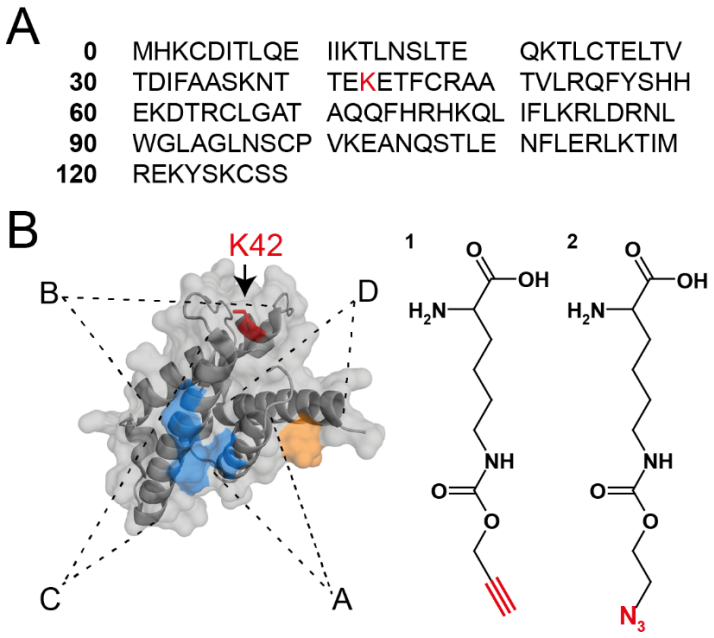

Fig. 1 **(A)** AA sequence of human IL-4. The codon for Lysine (K) 42 (shown in red) was exchanged to an amber stop codon for genetic code expansion. **(B)** Crystal structure of IL-4. PDB = 2B8U.[1] The 4-helix (A, B, C and D) bundle is indicated. Main receptor binding sites are highlighted: Orange colored residues (I11, R121, and Y124) are the binding site for receptor subunits IL-13Rα1/γc and blue colored residues (E9, T13, F82, R85, R88) the binding site for receptor subunit IL-4Rα.[1] K42 / the insertion site of the uAA is shown in red. **(C)** Structure of the uAAs propargyl-L-lysine (Plk; 1) and N3-pyrrolysine (N3; 2).

IL-4 belongs to the short chain 4-helix bundle cytokines with four anti-parallel α-helices. IL-4's receptor binding sites are localized on its A, C and D helices but not on the B helix (Figure 1B).[7] These structural insights were seminal in that hypothetically any introduction of uAA into appropriate sites of the B helix will not interfere with the receptor binding sites and providing the cytokine's overall conformation remains unaltered. This rationale selection of insertion sites may be a general approach for the design of protein/cytokine-decorated surfaces as exemplarily shown here for IL-4. Based on this strategy, a surface exposed lysine (Lys) residue at position 42 in the α-helix B (residues 39–66) opposite to the receptor interaction epitopes formed an attractive replacement site for uAAs propargyl-L-lysine (Plk) (1) or N3-pyrrolysine (N3) (2). Figure 1B depicts the crystal structure of IL-4, in which the four α-helices (A, B, C and D) and the location with the Plk/N3-exchange (Lys-42–Plk or Lys-42-N3) is highlighted. Upon selection of the insertion site - driven by the aforementioned specifications (vide supra) - we introduced the uAA residues into IL-4 through amber codon (UAG) suppression using a pyrrolysyl-tRNA synthethase/tRNAPyl CUA pair originating from *Methanosarcina barkeri*, which tolerates incorporation of various pyrrolysine-based derivatives.[8]

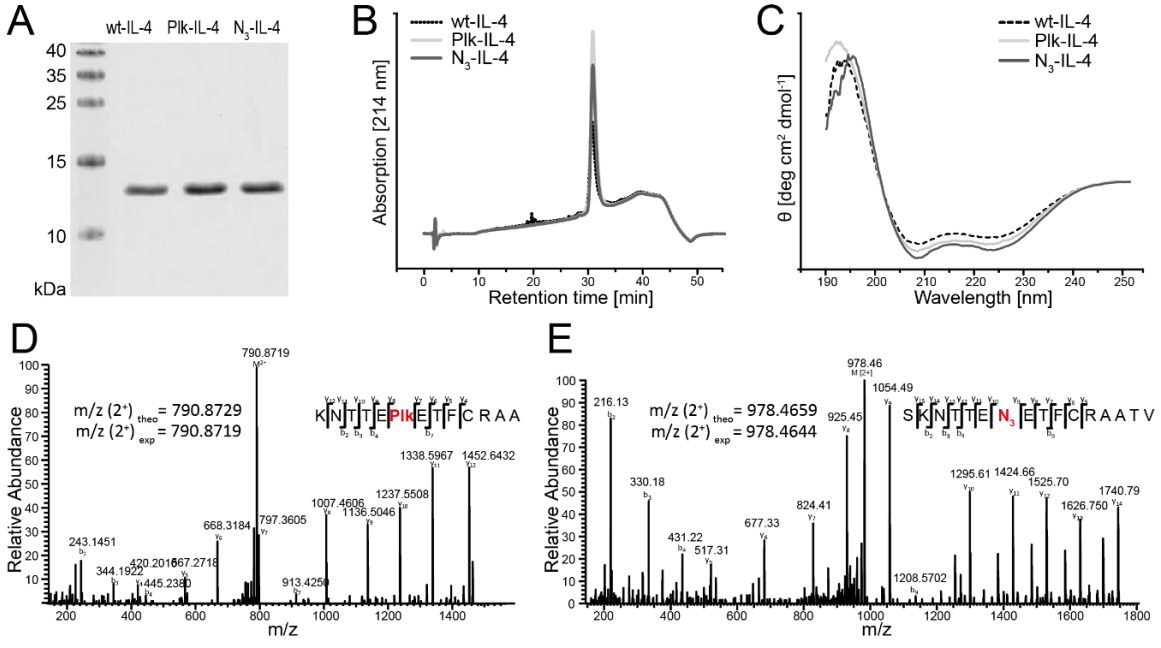

Fig. 2 **(A)** Reduced SDS-PAGE of wt-IL-4, Plk-IL-4 and N3-IL-4. **(B)** RP-HPLC analysis of wt-IL-4 (dashed line), Plk-IL-4 (light grey) and N3-IL-4 (dark grey). **(C)** CD spectra of wt-IL-4, Plk-IL-4 and N3-IL-4. **(D)** Fragments of elastase digested Plk-IL-4 as analysed by LC-MS/MS. **(E)** Fragments of elastase digested N3-IL-4 as analysed by LC-MS/MS. All b- and y-ions marked in the peptide sequence were found.

The muteins Plk-IL-4 and N3-IL-4 were expressed in the *E. coli* strain BL21 (DE3) with average overall process-yields of about 3 mg/L – a comparable yield observed for analogously produced, other muteins[8c, 9] – and high purity (> 95 %) as determined by RP-HPLC and SDS-PAGE for both, the Plk-IL-4 and the N3-IL-4 mutein, respectively (Figure 2A,B). Circular dichroism measurements of Plk-IL-4 and N3-IL-4 in comparison to wt-IL-4 revealed comparable levels of helicity, suggesting a natively folded state of the muteins (Figure 2C). MALDI-MS analysis confirmed the calculated mass of both IL-4 muteins (Plk-IL-4: obs. average mass = 15173 Da, calc. average mass = 15170 Da; N3-IL-4 obs. average mass = 15201 Da, calc. average mass = 15207 Da; Figure S1, S2). Furthermore, the introduction of the uAAs Plk or N3 at position 42 into IL-4 was confirmed following elastase digest and LC-MS/MS analysis (Figure 2 D,E).

The potency of the muteins was determined by measuring the dose-dependent activity of the proteins in two different cell-lines and a primary cell culture system of human peripheral blood derived monocytes (PBDM). We deployed human TF-1 suspension cells as a model for hematopoietic cells - expressing both the type I and the type II IL-4 receptor - to analyze cell proliferation in response to IL-4 concentration. As non-hematopoietic cell-line, kidney derived HEK293T cells - expressing only the type II receptor - were cotransfected with a STAT-6 expression vector for reporter gene expression of either enhanced yellow fluorescence protein (eYFP) or secreted alkaline phosphatase (SEAP).[10] IL-4R activation leads to STAT-6 phosphorylation as primary signaling pathway.[11] Both IL-4 muteins were as active as wt-IL-4 in all cell culture setups, establishing the Lys 42 residue as a suitable uAA insertion site for the purpose of generating constitutively active IL-4 muteins with site-specific anchor sites serving subsequent decoration purposes (Figure 3 A–C). The muteins' polarization potential on M-CSF generated human Mϕ was assessed by RT-PCR using M1 and M2 gene expression markers.[12] Positive controls for M1 polarization were Mϕ exposed to a mixture of lipopolysaccharides (LPS) and interferon ɣ (IFNɣ) for 24 hours or - to induce the M2 Mϕ polarization state - by incubation with 20 ng/mL of IL-4 or Plk-IL-4 in the presence of M-CSF. The IL-4 concentration of 20 ng/mL was selected as it provided maximal TF-1 proliferation (Figure 3A) and maximal relative ALOX15 gene expression in primary macrophages as measured in quantitative dose gene-expression curves obtained from cells originating from two different donors (Figure S3). Plk-IL-4 induced M2 markers with the same potency and efficacy as wt-IL-4, but did not induce M1 markers (Figure S4; N3-IL-4 insertion was not tested with respect to Mϕ polarization, but provided comparable results to Plk-IL-4 with respect to TF-1 proliferation). Binding affinities of IL-4 muteins to the

extracellular domain of IL-4Rα were studied by surface plasmon resonance (SPR) based interaction analysis. For preparation of the sensor chip, the ybbR-tagged N-terminus of the IL-4Rα ectodomain was enzymatically modified with the substrate CoA-biotin by Sfp phosphopantetheinyl transferase and site-specifically immobilized on a streptavidin modified sensor chip as previously described.[1, 13] Wt-IL-4 and both clickable IL-4 muteins (Plk-IL-4, and N3-IL-4) show identical binding kinetics for the interaction with surface immobilized IL-4Rα. Sensograms were analyzed to yield association and dissociation rate constants employing a simple Langmuir type 1:1 interaction model. All IL-4 proteins had a very fast association with a rate constant (kon) in the range of 3-5 x 106 M-1s-1 and a rather slow dissociation (koff) in the range of 5 x 10-4 s-1 indicating that the exchange of Lys 42 did not alter binding kinetics nor complex stability (Figure 3 D–F). Binding affinities were calculated from the kinetic rate constants and yielded equilibrium binding constants of 143 pM for wt-IL-4, which is in accordance to the literature. [5]

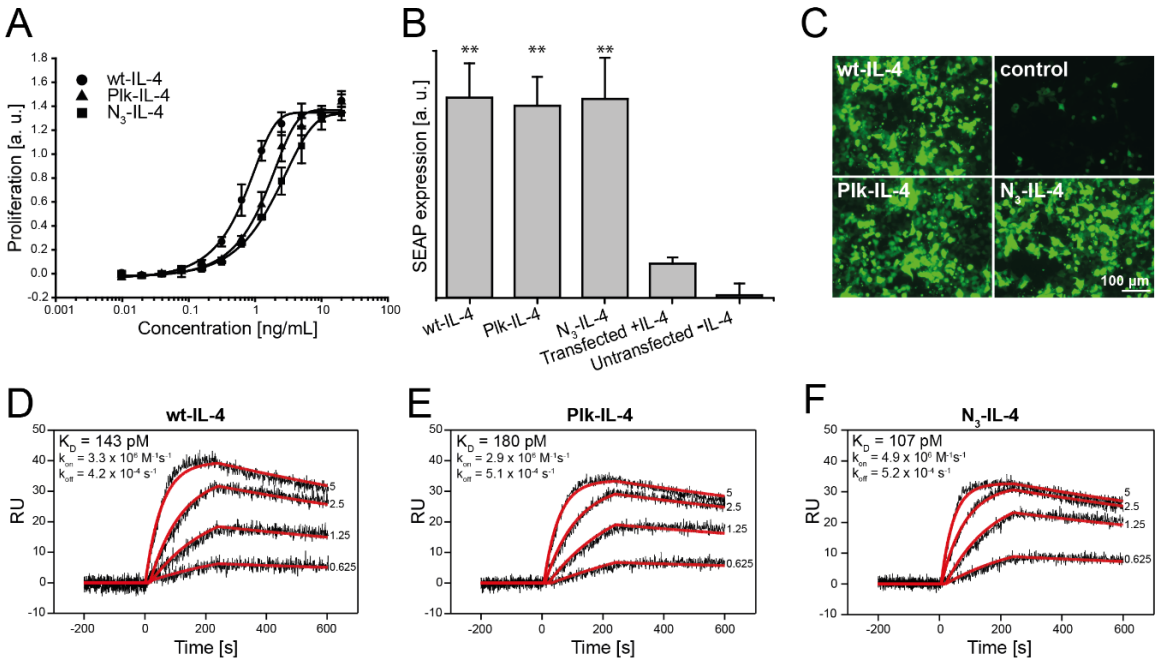

Fig. 3 **(A)** TF-1 proliferation assay of wt-IL-4, Plk-IL-4, N_3-IL-4 (mean ± standard deviation, n = 3). **(B)** SEAP reporter gene assay of HEK 293T cells transfected with pSTAT6–SEAP and pSTAT6 after stimulation with wt-IL-4, Plk-IL-4 and N_3-IL-4 (mean ± standard deviation, n = 3) and in comparison to controls. **(C)** eYFP reporter gene assay of HEK 293T cells transfected pSTAT6–eYFP and pSTAT6 after stimulation with wt-IL-4, Plk-IL-4 and N_3-IL-4. **(D–F)** Surface plasmon resonance interaction analysis for wt-IL-4 (D), Plk-IL-4 (E) and N_3-IL-4 (F) with the ectodomain of human IL-4Rα immobilized on the sensor surface. Rate constants. k_{on} and k_{off} as well as equilibrium binding constants K_D are shown. Asterisks indicate statistically significant differences among groups ($p \leq 0.01$ (**)).

Very similar values were obtained for the Plk-IL-4 (KD = 180 pM) and N3-IL4 (KD = 120±11 pM), respectively. Binding of the binary complex between IL-4 muteins and IL-4Rα to the extracellular domains of the low affinity receptors IL-13Rα or of γc was detailed in parallel (Figure S5). Co-inject sensograms of wild type IL-4 compared to the two variants N3-IL-4 and Plk-IL-4 indicate that binding of the latter two IL-4 variants to both low-affinity receptor subunits IL-13Rα (Figure S5 B,C) and βc (Figure S5 E,F) is indistinguishable from the wild type protein IL-4 (Figure S5 A,D). In conclusion, both clickable IL-4 muteins retained wild-type-like biological activity and conformation. Furthermore, the inability of the wt-IL-4 and its muteins to induce an unfavorable M1-Mϕ polarization provided evidence that the downstream processing efficiently removed LPS from the bacterial expression host. Starting off these results we analyzed the ability for site-directed modification of the IL-4 position 42 muteins in solution and for anchorage on surfaces.

To address the accessibility of the alkyne functionality introduced at position 42 through Plk-IL-4 for chemical modification, a small azide-fluorophore was conjugated via copper-catalyzed alkyne azide cycloaddition (CuAAC) using copper (II) sulfate in the presence of sodium L-ascorbate as reducing agent with the water-soluble base tris(3-hydroxy-propyltriazolylmethyl) amine (THPTA) as previously described.[14] Fluorescent labeling of N3-IL-4 without metal catalyst was performed in parallel with a dibenzocyclooctyl (DBCO)-conjugated fluorophore, following copper free strain promoted azide alkyne cycloaddition (SPAAC), bio-orthogonal chemical conjugation strategies.[15] After click reaction, specific fluorescent bands with the expected electrophoretical mobility of IL-4 were observed in the SDS-PAGE upon fluorescence imaging, whereas controls did not show detectable fluorescence (Figure S6). Fluorescent labeling of Plk-IL-4 and N3-IL-4 was further detailed by MALDI-MS analysis demonstrating an equimolar decoration of IL-4 muteins for both the CuAAC and the SPAAC click chemistries (Figure S7, S8).

Anchoring of the IL-4 muteins was demonstrated on biocompatible agarose beads with a mean average diameter of 90 μm.[9] Firstly, the agarose surfaces were functionalized by NHS chemistry, thereby introducing N3-groups (azido-undecane azide) for CuAAC (Scheme 1A) and DBCO-groups (dibenzocyclooctyne amine) for SPAAC (Scheme 1B), respectively. Agarose-surface anchored IL-4 muteins – either by CuAAC or SPAAC – were visualized by using fluorescent IL-4 proteins, which were labeled with a NHS-fluorophore before surface anchoring. Strong fluorescence of each agarose surface was observed after immobilization by CuAAC or SPAAC and in contrast to negative controls, which lacked the

copper (I) catalyst (control for CuAAC) or when using wt-IL-4 (control for SPAAC; Figure S9).

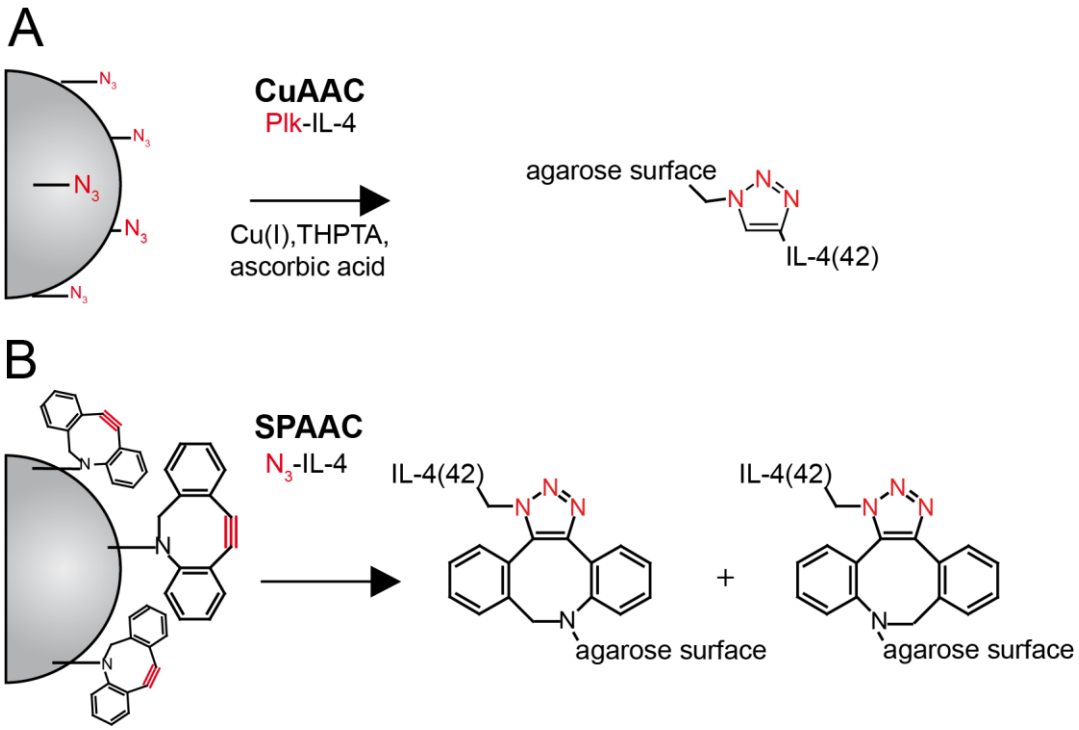

Scheme 1 **(A)** Copper-catalyzed and **(B)** copper-free strain promoted 1,3-dipolar azide alkyne cycloadditions between functionalized agarose surfaces and IL-4 muteins. Defined amounts of NHS-activated agarose beads (4 µmol NHS/100 µL bead volume) were equimolar modified with the respective clickable functional groups dibenzocyclooctyne-amine or azido-undecane-amine, respectively.

To differentiate non-specifically adsorbed IL-4 from covalently bound IL-4, IL-4 decorated agarose surfaces and corresponding controls were characterized after manufacture and after washing in PBS for up to 6 days. The IL-4 concentration in the supernatant was quantified by enzyme-linked immunosorbent assay (ELISA) at different time points (Figure S10). While CuAAC prepared surfaces were releasing small amounts of IL-4 mutein and in the range of what was observed for the control experiment, significantly (about 10 fold) more IL-4 mutein was found in the supernatant of surfaces decorated with SPAAC suggesting better covalent decoration success for the CuAAC. We speculate that the hydrophobic DBCO moiety on agarose surfaces as used for the SPAAC here within facilitated hydrophobic interactions of wt-IL-4 and its mutein, thereby favoring non-specific adsorption over site-directed covalent conjugation. Future studies may replace DBCO by other, less hydrophobic cylcooctynes.

Subsequently, we addressed the duration of activity (sustained effect) of IL-4 mutein-decorated agarose surfaces - prepared by either CuAAC or SPAAC - with a TF-1 cell proliferation assay (Figure 4 A,D). Control agarose surfaces (blocked with ethanolamine) neither induced TF-1 proliferation nor impaired proliferation in response to wt-IL-4 (Figure S11). The bioactivity of IL-4-decorated agarose surfaces prepared by CuAAC was comparable to respective controls (using wt-IL-4) when tested right after manufacture (Figure 4A), hence, no differences were observed between the covalently decorated group and its control right after manufacture. This result is not surprising in light of the high IL-4 potency on TF-1 cells (EC50 = 0.05–0.2 ng/mL)[16] and the amount of IL-4 found in the supernatant right after manufacture (Figure S9A). The remaining question was to which extent the two groups maintain an IL-4 effect when washed over time. Interestingly, washing in PBS for 6 days provided quite disparate results between the CuAAC decorated surfaces and its control. A 100 fold potency loss was observed for the control. In contrast, CuAAC decorated surfaces fully retained their TF-1 cell proliferation potency. These results indicated that the CuAAC surfaces provided sustained potency, whereas surface adsorbed IL-4 (control) failed to do so (Figure 4A). In parallel, we assessed the ability of SPAAC chemistry for the same purpose (local and sustained activity; Figure 4D). In analogy to the results obtained for immobilization by CuAAC, DBCO-functionalized agarose surfaces modified with N3-IL-4 resulted in TF-1 cell proliferation equal to its wt-IL-4 control when used right after manufacture. However, in contrast to CuAAC decorated surfaces, SPAAC decoration failed to provide sustained bioactivity after washing in PBS for 6 days, indicating incomplete covalent decoration and inferior performance regarding sustained activity. The about 10 fold better performance of SPAAC-decorated surfaces as compared to its wt-IL-4 control after 6-day-wash may provide evidence that improved SPAAC protocols are to be developed to yield better outcome in terms of increasing covalent decoration while decreasing nonspecific adsorption. Interestingly, a comparison of the controls for the CuAAC (Figure 4A) and SPAAC (Figure 4D) surfaces indicated a higher potency for the SPAAC control, perhaps reflecting increased non-specific IL-4 adsorption on the more hydrophobic DBCO functionalized surfaces in contrast to the more hydrophilic, azido-functionalized surfaces used for CuAAC. This provides more evidence for non-specific IL-4 adsorption during SPAAC rather than CuAAC conjugation corroborated by the outcome from the TF-1 cell proliferation assay (vide supra). Replacing DBCO by less hydrophobic cyclooctynes with higher reaction rates may improve the SPAAC outcome. The impact of the decoration strategies on cellular performance was tested using primary human (M-CSF differentiated)

Mϕ (Figure 4 B,C and 4E,F for CuAAC and SPAAC, respectively). IL-4 agarose surfaces - washed in PBS for 6 days for assessment of their sustained activity - were used. The ability of these surfaces for driving Mϕ polarization was

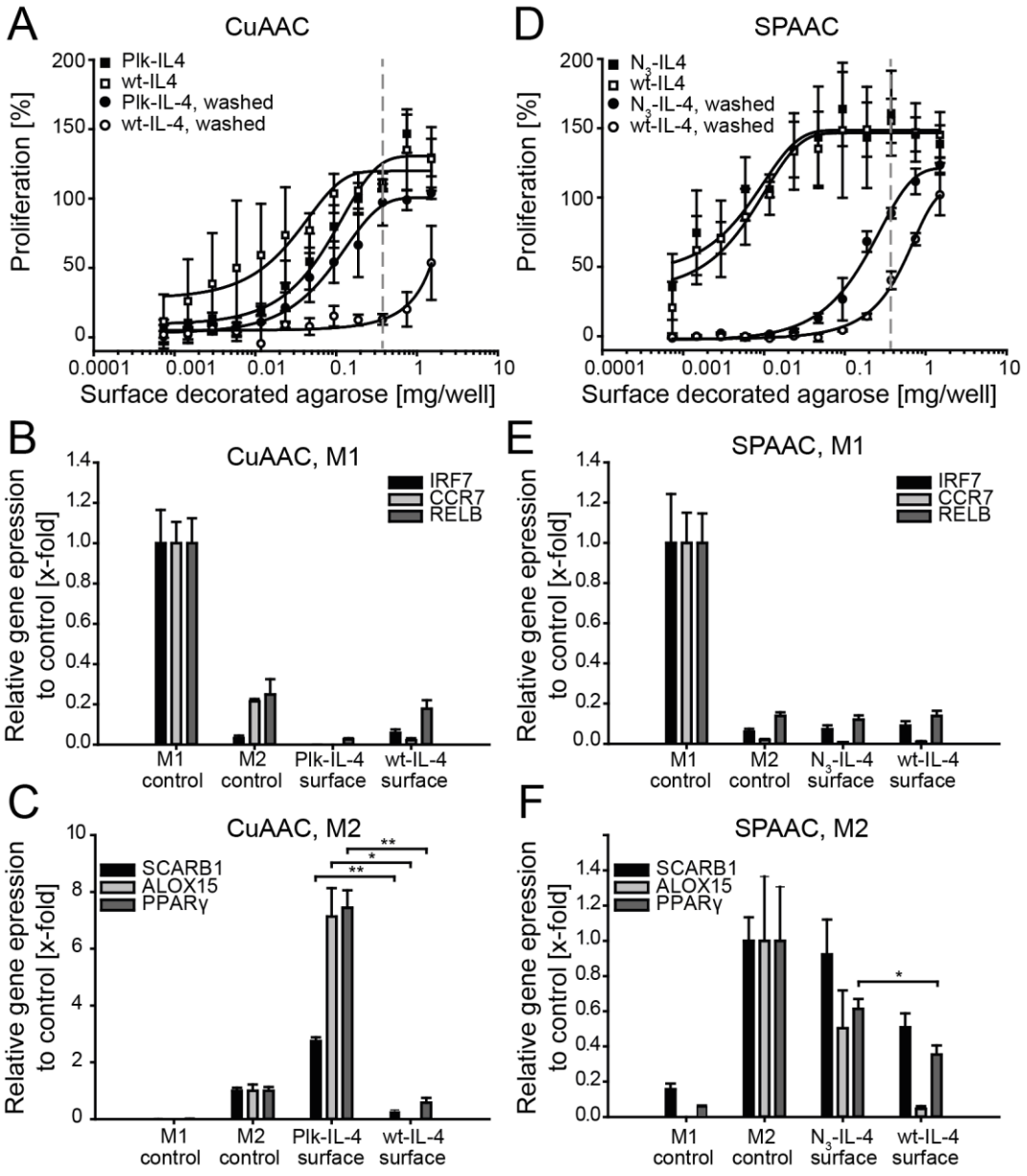

Fig. 4 **(A,B,C)** Bioactivity of IL-4-decorated agarose surfaces after CuAAC and **(D,F,E)** after SPAAC. **(A)** TF-1 proliferation assay of wt-IL-4, Plk-IL-4 and N3-IL-4 immobilized to agarose carriers after CuAAC and **(C)** after SPAAC. The dashed line indicates the concentrations selected for experiments as shown in B, C, and E, F, respectively. Data are expressed as percentage of maximal soluble IL-4 stimulation (mean ± standard deviation, n = 3). **(B,C,E,F)** Gene expression of PDBM derived M-CSF generated macrophages analyzed for M1 **(B,E)** and for M2 **(C,F)** gene markers after treatment with IL-4-decorated agarose surfaces which were washed in PBS for 6 days (used concentration as shown by dashed line in A,D) and in comparison to soluble controls. Data are expressed relatively to mRNA levels of M1 / M2 soluble controls, set at a value of one (mean ± standard deviation, n = 3). Asterisks indicate statistically significant differences among groups ($p \leq 0.05$ (*) and $p \leq 0.01$ (**)).

studied at concentrations selected from the TF-1 cell proliferation assay (Figure 4; concentrations selected for the gene expression analysis in Mϕ are indicated by dashed line in Figure 4 A and D; wt-IL-4 - serving as soluble control - was used at concentrations of 20 ng/mL, yielding 100 % relative activity in the TF-1 cell proliferation assay as seen in Figure 3A; similarly, 20 ng/mL maximally stimulated relative ALOX 15 expression in human primary (CSF1 induced) Mϕ originating from 2 donors as shown in Figure S3). At first we used M1 gene markers to study the influence of the CuAAC-prepared agarose carrier on Mϕ responses in comparison to controls exposed to LPS and IFNɣ (Figure 4B). Agarose surfaces decorated with Plk-IL-4 or wild-type IL-4 after CuAAC did not induce M1 gene markers. Similarly, the second control (soluble wt-IL-4 at a concentration of 20 ng/mL) did not induce M1-Mϕ polarization. Subsequently, we used M2 gene markers for the analysis of the responses. Exposure to CuAAC-decorated IL-4 agarose surfaces triggered M2 polarization such that a > 15 fold upregulation for ALOX15 and PPAR was observed, and as compared to the CuAAC control (Figure 4C). Interestingly, the response on Mϕ polarization by CuAAC-decorated surfaces was stronger as observed for the soluble IL-4 control. This outcome points to the question if surface-presented IL-4 can induce M2-Mϕ polarization better than soluble IL-4 when both are presented at levels previously linked to 100 % relative activity in the TF-1 cell proliferation assay (Figure 3A). Analogous to previous studies, future studies should corroborate the M2 vs. M1 polarization on the protein level, including for example TNF-α, IL-1β, CCL17, or IL-12. [17]

SPAAC functionalized agarose surfaces (Figure 4E, F) - used at concentrations as detailed by the dashed line in Figure 4D - did not induce M1-Mϕ polarization similar to what was observed for Plk-IL-4 functionalized CuAAC surfaces (Figure 4E). In contrast to CuAAC-prepared surfaces and in analogy to what was demonstrated before for TF-1 cell proliferation (Figure 4A, D), SPAAC-prepared surfaces failed to drive M2-Mϕ polarization resulting in a pattern similar to controls (Figure 4F).

In conclusion, site-directed anchoring of 'clickable IL-4 muteins' on surfaces by CuAAC chemistry can provide sustained immune modulating stimuli. Respective controls perform comparably well right after manufacture, but fail to provide sustained activity after washing protocols lasting for 6 days. Whereas CuAAC chemistry resulted in striking in vitro performances, SPAAC failed to do so. Ongoing studies evaluate the in vivo potential of CuAAC decorated IL-4 surfaces on M2 Mϕ polarization efficiency.

Experimental Section

Materials and experimental details are given in the SI.

Acknowledgements

Support by DFG (grant ME 3920/3-1 'Macrophage plasticity deployed for efficient bone (re-)generation'), the Sino-German center, and the Germany Federal Ministry of Education and Research (grant 13N13454) are gratefully acknowledged. We thank Dr. Hermann Gram and Dr. Klaus Seuwen (Novartis Pharmaceuticals AG, Basel, Switzerland) for critical discussion and for providing M-CSF and Wilfried Weber (Center for biological signaling studies, University of Freiburg) for the secreted alkaline phosphatase (SEAP) and yellow fluorescent protein (eYFP) reporter gene assays and Karl-Heinz Wiesmüller (EMC Microcollections GmbH (Tübingen, Germany) for providing S)-2-amino-6-((2-azidoethoxy)carbonylamino)hexanoic acid.

References

1. M. Kraich, M. Klein, E. Patino, H. Harrer, J. Nickel, W. Sebald, T. D. Mueller, *BMC Biol* **2006**, 4, 13.

2. B. Chazaud, *Immunobiology* **2014**, 219, 172-178.

3. **a** D. M. Mosser, J. P. Edwards, *Nat Rev Immunol* **2008**, 8, 958-969;

   b P. J. Murray, J. E. Allen, S. K. Biswas, E. A. Fisher, D. W. Gilroy, S. Goerdt, S. Gordon, J. A. Hamilton, L. B. Ivashkiv, T. Lawrence, M. Locati, A. Mantovani, F. O. Martinez, J. L. Mege, D. M. Mosser, G. Natoli, J. P. Saeij, J. L. Schultze, K. A. Shirey, A. Sica, J. Suttles, I. Udalova, J. A. van Ginderachter, S. N. Vogel, T. A. Wynn, *Immunity* **2014**, 41, 14-20.

4. **a** I. S. Junttila, K. Mizukami, H. Dickensheets, M. Meier-Schellersheim, H. Yamane, R. P. Donnelly, W. E. Paul, *J Exp Med* **2008**, 205, 2595-2608;

   b T. Hemmerle, F. Doll, D. Neri, *Proc Natl Acad Sci USA* **2014**, 111, 12008-12012.

5. V. Duppatla, M. Gjorgjevikj, W. Schmitz, H. M. Hermanns, C. M. Schafer, M. Kottmair, T. Muller, W. Sebald, *Bioconjug Chem* **2014**, 25, 52-62.

6. **a** R. P. Whitehead, D. Lew, R. C. Flanigan, G. R. Weiss, V. Roy, M. L. Glode, S. R. Dakhil, E. D. Crawford, *J Immunother* **2002**, 25, 352-358;

   b J. A. Sosman, S. G. Fisher, C. Kefer, R. I. Fisher, T. M. Ellis, *Ann Oncol* **1994**, 5, 447-452.

7. S. L. LaPorte, Z. S. Juo, J. Vaclavikova, L. A. Colf, X. Qi, N. M. Heller, A. D. Keegan, K. C. Garcia, *Cell* **2008**, 132, 259-272.

8. **a** S. Eger, M. Scheffner, A. Marx, M. Rubini, *J Am Chem Soc* **2010**, 132, 16337-16339;

   b S. Eger, M. Scheffner, A. Marx, M. Rubini, *Methods Mol Biol* **2012**, 832, 589-596;

   c D. P. Nguyen, H. Lusic, H. Neumann, P. B. Kapadnis, A. Deiters, J. W. Chin, J Am Chem Soc 2009, 131, 8720-8721; dW. Wan, J. M. Tharp, W. R. Liu, *Biochim Biophys Acta* **2014**, 1844, 1059-1070.

9. T. Lühmann, G. Jones, M. Gutmann, J.-C. Rybak, J. Nickel, M. Rubini, L. Meinel, *ACS Biomaterials Science & Engineering* **2015**, 1, 740-746.

10. **a** P. S. Lienemann, M. Karlsson, A. Sala, H. M. Wischhusen, F. E. Weber, R. Zimmermann, W. Weber, M. P. Lutolf, M. Ehrbar, *Adv Healthc Mater* **2013**, 2, 292-296;

    b E. H. Christen, M. Karlsson, M. M. Kämpf, R. Schoenmakers, R. J. Gübeli, H. M. Wischhusen, C. Friedrich, M. Fussenegger, W. Weber, *Adv Funct Mater* **2011**, 21, 2861-2867.

11. S. M. McCormick, N. M. Heller, *Cytokine* **2015**, 75, 38-50.

12. M. Jaguin, N. Houlbert, O. Fardel, V. Lecureur, *Cell Immunol* **2013**, 281, 51-61.

13. J. Yin, P. D. Straight, S. M. McLoughlin, Z. Zhou, A. J. Lin, D. E. Golan, N. L. Kelleher, R. Kolter, C. T. Walsh, *Proc Natl Acad Sci USA* **2005**, 102, 15815-15820.

14. **a** S. I. Presolski, V. P. Hong, M. G. Finn, *Curr Protoc Chem Biol* **2011**, 3, 153-162;

b H. Zhao, E. Heusler, G. Jones, L. Li, V. Werner, O. Germershaus, J. Ritzer, T. Luehmann, L. Meinel, *J Struct Biol* **2014**, 186, 420-430.

15. M. Gutmann, E. Memmel, A. C. Braun, J. Seibel, L. Meinel, T. Luhmann, *Chembiochem: a European journal of chemical biology* **2016**, 17, 866-875.
16. T. Kuwaki, T. Kitamura, A. Tojo, S. Matsuki, Y. Tamai, K. Miyazono, F. Takaku, *Biochem Biophys Res Commun* **1989**, 161, 16-22.
17. M. Jaguin, N. Houlbert, O. Fardel, V. Lecureur, *Cell. Immunol.* **2013**, 281, 51-61.

Supporting information

Materials & Methods

Materials

DMEM, RPMI-1640 medium, L-glutamine, L-alanyl-L-gluatime, sodium pyruvate, bovine serum albumin solution 7.5 %, lipid medium supplement, copper (II) sulfate, sodium L-ascorbate, tris(3-hydroxypropyltriazolylmethyl) amine (THPTA), dibenzocyclooctyne-amine, lipopolysaccharides (LPS) from *E.coli 0111:B4* were purchased from Sigma-Aldrich (Schnelldorf, Germany). Penicillin G and streptomycin solution (Pen/Strep) were purchased from Biochrom AG (Berlin, Germany). Fetal bovine serum (FBS), Opti-MEMI, FreeStyle™ 293 medium and recombinant human interferon γ (IFNγ) were from GIBCO life technologies (Carlsbad, CA). Serum-free IPL-41 medium was purchased from Genaxxon bioscience (Ulm, Germany). Pluronic F-68 was purchased from Applichem (Darmstadt, Germany). Linear polyethylenimine (PEI) 25 kDa was from Polysciences, Inc (Hirschberg, Germany). Sfp phosphopantetheinyl transferase, CoA-biotin substrate and restriction endonucleases were purchased from NEB (Frankfurt a. M., Germany). PageRuler™ Prestained Protein Ladder (10 – 170 kDa) and Alexa Fluor® 488 NHS Ester were from Thermo Fisher Scientific (Dreieich Germany). DBCO-PEG4-5/6-Carboxyrhodamine 110 was from Jena Bioscience (Jena, Germany). (S)-2-amino-6-((2-azidoethoxy)carbonylamino)hexanoic acid (N_3) was purchased from IRIS Biotech GmbH (Marktredwitz, Germany) or was kindly provided by EMC Microcollections GmbH (Tübingen, Germany). TaqMan Gene Expression Master Mix, high Capacity cDNA Reverse Transcription Kit, GAPDH-, IRF7-, relB, CCR7-, SCARB 1-, ALOX 15- and PPARγ TaqMan Gene Expression Assay were purchased from Applied Biosystems (Foster City, CA, USA). NHS activated agarose TM4 Fast flow, HiTrap SP XL and HiTrap SP HP ÄKTA columns were from GE Healthcare (Buckinghamshire, GB). CD14 MicroBeads and Auto-MACS columns were from Miltenyi Biotec (Bergisch Gladbach, Germany). Anti-CD14 antibody was from Abcam (Cambridge, UK). Recombinant human interleukin 4 (IL-4), granulocyte macrophage colony-stimulating factor (GM-CSF) and ELISA Human IL-4 Kit were from R&D (Minneapolis, MN). Macrophage colony-stimulating factor (M-CSF) was kindly provided by Novartis AG (Basel, Switzerland). Vivaspin centrifugal concentrators were from Sartorius AG (Göttingen, Germany). WST-1 was purchased from Roche (Basel, Switzerland). Buffy coat was purchased from Blutspendedienst des Bayerischen Roten Kreuzes (München, Germany). Quanti-Blue™ alkaline phosphatase detection medium was from InvivoGen (San Diego). All other

chemicals used were at least of pharmaceutical grade and were purchased from Sigma-Aldrich (unless noted otherwise).

Methods

Chemical synthesis of Propargyl-L-lysine

Propargyl-L-lysine (Plk) was prepared as HCl-salt following procedures described by Milles et al.[1] and Li et al.[2] NMR spectra were acquired on a Bruker Advance 400 MHz spectrometer for confirmation of the product as reported in.[3]

Cloning and expression of TAG-IL-4 and wild-type IL-4

The gene encoding for full length human IL-4 (gene bank reference ID: AF395008.1, amino-acids 25-153) was purchased from Sino Biological (Beijing, P.R. China). Wild-type IL-4 cDNA was amplified using the forward primer 5` CCCCATATG CACAAGTGCGATATCACCTTACAGG 3′ and the reverse primer 5′ CCCGGATCC TCAGCTCGAACACTTTGAATATTTCTCTC 3′ for PCR amplification. The resulting IL-4 cDNA was subcloned with the restriction endonucleases NdeI and BamHI into the backbone of the pETIIa plasmid, resulting plasmid IL-4 pETIIa.

Mutant 42(TAG)-IL-4 cDNA was customized designed with NdeI and BamHI restriction endonuclease sites and synthesized and subcloned in the transfer plasmid pUC47 by GenScript. pUC47 plasmid DNA was digested with the restriction endonucleases NdeI and BamHI and the resulting DNA-fragment of 42(TAG)-IL-4 was subcloned into the backbone of a pETIIa construct yielding plasmid 42(TAG)-IL-4 pETIIa, already containing the gene for the pyrrolysine tRNA and the lipoprotein promotor lpp and the terminator RRN b/c as described in Eger et al.[4]. Correct insert sequences of all constructs were confirmed by DNA sequencing using a T7-promoter sequencing primer. For TAG-IL-4 expression the pETIIa plasmid was co-transformed with a pRSF-duet construct, encoding for the gene of the pyrrolysine tRNA synthetase pylS into *E. coli* BL21(DE3) for expression as previously described.[5]

Cells were cultured at 37°C and the uAA substrate was added at a final concentration of 2 mM at OD_{600} = 0.3 in standard TB (Terrific Broth) medium. Protein expression was subsequently induced with 1 mM IPTG at OD_{600} = 0.6 at 37°C. After 6 hours the cells were harvested and the bacterial pellet was resuspended in lysis buffer (50 mM Tris-HCl, 50 mM

NaCl, 1 mM EDTA, pH 8.0, supplemented with 0.1 mM PMSF) and treated by ultrasonication at 4 °C. After centrifugation, the protein was extracted with lysis buffer containing 5 M guanidine-HCl supplemented with 2 mM reduced and 0.2 mM oxidized glutathione. The protein solution was subsequently refolded using a glutathione redox buffer system as described.[6] After refolding the solution was centrifuged and the supernatant containing TAG-IL-4 was subjected to ion exchange affinity chromatography using an FPLC system (GE Healthcare Äkta Purifier, Life sciences, Freiburg, Germany). After purification, fractions containing IL-4 proteins were extensively dialyzed against PBS and stored at -80 °C. Wild-type IL-4, Plk-IL-4 and N_3-IL-4 concentrations were determined by UV-absorbance at 280 nm, using a molar extinction coefficient of 8860 $M^{-1} \cdot cm^{-1}$.[7]

MALDI-MS and NanoLC MS/MS

The samples were desalted using ZipTipC18-tips following the manufacturer's instructions. Matrix-assisted laser desorption ionization (MALDI-MS) spectra were acquired in the linear positive mode by using an Autoflex II LRF instrument (Billerica, USA). Mass spectra were calibrated externally with a protein standard I from Bruker Daltonics Inc. (Billerica, USA), containing insulin, ubiquitin, myoglobin and cytochrome C.

For in-gel digestion the excised gel bands were destained with 30 % ACN, shrunk with 100 % acetonitrile, and dried in a vacuum concentrator (Concentrator 5301, Eppendorf, Hamburg, Germany). Proteolysis with elastase was performed overnight at 37 °C in 0.1 M NH_4HCO_3 (pH 8.0). About 0.1 µg of protease was used for one gel band. Peptides were extracted from the gel slices with 5 % formic acid. NanoLC-MS/MS analysis was performed as described before.

SDS-PAGE

Recombinant proteins used in click reactions were analyzed by standard Tris-glycine SDS-PAGE as outlined before [8]. Gels were stained with Coomassie Brilliant Blue G250 and photographed using a FluorChem FC2 imaging system (Protein Simple, Santa Clara, CA).

RP-HPLC analysis

Protein purity was assessed on a RP-HPLC system using a VWR Hitachi LaChrom HPLC system (Darmstadt, Germany). Approximately twenty µg protein sample was applied to a ZORBAX Eclipse XDB-C18 column (4.6 mm internal diameter, 150 mm length (Agilent, Santa Clara, CA)), equilibrated with water containing 0.1 % TFA and acetonitrile (ACN) containing 0.1 % TFA (90:10 v/v). Wild-type IL-4 and IL-4 muteins were eluted by a linear gradient of 10 – 50 % ACN containing 0.1 % TFA with a gradient of 1 % ACN/min and a flow rate of 1 mL/min. Column temperature was kept at 42°C and UV-absorbance was monitored at 214 nm.

Expression, purification and biotinylation of the extracellular domain of human IL-4Rα

The extracellular domain (ectodomain) of human IL-4Rα (IL-4Rα_{ECD}) comprising residues Lys 27 to Leu 233 was expressed in baculovirus-transfected insect cells as described before.[9] The expression construct harbors an N-terminal gp64 signal peptide for secretion into the medium followed by a 13mer peptide termed ybbR-tag, which contains a sequence that can be specifically and covalently modified with substrates of the Sfp phosphopantetheinyl transferase.[10] For purification and immunodetection the IL-4Rα_{ECD} protein was fused at the C-terminus to a V5 epitope and a decahistidine peptide. The unpaired Cys residue at position 183 was exchanged for alanine to avoid multimerization due to intermolecular disulfide bond formation. HighFive insect cells growing in suspension in serum-free IPL-41 medium containing 1.5 % (v/v) Lipid Medium Supplement and 0.15 % (v/v) Pluronic F-68 were transfected with recombinant bacoluvirus encoding for the above protein with a multiplicity of infection (MOI) of 5. Protein expression was performed for 5 days at 27 °C and 80 rpm in 2 L shaking flasks. After clarifying the protein-containing medium from cell debris by centrifugation the supernatant was dialyzed against PBS. For subsequent metal affinity chromatography (IMAC) the protein solution was supplemented with 5 mM imidazole, the sodium chloride concentration was raised to 500 mM and the pH was adjusted to 8.0. The protein was applied to a 5 mL HisTrap FF column, which was then washed with 10 column volumes (CV) 50 mM sodium phosphate, 500 mM sodium chloride, 10 mM imidazole pH 8.0. YbbR-tagged IL-4Rα_{ECD} was eluted with the same buffer containing 300 mM imidazole. After SDS-PAGE analysis protein-containing fractions were pooled and dialyzed against PBS. Aliquots were flash-frozen in liquid nitrogen and stored at -80 °C.

For site-specific biotinylation, the ybbR-tagged IL-4Rα_{ECD} was diluted to a concentration of 10 µM in buffer containing 50 mM HEPES pH 7.5, 10 mM $MgCl_2$, 0.5 µM Sfp phosphopantetheinyl transferase and 10 µM CoA-biotin substrate. After incubation at 22 °C for 2 hours and subsequent reaction at 8 °C over night unreacted CoA-biotin was removed from IL-4Rα_{ECD} protein by exchanging the buffer for PBS using ultrafiltration (Vivaspin 4, 5K MWCO PES; Sartorius, Göttingen, Germany). Successful biotinylation was confirmed by Western blot analysis and using horseradish-coupled streptavidin for detection. Aliquots of biotinylated IL-4Rα_{ECD} were stored at -80 °C until further use.

Expression and purification of the extracellular domains of IL-13Rα1 and γc

For the measurement of ternary complex formation of the binary complex of IL-4:IL-4Rα with the low affinity receptor chains IL-13Rα1 and γc, both receptor ectodomains were produced in eukaryotic expression systems. The ectodomain of human IL-13Rα1 comprising residues Thr 29 to Thr 343 was produced in Baculovirus-transfected HighFive insect cells as described[9] and purified by metal affinity chromatography. For the preparation of the ectodomain of γc (CD132) a transient expression was utilized employing FreeStyle 293F cells that are a high-expression clone of HEK293 cells adapted to grow in suspension under serum-free conditions. FreeStyle293 cells were grown in FreeStyleTM 293 medium in polycarbonate Erlenmeyer flasks at 37°C, 150 rpm, 8 % (v/v) CO2 and 65 % relative humidity. When the cell density reached 2-3x106 cells per ml, cells were passaged to a cell density of 5.5x105 cells per mL. For the expression of γc, the cDNA encoding for residues Trp 23 to Ala 263 of murine γc was cloned between the restriction sites AgeI and KpnI of the expression vector pHLsec, which harbors an optimized signal sequence for secretion and provides for a C-terminal hexahistidine tag for purification [11]. This construct was then used for transient transfection of the FreesStyle 293F cells. Per mL expression culture 1 µg vector DNA culture in 35 µL Opti-MEMI was mixed with 2 µg linear PEI 25 kDa dissolved in 35 µl Opti-MEMI and incubated at room temperature for 20 min. Then the DNA-PEI mixture was added to the cell suspension (cell density of 5.5x 106 cells/mL) and the transfected cells were incubated for 4 to 5 days. Thereafter the supernatant was cleared from cells and debris by centrifugation (6000 x g, 15 min, 4°C). For purification the protein solution was dialyzed twice against 10 volumes of 20 mM Tris-HCl pH 7.4, 300 mM NaCl and subjected to a 1 mL HisTrap Excel column (GE Healthcare). The column was first washed with increasing concentrations of imidazole (up to 30 mM) to remove impurities unspecifically bound to

the column, γc was then eluted by buffer (20 mM Tris-HCl pH 7.4, 300 mM NaCl) supplemented with 500 mM imidazole. After SDS-PAGE analysis protein-containing fractions were pooled and dialyzed against PBS. Aliquots were flash-frozen in liquid nitrogen and stored at -80 °C.

Interaction analysis using surface plasmon resonance

Surface plasmon resonance (SPR) analyses for the measurement of *in vitro* interactions were performed using a ProteOn™ XPR36 system (BioRad, Hercules, CA). HBS150T (10 mM HEPES, 150 mM NaCl, 3.4 mM EDTA, pH 7.5, 0.005 % (v/v) Tween 20) was used as running buffer, the temperature for all measurements was set to 25 °C. Recombinant human site-specific biotinylated IL-4Rα_{ECD} protein was used as ligand, wild type IL-4 and the variants N_3- and Plk-IL-4, in which lysine 42 was exchanged for the uAA, were used as analytes. For immobilization onto the chip surface a ProteOn GLC sensor chip (BioRad) was activated using EDC/Sulfo-NHS (BioRad) according to manufacturer's recommendation and subsequently coated with streptavidin (Sigma-Aldrich; 40 ug/mL in 10 mM sodium acetate pH 4.0) until a density of about 2100 to 2300 RU was achieved, free activated sites were quenched by perfusion with 1M ethanolamine pH 8.5. Then biotinylated IL-4Rα_{ECD} (150 nM in running buffer) was immobilized (in vertical direction) onto a single flow channel at a density of about 400 RU. For data acquisition the IL-4 proteins were dissolved in running buffer and perfused over the sensor surface oriented in horizontal direction (single shot kinetic setup) and simultaneously injecting the analyte at five different concentrations (5, 2.5, 1.25, 0.625, and 0.3125 nM). The association was monitored for 240 seconds at a flow rate of 100 µL/min. Data for dissociation were acquired for 300 seconds by perfusing HBS150T buffer at a flow rate of 100 µl/min. Unspecific binding and bulk face effects were removed by subtracting the interaction of the analyte with an empty streptavidin surface at the so-called interspot regions on the ProteOn sensor chip. The chip surface was regenerated for further measurements by injecting two 18 s pulses of 10 mM glycine pH 1.5 and one 18 s pulse of 4 M $MgCl_2$ employing a flow rate of 100 µL/min. Binding affinities were determined from the rate constants for association and dissociation using the ProteOn™ Manager 3.1 software (Bio-Rad) and applying a simple 1:1 Langmuir type interaction model. All variables were fitted globally for all five analyte concentrations. All experiments were performed as independent duplicates. For the measurement of ternary complex formation, i.e. the binding of the low-affinity receptor subunits IL-13Rα1 and γc (CD132 or common

gamma chain) to the binary complex comprising IL-4Rα and IL-4 or variants thereof, the same setup with the biotinylated extracellular domain of IL-4Rα immobilized on a streptavidin-coated sensor chip was used. First the immobilized IL-4Rα was saturated by perfusing the sensor chip with 50 nM of IL-4 (or the variants IL-4 N_3 or Plk-IL-4) at a flow rate of 100µL min^{-1} and 120s. The dissociation time was set to 0s. Thereafter a solution of 50 nM IL-4 protein (or the respective variants) mixed either with 0.25, 0.5 and 1 µM IL-13Rα1 or 0.375, 0.75 and 1.5 µM γc protein (extracellular domain) was perfused over flow channels 1, 2, and 3 for 90s at a flow rate of 100 µL min^{-1}. Dissociation of the ternary complex was initiated by injecting running buffer and recorded for 240s. Binding of IL-13Rα1 and γc protein to IL-4Rα alone was monitored using the same measurement parameters but without perfusion of IL-4 protein.

Circular dichroism spectroscopy

IL-4 samples were dialyzed against 20 mM sodium phosphate buffer pH 7.0, with the same buffer serving as a blank. CD-spectra were recorded with a J715 spectropolarimeter (JASCO Labor- und Datentechnik GmbH, Groß-Umstadt, Germany) with protein solutions with a final concentration of 0.2 mg/mL in a cell with 2 mm path length. The following scan parameters were used: 100 mdeg sensitivity, 0.1 nm step resolution, 50 nm/min scan speed, 2 s time constant. Three accumulations per scan were averaged. Data processing included solvent background correction and adjustment for pathlength and concentration.

Copper-catalyzed azide-alkyne Huisgen cycloaddition (CuAAC) and strain promoted azide-alkyne cycloaddition (SPAAC)

10 µg Plk-IL-4 and a 10-fold molar excess of the fluorescent dye Azide Fluor 488 was used. The click reaction was performed in the presence of 5 mM L-ascorbic acid, 500 µM THPTA and 100 µM $CuSO_4$ at room temperature. Copper (II) sulfate and THPTA were premixed and incubated with L-ascorbic acid under air exclusion for 10 min. to quench occurring ROS species. After 1 h incubation, the click reaction was stopped by the addition of 5 mM EDTA. 10 µg N_3-IL-4 and a 10-fold molar excess of the fluorescence dye DBCO-PEG4-5/6-carboxyrhodamine 110 was used. The click reaction was performed at room temperature for 24 h. The proteins were subsequently analyzed by SDS-PAGE and MALDI-MS analysis.

Cell culture

TF-1 cells (ATCC number CRL-2003, ATCC, and Manassas, VA) were harvested from exponentially growing suspension cultures. The cells were maintained in 75 cm^2 culture flasks in growth medium (RPMI-1640 medium, supplemented with 10 % heat-inactivated FBS, 1 % Pen/Strep solution, 4.5 g/L D-glucose, 2 mM L-glutamine, 2 mM l-alanyl-l-glutamine, 1 mM sodium pyruvate and 2 ng/mL human GM-CSF) at 37 °C and 5 % CO_2. HEK 293T cells (ATCC number CRL-1573, ATCC, Manassas, VA) were harvested from exponentially growing subconfluent monolayers in growth medium (DMEM containing 10 % heat-inactivated FBS and 1 % Pen/Strep solution) at 37 °C and 5 % CO_2.

WST-proliferation assay

TF-1 cells were seeded in a 96-well plate format (5 x 10^4 cells/well) in WST-1 assay medium (RPMI-1640 medium, supplemented with 10 % (v/v) FBS, 1 % Pen/Strep, 0.5 % (w/v) BSA), supplemented with dilution series of wild-type IL-4 and Plk/N_3-IL-4 variants ranging from 0.01 to 20 ng/mL or with dilution series of decorated/control agarose particles ranging from 0.0007 to 1.5 mg/well, respectively. After stimulation for 48 hours, the cells were incubated with WST-1 for 4 hours at 37 °C according to the manufacturer's instructions. The absorbance of the soluble formazan product was determined at 450 nm using a Spectramax 250 microplate reader (Molecular Devices, Sunnyvale). Relative proliferation is expressed in comparison to soluble wt-IL-4.

Secreted alkaline phosphatase and enhanced yellow fluorescent protein reporter gene assay

For the secreted alkaline phosphatase (SEAP) reporter gene assay 2 x 10^3 HEK 293T cells were cotransfected in 96 well plates with 0.2 µg of the plasmid pHW003 (P_{STAT6} –SEAP) and 0.2 µg of the constitutive STAT6 expression plasmid pSTAT6 (Genebank accession N-BC075852.1). After exchange of the transfection against growth medium supplemented with 20 ng/mL wild type IL-4 or Plk/N_3-IL-4, respectively, the cells were stimulated for 48 hours at 37 °C and 5 % CO_2. Then 20 µL of the medium supernatant were incubated with 200 µL Quanti-Blue™ alkaline phosphatase detection medium and SEAP activity was monitored at 650 nm using a Spectramax 250 microplate reader (Molecular Devices, Sunnyvale, CA). Detailed information about STAT-6 gene reporter plasmids is given elsewhere. [12]

For the enhanced yellow fluorescent protein (eYFP) reporter gene assay 1.5 x 10^4 HEK 293T cells were cotransfected in 24 well plates with 1 µg of the plasmid pHW0040 (P_{STAT6} –eYFP) and 1 µg of the constitutive STAT6 expression plasmid pSTAT6 (Genbank accession N-BC075852.1). After exchange of the transfection medium against growth medium supplemented with 20 ng/mL wild type IL-4 or Plk/N_3-IL-4, respectively, the cells were stimulated for 48 hours at 37 °C and 5 % CO_2. Thereafter eYFP expression was detected with an Axiovert 200M inverted microscope (Zeiss, Oberkochen, Germany).

Fluorescent labelling of IL-4

Wild type IL-4 was reacted with a 10-fold molar excess of the fluorescence dye Alexa Fluor® 488 NHS Ester in PBS at room temperature. After 2 hours of incubation, unreacted dye was removed using a Vivaspin 500 MWCO 10,000 Da centrifugal concentrator.

Decoration of NHS-activated agarose particles

NHS-activated agarose particle slurry solution (100 µL solution corresponds to 4 µmol NHS) was modified equimolar with 11-azido-3,6,9-trioxaundecan-1-amine (referred to azido-undecane-amine herein), dibenzocyclooctyne-amine (DBCO-amine) or ethanolamine in PBS buffer at pH 7.4 for 4 hours with gentle shaking, respectively. DBCO-amine was dissolved in DMF prior before use. After incubation, the particle solution was subsequently blocked with 500 mM ethanolamine in 100 mM Tris-HCl buffer (pH 8.3), containing 0.5 M NaCl, for 1 hour. After washing with PBS, the modified particle solutions were kept in 20 % ethanol at 4 °C until further use.

Immobilization of IL-4 onto agarose particles via CuAAC and SPAAC

Decorated agarose particles were reacted with 0.5 µg of respective IL-4 variants per mg of agarose particles in PBS (pH 7.4). Concentration of IL-4 proteins in the reaction mixture was 0.2 mg/mL. The particle volume was included in the reaction volume. For CuAAC, 500 µM THPTA, 100 µM $CuSO_4$ and 5 mM ascorbic acid were added and immobilization was performed at 37 °C for 2 h as described above. SPAAC was performed at 4 °C for 24 h. Particles were washed ten times with PBS prior to use.

Incubation of IL-4 decorated agarose particles

40 mg IL-4 decorated agarose particles were incubated in 60 µL PBS containing 0.02 % sodium azide (CuAAC) or 1 % Pen/Strep (SPAAC) at 37 °C, 800 rpm for 6 days. Supernatant was exchanged for fresh buffer after 1, 2, 3 and 6 days. Supernatants were analyzed by ELISA. Particles were washed ten times with PBS before further analysis.

IL-4 quantification by Enzyme Linked Immunosorbent Assay (ELISA)

Supernatants of incubated agarose particles were analyzed for IL-4 content at different time points. The ELISA was performed according to the manufacturer's instructions. The absorbance of the acidified 3,3',5,5'-tetramethylbenzidine diimine product was determined at λ = 450 nm using a Spectramax 250 microplate reader (Molecular Devices).

Monocyte isolation, differentiation and polarization

Monocytes were isolated from peripheral blood mononuclear cells (PBMC) obtained from blood buffy coats by a two-step density gradient centrifugation using Histopaque-1077 (Sigma Aldrich) and Percoll (GE Healthcare, Buckinghamshire, GB). Magnetic associated cell sorting with CD14 microbeads was performed using an auto-MACS system (Miltenyi Biotec, Bergisch Gladbach, Germany), following the manufacturer's instructions. The viability of the isolated monocyte fraction was assessed by trypan blue dye exclusion and was typically higher than 90 % of living cells. To determine the degree of $CD14^+$ cells, monocytes were incubated with a FITC conjugated anti-CD14 antibody for 45 minutes at 4 °C. 1 x 10^4 cells were analyzed by recording forward scatter, sideward scatter and fluorescence signals at λ = 488 nm and detection at λ = 530 ± 30 nm using a FACS Calibur system (Becton Dickinson, NY). Analysis was performed with the Flowing Software 2.5.0. (Perttu Terho, Turku Centre for Biotechnology, Turku, Finland).

Monocytes were resuspended in macrophage (Mϕ) activation medium (RPMI-1640 medium supplemented with 10 % heat-inactivated FBS, 1 % Pen/Strep and 50 ng/mL M-CSF; unpolarized Mϕ) at a final cell concentration of 1x106 cells/mL and were incubated for 6 days at 37 °C and 5 % CO2. After 6 days the medium was exchanged for fresh RPMI-1640 medium supplemented with 5 % FBS, 1 % Pen/Strep, 100 ng/ml LPS and 20 ng/mL IFNγ for M1-Mϕ polarisation. For M2-Mϕ polarisation, RPMI-1640 medium was supplemented with 5 % FBS, 1 % Pen/Strep, 10 ng/mL M-CSF and 20 ng/mL IL-4 or 42TAG-IL-4, respectively.

Mϕ exposed to fresh macrophage activation medium was used as control. All activation media were incubated with the cells for 24 h prior to RNA isolation.

RT-PCR

Total RNA of all conditions was isolated by using the RNeasy Mini Kit (Qiagen, Hilden, Germany) following the manufacturer's instructions. cDNA was prepared from equal amounts of total RNA using oligo(dT) primers and MultiScribe™ MuLV reverse transcriptase of the High Capacity cDNA Reverse Transcriptase Kit (Thermofisher, Waltham, MA). 100 ng of cDNA was amplified in an ABI prism7900 HT Real-Time PCR System (Applied Biosystems, Foster City, CA) using TaqMan Gene Expression Master Mix and appropriate probes (Table SI 1). Gene markers for M1- and M2-Mϕ polarization were chosen according to previously published literature [13]. cDNA levels were normalized to the expression of the housekeeping gene GAPDH and relative values were calculated using the comparative C_T Method [14].

Statistical analysis

Data were analyzed using a one-way ANOVA and differences between individual means were determined *post-hoc* using the Tukey-Kramer procedure. SigmaPlot (Systat Software Inc., San Jose, CA) and Minitab 16 (Minitab, Coventry, UK) were used. Results were considered statistically significant at $p \leq 0.05$ (*) and $p \leq 0.01$ (**) and results are displayed as mean with standard deviation (SD).

Supporting tables and figures

Table SI 1 TaqMan Gene Expression primers; species = human; Fluorescent dye = fluorescein amidite (FAM).

Applied Biosystems Assay ID	Gene
Hs02758991_g1	GAPDH
Hs01014809_g1	IRF7
Hs00232399_m1	RELB
Hs01013469_m1	CCR7
HS00969821_m1	SCARB1
Hs00993765_g1	ALOX15
HS01115513_m1	PPARG

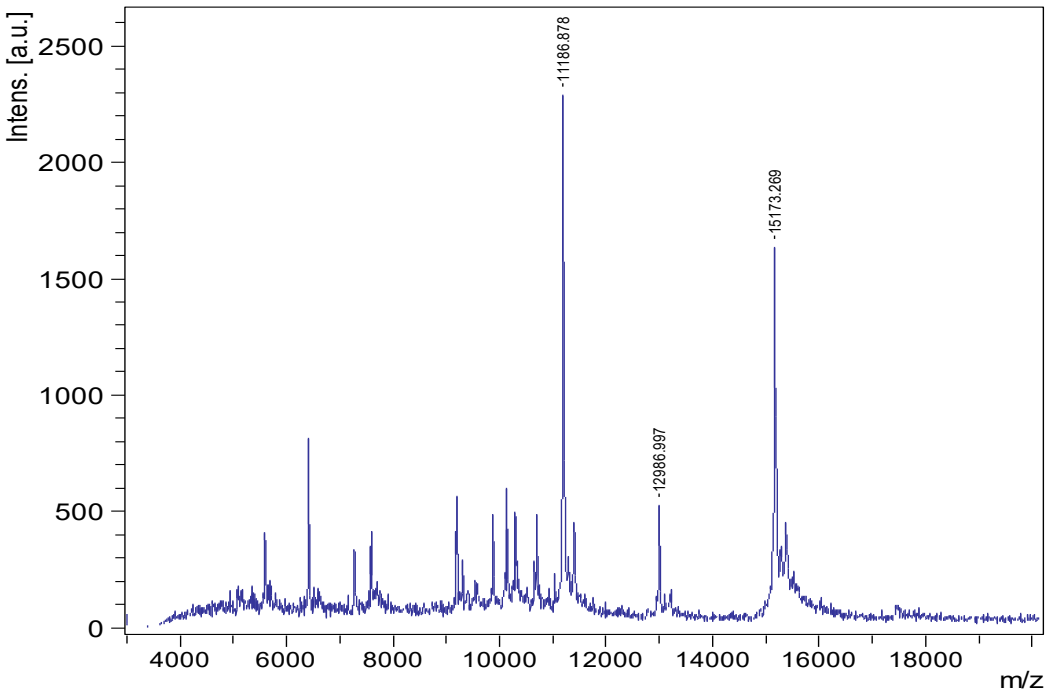

Fig. SI 1 MALDI-MS analysis of Plk-IL-4. Observed average mass 15,173.269 Da, calculated average mass 15,170.381 Da (oxidized cysteines).

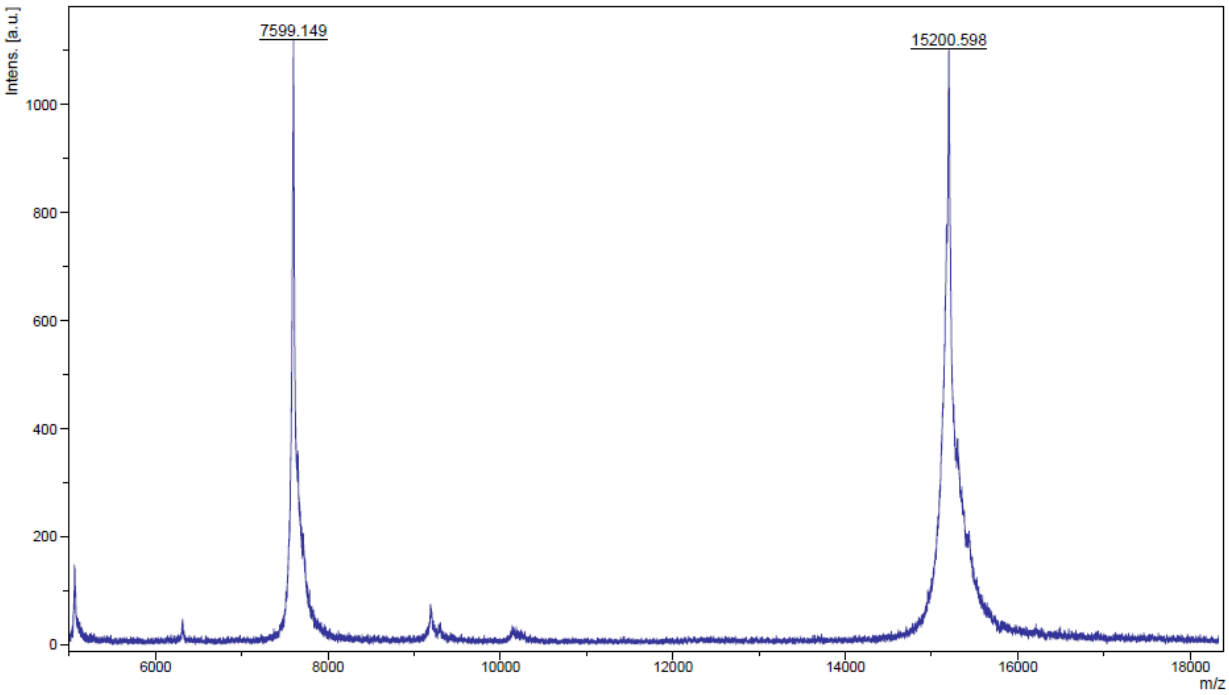

Fig. SI 2 MALDI-MS analysis of N3-IL-4. Observed average mass 15,200.589 Da, calculated average mass 15,207.478 Da (oxidized cysteines).

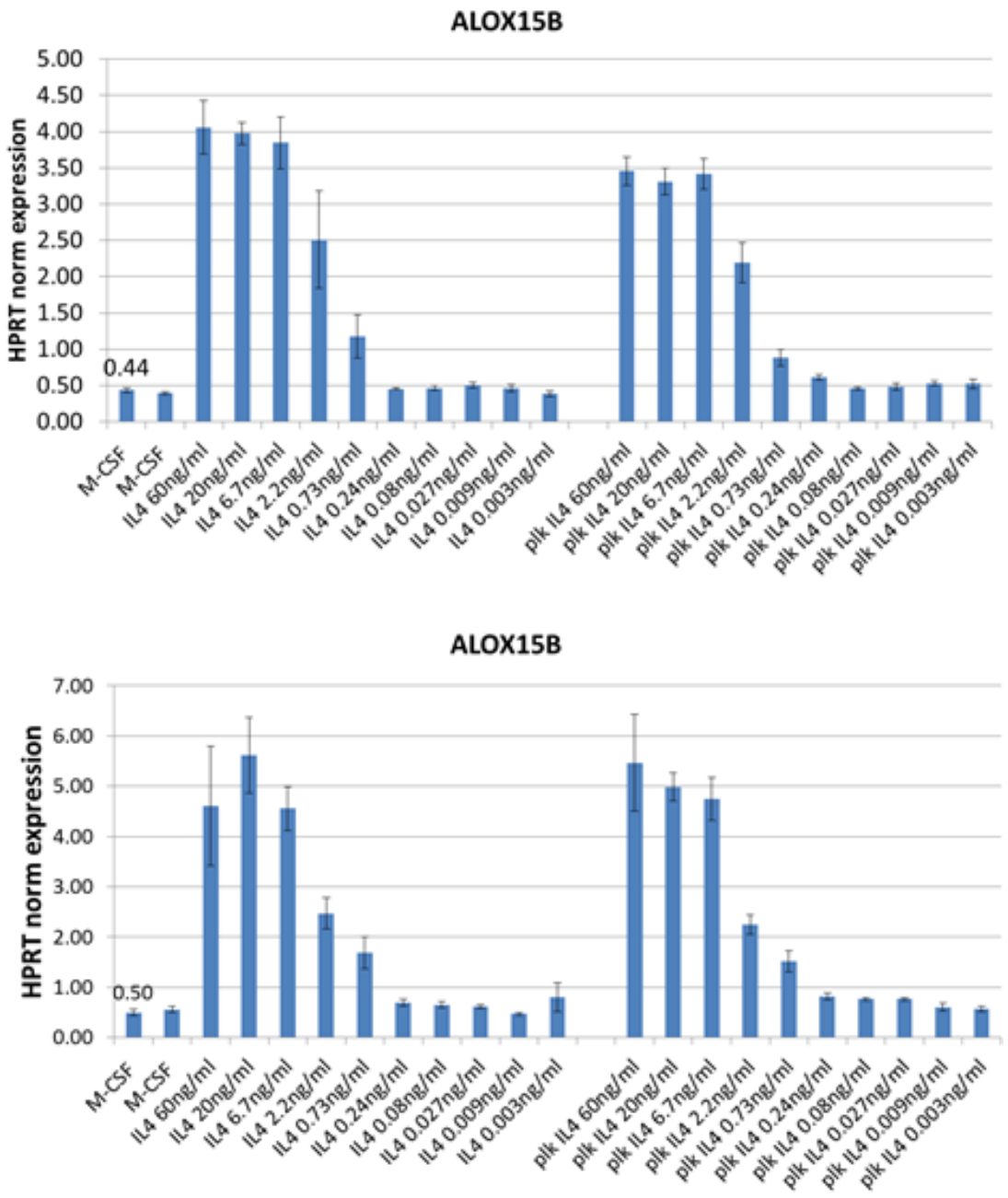

Fig. SI 3 Quantitative PCR of relative arachidonate 15-lipoxygenase (ALOX15) gene expression in human primary macrophages relative to Hypoxanthine-guanine phosphoribosyltransferase (HPRT) as housekeeping gene as a function of wt-IL-4 (left) and plk-IL-4 concentrations, respectively. Responses are identical for wt-IL-4 and plk-IL-4. 20 ng/mL induced maximal ALOX15 expression in analogy to the observation on TF-1 proliferation, which was also maximal at 20 ng/mL (Figure 4). Measurements were n = 3 and in cells originating from two different donors donor 1 top, donor 2 bottom.

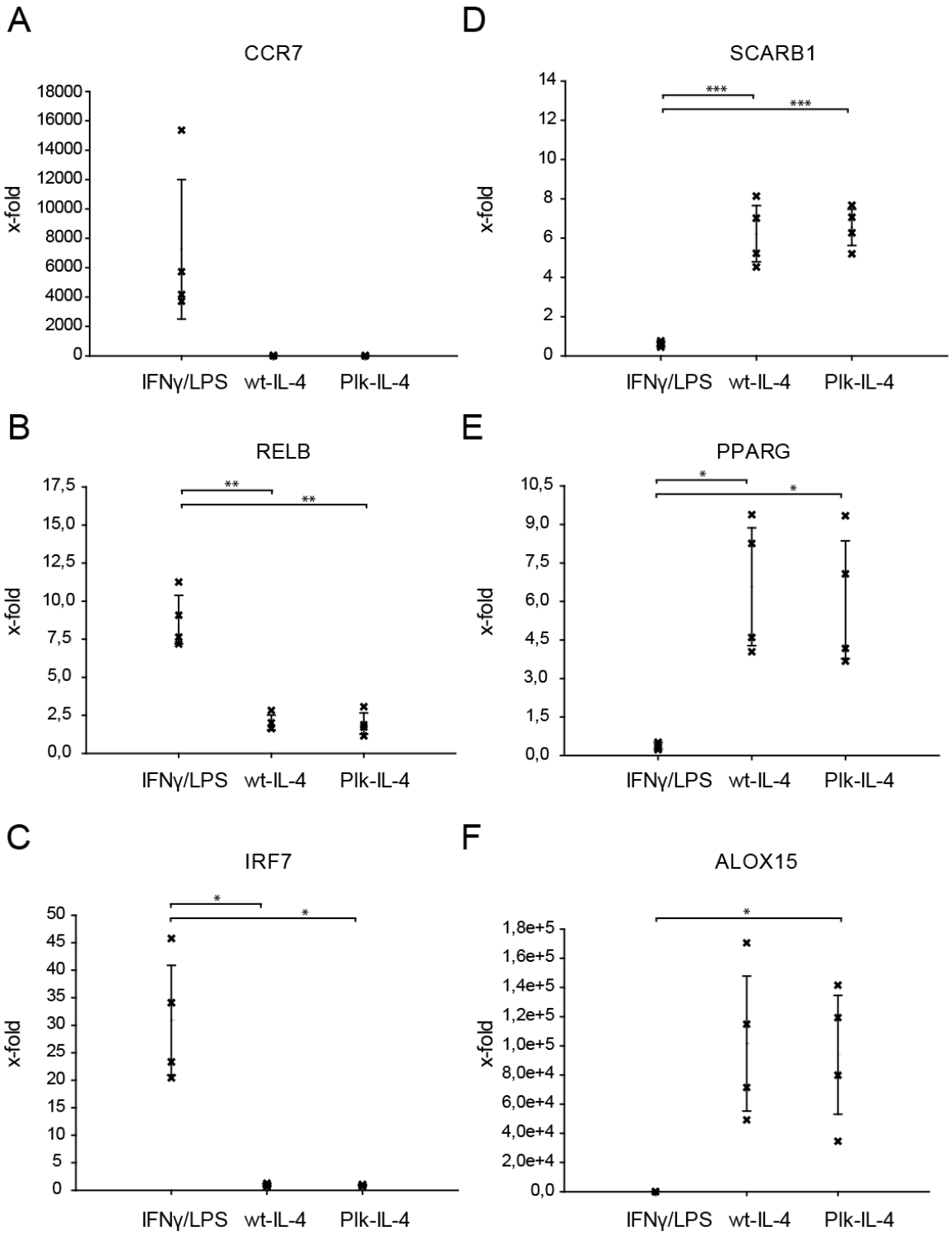

Fig. SI 4 mRNA expression of M-CSF Mϕ after treatment with IFNɣ/LPS or with wt-IL-4 or Plk-IL-4 in the presence of M-CSF, respectively. M1-Mϕ markers are shown in (A) – (C), M2-Mϕ markers are displayed in (E) – (F). Data are expressed relatively to mRNA levels in M0-M (not shown), set at a value of zero (mean ± standard deviation, n = 4). *$p < 0.05$, ** $p < 0.01$.

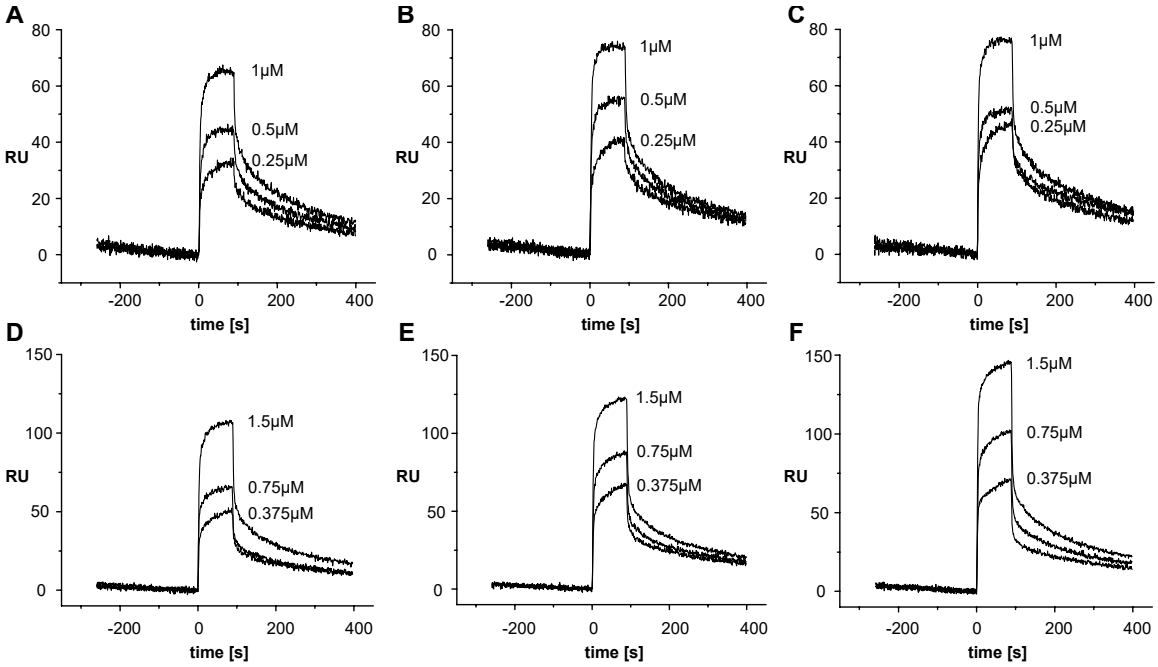

Fig. SI 5 Surface plasmon resonance analysis of the interaction of the extracellular domain of IL-13Rα1 (A, B, C) or of γc (D, E, F) with the binary complex of IL-4 bound to IL-4Rα. For measurement of ternary complex formation a biosensor, which was coated with 400RU IL-4Rα (ectodomain), was saturated with IL-4 by perfusing either with 50 nM IL-4 wild type (A,D), Plk-IL-4 (B,E), or IL-4 N3 (C,F). Thereafter a mixture of 50 nM of the respective IL-4 protein with different concentrations of either IL-13Rα1 ectodomain protein (A-C) or γc (D-F) was injected onto the biosensor (injection starts at time point 0s). After 90s for recording the association, dissociation of the ternary complex was monitored by perfusion of running buffer for 240s. Due to the fact that no (covalently) fixated binary complex of IL-4 attached to IL-4Rα was immobilized on the sensor chip, these co-inject SPR experiments only present qualitative binding data. Quantitative analyses are not possible as for instance the dissociation comprises not only the dissociation of IL-13Rα1 or γc from the binary complex, but also the dissociation of IL-4 proteins from the immobilized IL-4Rα.

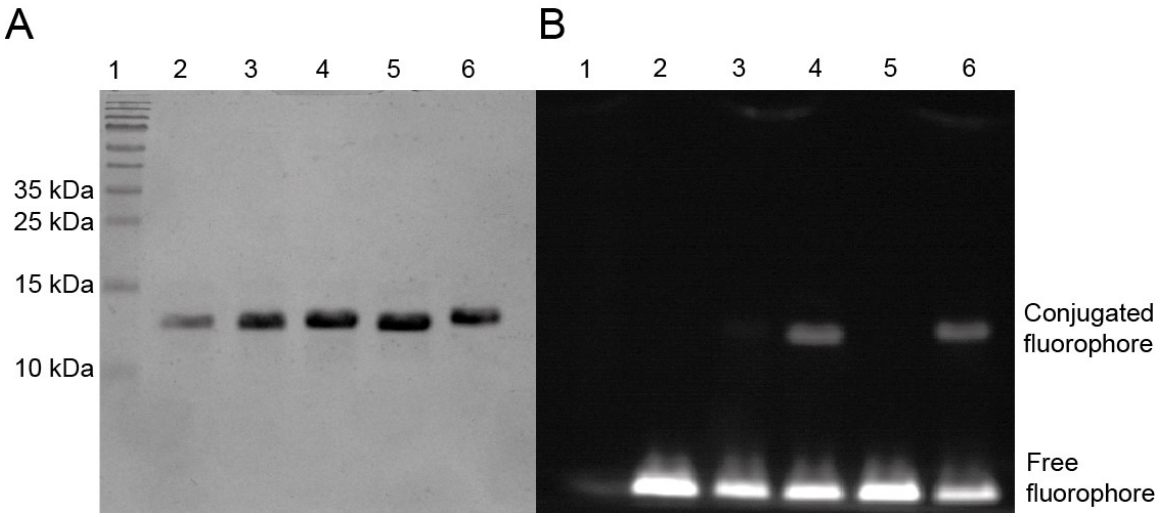

Fig. SI 6 SDS-PAGE of IL-4-fluorescent dye conjugates. **A:** Coomassie staining **B:** Fluorescence detection. **1** Page Ruler™ Prestained Protein Ladder (10 – 170 kDa), **2** wt-IL-4 + Azide Fluor 488, **3** wt-IL-4 + DBCO-PEG4-5/6-Carboxyrhodamine 110, **4** Plk-IL-4 + Azide Fluor 488 (+Cu), **5** Plk-IL-4 + Azide Fluor 488 (-Cu), **6** N_3-IL-4 + DBCO-PEG4-5/6-Carboxyrhodamine 110.

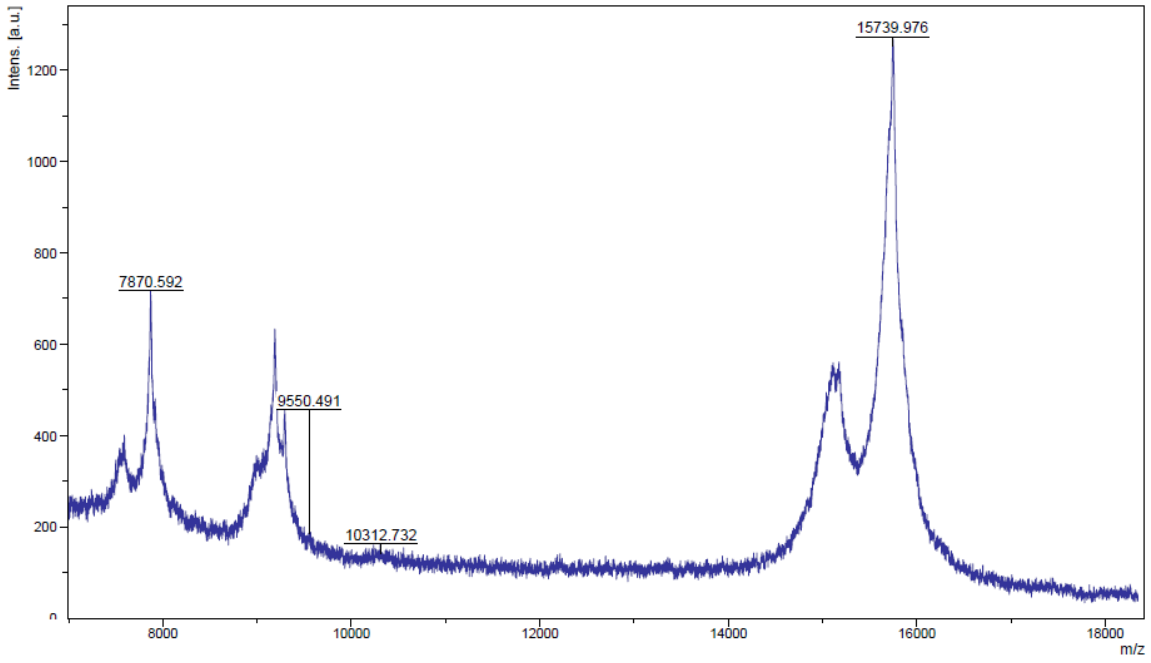

Fig. SI 7 MALDI-MS analysis of Plk-IL-4 – Azide Fluor 488 conjugate. Observed average mass 15,739.976 Da, calculated average mass 15,744.787 Da (oxidized cysteines).

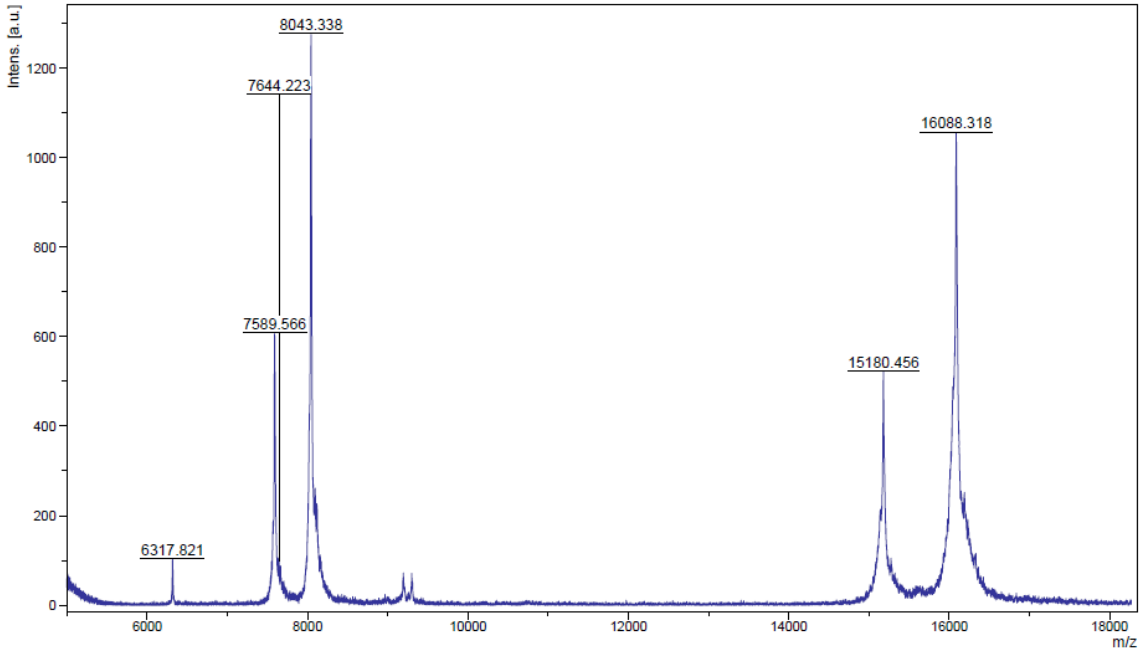

Fig. SI 8 MALDI-MS analysis of N3-IL-4 – DBCO-PEG4-5/6-Carboxyrhodamine 110 conjugate. Observed average mass 16,088.318 Da, calculated average mass 16,085.135 Da (oxidized cysteines).

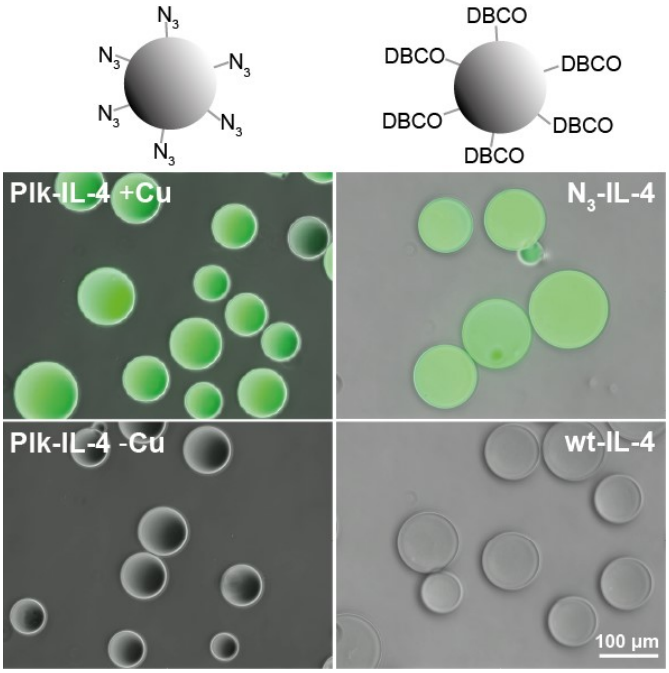

Fig. SI 9 Fluorescence microscopy of azide- or DBCO-functionalized agarose particles decorated with fluorescently labelled Plk-IL-4 or N3-IL-4, respectively. Controls: Plk-IL-4 with azide particles without copper, wt-IL-4 incubated with DBCO particles.

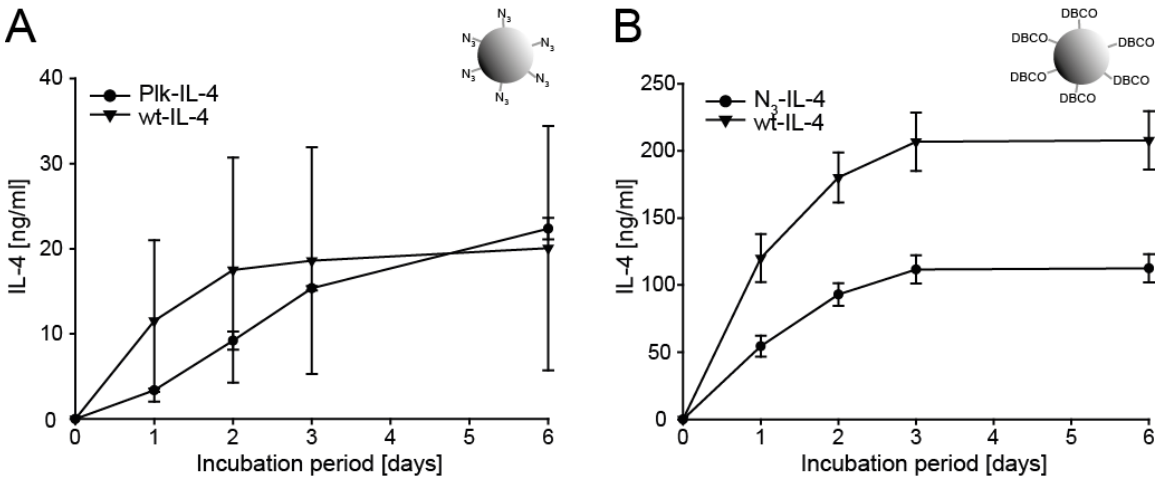

Fig. SI 10 IL-4 concentrations in supernatants of washed agarose surfaces of 40 mg agarose beads (hence 4 times more as the highest concentration used for the TF-1 and macrophage experiments as shown in Figure 4) stored in 60 µL PBS after 1, 2, 3 and 6 days. Azide- or DBCO-functionalized agarose surfaces were reacted with the corresponding IL-4 muteins or with wt-IL-4 as a control. Surfaces were incubated in PBS and supernatants were exchanged after 1, 2, 3 and 6 days and subsequently analyzed by ELISA.

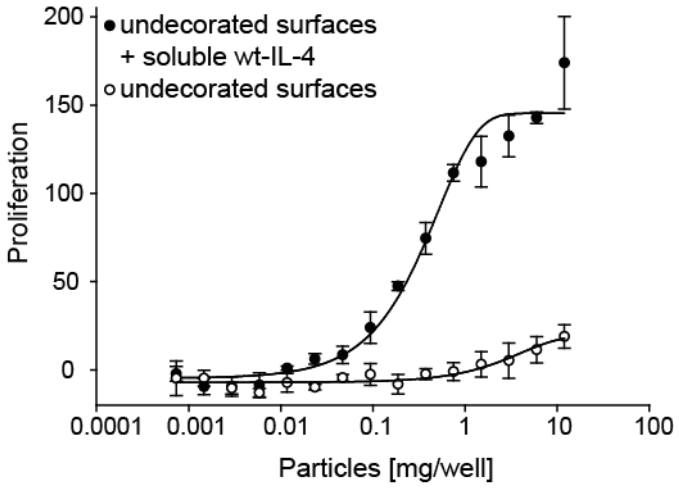

Fig. SI 11 WST1 proliferation assay of TF-1 cells incubated with undecorated ethanolamine-blocked agarose surfaces with and without wt IL-4. A stock solution of wt- IL-4 and blocked surfaces was diluted (highest wt-IL-4 concentration tested was 20 ng/mL with 10 mg/well particles and this highest concentration was log2 diluted, thereafter). 20 ng/mL also induced maximal relative ALOX15 expression in primary human (CSF1 differentiated) macrophages from two donors (Figure S3). Data are expressed as percentage of maximal stimulation by soluble IL-4 (mean ± standard deviation, n = 3).

References (SI)

1. S. Milles, S. Tyagi, N. Banterle, C. Koehler, V. VanDelinder, T. Plass, A. P. Neal, E. A. Lemke, *Journal of the American Chemical Society* **2012**, *134*, 5187-5195.
2. F. Li, H. Zhang, Y. Sun, Y. Pan, J. Zhou, J. Wang, *Angew Chem Int Ed Engl* **2013**, *52*, 9700-9704.
3. T. Lühmann, G. Jones, M. Gutmann, J.-C. Rybak, J. Nickel, M. Rubini, L. Meinel, *ACS Biomaterials Science & Engineering* **2015**, *1*, 740-746.
4. S. Eger, M. Scheffner, A. Marx, M. Rubini, *J Am Chem Soc* **2010**, *132*, 16337-16339.
5. **a** S. Eger, M. Scheffner, A. Marx, M. Rubini, *J Am Chem Soc* **2010**, *132*, 16337-16339.

   b S. Eger, M. Scheffner, A. Marx, M. Rubini, *Methods Mol Biol* **2012**, *832*, 589-596.
6. A. van Kimmenade, M. W. Bond, J. H. Schumacher, C. Laquoi, R. A. Kastelein, *Eur J Biochem* **1988**, *173*, 109-114.
7. Y. Wang, B. J. Shen, W. Sebald, *Proc Natl Acad Sci U S A* **1997**, *94*, 1657-1662.
8. O. Germershaus, I. Schultz, T. Luhmann, M. Beck-Broichsitter, P. Hogger, L. Meinel, *Eur J Pharm Biopharm* **2013**, *85*, 61-68.
9. M. Kraich, M. Klein, E. Patino, H. Harrer, J. Nickel, W. Sebald, T. D. Mueller, *BMC Biol* **2006**, *4*, 13.
10. J. Yin, P. D. Straight, S. M. McLoughlin, Z. Zhou, A. J. Lin, D. E. Golan, N. L. Kelleher, R. Kolter, C. T. Walsh, *Proc Natl Acad Sci U S A* **2005**, *102*, 15815-15820.
11. A. R. Aricescu, W. Lu, E. Y. Jones, *Acta Crystallogr D Biol Crystallogr* **2006**, *62*, 1243-1250.
12. E. H. Christen, M. Karlsson, M. M. Kampf, R. Schoenmakers, R. J. Gubeli, H. M. Wischhusen, C. Friedrich, M. Fussenegger, W. Weber, *Adv Funct Mater* **2011**, *21*, 2861-2867.
13. **a** M. Jaguin, N. Houlbert, O. Fardel, V. Lecureur, *Cell Immunol* **2013**, *281*, 51-61.

    b P. J. Murray, J. E. Allen, S. K. Biswas, E. A. Fisher, D. W. Gilroy, S. Goerdt, S. Gordon, J. A. Hamilton, L. B. Ivashkiv, T. Lawrence, M. Locati, A. Mantovani, F. O. Martinez, J. L. Mege, D. M. Mosser, G. Natoli, J. P. Saeij, J. L. Schultze, K. A. Shirey, A. Sica, J. Suttles, I. Udalova, J. A. van Ginderachter, S. N. Vogel, T. A. Wynn, *Immunity* **2014**, *41*, 14-20.
14. T. D. Schmittgen, K. J. Livak, *Nature protocols* **2008**, *3*, 1101-1108.

Chapter 3: Creating an inflammation-responsive cytokine depot by co-injection with FXIIIa

Valerie Spieler[1], Yejun Hu[2], Katharina Güntzel[1], Hongwei Ouyang[2], Tessa Lühmann[1], Lorenz Meinel[1]

[1] Institute for Pharmacy and Food Chemistry, University of Würzburg, Würzburg, Germany

[2] Center for Stem Cell and Tissue Engineering, School of Medicine, Zhejiang University, Hangzhou, China

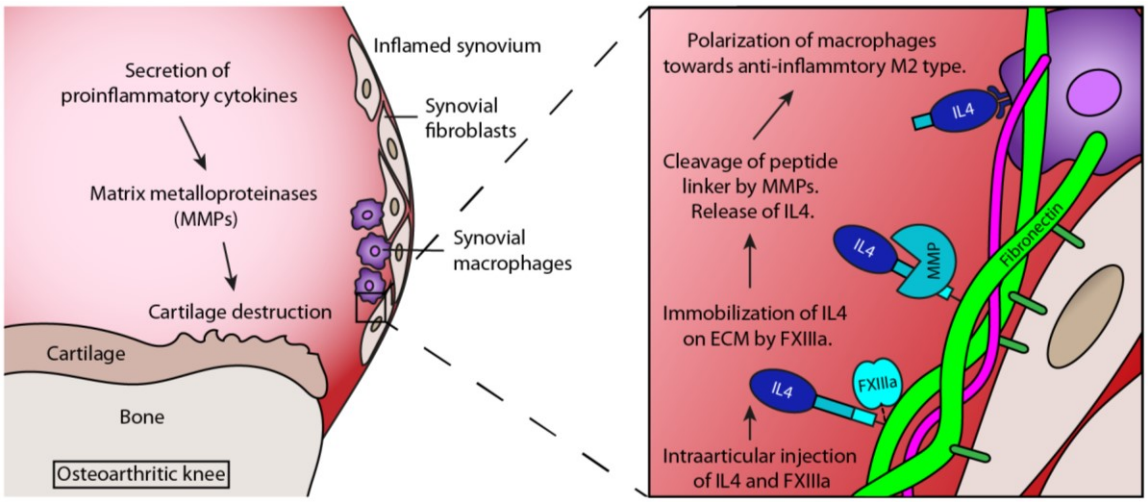

Unpublished manuscript

Abstract

Cytokines have great therapeutic potential but are challenged by short half-life and dose-limiting toxicities when given systemically. In the body, cytokine levels are regulated on the transcriptional level, but also by storing them in the extracellular matrix (ECM) and releasing them when they are needed during tissue remodeling processes. Here we describe an injectable solution of IL4 for enzymatic depot formation by covalent binding to extracellular matrix (ECM) components. Upon binding, the construct features bioresponsive release from the ECM by inflammatory matrix-metalloproteinases (MMPs) to precisely adjust spatiotemporal cytokine activity to the pathogenesis of the flaring disease. Attaching a peptide sequence featuring both, the protease-sensitive peptide linker (PSL) and a sequence by which the cytokine covalently immobilizes to the ECM when co-injected with activated human transglutaminase FXIIIa (TGase), to an unnatural amino acid at IL4 position 42 preserved wild type potency of the mutein. The PSL responded to MMPs and the construct was bound to the fibronectin of the ECM by TGase. Muteins displaying all these functionalities were necessary and sufficient in reducing inflammation and protecting non-load bearing cartilage and the anterior cruciate ligament from degradation as evaluated in an osteoarthritis model in rabbits created by surgical destabilization of the animals' medial menisci (DMM). In conclusion, a minimally invasive treatment option featuring bioresponsive IL4 depots with potential clinical value in osteoarthritis and potentially other inflammatory conditions has been established.

Introduction

Cytokines are potent biological agents with a variety of pleiotropic effects, some of which make them interesting for therapeutic purposes.[1,2] Unfortunately, they suffer from a short half-life and need to be administered at high concentrations systemically to achieve biologically active concentrations in the targeted tissue. This leads to dose-limiting systemic toxicities that hinder their therapeutic use.[3,4] Cytokine expression is mainly controlled (post-)transcriptionally[5] but an additional level of regulation is found in cytokines that are bound by the extracellular matrix (ECM) and released by tissue remodeling processes like they occur in inflammation and wound healing.[6] With focus on osteoarthritis, an inflammatory joint disease ultimately compromising cartilage and subchondral bone[7] and with natures design of bioresponsive cytokine depots in mind, we have engineered a cytokine that was modified allowing enzymatic binding to the ECM of the damaged joint

cavity upon minimally invasive injection. Interleukin-4 (IL4) was selected as of its established anti-inflammatory role including the reduction of matrix metalloproteinase (MMP) activation and thereby protecting the ECM components of cartilage such as aggrecan.[8] Further, the cytokine conjugate features a **p**rotease **s**ensitive **l**inker (**PSL**) by which active IL4 gets liberated from the ECM through MMP activity[9–11] in an effort to effectively modulate the arthritis outcome through bioresponsive control of spatiotemporal IL4 delivery. We developed the conjugate to bind to the ECM in presence of FDA-approved **t**rans**g**lutamin**ase** (**TGase**) FXIII leading to a stable, covalent IL4 decoration of the joint cavity. TGase catalyzes the formation of ε-(γ-glutamyl)lysine isopeptide bonds between specific Gln and Lys residues in blood clotting, wound healing or binding of growth factors to the ECM molecules or fibrin fibrils.[12,13] Previous reports have demonstrated that intra-articular injection of IL4 may have the potential to prevent proteoglycan loss and promotion of matrix synthesis through inhibition of NO production in the early phase of cartilage destruction but the pre-clinical benefit of these studies was limited likely as of rapid diffusion of IL4 from the joint upon injection.[14] The IL4 variants presented here for TGase-tissue decoration have wild type bioactivity while effectively binding to fibronectin or other extracellular matrix components in presence of TGase. The protease-sensitive linker is selectively recognized and cleaved by MMPs, liberating intact and active IL4 from the ECM. Only this form but not un-cleavable controls or wild type IL4 demonstrated disease modifying activity in a rabbit osteoarthritis model.

Results

Structural considerations

Several novel human IL4 variants were created, containing a TGase substrate sequence for immobilization on extracellular matrix components and an intervening protease-sensitive linker enabling release of IL4 by MMPs to allow diffusion from the depot site (Fig.).

The peptide extension was genetically fused to the N- or C-terminus of IL4, respectively. It was previously observed that fusion of proteins to the C-terminus of IL4 greatly reduces its affinity[16] and exchanging amino acids in the binding site for the γc receptor subunit close to the C-terminus creates IL4 antagonists.[17] Therefore, in another approach, the peptide extension was attached to IL4 via an unnatural amino acid introduced by genetic codon expansion during expression in *E. coli*. As we showed before, human IL4 can be modified

with this unnatural amino acid for click chemistry (propargyl-L-lysine, Plk) at position K42 and conjugated to particles or polymers while retaining full bioactivity.[18,19]

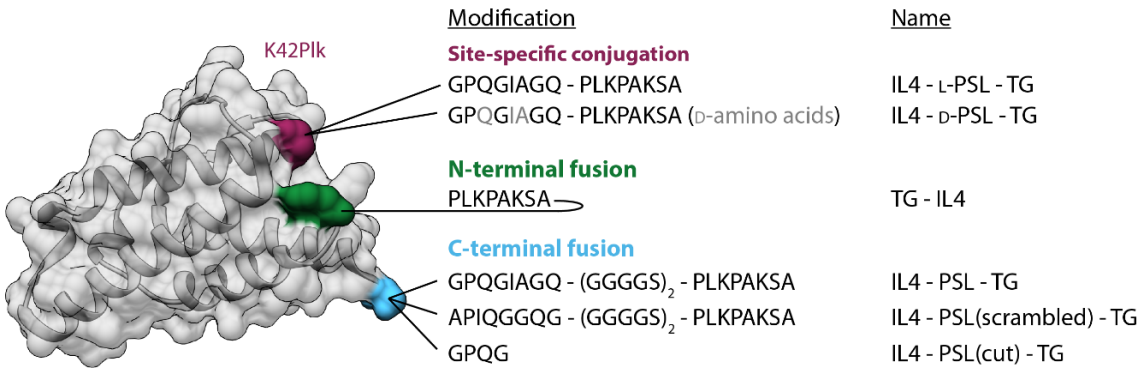

Fig. 1 Schematic representation of IL4 variants including modification site and amino acid sequence of attached peptide. Molecular graphics were created with Chimera.[15]

The TGase lysine-donor substrate sequence ('TG', amino acid sequence: PLKAPAKSA) was derived from insulin-like growth factor 1.[9] Previous studies described the FXIIIa-mediated covalent binding of IGF-1 through its K68 in the C-terminal D-domain to components of the extracellular matrix (ECM)[20] or used it for site-specific PEGylation[9]. Taking advantage of this natural mechanism, we used the IGF-1 D-domain as a TGase substrate sequence for immobilization of IL4 on extracellular matrix molecules.

The protease-sensitive linker sequence ('PSL', amino acid sequence: GPQGIAGQ) is derived from type I collagen and facilitates release of IL4 from the ECM by MMPs.[9,21–23] For the IL4 conjugates, a PSL version with D-amino acids at the MMP recognition site in the protease-sensitive linker (D-PSL) was synthesized to serve as a non-cleavable control to be compared to the cleavable version (L-PSL) with standard L-amino acids. As this is not an option for the IL4 fusion proteins, a scrambled version of the PSL (amino acid sequence: APIQGGQG) was used, as well as a "pre-cut" version (amino acid sequence: GPQG).

Production of interleukin-4-peptide conjugates

All proteins were expressed in *E. coli* with a yield of ~1 mg per liter of expression culture, except for wild type IL4, which yielded more than 10 mg/l. The proteins were refolded from inclusion bodies and purified by cation exchange chromatography. IL4 K42Plk was further processed by conjugation with the peptides "N_3-L-PSL-TG" and "N_3-D-PSL-TG" via copper(I)-catalyzed alkyne-azide cycloaddition (CuAAC), resulting in "IL4-L-PSL-TG" and

"IL4-D-PSL-TG". The peptides were prepared by solid phase peptide synthesis and purified by RP-HPLC yielding 7.5 mg (N_3-L-PSL-TG peptide) and 3.7 mg (N_3-D-PSL-TG peptide) per 100 µmol

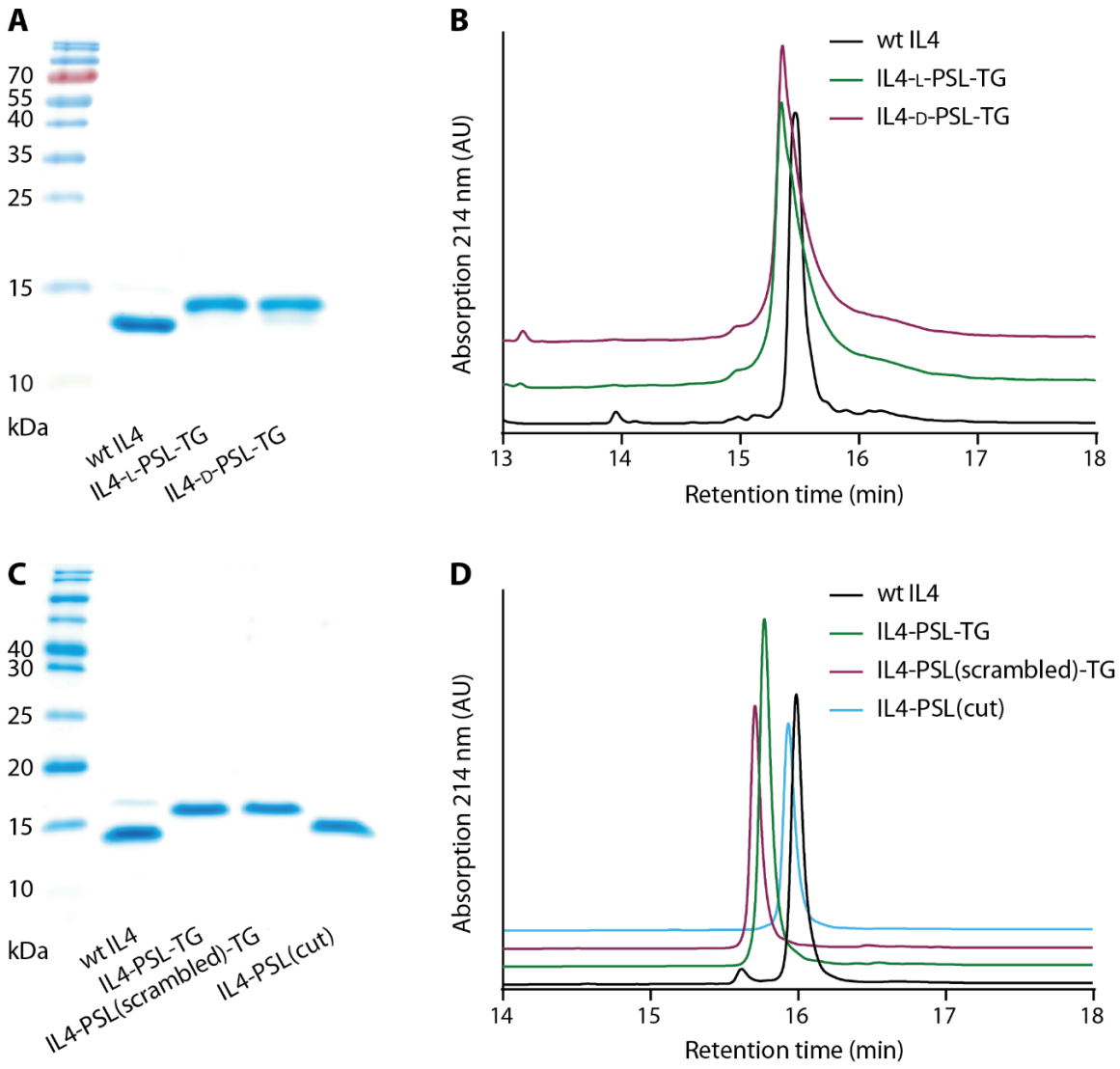

Fig. 2 Characterization of IL4 variants. **(A)** SDS-PAGE analysis of purified IL4-conjugates (Molecular-weight marker (PageRuler Prestained Protein Ladder, 10 to 180 kDa; Thermo Fisher Scientific, Darmstadt, Germany); wild type IL4 (15.1 kDa); IL4-L-PSL-TG (16.4kDa); IL4-D-PSL-TG (16.4 kDa). **(B)** Reversed phase chromatography profile of purified IL4-PSL-TG-conjugates in comparison to wt IL4. **(C)** SDS-PAGE analysis of purified IL4-PSL-TG fusion proteins (Molecular-weight marker (PageRuler Unstained Broad Range Protein Ladder, 5 to 250 kDa; Thermo Fisher Scientific, Darmstadt, Germany); wild type IL4 (15.1 kDa); IL4-PSL-TG (17.2 kDa); IL4-PSL(scrambled)-TG (17.2 kDa); IL4-PCL(cut) (15.4 kDa). **(D)** Reversed phase chromatography profile of purified IL4-PSL-TG fusion proteins in comparison to wt IL4.

batch, respectively. RP-HPLC analysis showed >90% purity and the molecular weight (1603 Da) of the peptides was confirmed by MALDI-MS (Fig. SI 12 - Fig. SI 3). The resulting IL4-peptide conjugates were purified by size exclusion chromatography.

Purity of the C-terminal IL4 fusion proteins and IL4-peptide-conjugates was analyzed by SDS-PAGE and RP-HPLC (Fig. 2). All proteins showed single bands of the expected size in the SDS-PAGE (wt IL4: 15.1 kDa, IL4-L-PSL-TG: 16.4 kDa, IL4-D-PSL-TG: 16.4 kDa, IL4-PSL-TG: 17.2 kDa, IL4-PSL(scrambled)-TG: 17.2 kDa, IL4-PCL(cut): 15.4 kDa) and were >95% pure. The correct mass of the C-terminal IL4 fusion proteins and IL4-peptide-conjugates was confirmed by MALDI-MS (Fig. SI 4 - Fig. SI 8).

The MALDI-MS spectrum of the N-terminally modified TG-IL4 showed a lower mass than expected (Fig. SI 9, observed average mass 16473.417 Da, calculated average mass 16824.189 Da), which indicates that several amino acids are missing. Additionally, the TG tag was not functional when tested in a TGase catalyzed reaction with fibronectin (Fig. SI 11). Hence, the development of this IL4 variant was not further pursued.

Characterization of the IL4 depot system in vitro

Bioactivity of IL4 variants

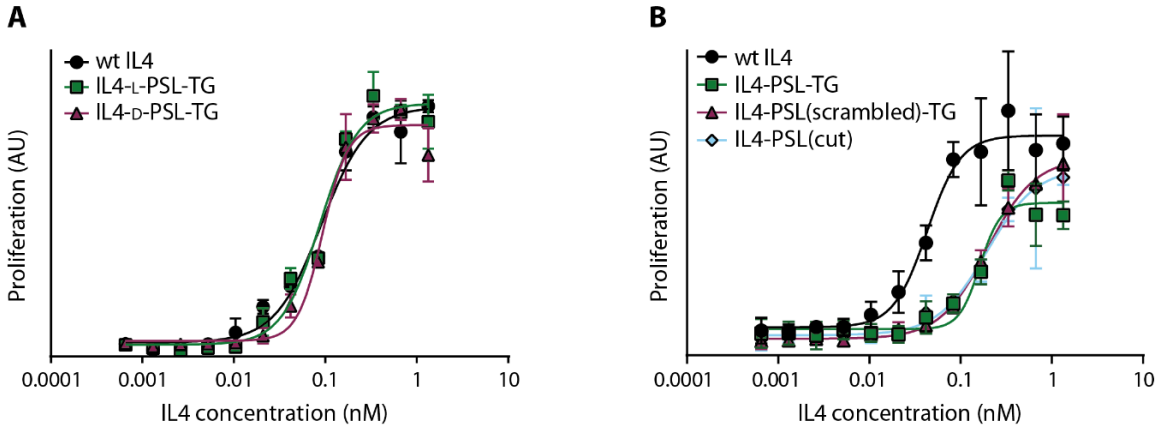

Fig. 3 Bioactivity of IL4 variants **(A)** Proliferation assay of IL4-PSL-TG-conjugates. Different concentrations of IL4-conjugates were incubated with human TF-1 cells and proliferation was assessed after 48 h using WST-1 reagent. EC50 values: wt IL4 0.090 nM, IL4-L-PSL-TG 0.087 nM, IL4-D-PSL-TG 0.093 nM. **(B)** Proliferation assay of IL4-PSL-TG fusion proteins. Different concentrations of IL4-PSL-TG fusion proteins were incubated with human TF-1 cells and proliferation was assessed after 48 h using WST-1 reagent. EC_{50} values: wt IL4 0.043 nM, IL4-PSL-TG 0.163 nM, IL4-PSL(scrambled)-TG 0.198 nM, IL4-PSL(cut) 0.195 nM.

IL4 is a cytokine with anti-inflammatory effects, including reduction of MMP activation and thereby protecting ECM components from degradation. To assess the influence of the PSL-TG tag extension on the cytokine, the bioactivity of the IL4-PSL-TG conjugates and fusion proteins was assessed via proliferative response of TF-1 cells in vitro and compared to that of wild type IL4 (Fig. 3). Proliferation of TF-1 cells was induced by wild type IL4 and the IL4-PSL-TG conjugates and fell within a 5% range (EC_{50} values: wt IL4 0.090 nM, IL4-L-PSL-TG 0.087 nM, IL4-D-PSL-TG 0.093 nM)(Fig. 3A). This is in line with our previous findings, that modification of IL4 at position 42 yields fully active bioconjugates.[18,19] Cleavage of the PSL by MMPs results in a short peptide tag of four amino acids remaining attached to the IL4 molecule. The proliferation assay shows that this is not expected to interfere with the biologic activity of the cytokine. The proliferative response of the TF-1 cells incubated with the IL4 fusion proteins was more than 4-fold lower compared to wild type IL4 (EC_{50} values: wt IL4 0.043 nM, IL4-PSL-TG 0.163 nM, IL4-PSL(scrambled)-TG 0.198 nM, IL4-PSL(cut) 0.195 nM) (Fig. 3B). The C-terminally attached peptide significantly reduces the bioactivity of IL4, and it is not restored by cleavage of the PSL. The IL4 variant modified with the four amino acids remaining after cleavage, IL4-PSL(cut), has the same reduced bioactivity as the variants with the full length peptide tag. Due to the impaired bioactivity, the development of the C-terminally modified IL4 fusion proteins was not further pursued.

The protease sensitive linker attached to the cytokine facilitates the release of IL4 from the ECM through MMP activity. To measure the MMP concentration required for efficient cleavage of the PSL, a dose escalation study with a combination of different activated MMP isoforms (MMP-1, -8 and -9) was performed (Fig. 4A). The N_3-PSL-TG peptides were incubated with an equimolar MMP mixture at six total MMP concentrations (1, 5, 12, 16, 18 and 24 nM). RP-HPLC analysis revealed complete cleavage of N_3-L-PSL-TG after 24 h for MMP concentrations higher than 18 nM (Fig. 4B). With a total MMP concentration of 12 nM around 90% cleavage is reached after 48 h. N_3-D-PSL-TG is not susceptible to MMP cleavage.

A similar experimental setup was used to assess the MMP cleavage of the IL4- L-PSL-TG conjugate. A cleavage study with an equimolar mixture of MMP-1, -8, and -9 was performed at four total concentrations (1 nM, 3 nM, 6 and 12 nM) (Fig. 4C). After 24 h incubation about 80% cleavage of the PSL could be achieved with 12 nM MMPs. The same concentration of MMPs was used to analyze cleavage over time (Fig. 4D). Complete cleavage of the IL4-L-PSL-TG was achieved within 48 hours. IL4-D-PSL-TG showed no cleavage. Neither the cytokine nor the D-amino acid modified peptide is an MMP substrate.

Characterization of the protease-sensitive linker

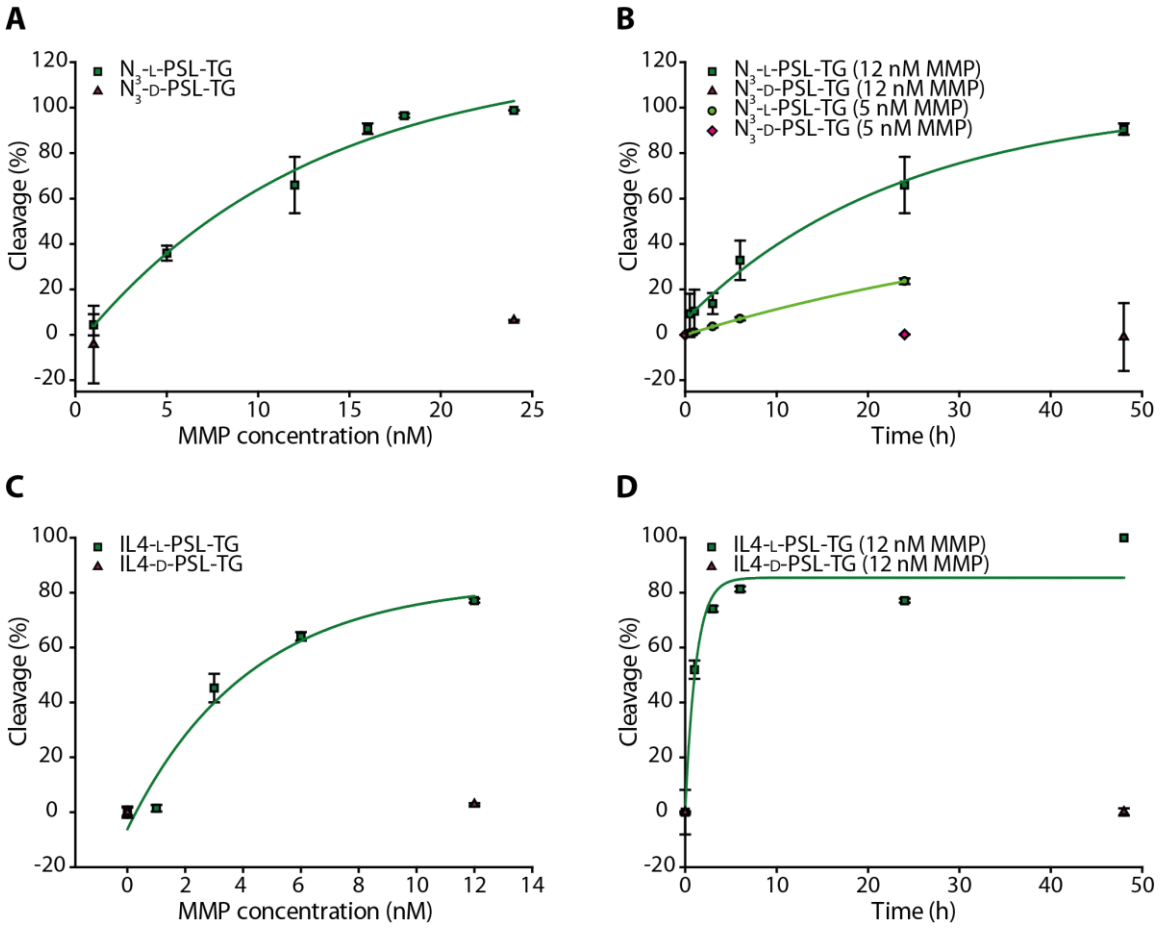

Fig. 4 Cleavage experiments N_3- PSL-TG peptides and IL4-PSL-TG conjugates with matrix metalloproteinases. After inactivation of the enzymes, the reaction was analyzed by reversed phase HPLC and percentage of cleavage was determined by analyzing peak areas. **(A)** N_3-L-PSL-TG and N_3-D-PSL-TG peptides were incubated with different concentrations of an equimolar mixture of MMP-1, -8, -9 for 24 h at 37 °C. **(B)** N_3-L-PSL-TG and N_3-D-PSL-TG peptides were incubated with equimolar mixture of MMP-1, -8, -9 (12 nM) for different time spans up to 48 h at 37 °C. **(C)** IL4-L-PSL-TG and IL4-L-PSL-TG were incubated with different concentrations of an equimolar mixture of MMP-1, -8, -9 for 24 h at 37 °C. **(D)** IL4-L-PSL-TG and IL4-D-PSL-TG were incubated with an equimolar mixture of MMP-1, -8, -9 (12 nM) for different time spans up to 48 h at 37 °C.

This shows, that the PSL contained in the IL4-PSL-TG conjugate behaves very similarly to the PSL contained in the N_3-PSL-TG peptide, which means that the MMPs are not influenced by the added "bulk" in the form of IL4. The levels of active MMPs in synovial fluid differ between osteoarthritis patients but are reported for being in the very low nanomolar range.[24–26] These MMP levels should facilitate a slow release of IL4 from the ECM depot, regulated in a negative feedback loop, as IL4 prevents activation of pro-MMPs.[8]

Conjugation to fibronectin

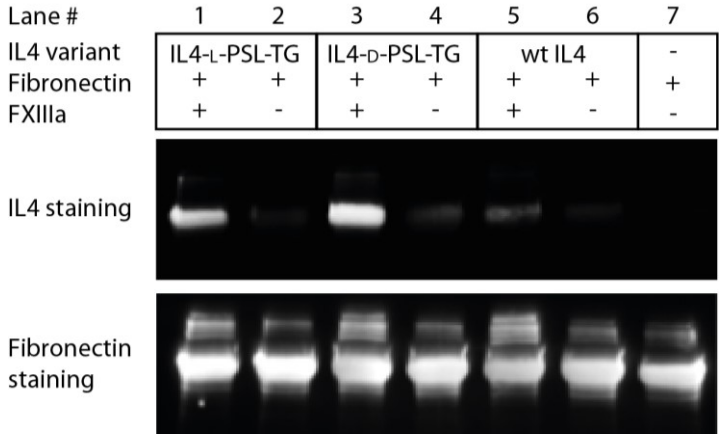

Fig. 5 Western blot analysis of FXIIIa mediated bioconjugation of IL4-PSL-TG conjugates with fibronectin. IL4-L-PSL-TG, IL4-D-PSL-TG and wt IL4 were incubated with fibronectin and FXIIIa at 37 °C for 1 h. Samples were run on a 5-20% SDS-PAGE gradient gel and transferred to a nitrocellulose membrane. Blot was stained for IL4 (top) and afterwards stripped and re-probed for fibronectin (bottom).

The IL4 conjugate was developed to be covalently attached to the ECM of the joint cavity in presence of the transglutaminase FXIIIa to build a cytokine depot. FXIIIa catalyzes the formation of ε-(γ-glutamyl)lysine isopeptide bonds between specific Gln and Lys residues. The bond-formation between the Lys residues in the TGase substrate sequence (PLKPAKSA) of the IL4-PSL-TG conjugates and the Gln residues of fibronectin, a major fibrillar glycoprotein within the ECM, was qualitatively assessed using western immunoblotting with sequential detection of IL4 and fibronectin (Fig. 5). A reducing gradient SDS-PAGE (5-20%) was used to resolve the large protein fibronectin (220 kDa) and the small IL4 variants (wt IL4: 15.1 kDa, IL4-PSL-TG conjugates: 16.4 kDa). The western blot shows a clear co-localization of the IL4-PSL-TG conjugates and fibronectin, indicating that a covalent linkage was formed between fibronectin and IL4. For wild type IL4 a faint band can be observed, probably due to unspecific conjugation with one of the several surface lysins of the cytokine. The IL4 -PSL-TG conjugates presented here for TGase-mediated tissue painting are effectively bound to fibronectin, an extracellular matrix component, in the presence of FXIIIa.

Depot system performance in an in vivo model of osteoarthritis

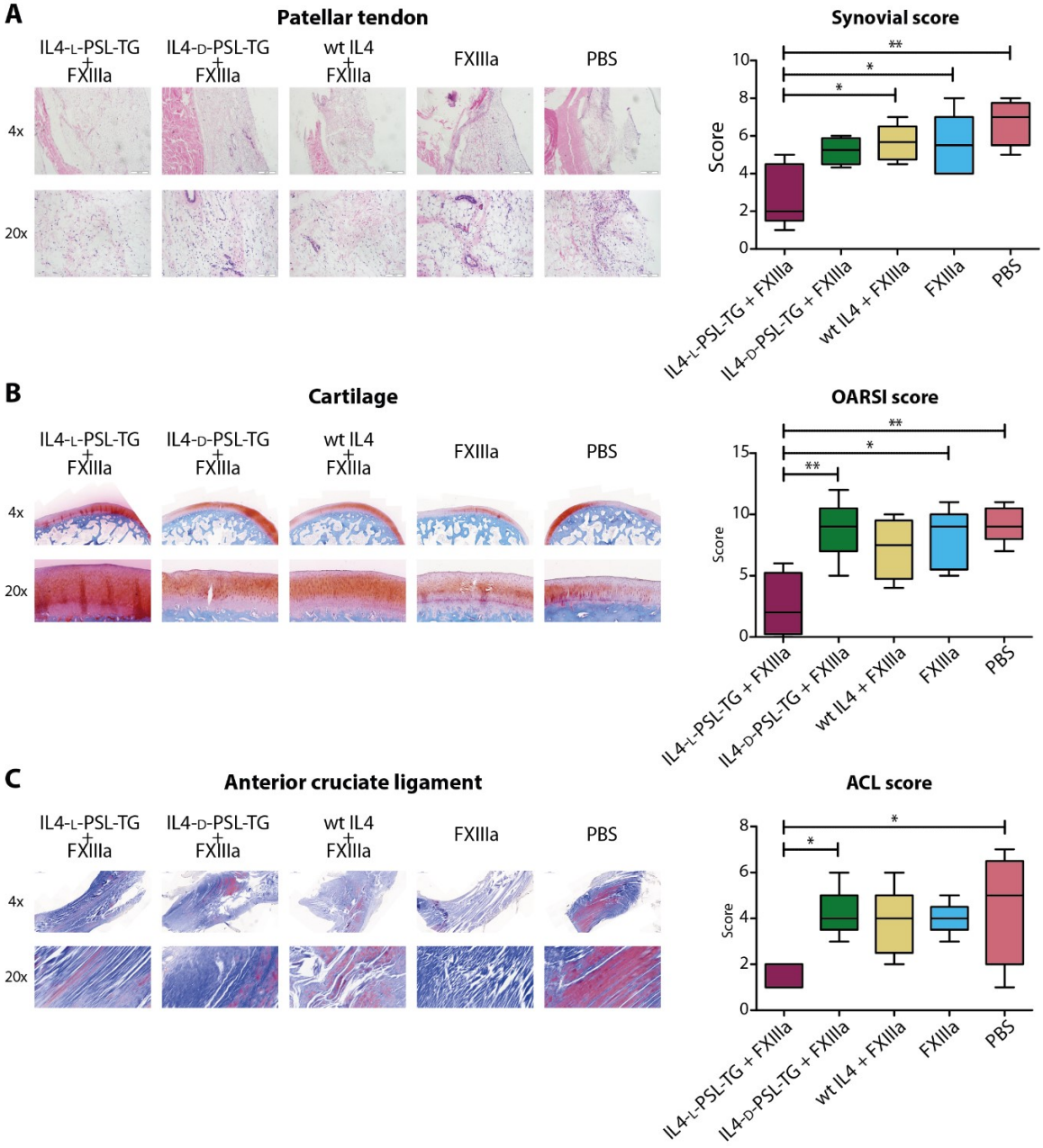

Fig. 6 Therapeutic activity of IL4-PSL-TG conjugates in a rabbit DMM model. Rabbits were sacrificed 8 weeks after surgery. **(A)** Left: Histological sections of the medial meniscus were subjected to HE staining to evaluate inflammation of patellar tendon and subsynovium. Right: Synovial score, includes sub-synovial inflammation, synovial fibrosis and vascular formation. **(B)** Left: Safranin O and type II collagen immunohistochemical staining of the cartilage of rabbit knee joints. Right: OARSI score, includes SO staining, cartilage structure, chondrocyte density and cluster formation. **(C)** Left: HE and Masson staining of the ACL of rabbit knee joints. Right: ACL score, includes inflammation, mucoid degeneration, chondrometaplasia, fibrocystosis and fiber orientation.

The injectable, minimally invasive system for enzymatic cytokine depot formation consisting of IL4-PSL-TG and FXIIIa was tested in vivo in a rabbit model of established osteoarthritis. Three days after surgical destabilization of the medial meniscus, rabbits were

injected intraarticularly with vehicle, FXIIIa alone or IL4-L-PSL-TG, IL4-D-PSL-TG and wt IL4 in combination with FXIIIa, respectively, to investigate the effects of IL4, immobilization and release. Evaluation by HE and SO staining was performed after 8 weeks. The gross view of the meniscus shows that the release of IL4 improves regrowth of the medial meniscus (Fig. SI 12). Fig. 6 shows that administration of IL4-L-PSL-TG results in significant amelioration of the sub-synovial inflammation, resulting in a reduced number of inflammatory cells, fibrosis and vascular formation. An increase in the OARSI score can be seen in animals treated either with vehicle, IL4-D-PSL-TG, wild type IL4 or FXIIIa alone, whereas significantly decreased disease activity was noted after treatment with IL4-L-PSL-TG. The SO staining shows that IL4 release leads to a delayed destruction of ECM. The non-load bearing area of the cartilage has a delayed regeneration and the anterior cruciate ligament (ACL) is also protected from OA induced degeneration.

In conclusion, only when all components of the injectable cytokine depot system – anti-inflammatory activity of IL4, bioresponsive release by MMPs and immobilization on ECM of the joint – are present, disease modifying activity can be achieved.

Discussion

In this study we explored different design strategies to create a bioinspired cytokine depot system by extending the cytokine with a protease-sensitive linker and a TGase substrate sequence. IL4 was used as a model cytokine because of its potent anti-inflammatory properties but pharmacokinetic shortcomings. While IL4 is susceptible to C-terminal fusion, the N-terminally attached TGase substrate sequence was nonfunctional after expression in *E. coli*, probably due to degradation. This leaves the site-directed bioconjugation approach via the unnatural amino acid at position 42 as the best option to yield a bioactive IL4 modified with a functional protease-sensitive linker and TGase substrate sequence. The in vitro characterization of the constructs shows that IL4 remains fully bioactive upon conjugation with the bifunctional peptide at amino acid 42, like it was expected from previous studies.[19,27] The protease-sensitive linker is selectively cleaved by MMPs, while IL4 remains intact. The IL4 constructs are conjugated to fibronectin by FXIIIa via the TGase substrate sequence contained in the bifunctional peptide. Further, we were able to demonstrate an enhanced therapeutic effect of IL4 by MMP-responsive release in a rabbit OA model. Compared to the control groups, bioresponsive release of IL4 lead to a

delayed degeneration of non-load bearing cartilage and protection of the anterior cruciate ligament.

Bioresponsive release of anti-inflammatory cytokines from an immobilized depot in the joint may be a useful therapeutic strategy in OA because it expands the administration intervals. Normally, IL4 treatment must be given by repeated daily injection or continuous administration, because it is rapidly cleared from the circulation.[28,29] This makes it inapplicable for treatment in a clinical setting. Also, it requires high systemic doses to achieve efficacy and that prevents its use because of unwanted side effects, including capillary leak syndrome and gastrointestinal haemorrhage.[30] While these side effects exclude systemic administration as an option, local administration is limited due to the risk of infection after arthroscopic visits. One way to overcome these problems is with immobilizing the cytokine by minimally invasive local co-injection with the transglutaminase FXIIIa to create a drug depot with a prolonged effect and with a local release in response to inflammatory proteases to reduce systemic impact and achieve high local concentrations. Our study is the first to demonstrate the use of peptides to paint cytokines to synovial tissue with release in response to presence of MMP. The IL4 conjugates constructed in this study have been shown to increase the therapeutic effect of the cytokine and have the capacity to reduce degradation of non-load bearing cartilage and the anterior cruciate ligament with a single injection. The in vivo results show, that the release of IL4 by MMPs reduces the OA score, most likely through improved diffusion and thereby being able to reach target cells which are not in contact with the synovial extracellular matrix. The release of IL4 is regulated in a negative feedback loop, with an on-demand release of the therapeutic, thereby slowing disease progression und preventing the spreading to healthy structures in the rabbit OA model.

Surgically destabilizing the meniscus is currently one of the most consistent models of human knee OA.[31] While the rabbit knee is similar to the human knee in gross appearance[32], the biomechanics and histology is different, e.g. it has greater cellularity and less vascular penetration[33]. An additional problem of the rabbit model is the capability of rabbits up to 8 month old to regenerate articular cartilage.[34] Many treatments that were promising in animal models, were not successful in humans because they were started to late, as humans remain asymptomatic until late in the disease progression. One example are matrix metalloproteinase inhibitors that were able to reduce cartilage degradation preclinical disease models[35–37], but failed in the clinic and led to significant musculoskeletal adverse effects.[38] We circumvented this by not directly inhibiting MMPs, but using them as targets

to locally release a MMP-downregulating cytokine which additionally suppresses inflammation, one of the key mediators of the pathogenesis of OA.[39] Further in vivo experiments are necessary to further assess the pharmacological properties of our system, with focus on the precise influence of the single components on the therapeutic outcome.

The presented system for the delivery of therapeutics in response to inflammation is a versatile platform approach that provides all necessary building blocks to adapt the system to future needs. Bioresponsive release profiles can be easily altered by exchanging the PSL, e.g. aiming at slower/faster release or sensitivity to other proteases.[2l] Intraarticular injection is only an option when performed every few month at maximum. By choosing a PSL with slower release, these intervals of administration could be achieved. The transglutaminase sequence and corresponding transglutaminase might be exchanged to provide specificity for a different scaffold or even might be replaced by a targeting moiety which binds to the diseased tissue and enables systemic administration, completely circumventing intraarticular injection.[40,41] Finally, this approach detailed for IL4 can be extended to other proteins, peptides or small molecules, e. g. the release of growth factors to improve cartilage regeneration subsequent to repressing the inflammation.

In conclusion, this study provides a framework for engineering therapeutic proteins that can exploit fundamental features of inflammatory diseases. The delivery strategy shown here for IL4 is paving the way for future cytokine and growth factor constructs leveraging the pharmacokinetic advantages of immobilization with the benefit of fully regained performance after bioresponsive release. The system also enables tailored treatment of individual patients. Patients could be stratified according to protease activities using a diagnostic version of this system, in which the drug would be replaced by a mass tag.[42] The building blocks could then be easily adapted based on individual expression patterns in different patients. Thereby, this novel delivery strategy has the potential to allow effective and safe personalized treatment.

Methods

Peptide synthesis and purification

The linker peptides N_3-L-PSL-DC and N_3-D-PSL-DC were synthesized by solid phase peptide synthesis (SPPS) using an Initiator+ SP Wave semi-automated peptide synthesizer (Biotage, Uppsala, Sweden). Fmoc-Rink Amide AM resin (Iris Biotech, Marktredwitz, Germany) as

solid support was deprotected using 25% (v/v) piperidine in DMF for 3 min at 75 °C followed by six washing steps with dimethylformamide (DMF). A 5-fold molar excess of Fmoc-protected amino-acid (all purchased from Iris Biotech, Marktredwitz, Germany) in regard to the functional groups on the resin was dissolved in 3 ml 0.5 M hydroxybenzotriazole in DMF. 100 µl *N,N'*-diisopropylcarbodiimide was used as activator of the amino acids carboxylic function and 100 µl *N,N*-diisopropylethylamine was used as activator base. The amino acid cocktail was loaded onto the resin and incubated for 10 min at 50 °C followed by six washing steps using DMF. The azido group was introduced by a 2.5-fold molar excess or 2-azidoacetic acid. Final peptide cleavage from the resins was performed with 95% TFA in dichloromethane for 3 h followed by precipitation with diethyl ether at -20 °C. The precipitate was washed twice with ice cold diethyl ether and then air dried. The resulting precipitate was dissolved in 3% acetonitrile and 0.1% TFA in water. The peptides were purified by reversed phase chromatography using a Jupiter 15u C18 300A column (21.2 mm × 250 mm, Phenomenex LTD, Aschaffenburg, Germany), lyophilized and stored at -20 °C.

Preparation of interleukin-4 conjugates

Cloning, expression and purification of IL4 K42Plk were described before.[27] IL4 K42Plk was mixed with a 10-fold molar excess of N_3-L-PSL-DC or N_3-D-PSL-DC, respectively. 1/10 volume of CuAAC master mix (20 mM THPTA, 10 mM $CuSO_4$, 100 mM ascorbic acid) was added. Reaction was carried out for 2 h at 37 °C. Product was separated by size exclusion chromatography using a Superdex75 10/300 GL column (GE Healthcare Life Sciences, Freiburg, Germany) with PBS pH 7.4 at a flowrate of 0.25 ml/min at 4 °C.

Preparation of interleukin-4 fusion proteins

The DNA fragments for wild type human IL4 were N- or C-terminally elongated with oligonucleotides (Sigma-Aldrich, Schnelldorf, Germany) encoding the different linker variants using Gibson Assembly Master Mix (NEB, Frankfurt a. M., Germany). The cDNAs were inserted into the expression vector pET28b (Novagen, Merck KGaA, Darmstadt, Germany) and transformed into the expression host *E. coli* BL21(DE3).

Bacteria were grown in TB medium plus kanamycin (100 µg/ml) on a rotatory shaker at 37 °C to an optical density of 1.0 and IL4 protein expression was then induced by addition of 1 mM isopropylthiogalactopyranoside (IPTG) for 3 h. The bacteria were sedimented by

centrifugation at 5000 g, 15 min at 4 °C and resuspended in 1/200 culture volumes of resuspension buffer (50 mM Tris-HCl pH 8.0, 50 mM NaCl, 1 mM EDTA) and PMSF (final concentration 100 µM) and lysozyme (final concentration 75 µg/ml) were added. The cells were lysed by sonication (Sonopuls HD3100, Bandelin, Berlin, Germany) with the cell suspension cooled on ice. The sediment was resuspended in a quarter volume of the resuspension buffer used above and sonicated again. The insoluble fraction ("inclusion bodies") was separated by centrifugation and washed once with resuspension buffer plus 1% Triton X-100 and twice with resuspension buffer. The final sediment was kept frozen at temperatures -80 °C

The IL4 protein was extracted from the inclusion bodies using unfolding buffer (50 mM Tris-HCl pH 8.0, 50 mM NaCl, 1 mM EDTA, 5 M guanidine-HCl, 2 mM glutathione reduced, 0.2 mM glutathione oxidized, 9 ml per g wet weight). For refolding of the IL4, the clarified protein extract was diluted with two volumes of refolding buffer (0.5 M arginine, 50 mM Tris-HCl pH 8.0, 50 mM NaCl, 1 mM EDTA, 2 mM glutathione reduced, 0.2 mM glutathione oxidized) and dialyzed against 20 volumes of refolding buffer for 4 h at room temperature. Then, the solution was dialyzed against 40 volumes of 25 mM ammonium acetate pH 5.0 overnight at 4 °C. The solution was clarified by centrifugation, and the supernatant was filtered (0.22 µm) and loaded onto a HiTrap SP XL 5 ml column (GE Healthcare Life Sciences, Freiburg, Germany) that was equilibrated with 25 mM ammonium acetate pH 5.0 (A). The IL4 protein was eluted via a gradient using buffer containing 2 M sodium chloride (B). The peak eluting around 25% B was collected and buffer exchange to A and concentration to 10 ml were achieved via ultrafiltration (MWCO 9 kDa). The process was repeated with two HiTrap SP HP 1 ml columns (GE Healthcare Life Sciences, Freiburg, Germany). Natively folded IL4 eluting as the major peak at 30% B was dialyzed against PBS pH 7.4, frozen in liquid nitrogen and stored in aliquots at -80 °C until further use. Protein concentrations were determined by BCA assay against a BSA standard (Thermo Fisher Scientific, Darmstadt, Germany).

SDS-PAGE

Protein samples were analyzed by discontinuous SDS-PAGE under denaturing conditions as described elsewhere.[43] Protein bands were stained with Coomassie Brilliant Blue G-250.[44]

RP-HPLC

Protein purity was assessed by RP-HPLC using a Hitachi LaChrom HPLC system (VWR, Darmstadt, Germany). Approximately 20 µg protein sample was applied to a Zorbax 300SB-CN column (Agilent, Waldbronn, Germany), equilibrated with water containing 0.1 % TFA and acetonitrile (ACN)(VWR, Darmstadt, Germany) containing 0.1% TFA (95:5 v/v). Proteins were eluted by a linear gradient of 5 - 95% ACN containing 0.1% TFA with a gradient of 5% ACN/min and a flow rate of 1 ml/min. Column temperature was kept at 22 °C and UV absorbance was monitored at 214 nm.

MALDI-MS

Protein samples were desalted using ZipTip C18 pipette tips (Merck Millipore, Darmstadt, Germany) following the manufacturer's instructions. Matrix-assisted laser desorption ionization (MALDI-MS) spectra were acquired in the linear positive mode with an Autoflex II LRF instrument (Billerica, MA, USA). Mass spectra were calibrated externally with the Protein Calibration Standard I (Bruker Daltonics; Billerica, MA, USA), containing insulin, ubiquitin, myoglobin and cytochrome C.

TF-1 cell proliferation assay

TF-1 cells (CRL-2003; ATCC, Manassas, VA, USA) were maintained in T75 flasks in growth medium (RPMI-1640 containing 10% heat-inactivated FCS (Thermo Fisher Scientific, Darmstadt, Germany), 2.5 ng/ml GM-CSF (R&D Systems, Wiesbaden, Germany), penicillin G (100 U/ml) and streptomycin (100 mg/ml) at 37 °C and 5% CO_2.

For the proliferation assay, TF-1 cells were seeded in a 96-well plate at 50,000 cells/well in assay medium (RPMI-1640 containing 10% heat-inactivated FCS, 0.5% BSA, penicillin G (100 U/ml) and streptomycin (100 mg/ml)), supplemented with a dilution series of IL4 variants, ranging from 0.01 to 20 ng/mL, respectively. After stimulation for 48 h, 10 µl of WST-1 (Roche, Mannheim, Germany) per well were added and the cells were incubated for 2-4 h at 37 °C. The absorbance of the soluble formazan product was determined at 450 nm using a Spectramax 250 microplate reader (Molecular Devices, Sunnyvale, CA, USA). Relative proliferation is expressed in comparison to wild type IL4 (R&D Systems, Wiesbaden, Germany).

MMP cleavage

Pro-MMPs (MMP-1, MMP-8 and MMP-9)(444208 / 444229 / 444231, EMD Millipore, Billerica, USA) were activated with 4-aminophenylmercuric acetate (APMA) as described before.[45]

Protease-sensitive linker

For the experiments targeting the MMP concentration-dependent cleavage of the PSL, a mixture of MMP-1, -8, and -9 was used. 0.45 mM PSL was incubated with equimolar amounts of MMP-1, -8 and -9 to reach total concentrations of 1 to 24 nM in 200 µl MMP buffer (200 mM NaCl, 50 mM Tris-HCl, 5 mM $CaCl_2$, 1 µM $ZnCl_2$, pH 6.8–7.0) at 37 °C for 24 h. Protease activity was stopped with 1 mM EDTA and heating to 95 °C for 5 min.

For the time-dependent cleavage profile, the PSL was incubated with as above but with 5 nm or 12 nM MMP mix and the reaction was stopped after 0.5, 1, 3, 6, 24 and 48 h. For each measured time point, a control of PSL in MMP buffer without MMPs was incubated under the same conditions to exclude unspecific degradation. The samples were analyzed by RP-HPLC using a Hitachi LaChrom HPLC system (VWR, Darmstadt, Germany) with a ZORBAX 300SB-CN column (4.6 mm× 150 mm, 5µm, Agilent, Santa Clara, CA, USA) equilibrated with a solution of 95% water containing 0.1% TFA and 5% acetonitrile (ACN) containing 0.1% TFA. PSL and cleaved fragments were eluted by a stepwise gradient of 5–60% ACN, 0.1% TFA in 18 min and 60-95% ACN, 0.1 %TFA in 5 min with a flow rate of 1 ml/min. Column temperature was kept at 22 °C and absorbance was monitored at λ = 214 nm.

IL4 conjugates

IL4 was dialyzed against MMP buffer (200 mM NaCl, 50 mM Tris-HCl, 5 mM $CaCl_2$, 1 µM $ZnCl_2$, pH 6.8–7.0) prior to cleavage experiments. For MMP concentration-dependent cleavage of IL4 variants, 20 µg IL4 were incubated with the MMP mixture (as described above) in 50 µl reaction volume at 37 °C for 24 h / 48 h. Protease activity was stopped with 10 mM EDTA. For the time-dependent cleavage profile, IL4 was incubated with 12 nM MMP mix and the reaction was stopped after 1, 3, 6, 24 and 48 hours. For each measured time point, a control of protein in MMP buffer without MMPs was incubated under the same conditions to exclude unspecific degradation. The samples were analyzed by RP-HPLC using a Hitachi LaChrom HPLC system (VWR, Darmstadt, Germany) with a Zorbax 300SB-CN column (Agilent, Waldbronn, Germany), equilibrated with water containing 0.1 % TFA and acetonitrile (ACN)(VWR, Darmstadt, Germany) containing 0.1% TFA (95:5 v/v). Proteins were eluted by a linear gradient of 5 - 95% ACN containing 0.1% TFA with a gradient of 5%

ACN/min and a flow rate of 1 ml/min. Column temperature was kept at 22 °C and UV absorbance was monitored at 214 nm.

Conjugation with fibronectin and western blot analysis

Human blood coagulation Factor XIII-A_2 (FXIII, A subunit, Zedira, Darmstadt, Germany) was activated in the presence of 2.5 mM $CaCl_2$ with 20 U/ml thrombin in TBS (20 mM Tris-HCl, 150 mM NaCl, pH 7.6) for 30 min at 37 °C. Small aliquots (200 U/ml) of activated FXIIIa were stored at -80 °C until further use. Fibronectin was incubated with a 10-fold molar excess of IL4 in the presence of 10 U/ml FXIIIa at 37 °C for 1 h in 20 µl reaction volumes in in TBS with 5 mM $CaCl_2$. The reaction products were analyzed on SDS-PAGE gradient gels (5-20%) under reducing conditions and western blotting. Proteins were transferred to a nitrocellulose membrane at 80 V for 90 minutes. Transfer was confirmed by Ponceau S staining. The membrane was blocked with Roti®-Block (Carl Roth, Karlsruhe, Germany) for 1 h at room temperature, prior to incubation with goat anti-hIL4 antibody (AB-204-NA, R&D Systems, Wiesbaden, Germany) in TBS containing 0.1% (w/w) Tween 20 (TBST) at 4 °C overnight under agitation. The membrane was then washed with TBST and incubated with goat anti-hIL4 antibody (AB-204-NA, R&D Systems, Wiesbaden, Germany) for 90 min at RT. Protein detection was performed using SuperSignal West Pico chemiluminescent substrate (Thermo Fisher Scientific, Darmstadt, Germany) and a FluorChem FC2 imaging system (Protein Simple, Santa Clara, CA, USA).

Afterwards the membrane was stripped using harsh stripping buffer (62.5 mM Tris-HCl pH 6.8, 2% SDS, 0.8% ß-mercaptoethanol) at 50 °C for 45 min under agitation. After extensive washing with water and TBS, the membrane was blocked again and re-probed for fibronectin using a rabbit anti-fibronectin antibody (F3648; Sigma-Aldrich, St. Louis, MO, USA) followed by an anti-rabbit HRP antibody (#7074; Cell Signaling Technology, Frankfurt a. M., Germany) as described above.

Rabbit model of partial meniscectomy

Forty 5-month-old male New Zealand White rabbits (2.5-3.0 kg) were maintained singly in stainless-steel cages. After intramuscular and intravenous injection with 10% chloral hydrate (4 ml/kg), a medial parapatellar approach was made through the skin and subcutaneous tissue. Then flexing of the joint and exposure of the medial meniscus, partial meniscectomy was performed by resecting about 80% of the meniscus' front zone. The rabbits could walk freely in their cages. Injections were administered three days after

surgical destabilization of the medial meniscus. Rabbits were randomly assigned to one of five groups and received a single intraarticular injection of IL4-L-PSL-TG (56 μg) + FXIIIa (15 U), IL4-D-PSL-TG (56 μg) + FXIIIa (15 U), wt IL4 (50 μg) + FXIIIa (15 U) or PBS, all contained in 200 μl total volume of PBS into the right knee joint. The rabbits were sacrificed eight weeks after surgery.

Macroscopic and histological assessment

The tibial plateau with menisci was carefully separated from the femoral condyle. Macroscopic pictures were taken using a digital camera (Olympus IX71) on a dedicated medical photography platform. Quantification of the size of the regenerated meniscus was performed using AxioVision Rel software version 4.8 to measure the ratio of the whole area of the medial meniscus, including both the regenerated region and the normal region, to the whole area of the medial tibial plateau. Specimens were fixed in 4% paraformaldehyde, then decalcified in 10% EDTA. After decalcification of the samples, they were dehydrated and embedded within paraffin blocks. Histological sections (6 μm) were prepared using a microtome, and subsequently deparaffinized with xylene, hydrated using decreasing concentrations of ethanol, and then subjected to hematoxylin and eosin staining for morphological evaluation and safranin O staining for glycosaminoglycan distribution. Regenerated meniscus was evaluated using the modified Pauli score on a scale of 0–18 points. The cartilage surface was stained with Indian ink for macroscopic observation. The Cartilage degeneration of the medial tibia was evaluated using the Mankin score, on a scale of 0–14 points. Investigators were blinded to group identity, from group assignment through histologic scoring.

Immunohistochemistry

A series of 6 mm-thick sections were utilized for immunohistochemical staining (IHC). Endogenous peroxidase was firstly blocked with hydrogen peroxide before pepsin treatment for 20 min. Mouse anti-rabbit monoclonal antibody against collagen type I (1:200 dilution; Abcam Inc., Cambridge, MA, USA) and mouse anti-rabbit monoclonal antibody against collagen type II (1:200 dilution; Calbiochem, Darmstadt, Germany) were used to detect the expression of collagen type I and type II in cartilage. Monoclonal antibodies were applied for 1 h followed by incubation with goat anti-mouse (Beyotime Institute of Biotechnology Inc., Jiangsu, China) secondary antibody for 2 h at room temperature. The DAB substrate

system (Zsbio, Beijing, China) was used for color development. Hematoxylin staining was used to reveal the nuclei.

Statistical Analysis

The data was expressed as mean ± SD. One-way ANOVA was performed using GraphPad (GraphPad Software Inc., La Jolla, CA, USA) to assess statistically significant differences of data between groups, followed by pairwise comparison using Tukey's post-test. The threshold of statistical significance was set at values of * $P \leq 0.05$, ** $P \leq 0.01$, *** $P \leq 0.001$.

Material

All reagents were obtained from Sigma Aldrich unless stated otherwise.

References

1. Vilček, J. & Feldmann, M. Cytokines as therapeutics and targets of therapeutics. *Rheumatologia* **20**, 65–74 (2006).
2. Bootz, F. & Neri, D. Immunocytokines: A novel class of products for the treatment of chronic inflammation and autoimmune conditions. *Drug Discov. Today* **21**, 180–189 (2016).
3. Whitehead, R. P. *et al.* Phase II trial of recombinant human interleukin-4 in patients with advanced renal cell carcinoma: a southwest oncology group study. *J. Immunother.* **25**, 352–358 (2002).
4. Lundin, J. *et al.* Interleukin 4 therapy for patients with chronic lymphocytic leukaemia: A phase I/II study. *Br. J. Haematol.* **112**, 155–160 (2001).
5. Taniguchi, T. Regulation of Cytokine Gene Expression. *Annu. Rev. Immunol.* **6**, 439–464 (1988).
6. Robertson, I. B. *et al.* Latent TGF-β-binding proteins. *Matrix Biol.* **47**, 44–53 (2015).
7. Kapoor, M., Martel-Pelletier, J., Lajeunesse, D., Pelletier, J. P. & Fahmi, H. Role of proinflammatory cytokines in the pathophysiology of osteoarthritis. *Nat. Rev. Rheumatol.* **7**, 33–42 (2011).
8. Van Lent, P. L. E. M., Holthuysen, A. E. M., Slöetjes, A., Lubberts, E. & Van Den Berg, W. B. Local overexpression of adeno-viral IL-4 protects cartilage from metallo proteinase-induced destruction during immune complex-mediated arthritis by preventing activation of pro-MMPs. *Osteoarthr. Cartil.* **10**, 234–243 (2002).
9. Braun, A. C., Gutmann, M., Mueller, T. D., Lühmann, T. & Meinel, L. Bioresponsive release of insulin-like growth factor-I from its PEGylated conjugate. *J. Control. Release* **279**, 17–28 (2018).
10. Schense, J. C. & Hubbell, J. A. Cross-linking exogenous bifunctional peptides into fibrin gels with factor XIIIa. *Bioconjug. Chem.* **10**, 75–81 (1999).
11. Schmoekel, H. G. *et al.* Bone repair with a form of BMP-2 engineered for incorporation into fibrin cell ingrowth matrices. *Biotechnol. Bioeng.* **89**, 253–262 (2005).
12. Früh, S. M. *et al.* Functional modification of fibronectin by N-terminal FXIIIa-mediated transamidation. *ChemBioChem* **15**, 1481–1486 (2014).
13. Nikolajsen, C. L., Dyrlund, T. F., Poulsen, E. T., Enghild, J. J. & Scavenius, C. Coagulation factor XIIIa substrates in human plasma: Identification and incorporation into the clot. *J. Biol. Chem.* **289**, 6526–6534 (2014).
14. Yorimitsu, M. *et al.* Intra-articular injection of interleukin-4 decreases nitric oxide production by chondrocytes and ameliorates subsequent destruction of cartilage in instability-induced osteoarthritis in rat knee joints. *Osteoarthr. Cartil.* **16**, 764–771 (2008).
15. Pettersen, E. F. *et al.* UCSF Chimera - A visualization system for exploratory research and analysis. *J. Comput. Chem.* **25**, 1605–1612 (2004).

16. Debinski, W., Puri, R. K., Kreitman, R. J. & Pastan, I. A Wide Range of Human Cancers Express Interleukin 4 (IL4) Receptors That Can Be Targeted with Chimeric Toxin Composed of IL4 and Pseudomonas Exotoxin. *J. Biol. Chem.* **268**, 14065–14070 (1993).

17. Tony, H. -P, Shen, B. -J, Reusch, P. & Sebald, W. Design of human interleukin-4 antagonists inhibiting interleukin-4-dependent and interleukin-13-dependent responses in T-cells and B-cells with high efficiency. *Eur. J. Biochem.* **225**, 659–665 (1994).

18. Lühmann, T. *et al.* Interleukin-4 clicked surfaces drive M2 macrophage polarization. *Chembiochem* (2016).

19. Lühmann, T. *et al.* Site-Specific POxylation of Interleukin-4. *ACS Biomater. Sci. Eng.* acsbiomaterials.6b00578 (2017). doi:10.1021/acsbiomaterials.6b00578

20. Sivaramakrishnan, M. *et al.* Lysine residues of IGF-I are substrates for transglutaminases and modulate downstream IGF-I signalling. *Biochim. Biophys. Acta - Mol. Cell Res.* **1833**, 3176–3185 (2013).

21. Nagase, H. & Fields, G. B. Human matrix metalloproteinase specificity studies using collagen sequence-based synthetic peptides. *Biopolymers* **40**, 399–416 (1996).

22. Braun, A. C. *et al.* Matrix Metalloproteinase Responsive Delivery of Myostatin Inhibitors. *Pharm. Res.* **34**, 58–72 (2017).

23. Ritzer, J. *et al.* Diagnosing peri-implant disease using the tongue as a 24/7 detector. *Nat. Commun.* **8**, (2017).

24. Heard, B. J. *et al.* Matrix metalloproteinase protein expression profiles cannot distinguish between normal and early osteoarthritic synovial fluid. *BMC Musculoskelet. Disord.* **13**, 126 (2012).

25. Tchetverikov, I. *et al.* MMP protein and activity levels in synovial fluid from patients with joint injury, inflammatory arthritis, and osteoarthritis. *Ann. Rheum. Dis.* **64**, 694–698 (2005).

26. Yoshihara, Y. *et al.* Matrix metalloproteinases and tissue inhibitors of metalloproteinases in synovial fluids from patients with rheumatoid arthritis or osteoarthritis. *Ann. Rheum. Dis.* **59**, 455–61 (2000).

27. Lühmann, T. *et al.* Interleukin-4-Clicked Surfaces Drive M2 Macrophage Polarization. *ChemBioChem* **17**, 2123–2128 (2016).

28. Allen, J. B., Wong, H. L., Costa, G. L., Bienkowski, M. J. & Wahl, S. M. Suppression of monocyte function and differential regulation of IL-1 and IL-1ra by IL-4 contribute to resolution of experimental arthritis 2. *J Immunol.* **151**, 4344–4351 (1993).

29. Horsfall, A. C. *et al.* Suppression of collagen-induced arthritis by continuous administration of IL-4. *J. Immunol.* **159**, 5687–96 (1997).

30. Prendiville, J. *et al.* Recombinant human interleukin-4 (rhu IL-4) administered by the intravenous and subcutaneous routes in patients with advanced cancer-A phase I toxicity study and pharmacokinetic analysis. *Eur. J. Cancer* **29**, 1700–1707 (1993).

31. Gregory, M. H. *et al.* A Review of Translational Animal Models for Knee Osteoarthritis. *Arthritis* **2012**, 1–14 (2012).

32. Kraus, V. B., Huebner, J. L., DeGroot, J. & Bendele, A. The OARSI histopathology initiative - recommendations for histological assessments of osteoarthritis in the guinea pig. *Osteoarthr. Cartil.* **18**, S53–S65 (2010).

33. Chevrier, A., Nelea, M., Hurtig, M. B., Hoemann, C. D. & Buschmann, M. D. Meniscus structure in human, sheep, and rabbit for animal models of meniscus repair. *J. Orthop. Res.* **27**, 1197–1203 (2009).

34. Wei, X., Gao, J. & Messner, K. Maturation-dependent repair of untreated osteochondral defects in the rabbit knee joint. *J. Biomed. Mater. Res.* **34**, 63–72 (1997).

35. Janusz, M. J. *et al.* Moderation of iodoacetate-induced experimental osteoarthritis in rats by matrix metalloproteinase inhibitors. *Osteoarthr. Cartil.* **9**, 751–760 (2001).

36. De Bri, E. *et al.* Effect of an Inhibitor of Matrix Metalloproteinases on Spontaneous Osteoarthritis in Guinea Pigs. *Adv. Dent. Res.* **12**, 82–85 (1998).

37. Yu, L. P. *et al.* Reduction of the severity of canine osteoarthritis by prophylactic treatment with oral doxycycline. *Arthritis Rheum.* **35**, 1150–1159 (1992).

38. Krzeski, P. *et al.* Development of musculoskeletal toxicity without clear benefit after administration of PG-116800, a matrix metalloproteinase inhibitor, to patients with knee osteoarthritis: A randomized, 12-month, double-blind, placebo-controlled study. *Arthritis Res. Ther.* **9**, 1–11 (2007).

39. Robinson, W. H. *et al.* Low-grade inflammation as a key mediator of the pathogenesis of osteoarthritis. *Nat. Rev. Rheumatol.* **12**, 580–592 (2016).

40. Wythe, S. E. *et al.* Targeted delivery of cytokine therapy to rheumatoid tissue by a synovial targeting peptide. *Ann. Rheum. Dis.* **72**, 129–135 (2013).

41. Hemmerle, T., Doll, F. & Neri, D. Antibody-based delivery of IL4 to the neovasculature cures mice with arthritis. - SI. *Proc. Natl. Acad. Sci. U. S. A.* **111**, 12008–12 (2014).

42. Kwong, G. A. *et al.* Mass-encoded synthetic biomarkers for multiplexed urinary monitoring of disease. *Nat. Biotechnol.* **31**, 63–70 (2013).

43. Gallagher, S. R. One-dimensional SDS gel electrophoresis of proteins. *Curr. Protoc. Protein Sci.* **1**, (2012).

44. Lawrence, A.-M. & Besir, H. Staining of Proteins in Gels with Coomassie G-250 without Organic Solvent and Acetic Acid. *J. Vis. Exp.* 2–4 (2009). doi:10.3791/1350

45. O'Connell, J. P., Willenbrock, F., Docherty, A. J. P., Eaton, D. & Murphy, G. Analysis of the role of the COOH-terminal domain in the activation, proteolytic activity, and tissue inhibitor of metalloproteinase interactions of gelatinase B. *J. Biol. Chem.* **269**, 14967–14973 (1994).

Supporting information

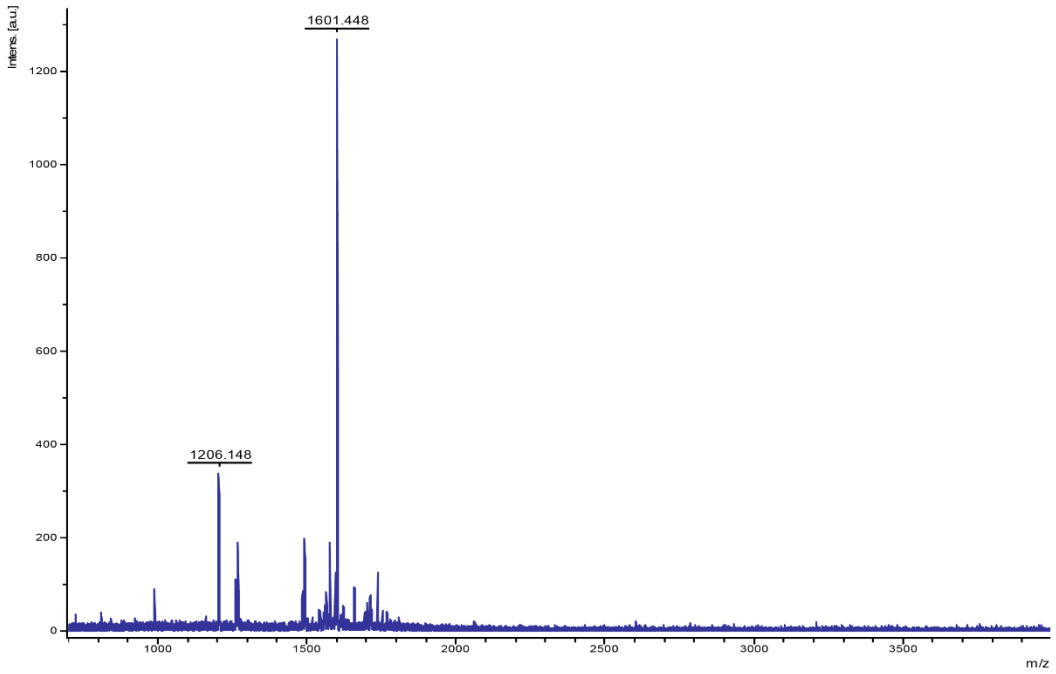

Fig. SI 12 MALDI-MS analysis of N_3-L-PSL-TG peptide: observed average mass 1601.448 Da, calculated average mass 1602.805 Da.

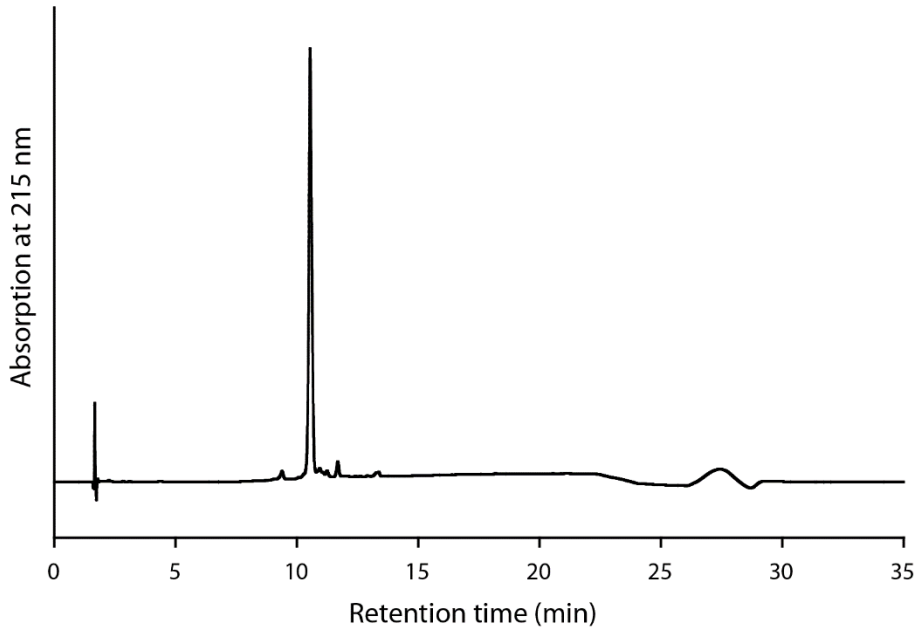

Fig. SI 1 HPLC purity analysis of N_3-L-PSL-TG peptide. Zorbax 300SB-CN column, equilibrated with water and ACN (95:5 v/v). Linear gradient 5 - 95% ACN, 5%/min, flow rate 1 ml/min. All solvents contained 0.1% TFA. The peptide elutes with a retention time of 13.65 min

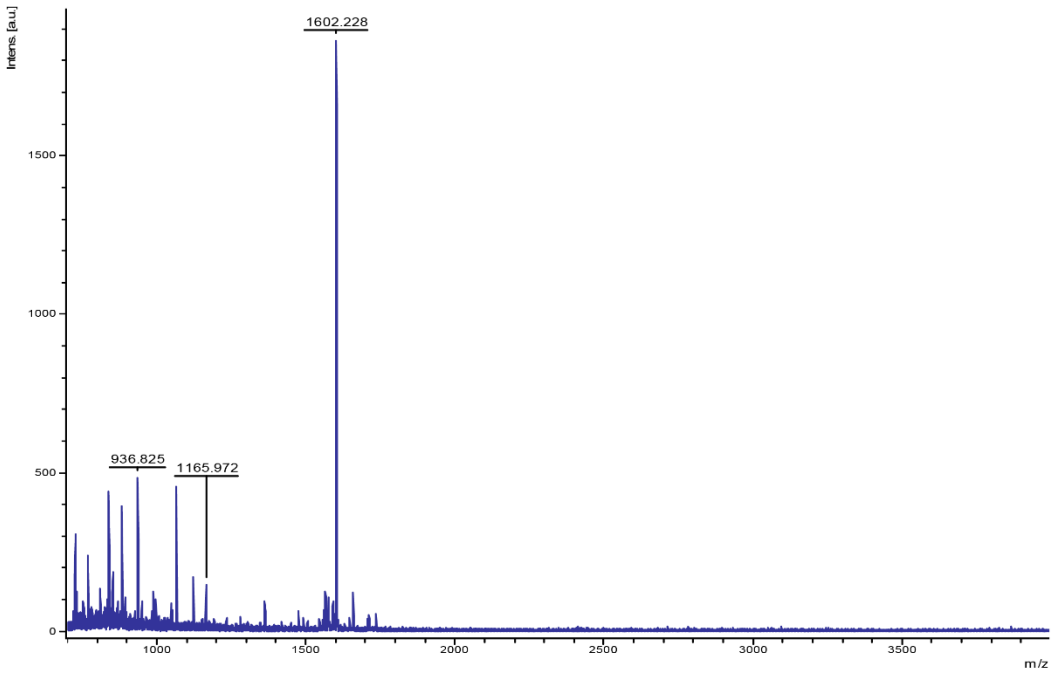

Fig. SI 2 MALDI-MS analysis of N_3-D-PSL-TG peptide: observed average mass 1602.228 Da, calculated average mass 1602.805 Da.

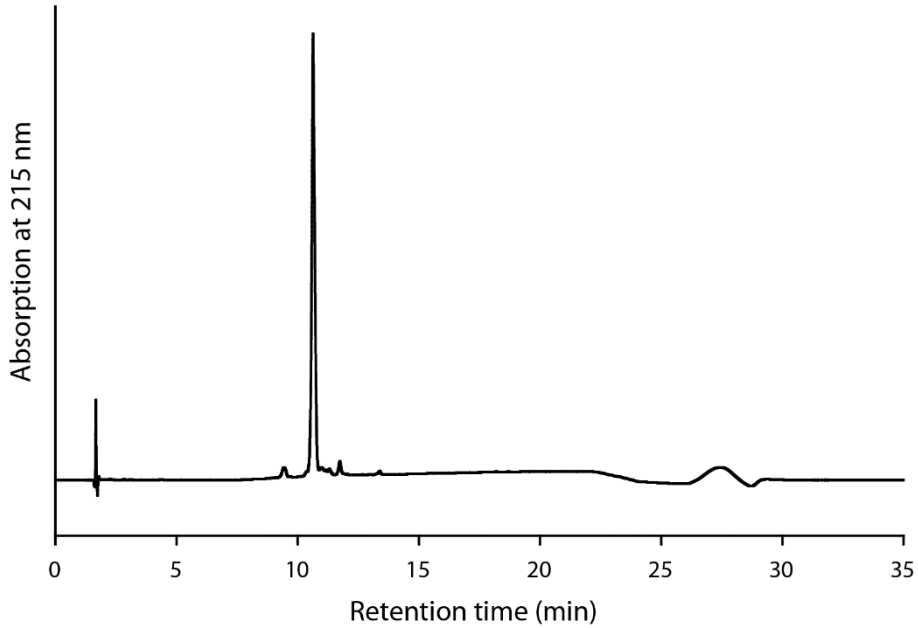

Fig. SI 3 HPLC purity analysis of N_3-D-PSL-TG peptide. Zorbax 300SB-CN column, equilibrated with water and ACN (95:5 v/v). Linear gradient 5 - 95% ACN, 5%/min, flow rate 1 ml/min. All solvents contained 0.1% TFA. The peptide elutes with a retention time of 13.65 min.

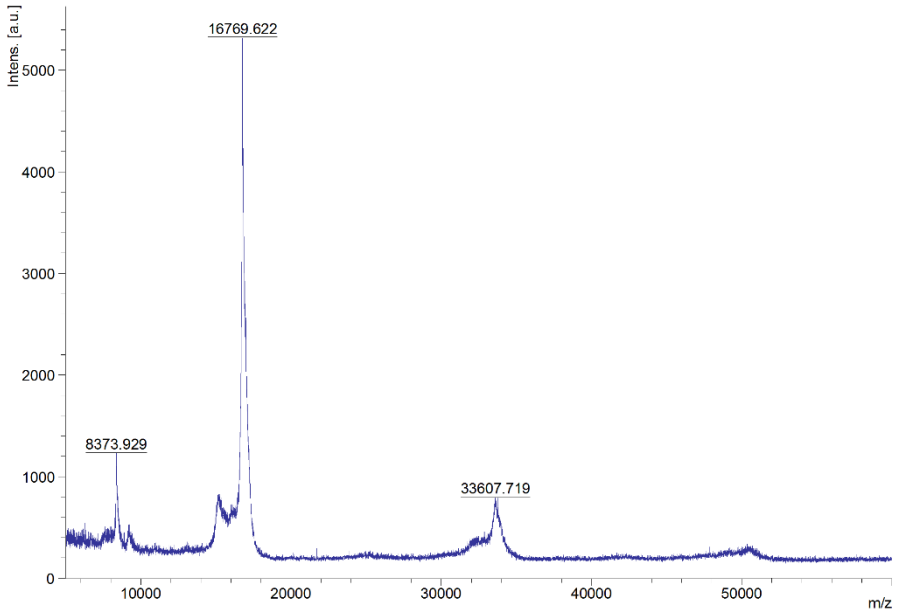

Fig. SI 4 MALDI-MS analysis of IL4-L-PSL-TG conjugate: observed average mass 16769.622 Da, calculated average mass 16642.047 Da (oxidized cysteines).

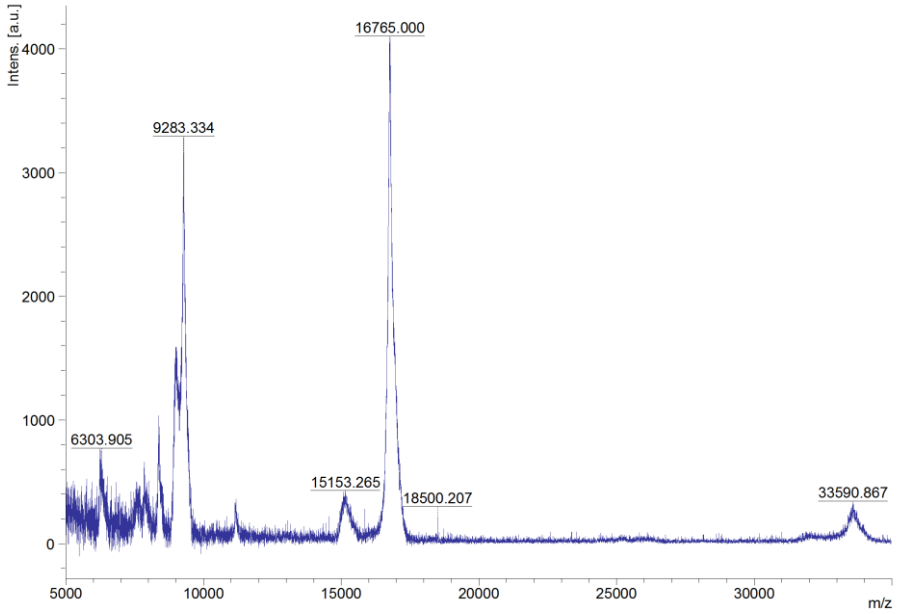

Fig. SI 5 MALDI-MS analysis of IL4-D-PSL-TG conjugate: observed average mass 16765.000 Da, calculated average mass 16642.047 Da (oxidized cysteines)

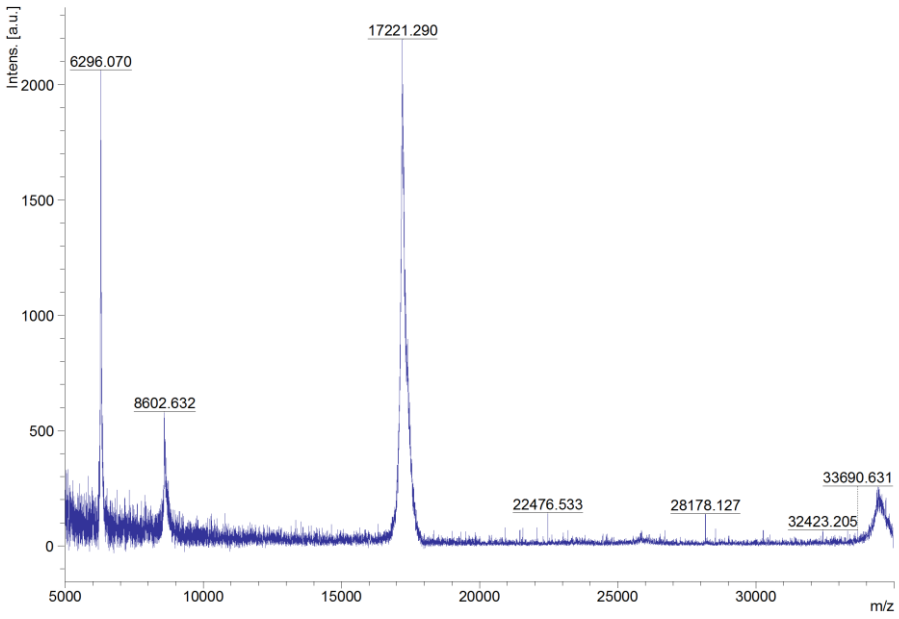

Fig. SI 6 MALDI-MS analysis of IL4-PSL-TG: observed average mass 17221.290 Da, calculated average mass 17220.697 Da (oxidized cysteines).

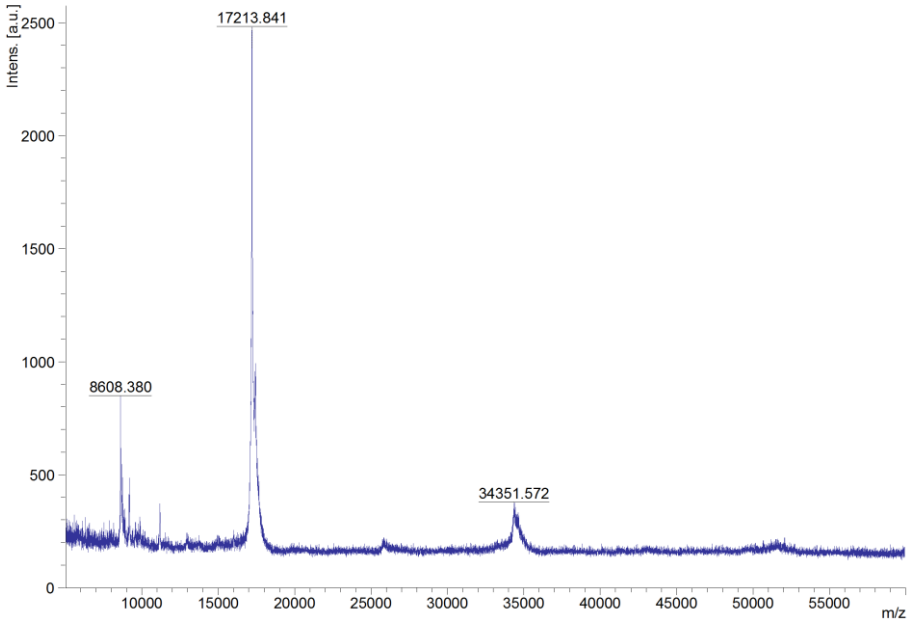

Fig. SI 7 MALDI-MS analysis of IL4-PSL(scrambled)-TG: observed average mass 17213.841 Da, calculated average mass 17220.697 Da (oxidized cysteines).

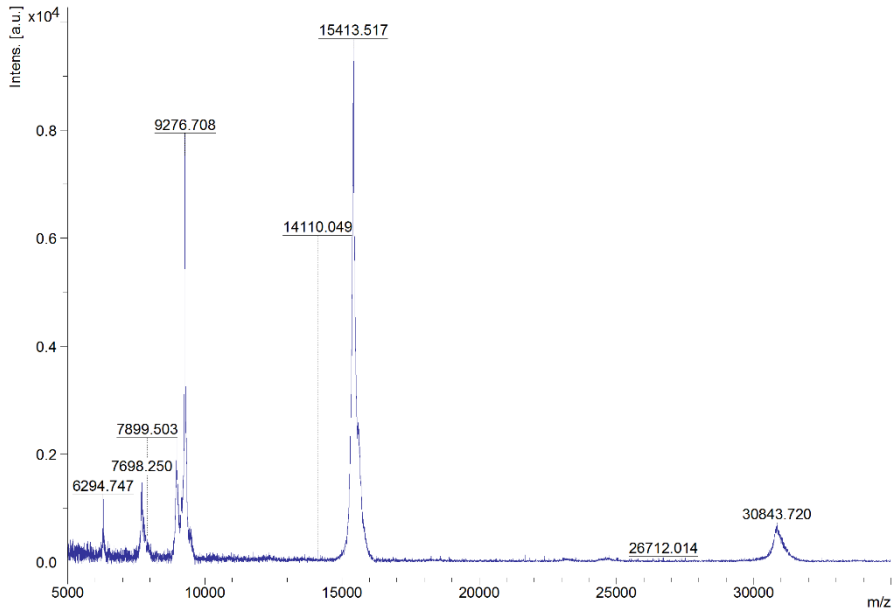

Fig. SI 8 MALDI-MS analysis of IL4-PSL(cut); observed average mass 15413.517 Da, calculated average mass 15427.731 Da (oxidized cysteines).

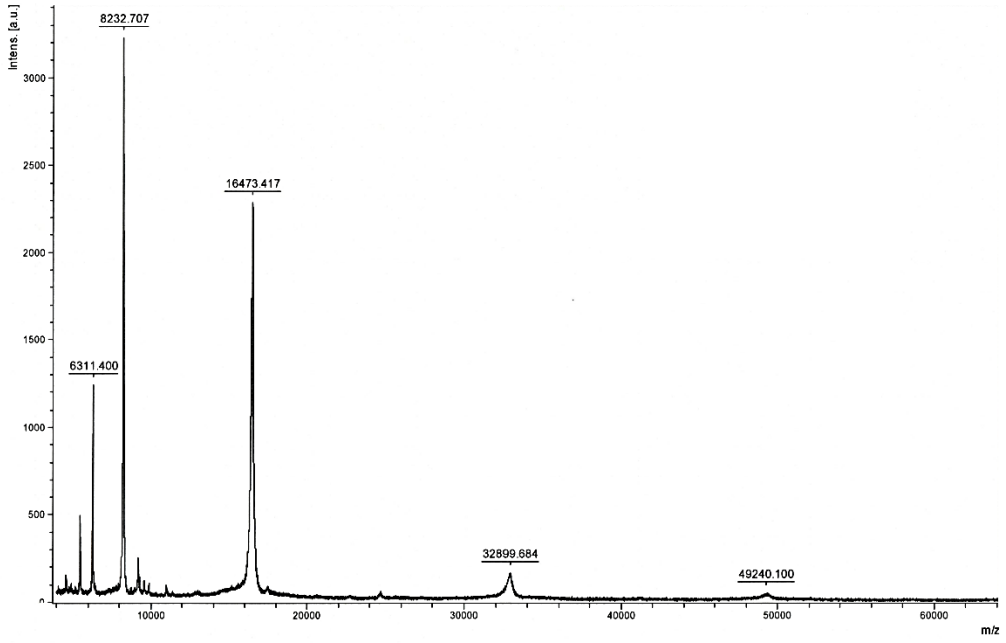

Fig. SI 9 MALDI-MS analysis of TG-IL4 fusion protein: observed average mass 16473.417 Da, calculated average mass 16824.189 Da (oxidized cysteines).

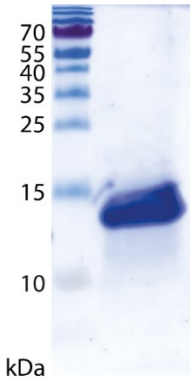

Fig. SI 10 SDS-PAGE analysis of purified TG-IL4 fusion protein. Left lane: molecular-weight marker (PageRuler Prestained Protein Ladder, 10 to 180 kDa; Thermo Fisher Scientific, Darmstadt, Germany), Right lane: TG-IL4 fusion protein (17.0 kDa).

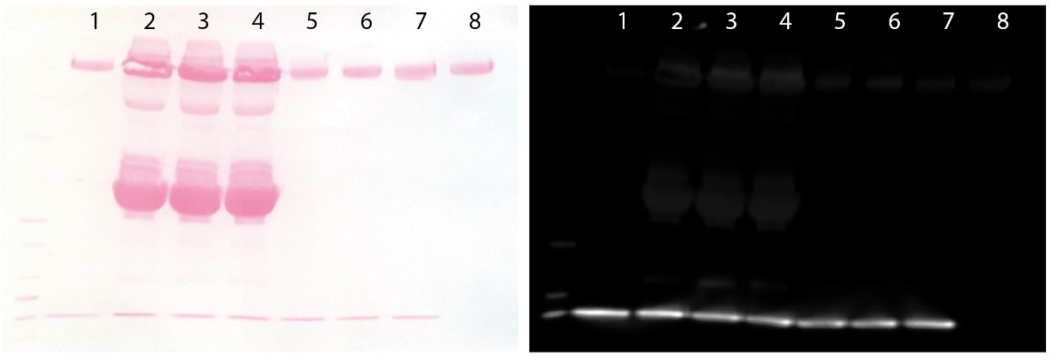

Fig. SI 11 Western blot analysis of FXIIIa mediated bioconjugation of TG-IL4 fusion with fibronectin. TG-IL4 fusion protein was incubated with fibronectin and FXIIIa (rFXIIIa (Zedira, Darmstadt, Germany): lane 1, 5, 6; activated Fibrogammin (CSL Behring, Marburg, Germany): lane 2, 3, 4) at 37 °C for 0.5 h, 1 h or 2 h respectively. Controls: lane 7 w/o FXIIIa, lane 8: w/o FXIIIa & w/o IL4. Samples were run on a 5-20% SDS-PAGE gradient gel and transferred to a nitrocellulose membrane. Protein transfer was detected using Ponceau S staining (left) and IL4 was detected using antibody staining (right).

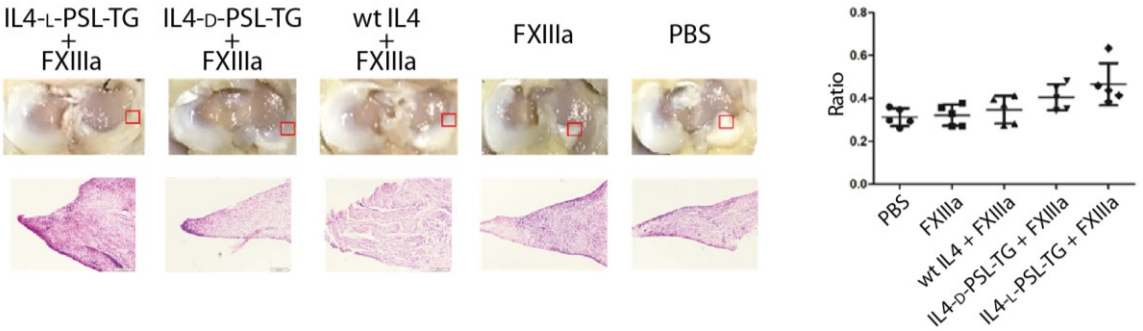

Fig. SI 12 Meniscus. Left: Gross view and histological sections. Right: Scoring.

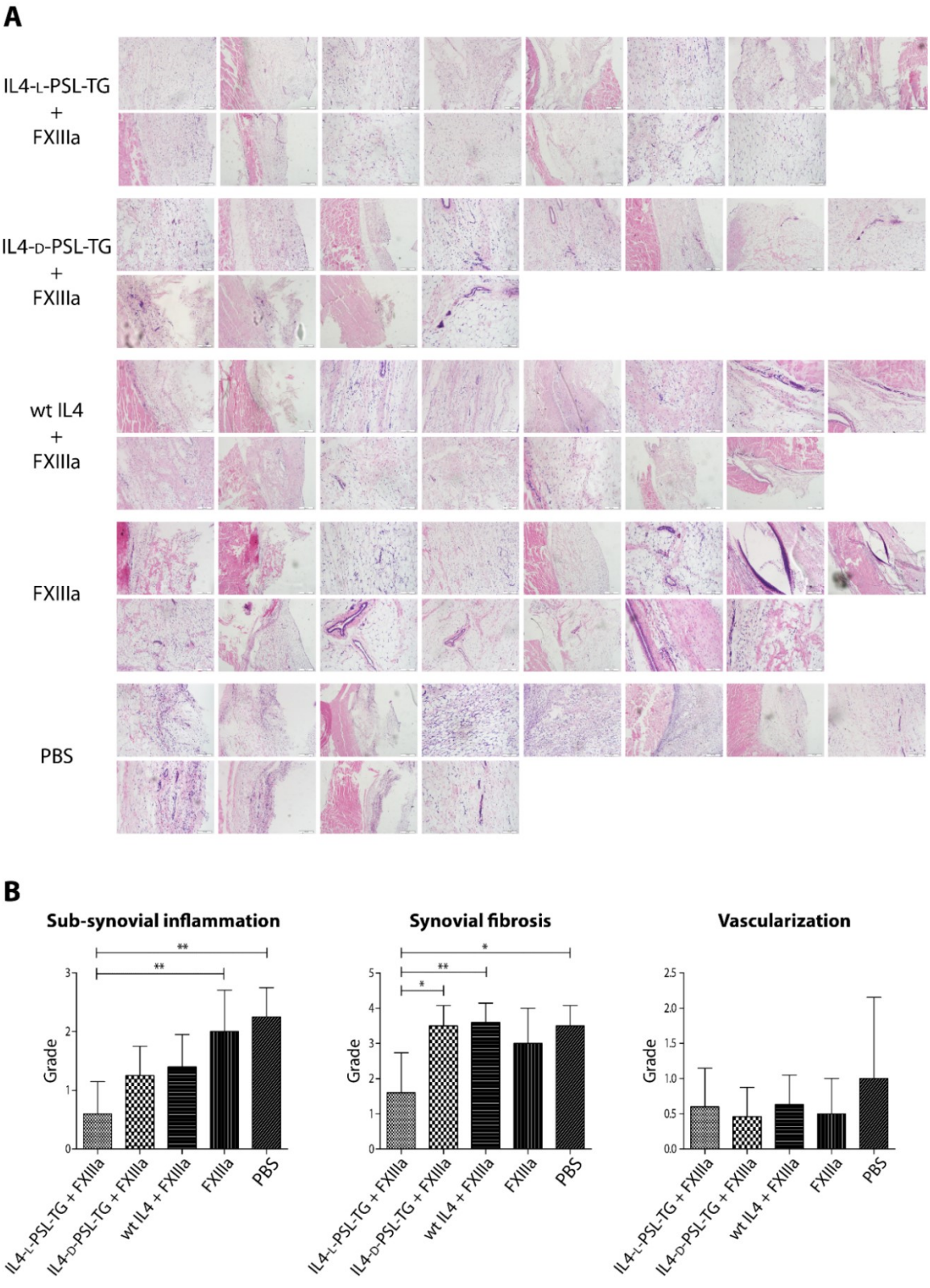

Fig. SI 13 Histological evaluation of the patellar tendon. A) Histological sections. B) Scoring.

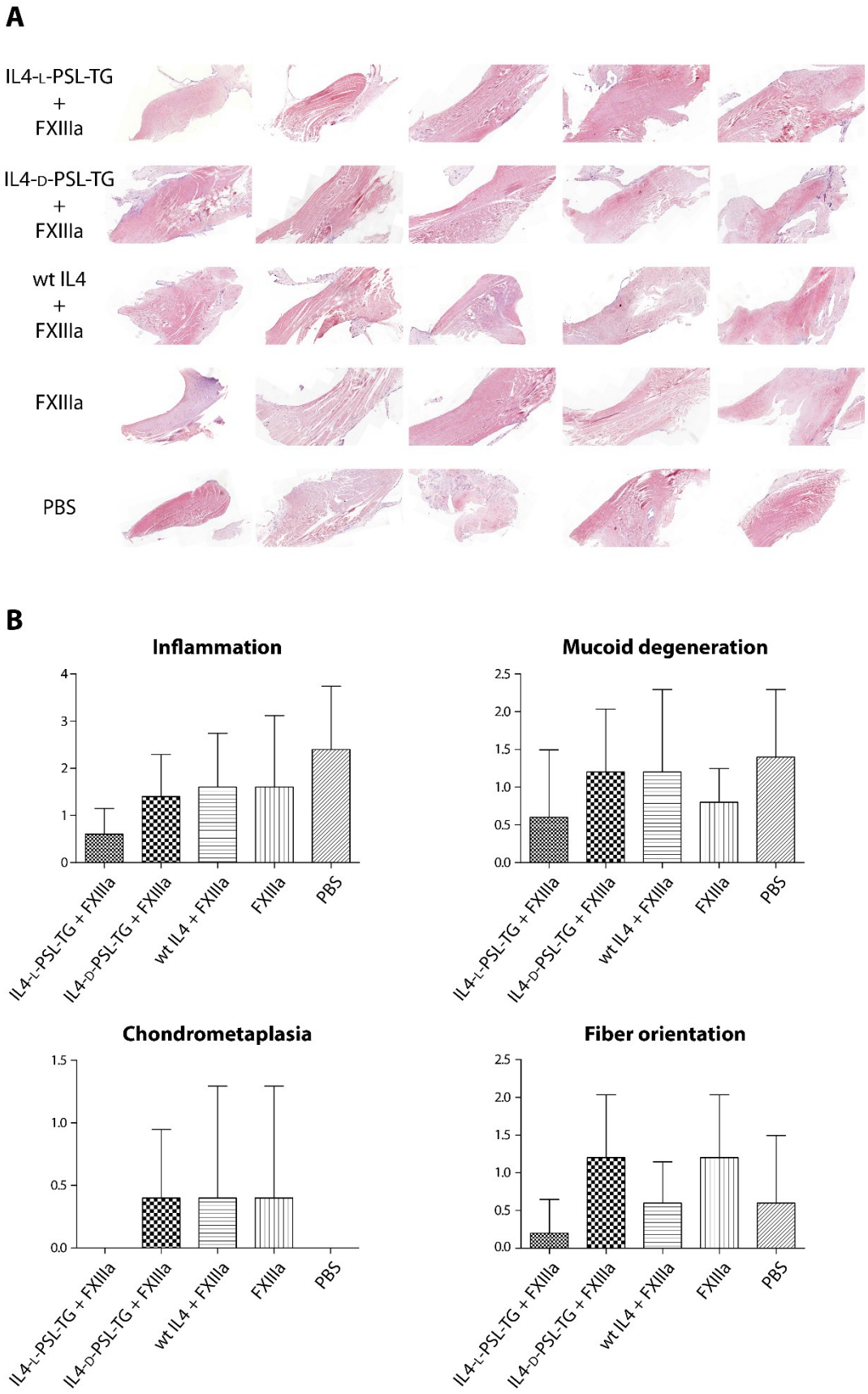

Fig. SI 14 Histological evaluation of the anterior cruciate ligament (ACL). A) Histological sections. B) Scoring.

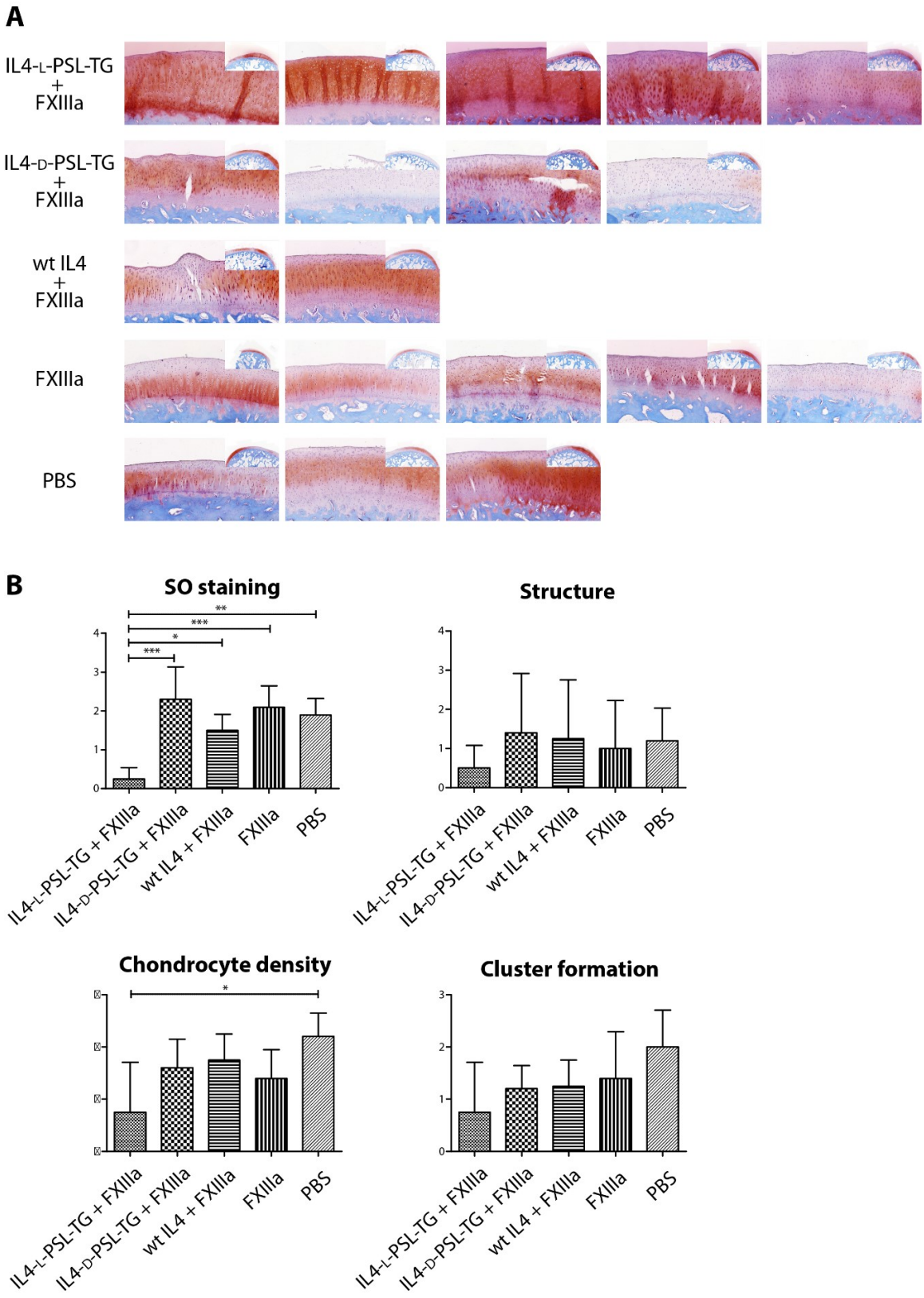

Fig. SI 15 Histological evaluation of cartilage. A) Histological section (SO staining). B) Scoring.

Chapter 4: Improved interleukin-4 fusion proteins for bioresponsive depot formation

Valerie Spieler[1], Katharina Güntzel[1], Tessa Lühmann[1], Lorenz Meinel[1]

[1] Institute for Pharmacy and Food Chemistry, University of Würzburg, 97074 Würzburg, Germany

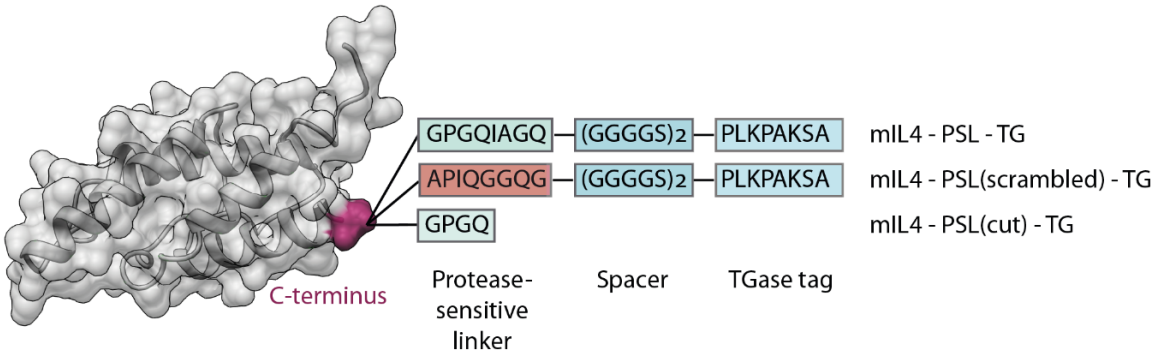

Unpublished manuscript

Introduction

In chapter 3, we emulated the natural storage and release strategy for cytokines and growth factors in the ECM[1] to create a bioresponsive IL4 depot for the treatment of inflammatory diseases with minimally invasive administration regimens. In this first study, human IL4 was conjugated with a bifunctional peptide which contained a sequence for immobilization on the extracellular matrix via a transglutaminase and a sequence for bioresponsive release by upregulated matrix metalloproteinases during inflammation. One of the challenges with this approach was the production of the cytokine conjugate. Incorporation of an unnatural amino acid into the protein, separate synthesis of the bifunctional peptide as well as conjugation by click chemistry resulted in a low overall yield. Therefore, we established an improved version of this system by genetically fusing the bifunctional peptide via a flexible, 12-amino-acid spacer to murine IL4. While human IL4 loses activity when C-terminally elongated, the activity of murine IL4 is not affected by the modification. The second generation murine IL4 fusion protein presented here possesses wild type bioactivity while effectively binding to in vitro grown extracellular matrix in presence of TGase. The protease-sensitive linker is selectively recognized and cleaved by MMPs, liberating intact and active IL4. Murine IL4 offers the possibility to test the bioresponsive cytokine depot in several mouse models, which was not possible with human IL4 due to species selectivity.[7] The availability of better animal models will help us to deepen our understanding of how to best combine cytokine, protease-sensitive linker and immobilization tag to tackle different inflammatory diseases.

Results

Design, production and characterization of interleukin-4 fusion proteins

To simplify the production process of the IL4-PSL-TG constructs and expand the application towards mouse models, a second generation of the system was designed as fusion proteins. While human interleukin-4 is susceptible to C-terminal fusion (see chapter 3), murine IL4 can be C-terminally modified without influence on its bioactivity. Therefore, mIL4 was genetically fused with a spacer sequence ($(GGGGS)_2$), the protease-sensitive linker (GPGQIAGQ), and the TG tag (PLKPAKSA)(Fig.). The flexibility of the spacer sequence should allow better access of enzymes to the peptide tag, the FXIIIa substrate sequence enables immobilization on extracellular matrix molecules and the intervening protease-

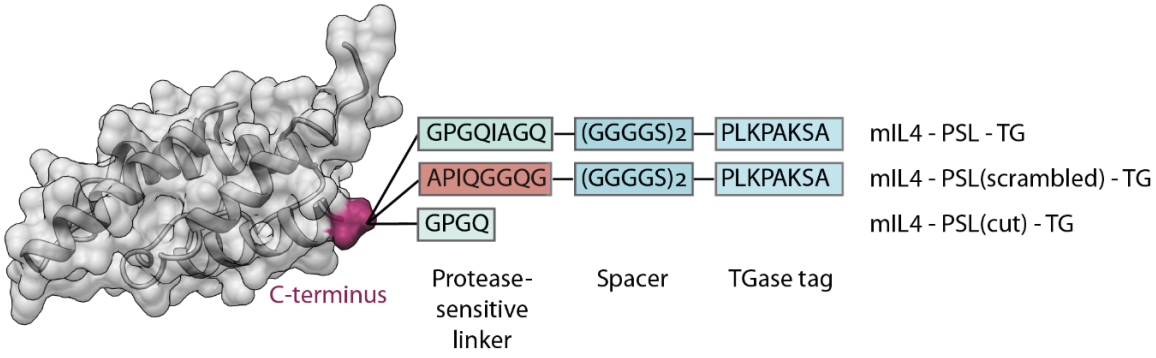

Fig. 1 Schematic structure of the mIL4-PSL-TG fusion protein and the control proteins (mIL4-PSL(scrambled)-TG: non-cleavable, mIL4-PSL(cut): "pre-cut", non-immobilizable). Molecular graphics were created with Chimera.[2]

sensitive linker allows release of IL4 by MMPs to facilitate diffusion. A scrambled and a pre-cut version of the protease-sensitive linker serve as a non-cleavable or non-immobilizable control, respectively.

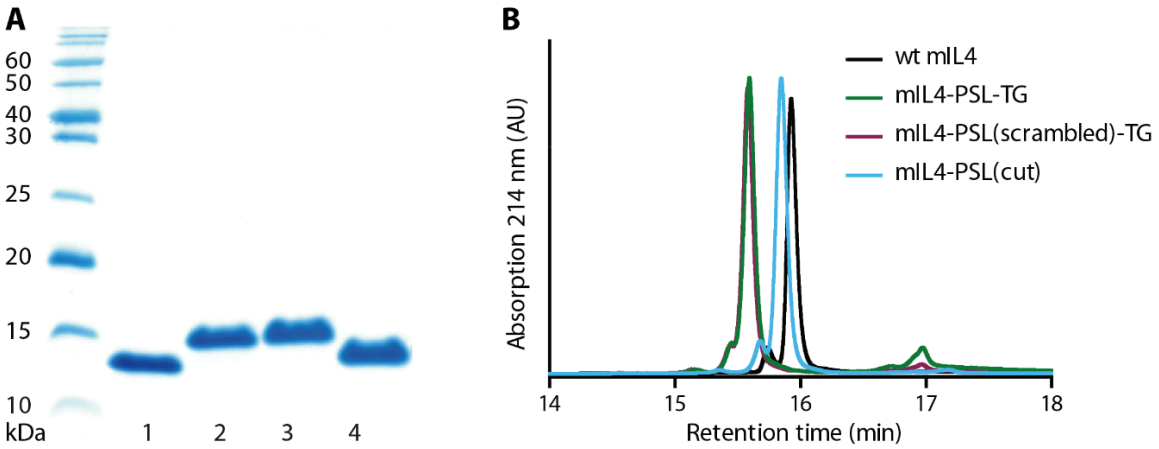

Fig. 2 Characterization of purified mIL4 fusion proteins. **(A)** SDS-PAGE (Molecular-weight marker (PageRuler Unstained Broad Range Protein Ladder, 5 to 250 kDa; Thermo Fisher Scientific, Darmstadt, Germany); 1, wild type IL4 (13.8 kDa); 2, IL4-PSL-TG (15.8 kDa); 3, IL4-PSL(scrambled)-TG (15.8 kDa); 4, IL4-PSL(cut) (14.0 kDa). **(B)** Reversed phase chromatography profile of purified IL4 fusion proteins in comparison to wt IL4.

All fusion proteins were expressed in *E. coli*, refolded from inclusion bodies and purified by two rounds of cation exchange chromatography. Purity of all IL4 variants was assessed by SDS-PAGE and RP-HPLC (Fig. 2). All proteins showed single bands of the expected size in the SDS-PAGE (wt IL4: 13.8 kDa, IL4- PSL-TG: 15.8 kDa, IL4-PSL(scrambled)-TG: 15.8 kDa, IL4-PSL(cut): 14.0 kDa) and were >95% pure, although the variants featuring a TG tag showed a second peak in the RP-HPLC analysis. The correct mass of the IL4 fusion proteins was confirmed by MALDI-MS (Fig. SI - Fig. SI 4).

Characterization of the IL4 depot system in vitro

Bioactivity of IL4 variants

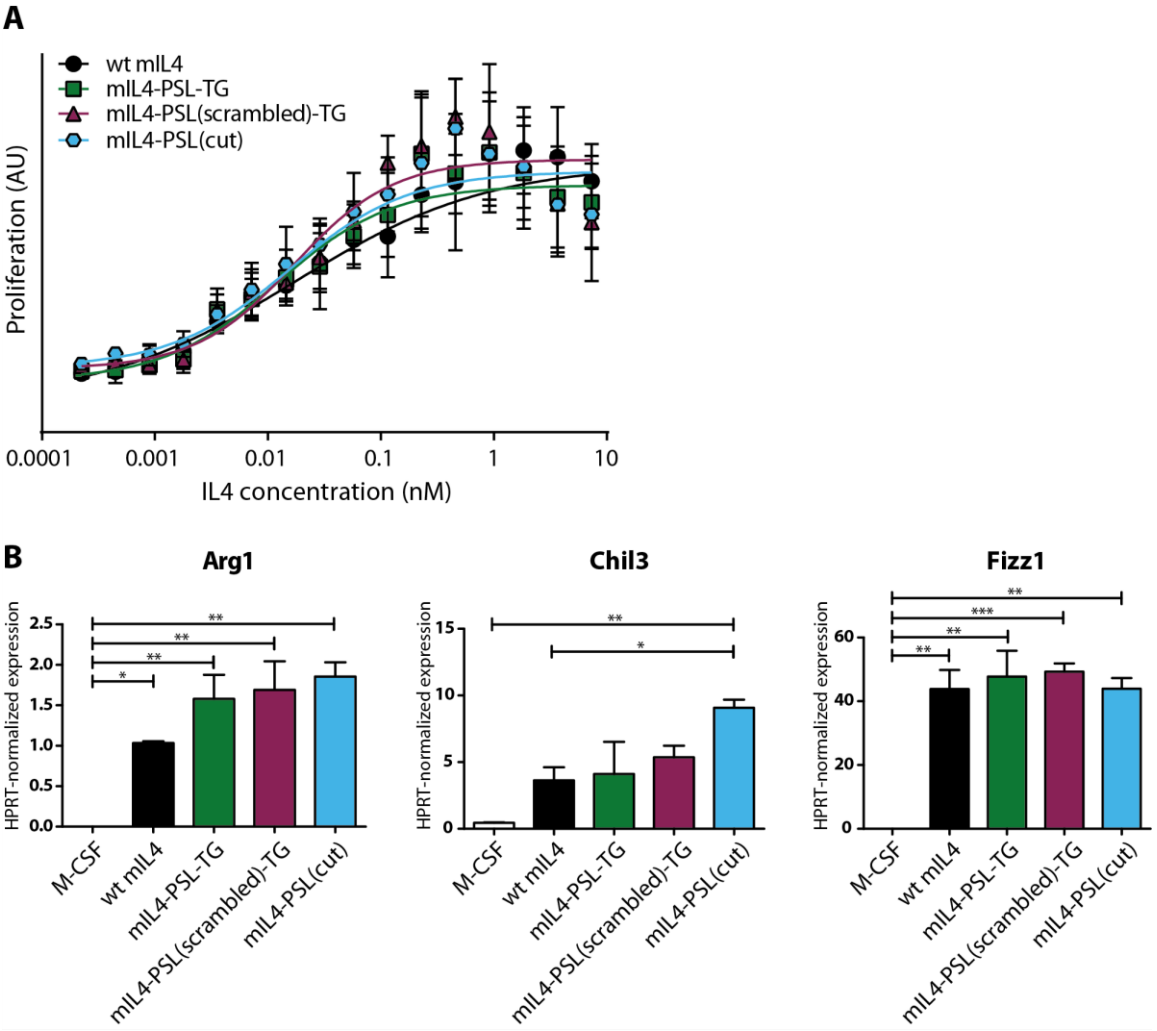

Fig. 3 Bioactivity of IL4 variants **(A)** Proliferation assay of IL4-PSL-TG-fusion proteins. Different concentrations of mIL4-PSL-TG-fusion proteins were incubated with murine HT2 clone A5E cells and proliferation was assessed after 24 h using WST-1 reagent. EC_{50} values: wt IL4 0.017 nM, IL4-PSL-TG 0.012 nM, IL4-PSL(scrambled)-TG 0.017 nM, IL4-PSL(cut) 0.016 nM. **(B)** qPCR analysis of macrophage polarization by murine IL4 variants in comparison to wild type IL4 (expression normalized to HPRT, polarization normalized to M-CSF induced macrophages).

The bioactivity of the different IL4 fusion proteins was measured via proliferative response of HT2 clone A5E cells in vitro and compared to that for wild type IL4 to assess the influence of the C-terminal fusion of the PSL-TG tag on the cytokine. Proliferation of HT2 A5E cells was induced by all four evaluated mIL4 variants and fell within a 30% range (EC_{50} values: wt mIL4 0.017 nM, mIL4-PSL-TG 0.012 nM, mIL4-PSL(scrambled)-TG 0.017 nM, mIL4-PSL(cut) 0.016 nM)(Fig. 3A).

IL4 exerts its positive effects mainly by polarizing macrophages towards an anti-inflammatory phenotype. The ability of the IL4 fusion proteins to polarize macrophages was

analyzed in a primary cell culture system of murine bone-marrow-derived monocytes (BMDMs)(Fig. 3B). Macrophage polarization after incubation with IL4 fusion proteins was evaluated by qPCR using different M2 gene expression markers compared to hypoxanthine guanine phosphoribosyltransferase (HPRT) expression. Cells incubated with M-CSF only were used for normalization, while wild type IL4 served as positive control. The macrophage polarization assay shows that the bioactivity of the modified IL4 variants is in the same range as wild type IL4.

Cleavage of the PSL results in a short peptide tag of four amino acids remaining attached to the IL4 molecule, which was simulated with mIL4-PSL(cut). Both bioactivity assays show that the residual amino acids do not interfere with the biologic activity of the cytokine.

Characterization of the protease-sensitive linker

The protease sensitive linker (PSL) fused to the cytokine facilitates the release of IL4 from the ECM by MMP activity. To quantify the MMP concentration required for efficient cleavage of the IL4-PSL-TG fusion proteins, a cleavage study with an equimolar mixture of MMP-1, -8, and -9 was performed at four total concentrations of 1, 3, 8 and 12 nM (Fig. 4A). The IL4-PSL-TG fusion protein had cleavage rates of less than 10% with the tested MMP concentrations after 24 h incubation time. After 7 days incubation time with a 12 nM MMP mixture approximately 20% were cleaved (Fig. 4B). IL4-PSL(scrambled)-TG was not cleaved. The significantly reduced hydrolysis sensitivity of the fusion protein compared to the stand-alone protease-sensitive peptide linker and the hIL4-PSL-TG conjugate (see chapter 3) is probably related to their tertiary structures. It is possible that the cleavage rate will also differ once the cytokine fusion protein is attached to the ECM.

The levels of active MMPs in synovial fluid differ between patients but are generally in the very low nanomolar range for osteoarthritis.[3–5] These MMP levels should facilitate a long-term release of IL4 from the ECM depot, which is regulated in a negative feedback loop, as IL4 prevents activation of proMMPs.[6] Several new linkers with spacers of different length and different PSL positions were already designed and are currently being tested, to evaluate how the cleavage rate can be influenced and thereby adapted to different disease profiles.

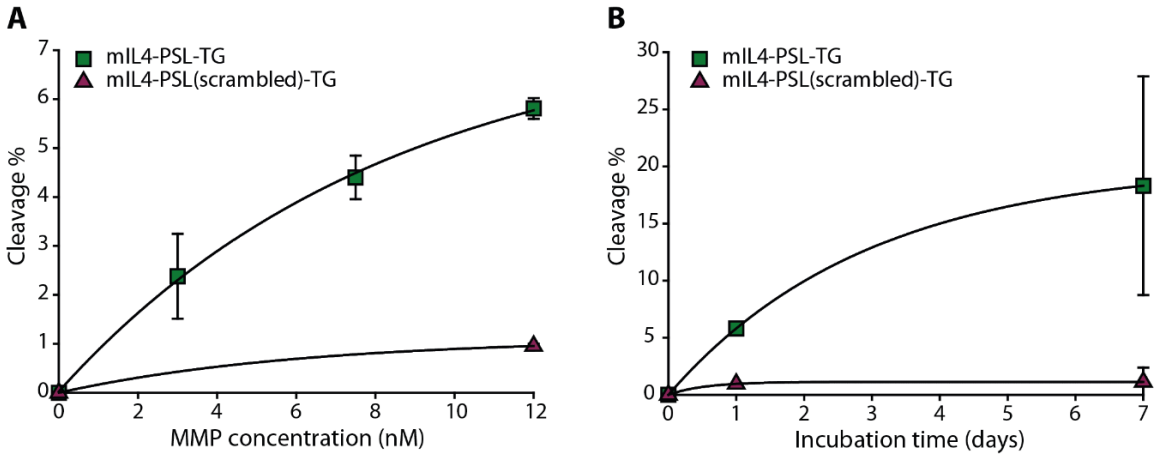

Fig. 4 Cleavage experiment of mIL4-PSL-TG fusion proteins with matrix metalloproteinases. mIL4-PSL-TG and mIL4-PSL(scrambled)-TG were incubated with an equimolar mixture of MMP-1, -8, -9 for 24 h at 37 °C. After inactivation of the enzymes, the reaction was analyzed by reversed phase HPLC and percentage of cleavage was determined by analyzing peak areas. **(A)** IL4-PSL-TG and IL4-PSL(scrambled)-TG were incubated with different concentrations of an equimolar mixture of MMP-1, -8, -9 for 24 h at 37 °C. **(B)** IL4-PSL-TG and IL4-PSL(scrambled)-TG were incubated with an equimolar mixture of MMP-1, -8, -9 (12 nM) for different time spans up to seven days at 37 °C.

Conjugation to cell derived matrices

The IL4-PSL-TG fusion protein was developed to be covalently attached to the ECM in presence of the transglutaminase FXIIIa to build a cytokine depot in the tissue. The bond-formation between the Lys residues in the TGase substrate sequence (PLKPAKSA) of IL4-PSL-TG and the Gln residues of extracellular matrix proteins, was visualized by coimmunostaining followed by confocal laser scanning microscopy (Fig. 5). A strong and defined fluorescence of high-order fibrillar structures was observed after the FXIIIa catalyzed reaction between IL4-PSL-TG or IL4-PSL(scrambled)-TG and cell-derived matrices (CDMs) grown from NIH 3T3 cells. These structures colocalized with antibody-stained fibronectin fibrils. This shows that IL4-PSL-TG and IL4-PSL(scrambled)-TG were effectively conjugated to fibrillar structures within the CDMs in the presence of FXIIIa (Fig. 5), whereas the reaction with IL4-PSL(cut) or without the catalyst showed only weak background fluorescence, demonstrating that the CDMs were selectively decorated by the therapeutic protein via the TG tag and FXIIIa.

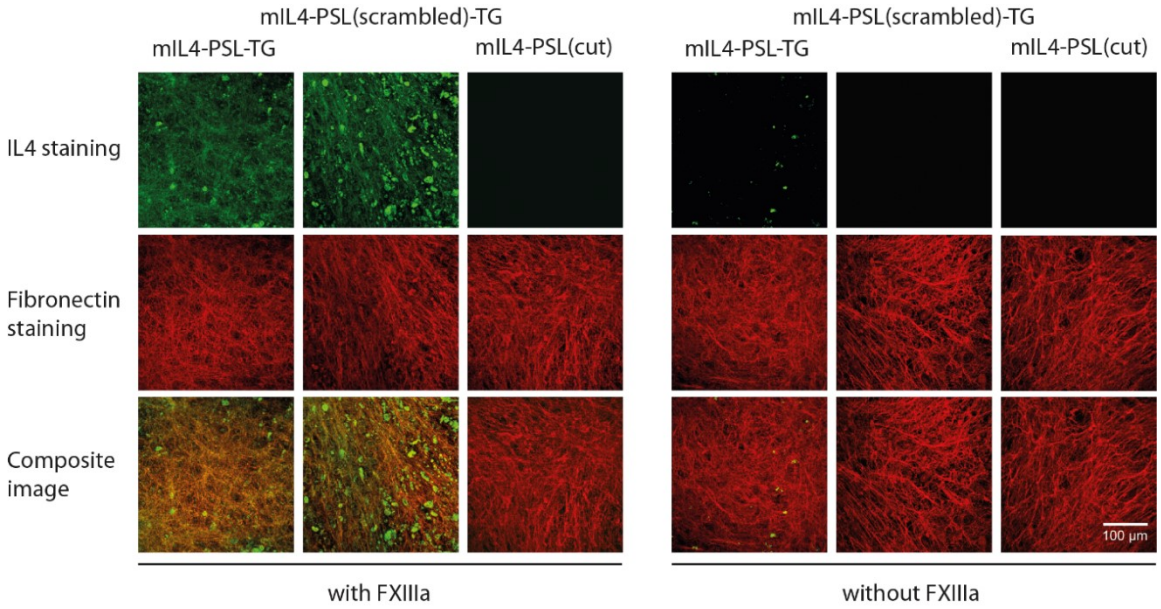

Fig. 5 Confocal microscopy analysis of FXIIIa mediated bioconjugation of mIL4-PSL-TG-fusion proteins with cell derived matrices in vitro. mIL4-PSL-TG-fusion proteins were incubated with cell derived matrices and FXIIIa at 37 °C for 1 h. CDMs were washed thoroughly and stained for mIL4 (green) and fibronectin (red).

Discussion

In this study we present an improved design of the bioinspired cytokine depot system featuring a protease-sensitive linker and a TGase substrate sequence. One of the challenges of the previous study was the production of the hIL4-PSL-TG conjugate. Incorporation of an unnatural amino acid, separate synthesis of the bifunctional peptide as well as conjugation of both by click chemistry resulted in a low overall yield. Therefore, we established the more straightforward, second-generation fusion protein with murine IL4 for easier production. In contrast to human IL4, the bioactivity of murine IL4 is not negatively influenced by C-terminal fusion of the PSL-TG tag-peptide. The in vitro characterization of the fusion proteins show that IL4 remains fully bioactive upon C-terminal fusion with the bifunctional peptide. During incubations with MMPs, the protease-sensitive linker is selectively cleaved, while IL4 remains intact. The cleavage rate is more than 10-fold slower than expected, i.e. compared the cleavage of the PSL peptide without IL4 attached. New designs and combinations of spacer, PSL and TG tag are currently being prepared for testing, to evaluate how the cleavage rate can be influenced by different setups. The IL4 fusion protein was successfully conjugated to cell derived matrices by TGase FXIIIa via the substrate sequence contained in the bifunctional peptide.

The second challenge was the species selectivity of IL4.[7] Human IL4 has no activity in mice, so we had to resort to a rabbit osteoarthritis model in which cartilage destruction is only partially caused by inflammation, but also wear-and-tear, and which additionally suffers from suboptimal availability of antibodies for immunohistochemistry. The new system built on murine IL4 opens the possibility to use the vast number of mouse models of protease-driven inflammatory diseases and to better understand the interplay between cytokine, protease-sensitive linker and TGase tag in different models and stages of disease. We are looking forward to testing the IL4-PSL-TG fusion protein in a mouse model of rheumatoid arthritis, which shows stronger inflammation and invasion by macrophages of the joint than OA and could benefit from IL4 therapy.[8]

In conclusion, we hope to gain better understanding of the effect of the different building blocks of our bioresponsive cytokine depot system with this new approach. The fusion proteins allow for easier modification and production, while using murine IL4 allows for wider testing in better animal models.

Methods

Preparation of interleukin-4 fusion proteins

The DNA fragment encoding for wt murine IL4 was purchased from Eurofins Genomics (Ebersberg, Germany). The DNA fragment was C-terminally elongated with oligonucleotides (Sigma-Aldrich, Schnelldorf, Germany) encoding the different linker variants using Gibson Assembly Master Mix (NEB, Frankfurt a. M., Germany). The cDNAs were inserted into the expression vector pET28b (Novagen, Merck KGaA, Darmstadt, Germany) and transformed into the expression host *E. coli* BL21(DE3).

Bacteria were grown in TB medium plus kanamycin (100 µg/ml) on a rotatory shaker at 37 °C to an optical density of 1.0 and IL4 protein expression was then induced by addition of 1 mM isopropylthiogalactopyranoside (IPTG) for 3 h. The bacteria were sedimented by centrifugation at 5000 g, 15 min at 4 °C and resuspended in 1/200 culture volumes of resuspension buffer (50 mM Tris-HCl pH 8.0, 50 mM NaCl, 1 mM EDTA) and PMSF (final concentration 100 µM) and lysozyme (final concentration 75 µg/ml) were added. The cells were lysed by sonication (Sonopuls HD3100, Bandelin, Berlin, Germany) with the cell suspension cooled on ice. The sediment was resuspended in a quarter volume of the resuspension buffer used above and sonicated again. The insoluble fraction ("inclusion

bodies") was separated by centrifugation and washed once with resuspension buffer plus 1% Triton X-100 and twice with resuspension buffer. The final sediment was kept frozen at temperatures -80 °C

The IL4 protein was extracted from the inclusion bodies using unfolding buffer (50 mM Tris-HCl pH 8.0, 50 mM NaCl, 1 mM EDTA, 5 M guanidine-HCl, 2 mM glutathione reduced, 0.2 mM glutathione oxidized, 9 ml per g wet weight). For refolding of the IL4, the clarified protein extract was diluted with two volumes of refolding buffer (0.5 M arginine, 50 mM Tris-HCl pH 8.0, 50 mM NaCl, 1 mM EDTA, 2 mM glutathione reduced, 0.2 mM glutathione oxidized) and dialyzed against 20 volumes of refolding buffer for 4 h at room temperature. Then, the solution was dialyzed against 40 volumes of 25 mM ammonium acetate pH 5.0 overnight at 4 °C. The solution was clarified by centrifugation, and the supernatant was filtered (0.22 µm) and loaded onto a HiTrap SP XL 5 ml column (GE Healthcare Life Sciences, Freiburg, Germany) that was equilibrated with 25 mM ammonium acetate pH 5.0 (A). The IL4 protein was eluted via a gradient using buffer containing 2 M sodium chloride (B). The peak eluting around 25% B was collected and buffer exchange to A and concentration to 10 ml were achieved via ultrafiltration (cutoff 9 kDa). The process was repeated with two HiTrap SP HP 1 ml columns (GE Healthcare Life Sciences, Freiburg, Germany). Natively folded IL4 eluting as the major peak at 30% B was dialyzed against PBS pH 7.4, frozen in liquid nitrogen and stored in aliquots at -80 °C until further use. Protein concentrations were determined by BCA assay against a BSA standard (Thermo Fisher Scientific, Darmstadt, Germany).

Characterization

SDS-PAGE

Protein samples were analyzed by discontinuous SDS-PAGE under denaturing conditions as described elsewhere.[9] Protein bands were stained with Coomassie Brilliant Blue G-250.[10]

RP-HPLC

Protein purity was assessed by RP-HPLC using a Hitachi LaChrom HPLC system (VWR, Darmstadt, Germany). Approximately 20 µg protein sample was applied to a Zorbax 300SB-CN column (Agilent, Waldbronn, Germany), equilibrated with water containing 0.1 % TFA and acetonitrile (ACN)(VWR, Darmstadt, Germany) containing 0.1% TFA (95:5 v/v).

Proteins were eluted by a linear gradient of 5 - 95% ACN containing 0.1% TFA with a gradient of 5% ACN/min and a flow rate of 1 ml/min. Column temperature was kept at 22 °C and UV absorbance was monitored at 214 nm.

MALDI-MS

Protein samples were desalted using Ziptip C18 pipette tips (Merck Millipore, Darmstadt, Germany) following the manufacturer's instructions. Matrix-assisted laser desorption ionization (MALDI-MS) spectra were acquired in the linear positive mode with an Autoflex II LRF instrument (Billerica, MA, USA). Mass spectra were calibrated externally with the Protein Calibration Standard I (Bruker Daltonics; Billerica, MA, USA), containing insulin, ubiquitin, myoglobin and cytochrome C.

HT2 clone A5E proliferation assay (murine interleukin-4)

HT2 clone A5E cells (92021401, ECACC, Salisbury, UK) were maintained in T75 flasks in growth medium (RPMI-1640 containing 10% heat-inactivated FCS, 0.05 mM β-mercaptoethanol, 100 IU/ml murine IL2, penicillin G (100 U/ml) and streptomycin (100 mg/ml) at 37 °C and 5% CO_2.

For the proliferation assay, HT2 cells were seeded in a 96-well plate at 50,000 cells/well in growth medium without IL2, but supplemented with a dilution series of IL4 variants, ranging from 0.05 to 100 ng/mL, respectively. After stimulation for 20 h, 10 µl of WST-1 (Roche, Mannheim, Germany) per well were added and the cells were incubated for 2-4 h at 37 °C. The absorbance of the soluble formazan product was determined at 450 nm using a Spectramax 250 microplate reader (Molecular Devices, Sunnyvale, CA, USA). Relative proliferation is expressed in comparison to wild type IL4 (R&D Systems, Wiesbaden, Germany).

Macrophage isolation, polarization and qPCR

Mouse BMDCs were obtained by flushing the femurs, humeri, and tibiae of C57BL/6J mice with PBS. Cells were incubated in Red Blood Cell Lysis Solution (Miltenyi Biotec, Bergisch Gladbach, Germany) and washed with PBS. Cells were seeded in 6-well plates at 3.6 million

cells/well in 2 ml WTM medium containing mM-CSF (45% F12 (Invitrogen 21765-037), 45% DMEM (Invitrogen 31885-049), 10% FCS (amimed 2-01F10-I), 40 ng/ml mM-CSF).

For in vitro stimulation of mouse macrophages 1.428 nM of each mIL4 variant was added to the cells on day 4 without removing the medium. On day 7, floating cells were removed, adherent cells were washed with PBS and harvested with 700 µl TRIzol reagent (Invitrogen, Karlsruhe, Germany) for RNA isolation according to the manufacturer's instructions.

cDNA was prepared using the SuperScript™ III First-Strand Synthesis System (Invitrogen, Karlsruhe, Germany). A QuantStudio 7 Flex System (Applied Biosystems) was used for quantitative PCR. The results are presented as relative quantification versus the basal condition using the comparative Ct method. Expression of all genes was measured using Taqman gene assays kits (Applied Biosystems) (Table SI 2).

MMP cleavage

Pro-MMPs (MMP-1, MMP-8 and MMP-9)(EMD Millipore, Billerica, USA) were activated with 4-aminophenylmercuric acetate (APMA) as described before.[11]

IL4 was dialyzed against MMP buffer (200 mM NaCl, 50 mM Tris-HCl, 5 mM $CaCl_2$, 1 µM $ZnCl_2$, pH 6.8–7.0) prior to cleavage experiments. For MMP concentration-dependent cleavage of IL4 variants, 20 µg IL4 were incubated with the MMP mixture (as described above) in 50 µl reaction volume at 37 °C for 24 h / 48 h. Protease activity was stopped with 10 mM EDTA. For the time-dependent cleavage profile, IL4 was incubated with 12 nM MMP mix and the reaction was stopped after 0 h, 24 h and 7 days. For each measured time point, a control of protein in MMP buffer without MMPs was incubated under the same conditions to exclude unspecific degradation. The samples were analyzed by RP-HPLC using a Hitachi LaChrom HPLC system (VWR, Darmstadt, Germany) or an Agilent 1260 Infinity II HPLC system with a Zorbax 300SB-CN column (Agilent, Waldbronn, Germany), equilibrated with water containing 0.1 % TFA and acetonitrile (ACN)(VWR, Darmstadt, Germany) containing 0.1% TFA (95:5 v/v). Proteins were eluted by a linear gradient of 5 - 95% ACN containing 0.1% TFA with a gradient of 5% ACN/min and a flow rate of 1 ml/min. Column temperature was kept at 22 °C and UV absorbance was monitored at 214 nm.

Conjugation with cell-derived matrices

Cell-derived matrices (CDMs) were produced as described in [12]. In short, NIH 3T3 fibroblasts (CRL-1658; ATCC, Manassas, VA, USA) were seeded (16.7x104 cells/ml, 300 µl growth medium per well) in in gelatin-coated NuncTM Lab-TekTM II Chamber SlideTM System 8 wells using growth medium (DMEM containing heat-inactivated BCS (10%), penicillin G (100 U/ml), streptomycin (100 mg/ml)) and incubated at 37 °C with 5% CO_2 for 24 h. After that the medium was changed every 24 h using growth medium supplemented with sodium L-ascorbate (50 µg/ml) for 6 days. CDMs were isolated by removing the cells with water, Triton-X- ammonia buffer and washing with PBS.

For the FXIIIa catalyzed reaction, the CDMs were incubated with 20 µg IL4 in the presence of 10 U/ml FXIIIa in 200 µl TBS with 5 mM $CaCl_2$ at 37 °C for 1 h. Afterwards the CDMs were washed with 25 mM ammonium acetate pH 5.0 with 1 M NaCl and TBST and blocked with Roti®-Block. The CDM was visualized by detecting fibronectin using a combination of rabbit anti-fibronectin antibody (F3648; Sigma-Aldrich, St. Louis, MO, USA)(1:500 in PBS, overnight at 4 °C) and goat anti-rabbit IgG-AF633 (A-21070; Thermo Fisher Scientific, Darmstadt, Germany) (1:200 in PBS, 90 min at RT). IL4 was detected using rat anti-mIL4 antibody (ab11524, Abcam, Cambridge, UK)(1:500 in PBS, overnight 4 °C) and goat anti-rat IgG-AF488 (A-11006; Thermo Fisher Scientific, Darmstadt, Germany)(1:200 in PBS, 90 min at RT). Analysis was performed on a high-resolution AOBS SP2 confocal laser scanning microscope (Leica Microsystems, Wetzlar, Germany) with a 63x N.A. 1.4-0.60 Oil I BL HCX PL APO I objective. To avoid cross talk the emission signals were collected independently. Images were processed using ImageJ (http://imagej.nih.gov/ij/).

Material

All reagents were obtained from Sigma Aldrich unless stated otherwise.

References

1. Robertson, I. B. *et al.* Latent TGF-β-binding proteins. *Matrix Biol.* **47,** 44–53 (2015).
2. Pettersen, E. F. *et al.* UCSF Chimera - A visualization system for exploratory research and analysis. *J. Comput. Chem.* **25,** 1605–1612 (2004).
3. Heard, B. J. *et al.* Matrix metalloproteinase protein expression profiles cannot distinguish between normal and early osteoarthritic synovial fluid. *BMC Musculoskelet. Disord.* **13,** 126 (2012).
4. Tchetverikov, I. *et al.* MMP protein and activity levels in synovial fluid from patients with joint injury, inflammatory arthritis, and osteoarthritis. *Ann. Rheum. Dis.* **64,** 694–698 (2005).
5. Yoshihara, Y. *et al.* Matrix metalloproteinases and tissue inhibitors of metalloproteinases in synovial fluids from patients with rheumatoid arthritis or osteoarthritis. *Ann. Rheum. Dis.* **59,** 455–61 (2000).
6. Van Lent, P. L. E. M., Holthuysen, A. E. M., Slöetjes, A., Lubberts, E. & Van Den Berg, W. B. Local overexpression of adeno-viral IL-4 protects cartilage from metallo proteinase-induced destruction during immune complex-mediated arthritis by preventing activation of pro-MMPs. *Osteoarthr. Cartil.* **10,** 234–243 (2002).
7. Mueller, T. D., Zhang, J. L., Sebald, W. & Duschl, A. Structure, binding, and antagonists in the IL-4/IL-13 receptor system. *Biochim. Biophys. Acta - Mol. Cell Res.* **1592,** 237–250 (2002).
8. Kinne, R. W., Bräuer, R., Stuhlmüller, B. & Palombo-Kinne, Ernesta Burmester, G.-R. Macrophages in rheumatoid arthritis. *Arthritis Res 2002* (2000).
9. Gallagher, S. R. One-dimensional SDS gel electrophoresis of proteins. *Curr. Protoc. Protein Sci.* **1,** (2012).
10. Lawrence, A.-M. & Besir, H. Staining of Proteins in Gels with Coomassie G-250 without Organic Solvent and Acetic Acid. *J. Vis. Exp.* 2–4 (2009). doi:10.3791/1350
11. O'Connell, J. P., Willenbrock, F., Docherty, A. J. P., Eaton, D. & Murphy, G. Analysis of the role of the COOH-terminal domain in the activation, proteolytic activity, and tissue inhibitor of metalloproteinase interactions of gelatinase B. *J. Biol. Chem.* **269,** 14967–14973 (1994).
12. Gutmann, M., Braun, A., Seibel, J. & Lühmann, T. Bioorthogonal Modification of Cell Derived Matrices by Metabolic Glycoengineering. *ACS Biomater. Sci. Eng.* **4,** 1300–1306 (2018).

Supporting information

Amino acid sequences

Wild type IL4

```
        10          20          30          40          50          60
MAHIHGCDKN HLREIIGILN EVTGEGTPCT EMDVPNVLTA TKNTTESELV CRASKVLRIF

        70          80          90         100         110         120
YLKHGKTPCL KKNSSVLMEL QRLFRAFRCL DSSISCTMNE SKSTSLKDFL ESLKSIMQMD

YS
```

IL4-PSL-TG

```
        10          20          30          40          50          60
MHIHGCDKNH LREIIGILNE VTGEGTPCTE MDVPNVLTAT KNTTESELVC RASKVLRIFY

        70          80          90         100         110         120
LKHGKTPCLK KNSSVLMELQ RLFRAFRCLD SSISCTMNES KSTSLKDFLE SLKSIMQMDY

       130         140
SGPQGIAGQG GGGSGGGGSP LKPAKSA
```

IL4-PSL(Scrambled)-TG

```
        10          20          30          40          50          60
MHIHGCDKNH LREIIGILNE VTGEGTPCTE MDVPNVLTAT KNTTESELVC RASKVLRIFY

        70          80          90         100         110         120
LKHGKTPCLK KNSSVLMELQ RLFRAFRCLD SSISCTMNES KSTSLKDFLE SLKSIMQMDY

       130         140
SAPIQGGQGG GGGSGGGGSP LKPAKSA
```

IL4-PSL(cut)

```
        10          20          30          40          50          60
MHIHGCDKNH LREIIGILNE VTGEGTPCTE MDVPNVLTAT KNTTESELVC RASKVLRIFY

        70          80          90         100         110         120
LKHGKTPCLK KNSSVLMELQ RLFRAFRCLD SSISCTMNES KSTSLKDFLE SLKSIMQMDY

SGPQG
```

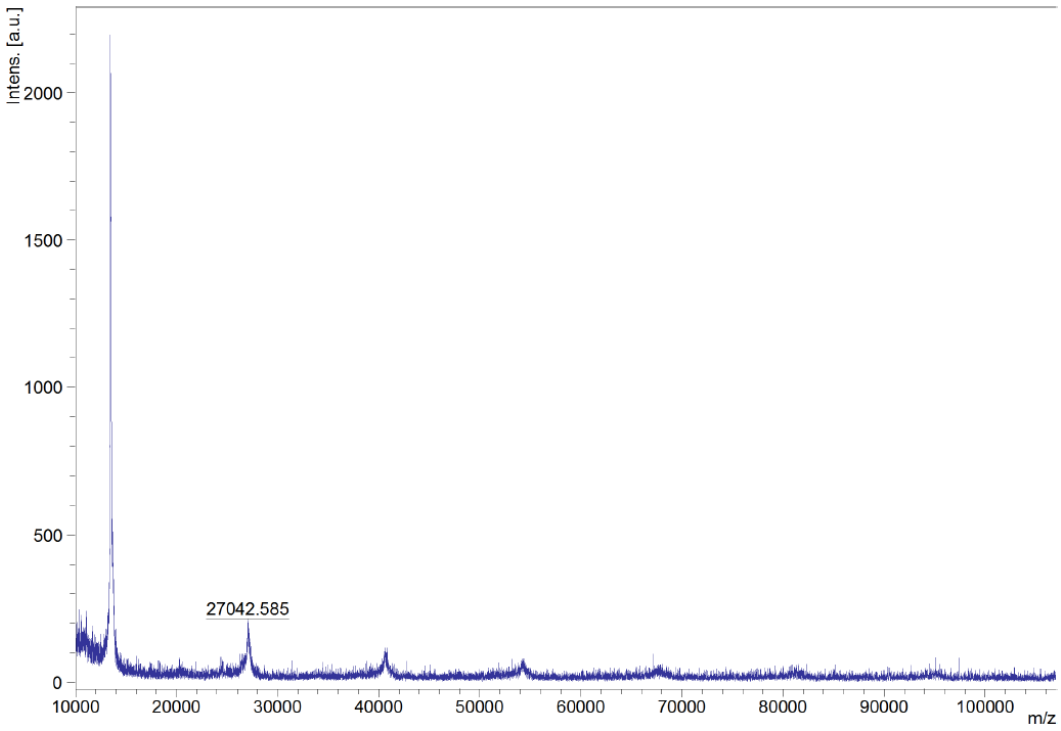

Fig. SI 1 MALDI-MS analysis of wt mIL4: observed average mass 13658.167 Da, calculated average mass 13622.801 Da (oxidized cysteines, without N-terminal methionine).

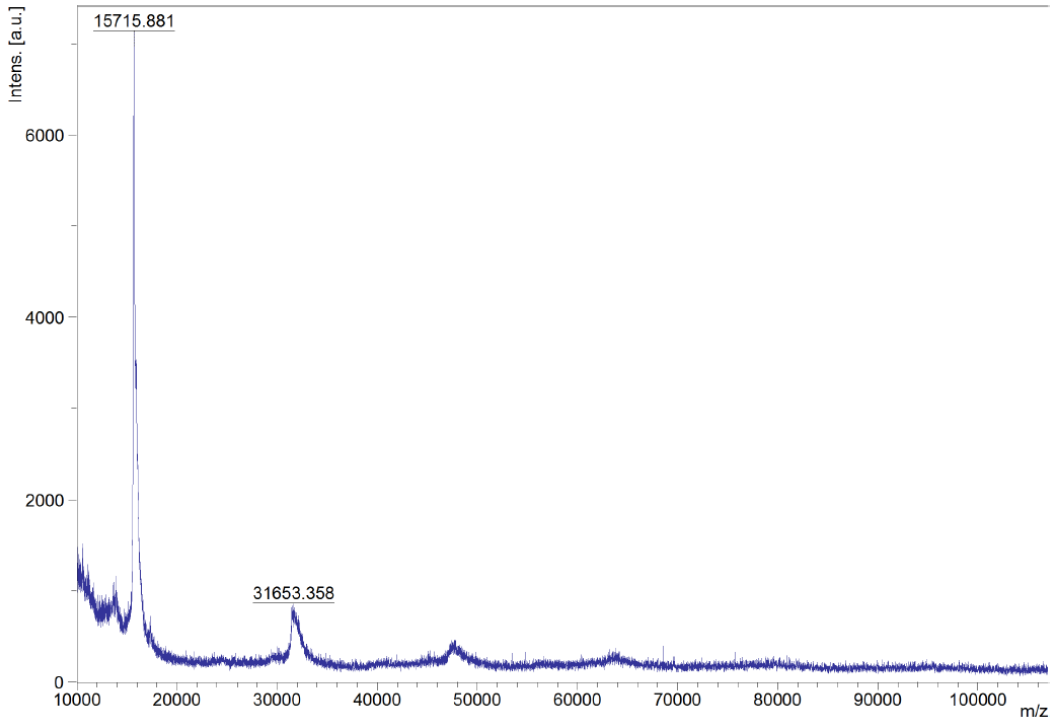

Fig. SI 2 MALDI-MS analysis of mIL4-PSL-TG: observed average mass 15715.881 Da, calculated average mass 15815.235 Da (oxidized cysteines).

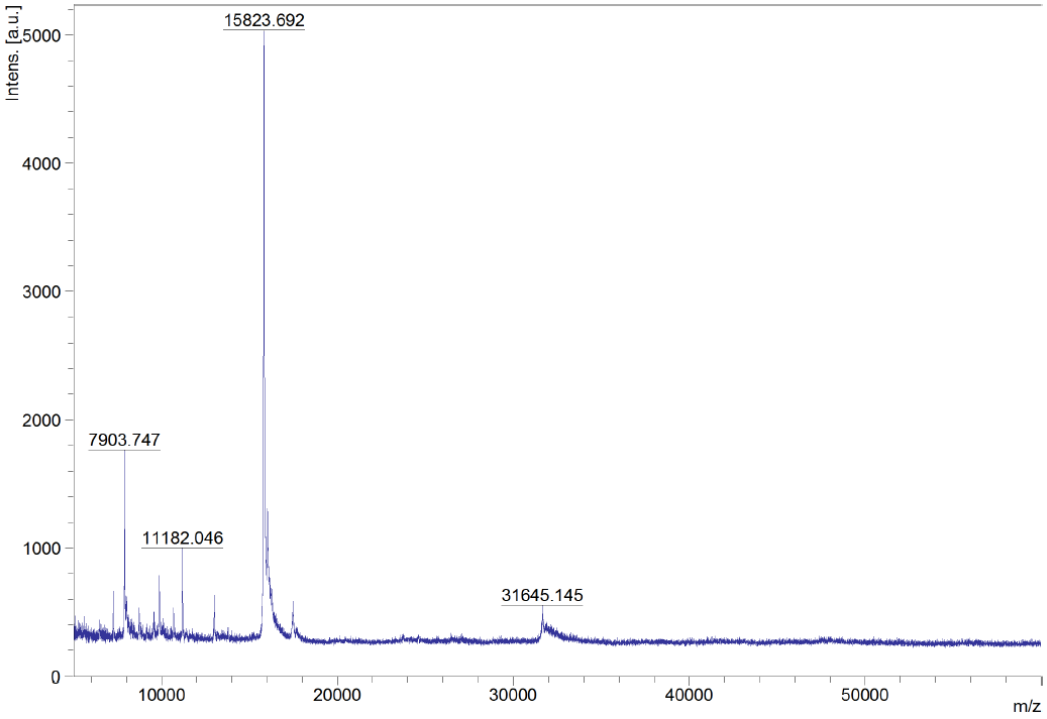

Fig. SI 3 MALDI-MS analysis of mIL4-PSL(scrambled)-TG: observed average mass 15823.692 Da, calculated average mass 15815.235 Da (oxidized cysteines).

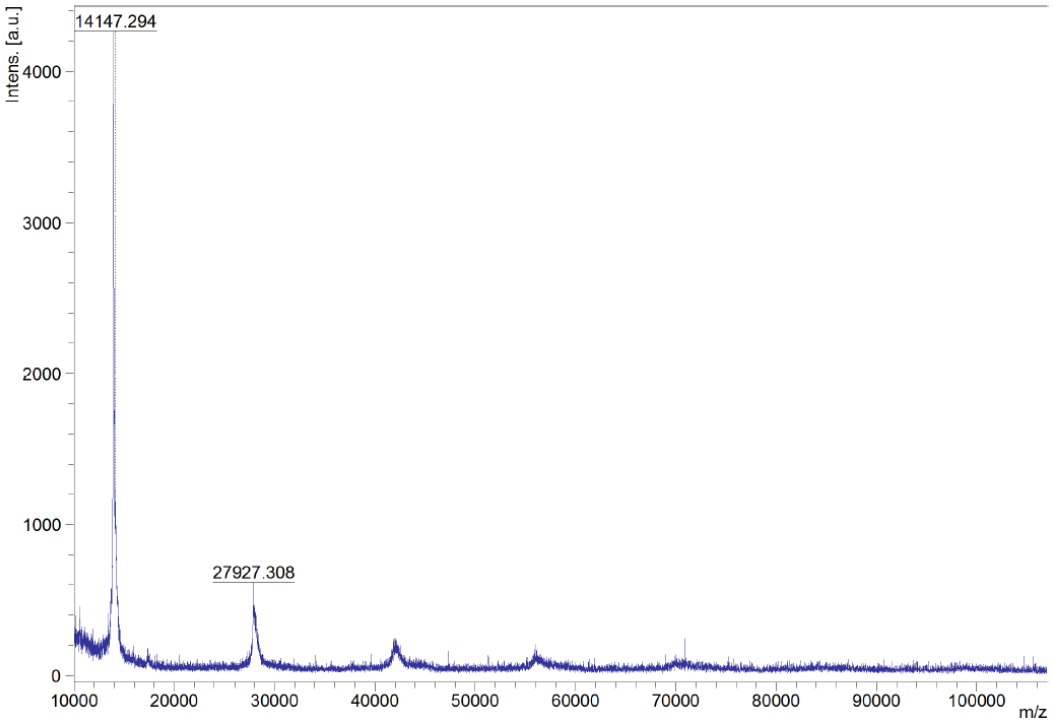

Fig. SI 4 MALDI-MS analysis of mIL4-PSL(cut); observed average mass 14147.294 Da, calculated average mass 14028.27Da (oxidized cysteines).

Table SI 2 qPCR probes

Gene Symbol	Gene Name	Assay ID
HPRT	hypoxanthine guanine phosphoribosyl transferase	Mm00446968_m1
Fizz1	resistin like alpha	Mm00445109_m1
Maoa	monoamine oxidase A	Mm00558004_m1
Chil3	chitinase-like 3	Mm00657889_mH
Arg1	arginase, liver	Mm00475988_m1

Chapter 5: IL4 conjugation with PEG-folate for improved targeting of activated macrophages

Valerie Spieler[1], Marie-Gabrielle Ludwig[2], Martina Raschig[1], Amanda Littlewood-Evans[2], Janet Dawson[2], Bruno Tigani[2], Tessa Lühmann[1], Lorenz Meinel[1]

[1] Institute for Pharmacy and Food Chemistry, University of Würzburg, Würzburg, Germany

[2] Novartis Institutes for BioMedical Research, Novartis Pharmaceuticals AG, Basel, Switzerland

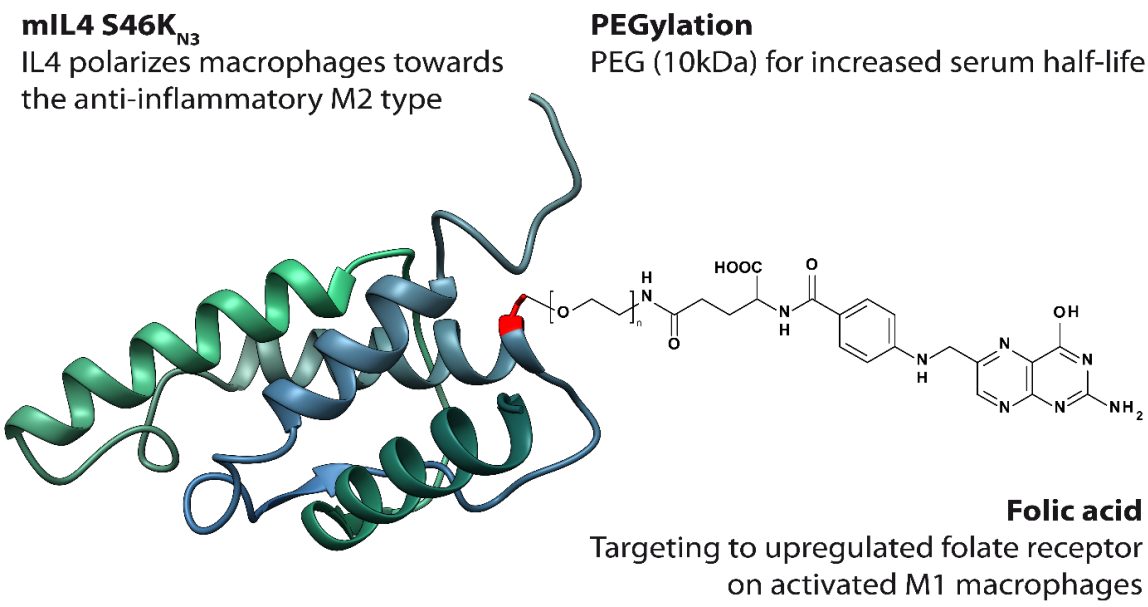

Unpublished manuscript

Abstract

Anti-inflammatory cytokines are a promising class of therapeutics for treatment of rheumatoid arthritis but are limited by their rapid clearance and dose-limiting toxicity. To increase the half-life and specifically target activated macrophages at disease sites, we have engineered a novel IL4 variant using the incorporation of an unnatural amino acid to modify the cytokine with a PEG-folate attachment. The bioactive cytokine conjugate has a high serum stability and the PEGylation confers a half-life of 4 h in vivo. Surprisingly, the folate moiety is not necessary to achieve a targeting effect to inflamed joints in an antigen-induced arthritis (AIA) mouse model. In this particular case, the targeting seems to be mediated by the cytokines itself. Then again, the modular nature of the IL4 conjugate would facilitate an easy adaption of the PEG chain length and targeting moiety to further improve the half-life and targeting function.

Introduction

Rheumatoid arthritis is the most common inflammatory arthritis and is a major cause of disability, affecting about 24.5 million people in 2015.[1] This systemic disease is characterized by infiltration of activated immune cells into the synovial membrane, leading to inflammation and bone and cartilage degradation.[2] Although unlikely to be the initiators, macrophages are critically involved in the pathogenesis of RA, as the degree of synovial macrophage infiltration correlates with the degree of joint erosion.[3] Activated M1 type macrophages overexpress and release pro-inflammatory cytokines, chemokines, matrix degrading enzymes, prostaglandins and reactive oxygen species (ROS), which can aggravate or accelerate damage to the tissue.[4] Depleting the inflamed tissues from macrophages or re-polarizing these into other phenotypes than M1, may therefore provide therapeutic benefit for affected joints in RA.[4] These macrophages present in inflamed RA joints express a folate receptor (FR) which is rather restricted to this pathophysiologically compromised tissue (and malignant cells) as well as physiologically found in normal kidney cells. This particular receptor allows selective targeting of folate-functionalized therapeutic agents to activated macrophages.[5] Interleukin-4 (IL4) is a pleiotropic T-cell derived cytokine with disease-modifying potential in relevant animal model systems of rheumatoid arthritis.[6–11] IL4 polarizes macrophages towards the anti-inflammatory M2 type[12] protecting against cartilage destruction during experimental arthritis regulating matrix metalloproteinases (MMP) and inhibiting pro-inflammatory interleukin-1 mRNA levels in the synovium.[7,10,13]

Unfortunately, the therapeutic value of IL4 is curtailed by improper pharmacokinetics (PK) and side effects when given systemically.[14–17] We are addressing these challenges by developing a PEGylated IL4 variant (accommodating for the improper PK properties[18]) with a folate moiety for targeting of activated M1 macrophages such as present in RA joints (to rapidly channel IL4 from the systemic circulation into the target tissue, thereby limiting systemic exposure and side effects). For that, we expressed in *E. coli* a murine IL4 mutein featuring an azide-bearing unnatural amino acid suitable for site-directed conjugation by strain-promoted alkyne-azide cycloaddition (SPAAC), refolded it from inclusion bodies and conjugated it with a DBCO-PEG-folate. The insertion site was analogous to the human IL4 variant we published before.[19,20] The PEGylated IL4 conjugate was active, stable in serum and had a half-life of around 4 hours in healthy mice. Following the NIR-labeled cytokine conjugate in an antigen-induced arthritis (AIA) mouse model showed targeting of IL4-PEG-folate to the inflamed knee joint. Unexpectedly, the targeting effect was exceeded by IL4-PEG, which was originally designed to be the negative control.

Results

Design, preparation and characterization of IL4 S46Alk

The first step in creating a novel IL4 variant for site-directed bioconjugation with DBCO-PEG-folate was to identify a position for the incorporation of an unnatural amino acid which enables bioorthogonal click reactions via its azido functionality while retaining the bioactivity of the IL4 mutein at wild type level. We started off with the human IL4 which we recently introduced being wild type active when modified at lysine 42.[20,23] For the murine variant developed here, we identified the analogous site within the murine IL4, which has a sequence similarity of 44%, a different disulfide bridge connectivity [24] and a shortened C-helix[25] as compared to human IL4. Since the 3D structure of murine IL4 is not known, we homology modeled it to a crystal structure of wild type human IL4 (2B8U.pdb)[26] and identified serine 46 of the mouse as being complementary to lysine 42 of human IL4 (Fig. 1).

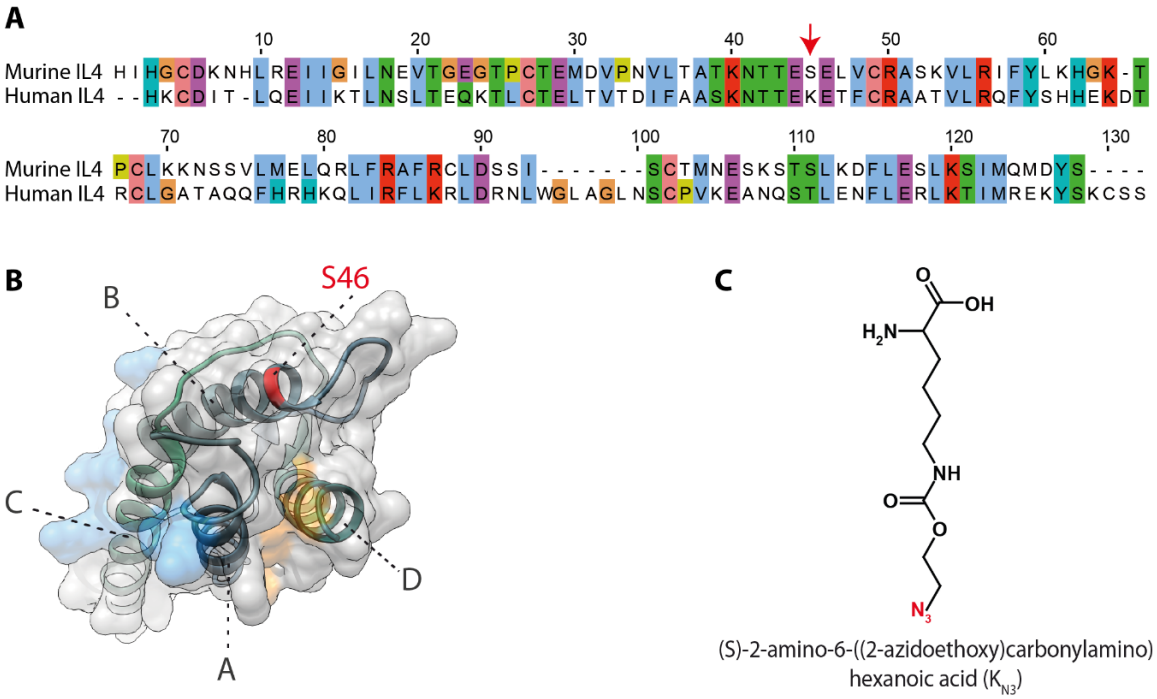

Fig. 1 Modeling of murine IL4. **(A)** Alignment of amino acid sequences of murine IL4 and human IL4 reveals mIL4 S46 as corresponding amino acid to hIL4 K42. Sequence alignment was created with Jalview.[21] **(B)** 3D structure of mIL4 (homology modeled using SWISS MODEL). Position S46, which was chosen to be exchanged for the unnatural amino acid is surface exposed and faces away from the receptor binding interface (indicated in orange and blue). The 4-helix bundle (A, B, C and D) is indicated. Molecular graphics were created with Chimera.[22] **(C)** Unnatural amino acid Alk.

After selection of the incorporation site, we genetically engineered the aliphatic azide (S)-2-amino-6-((2-azidoethoxy) carbonylamino)hexanoic acid (Alk) into mouse IL4. This unnatural amino acid, an azido-functionalized analogue of pyrrolysine, was introduced by genetic codon expansion using a pyrrolysyl-tRNA synthethase/tRNAPyl CUA pair originating from *Methanosarcina barkeri*.[27] Wild type IL4 and IL4 S46Alk were codon optimized to increase expression levels and thereby inclusion body purity (Fig. SI 2). Also, the formation of truncated protein products terminating at the introduced amber codon of IL4 S46Alk was reduced by choosing the right codon optimized sequence ("FF"). Wild type IL4 and IL4 S46Alk were expressed in *E. coli* BL21(DE3), refolded from inclusion bodies and purified by cation exchange chromatography. Purity of both IL4 variants was assessed by SDS-Page and reversed phase HPLC (Fig. 2) and the correct mass of both proteins was confirmed by MALDI-MS analysis (wt mIL4: obs. avg. mass 13658.167 Da, calc. avg. mass 13622.801 Da. mIL4 S46Alk: obs. avg. mass 13785.511 Da, calc. avg. mass 13777.983 Da)(Fig. SI 3, 4). The incorporation site of the unnatural amino acid Alk into IL4 S46Alk was analyzed by NanoLC-MS/MS following elastase digest and the incorporation of Alk at position 46 instead of serine was confirmed.

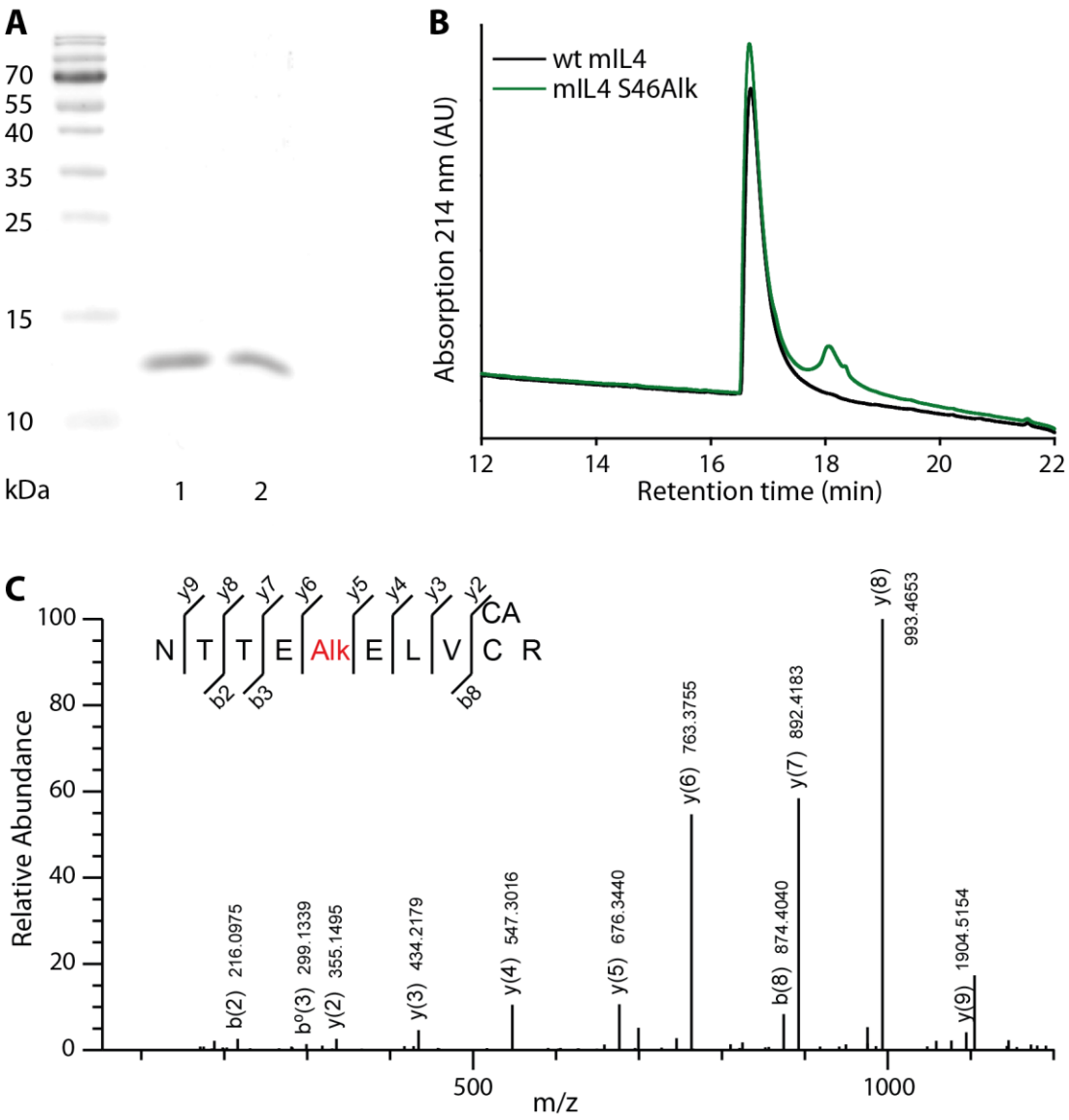

Fig. 2 Characterization of IL4 S46Alk. **(A)** SDS-PAGE analysis (Molecular-weight marker (PageRuler Prestained Protein Ladder, 10 to 180 kDa; Thermo Fisher Scientific, Schwerte, Germany); 1, wild type IL4 (13.6 kDa); 2, IL4 S46Alk (13.8 kDa). **(B)** Reversed phase chromatography profile of purified IL4 S46Alk in comparison to wild type IL4. **(C)** NanoLC-MS/MS analysis after elastase digest of IL4 S46Alk.

The bioactivity was determined by measuring the proliferation-inducing activity of the proteins on murine HT2 clone A5E suspension cells (IL2 dependent murine T lymphocytes responding to IL4) and was again confirmed in a primary cell culture system using murine peripheral-blood-derived monocytes (PBDMs) which are differentiated into macrophages by macrophage colony-stimulating factor (M-CSF)(Fig. 3). mIL4 S46Alk treated macrophages showed significant upregulation of M2 markers including arginase-1 (Arg1), chitinase-like protein 3 (Chil3), resistin-like beta (FIZZ1), monoamine oxidase A (MAOA) and mannose receptor

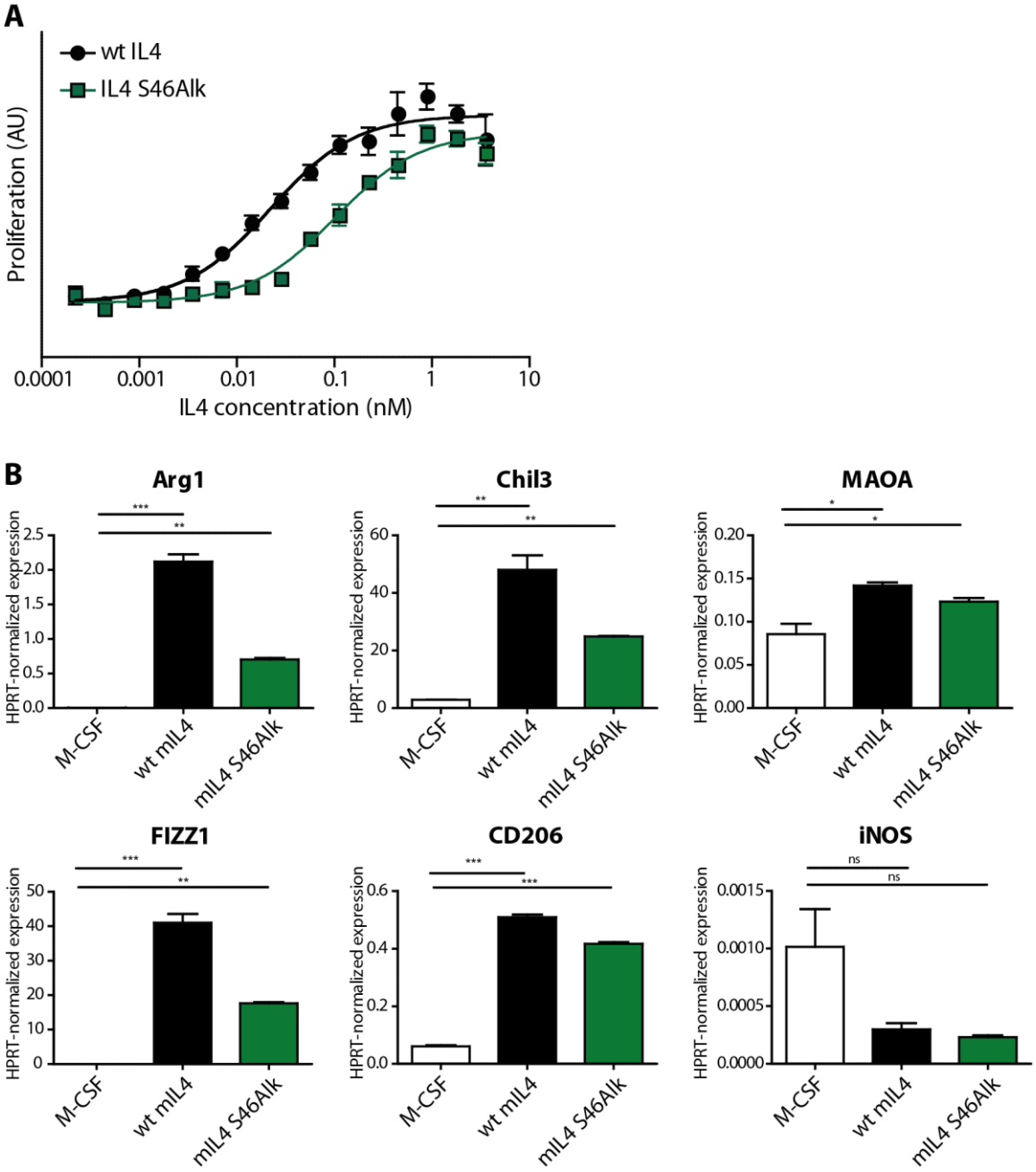

Fig. 3 Bioactivity of mIL4 S46Alk **(A)** HT2 clone A5E cell proliferation assay. EC_{50} values: wt IL4 0.0224 nM, IL4 S46Alk 0.105 nM. **(B)** qPCR analysis of macrophage polarization of IL4 S46Alk in comparison to wild type IL4 and M-CSF.

(CD206). The M1 marker inducible nitric oxide synthase (iNOS) served as a negative control and is not upregulated by mIL4 S46Alk. The IL4 mutein shows a reduced bioactivity compared to wild type IL4 in all cell culture assays, probably due to the incorporation of the unnatural amino acid.

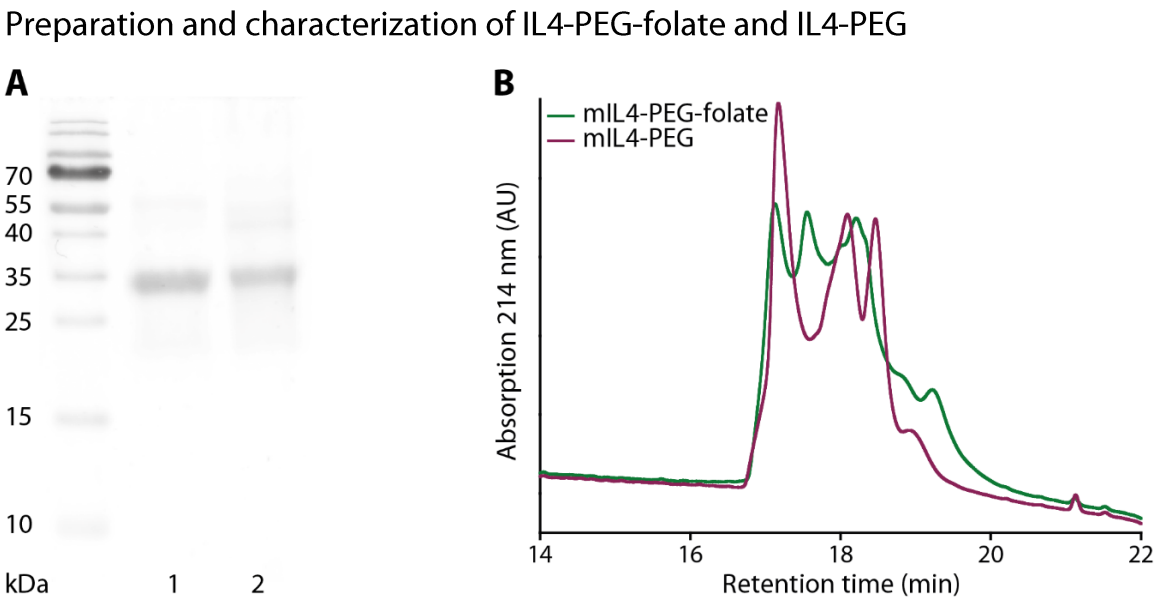

Fig. 4 Characterization of IL4-PEG-folate and IL4-PEG. **(A)** SDS-PAGE analysis (Molecular-weight marker (PageRuler Prestained Protein Ladder, 10 to 180 kDa; Thermo Fisher Scientific, Schwerte, Germany); 1, IL4-PEG-folate (25.7 kDa); 2, IL4-PEG (24.7 kDa). **(B)** Reversed phase chromatography profile of purified IL4-PEG-folate and IL4-PEG conjugates.

After successful design and production of a pure and bioactive IL4 variant harboring an unnatural amino acid suitable for click chemistry (IL4 S46Alk) the protein was further modified to improve serum half-life and targeting abilities. IL4 S46Alk was conjugated with DBCO-PEG(10k)-folate via strain-promoted alkyne-azide cycloaddition (SPAAC), resulting in IL4-PEG-folate. IL46Alk reacted with DBCO-PEG(10k) served as non-targeted control. The reactions had high yields of around 95% and the products were purified by size exclusion chromatography (data not shown). Purity of both IL4 conjugates was assessed by SDS-PAGE and RP-HPLC (85% mIL4-PEG, 80% mIL4-PEG-folate) (Fig. 4). The correct formation of IL4-PEG-folate and IL4-PEG was analyzed by MALDI-MS, resulting in an observed average mass of 25.7 kDa for IL4-PEG-folate and 24.7 kDa for IL4-PEG (Fig. SI 5, Fig. SI 6). The expected molecular weight is 23.8 kDa, which equals 13.8 kDa mIL4 S46Alk plus 10 kDa DBCO-PEG or DBCO-PEG-folate, respectively. The exact molecular weight of functionalized PEG molecules was not specified. Serum stability of the conjugates compared to wild type IL4 was assessed using western blot after incubation of IL4 with 10% serum for up to 48 h (Fig. SI 8). During the analyzed time span, no degradation was observed, which indicates a high serum stability.

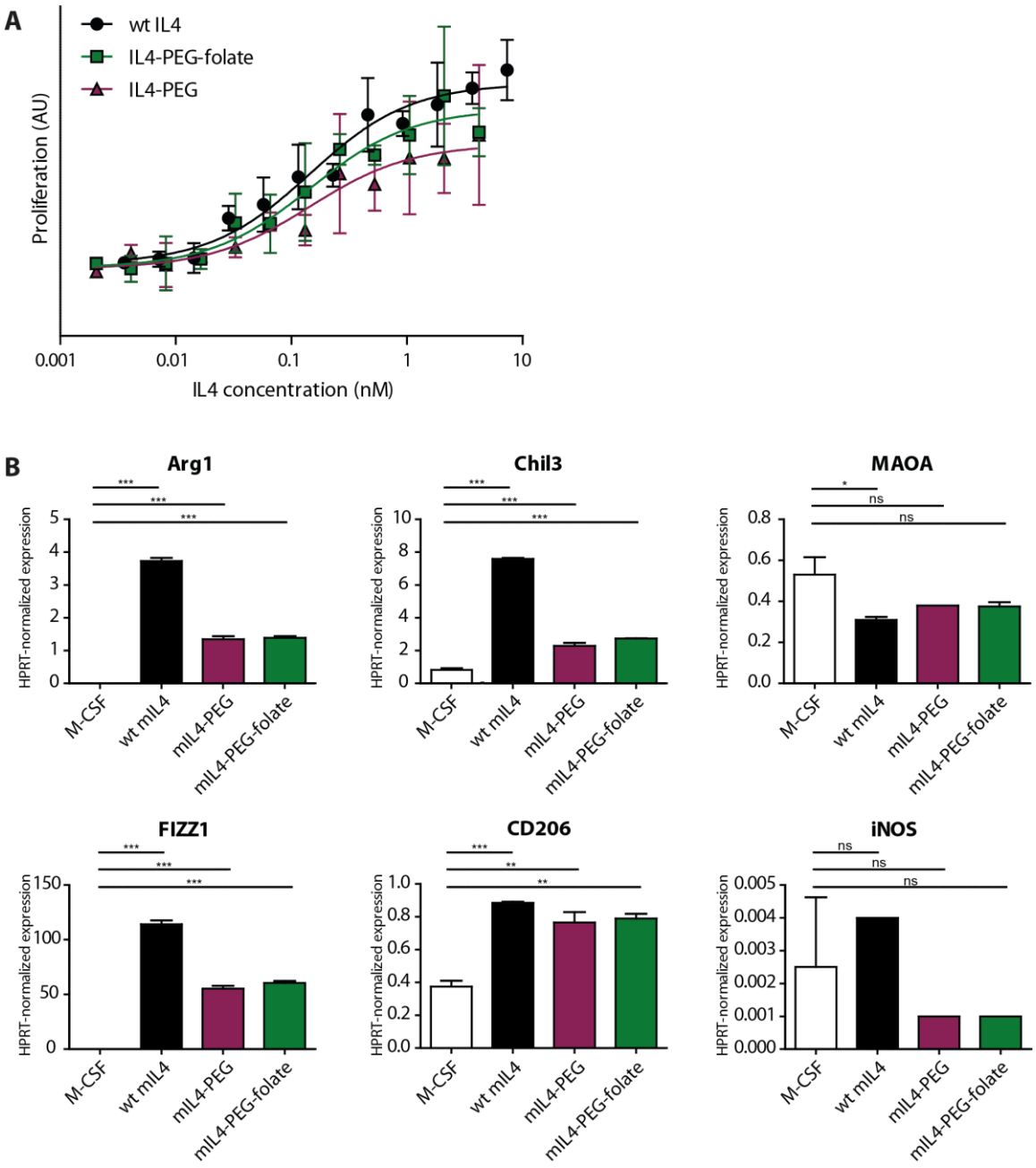

Fig. 5 Bioactivity of IL4-PEG-folate and IL4-PEG. **(A)** HT2 clone A5E cell proliferation assay. EC_{50} values: wt IL4 0.150 nM, IL4-PEG-folate 0.121 nM, IL4-PEG 0.187 nM. **(B)** qPCR analysis of macrophage polarization of IL4-PEG-folate and IL4-PEG conjugates in comparison to wild type IL4.

As before, the bioactivity of the IL4 conjugates was determined by measuring the activity of the proteins on murine HT2 clone A5E suspension cells (Fig. 5). The IL4 conjugates possess a bioactivity in the same range as the wild type protein. The primary cell culture system of murine bone-marrow-derived monocytes (BMDMs) was used to analyze the IL4 conjugates' polarization potential on mouse macrophages. Macrophage polarization after incubation with IL4 conjugates was assessed by qPCR using M1 and M2 gene expression markers. Cells incubated with wild type IL4 served as positive control. Macrophages incubated with mIL4-

PEG-folate or mIL4-PEG, respectively, showed significant upregulation of the M2 markers arginase-1 (Arg1), chitinase-like protein 3 (Chil3), resistin-like beta (FIZZ1) and mannose receptor (CD206). The M1 marker inducible nitric oxide synthase (iNOS) served as a negative control and was not upregulated by mIL4-PEG-folate or mIL4-PEG. The IL4 conjugates shows a reduced bioactivity compared to wild type IL4 regarding macrophage polarization, but not HT2 A5E proliferation. Overall, the bioactivity of the IL4-PEG-folate and IL4-PEG is comparable to that of mIL4 S46Alk, suggesting that the PEGylation has no negative influence on bioactivity.

Pharmacokinetics study

Before testing the targeting ability of IL4-PEG-folate, a pharmacokinetics (PK) study was performed to ensure that the conjugate stays long enough in circulation to reach its target - the folate receptors on activated macrophages at inflammation sites. Since the proteins were produced in *E. coli*, endotoxins were removed with an endotoxin removal resin, which uses poly(ε-lysine) as an affinity ligand to selectively bind endotoxins. All samples were sterile filtered, and the remaining endotoxin content was determined with a Limulus amebocyte lysate chromogenic endotoxin quantitation assay. The endotoxin content of the samples was between 5 – 8 EU/ml and therefore below the recommended endotoxin limit of 36 EU/ml for a 100 µl daily dose in mice.[28]

Pharmacokinetic evaluation was performed with healthy BALB/c mice. Fig. 6A shows the mean concentrations (±SD) of IL4-PEG-folate and IL4-PEG in serum at different time points after intravenous administration of 100 µg IL4 conjugate as determined by ELISA. Post-maximum concentrations decreased with a terminal half-life of 3.8 h for IL4-PEG-folate and 4.7 h for IL4-PEG. The area under the curve (AUC), which represents the total drug exposure across time, is 38072 ng*h*ml^{-1} for mIL4-PEG-folate and 16253 ng*h*ml^{-1} for mIL4-PEG (Fig. 6B).

The half-life of wild type murine IL4 was not assessed and could not be found in the literature. Recombinant human IL4 has a half-life of 19 ± 8.7 minutes after intravenous bolus injection in humans.[29] Given the similarity of both cytokines and using the rule-of-thumb $t_{1/2human} = 7.69*t_{1/2mouse}$ gives an estimate $t_{1/2}$ = 2.5 min of IL4 in mice.[30] PEGylation therefore significantly increased the half-life of IL4 and should, in combination with the long serum-stability, facilitate the therapeutic to reach its target before excretion.

A

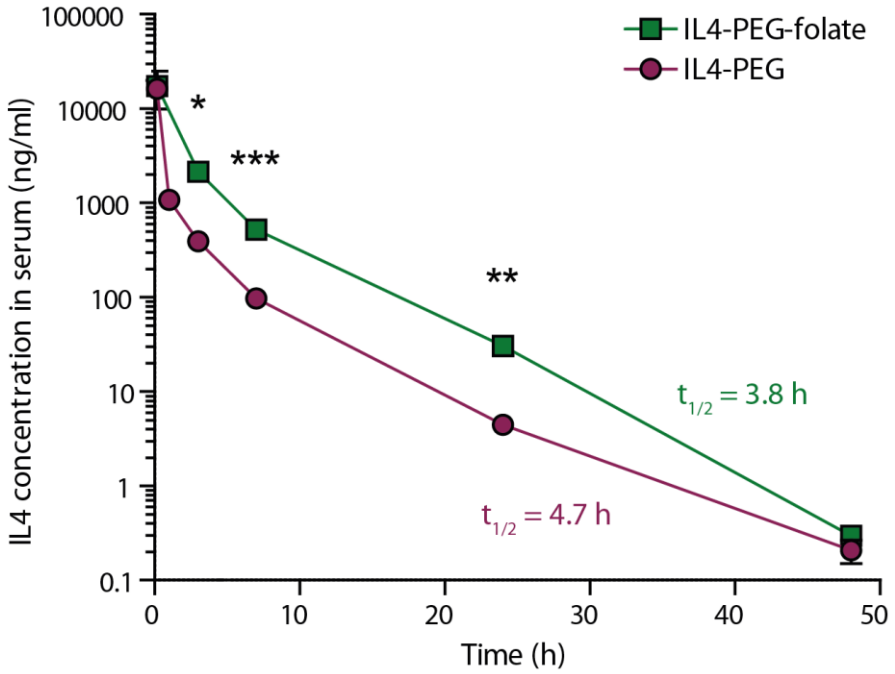

B

	Terminal half-life (h)	AUC (ng*h*ml^{-1})
mIL4-PEG-folate	3.8 ± 0.05	38072 ± 8121
mIL4-PEG	4.7 ± 0.20	16253 ± 10639

Fig. 6 Pharmacokinetics of IL4-PEG-folate and IL4-PEG in mice (n=3). **(A)** The IL4 conjugates were administered intravenously to BALB/c mice. Blood samples were taken at various times after administration. The IL4 concentration in serum was assessed by ELISA. **(B)** The terminal half-lives were calculated using the last three time points. AUC was calculated using GraphPad Prism. Values are expressed as mean ± SD.

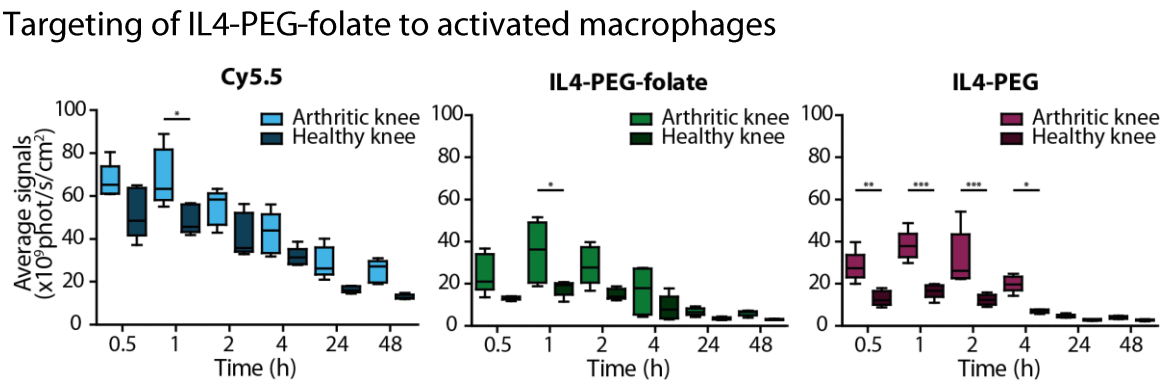

Fig. 7 Targeting experiment in mice with antigen-induced arthritis. Quantification of the NIR signal in the knees over 48 h after systemic injection of NIR-labeled IL4 conjugates. Box-and-whisker plot shows NIR intensity in arthritic vs. healthy knee, n = 5 per group.

The targeting of IL4-PEG-folate to synovial macrophages was tested in an antigen-induced arthritis (AIA) model in mice. This unilateral, T cell driven model is caused by injection of methylated bovine serum albumin (mBSA) into the knee joint of a Freund's Complete Adjuvant (FCA) preimmunized mouse. Afterwards, T cell mediated flares of inflammation can be induced by challenge with low dose mBSA.[31] The synovial macrophages in this model express the folate receptor and are involved in the development of the arthritis.[32] To visualize the targeting of IL4-PEG-folate to the macrophages within the inflamed joint, IL4 was labeled with a near-infrared (NIR) fluorescent dye. Two days after arthritis development, at the maximum of inflammation, the NIR-labeled IL4 conjugate was injected systemically and fluorescence signals were observed at different time points over the next 48 h (Fig. 7).

The NIR fluorescent dye Cy5.5 was used as a positive control to visualize the arthritic joints following induction of AIA in mice. Disordered new vessels have increased leakiness to macromolecules and these local permeability changes allow non-specific dye deposition.[33] Moreover, the enhanced ability to accumulate fluorescent cyanine dyes has also been associated with the activation of macrophages in arthritic lesions.[34] Cy5.5 demonstrates an approximately 1.5-fold higher fluorescence signal between 2 and 72 hours in arthritic compared with non-arthritic joints.[35]

As expected, an elevation of the Cy5.5 signal could be observed in the arthritic joint. The signals of IL4-PEG-folate and IL4-PEG were also higher in the inflamed than in the healthy joint. While the signal of IL4-PEG-folate was rather stable over time, IL4-PEG showed a clear maximum at 4 h after injection and showed a surprisingly high signal in general. All constructs also targeted the liver, but IL4-PEG-folate did so more than Cy5.5 and IL4-PEG (Fig. SI 11). The strong signal in the liver is not unexpected, as the liver harbors many

macrophages. Systemic activation of macrophages, especially in the liver, spleen and peritoneal cavity, in addition to local activation in the synovium, has been documented in the AIA model.[36]

Discussion

Application of anti-inflammatory cytokines like IL4 may be a useful strategy for treatment of RA but is hindered by the rapid clearance and dose-limiting toxicity of the small, pleiotropic cytokines. In this study we created a targeted cytokine conjugate consisting of PEG-folate conjugated to an IL4 modified with an unnatural amino acid enabling strain-promoted alkyne-azide cycloaddition. We were able to demonstrate the bioactivity of IL4-PEG-folate and an increased terminal serum half-life. The PEGylated cytokine has a serum half-life of around 4 h when injected intravenously in mice which is significantly longer than the expected half-life of several minutes.[29,30] The improved half-life could allow systemic administration by using lower dosages. Due to the modular design of the IL4 conjugate, the chain length of the PEG linker can easily be varied, and the half-life of the cytokine conjugate can thereby be fine-tuned according to different needs. Moreover, the long serum half-life and serum stability of IL4-PEG-folate should enable the therapeutic to circulate long enough to allow targeting to folate receptors on activated macrophages.

Targeting moieties specific for diseased tissues are another way to achieve lower dosages and thereby reduce side effects. The development of targeted cytokines for RA is an emerging field and preclinical studies are mostly focusing on using antibody fragments.[11,37] Our study attempted to use a folate to target cytokines to activated macrophages. The upregulated folate receptor allows selective targeting of folate-linked therapeutic agents to activated macrophages as they are present in the synovium of inflamed joints in RA. The imaging of the NIR-labeled cytokine conjugate in an antigen-induced arthritis mouse model demonstrated a targeting effect to the inflamed knee joint. The additional accumulation in the liver, which also harbors activated macrophages in this RA model, points out that the targeting specificity could be improved. Surprisingly, PEGylated IL4 without folate performed even better in targeting the arthritic joint of mice in the AIA model. It is known from immunocytokines, that in some cases cytokine-receptor interactions, rather than the targeting moiety, dictate the immunocytokine localization.[38] The targeting could be observed over the length of the experiment (48 h) and might be even increased by using a longer PEG

linker or another fusion partner like an Fc fragment or albumin, which additionally provide the benefit of FcRn-mediated recycling.

Methods

Synthesis of unnatural amino acid

The unnatural amino acid (S)-2-amino-6-((2-azidoethoxy) carbonylamino)hexanoic acid was synthesized as described elsewhere.[40] Briefly summarized, (S)-2-amino-6-((2-azidoethoxy) carbonylamino)hexanoic acid was synthesized starting from azidoethylchloroformate and commercial available Boc-L-Lys-OH with subsequent deprotection. Azidoethylchloroformate was synthesized in two reaction steps. In the first step a suspension of 1 eq. 2-bromoethanol and 2 eq sodium azide in water was stirred at 80 °C for 48 h to obtain 2-azidoethanol. After purification, a solution of 1 eq 2-azidoethanol and 1 eq triethylamine in THF were added slowly to a solution of 0.9 eq triphosgen in THF and stirred overnight at RT. After purification the solution containing the azidoethylchloroformate was added dropwise to a solution of 1.1 eq Boc-L-Lys-OH in THF and 1 M NaOH, stirred overnight and acidified with 6 M HCl. After deprotection with 2 M HCl in Et_2O and lyophilization, (S)-2-amino-6-((2-azidoethoxy) carbonylamino)hexanoic acid was obtained as a white powder.

Preparation of IL4

The DNA fragments encoding for wt murine IL4 and IL4 S46Alk were purchased from Eurofins Genomics (Ebersberg, Germany). The the cDNAs were inserted into the plasmid pETIIa which already contains the genes for the pyrrolysine tRNA, the lipoprotein promotor lpp and the terminator RRN b/c as previously described.[41] The plasmids were transformed into the expression host *E. coli* BL21(DE3). For expression of the unnatural amino acid containing mutein IL4 S46Alk, the pETIIa plasmid was cotransformed with a pRSF-duet construct, encoding for the gene of the pyrrolysine tRNA synthetase pylS as previously described.[41]

Bacteria were grown in TB medium plus carbenicillin (100 µg/ml, pETIIa) and kanamycin (100 µg/ml, pRSF) on a rotatory shaker at 37 °C to an optical density of 1.0 and IL4 protein expression was then induced by addition of 1 mM isopropylthiogalactopyranoside (IPTG) for 3 h. For IL4 S46Alk expression, Alk was added at a final concentration of 2 mM at OD_{600} =

0.5. The bacteria were sedimented by centrifugation at 5000 g, 15 min at 4 °C and resuspended in 1/200 culture volumes of resuspension buffer (50 mM Tris-HCl pH 8.0, 50 mM NaCl, 1 mM EDTA) and PMSF (final concentration 100 µM) and lysozyme (final concentration 75 µg/ml) were added. The cells were lysed by sonication (Sonopuls HD3100, Bandelin, Berlin, Germany) with the cell suspension cooled on ice. The sediment was resuspended in a quarter volume of the resuspension buffer used above and sonicated again. The insoluble fraction ("inclusion bodies") was separated by centrifugation and washed once with resuspension buffer plus 1% Triton X-100 and twice with resuspension buffer. The final sediment was kept frozen at temperatures -80 °C

The IL4 protein was extracted from the inclusion bodies using unfolding buffer (50 mM Tris-HCl pH 8.0, 50 mM NaCl, 1 mM EDTA, 5 M guanidine-HCl, 2 mM glutathione reduced, 0.2 mM glutathione oxidized, 9 ml per g wet weight). For refolding of the IL4, the clarified protein extract was diluted with two volumes of refolding buffer (0.5 M arginine, 50 mM Tris-HCl pH 8.0, 50 mM NaCl, 1 mM EDTA, 2 mM glutathione reduced, 0.2 mM glutathione oxidized) and dialyzed against 20 volumes of refolding buffer for 4 h at room temperature. Then, the solution was dialyzed against 40 volumes of 25 mM ammonium acetate pH 5.0 overnight at 4 °C. The solution was clarified by centrifugation, and the supernatant was filtered (0.22 µm) and loaded onto a HiTrap SP XL 5 ml column (GE Healthcare Life Sciences, Freiburg, Germany) that was equilibrated with 25 mM ammonium acetate pH 5.0 (A). The IL4 protein was eluted via a gradient using buffer containing 2 M sodium chloride (B). The peak eluting around 27% B was collected and buffer exchange to A and concentration to 10 ml were achieved via ultrafiltration (MWCO 9 kDa). The process was repeated with two HiTrap SP HP 1 ml columns (GE Healthcare Life Sciences, Freiburg, Germany) in series. Natively folded IL4 eluting as the major peak at 33% B was dialyzed against PBS pH 7.4, frozen in liquid nitrogen and stored in aliquots at -80 °C until further use. Protein concentrations were determined by BCA assay (Thermo Fisher Scientific, Schwerte, Germany) against a BSA standard.

PEGylation

IL4 S46Alk was mixed with a 5-fold excess of DBCO-PEG (Dundee Cell, Dundee, UK), or a 3-fold excess of DBCO-PEG-folate (Nanocs, New York, USA), respectively. Reaction was carried out at 4 °C overnight. Product was separated by size exclusion chromatography using a

Superdex75 10/300 GL column (GE Healthcare Life Sciences, Freiburg, Germany) with PBS pH 7.4 at a flowrate of 0.25 ml/min at 4 °C.

Endotoxin removal

Endotoxins were removed using the Pierce High-Capacity Endotoxin Removal Resin (Thermo Fisher Scientific, Schwerte, Germany) according to the manufacturer's instructions. In short, the resin was regenerated by incubation with 5 volumes of 0.2 N NaOH in 95% ethanol for 2 h at room temperature followed by 2 / 1 / 2 washing steps with 4 volumes of water / 2 M NaCl / water. The resin was equilibrated by two washing steps with two volumes of endotoxin-free PBS. The protein sample was incubated with the resin overnight at 4 °C, rolling. Endotoxin removal was confirmed by testing with the Pierce™ LAL Chromogenic Endotoxin Quantitation Kit (Thermo Fisher Scientific, Schwerte, Germany) according to the manufacturer's instructions.

SDS-PAGE

Protein samples were analyzed by discontinuous SDS-PAGE (15%) under denaturing conditions as described elsewhere.[42] Protein bands were stained with Coomassie Brilliant Blue G-250.[43]

RP-HPLC

Protein purity was assessed by RP-HPLC using a Hitachi LaChrom HPLC system (VWR, Darmstadt, Germany). Approximately 20 µg protein sample was applied to a Zorbax 300SB-CN column (Agilent, Waldbronn, Germany), equilibrated with water containing 0.1 % TFA and acetonitrile (ACN) containing 0.1% TFA (95:5 v/v). Proteins were eluted by a linear gradient of 5 - 95% ACN containing 0.1% TFA with a gradient of 5% ACN/min and a flow rate of 1 ml/min. Column temperature was kept at 22 °C and UV absorbance was monitored at 214 nm.

MALDI-MS

Protein samples were desalted using Ziptip C18 pipette tips (Merck Millipore, Darmstadt, Germany) following the manufacturer's instructions. Matrix-assisted laser desorption

ionization (MALDI-MS) spectra were acquired in the linear positive mode with an Autoflex II LRF instrument (Billerica, MA, USA). Mass spectra were calibrated externally with the Protein Calibration Standard I (Bruker Daltonics; Billerica, MA, USA), containing insulin, ubiquitin, myoglobin and cytochrome C.

Elastase digest and NanoLC-MS/MS

For in-gel digestion, 10 µg IL4 S46Alk were incubated with NuPAGE LDS Sample Buffer (4X) (Thermo Fisher Scientific, Schwerte, Germany) and 40 mM Dithiothreitol for 10 min at 70 °C. After cooling, iodoacetamide was added to obtain a final concentration of 80.5 mM. The mixture was incubated in the dark for 20 min at RT and was afterwards run on a 15% SDS-PAGE. After Coomassie staining, the band was excised, destained with 30% ACN, shrunk with 100% ACN and dried in a vacuum concentrator (Concentrator 5301, Eppendorf, Hamburg, Germany). The protein band was digested with 0.1 µg elastase overnight at 37 °C in 0.1 M NH_4HCO_3 (pH 8.0). Peptides were extracted from the gel slice with 5% formic acid and analyzed using a NanoLC-MS/MS LTQ-Orbitrap Velos Pro equipped with an EASY-Spray Ion Source coupled to an EASY-nLC 1000 (Thermo Fisher Scientific, Schwerte, Germany). The separation was performed on a trapping column (2 cm × 75 µm ID. PepMap C18 3 µm particles, 100 Å pore size) and EASY-Spray column (25 cm × 75 µm ID, PepMap C18 2 µm particles, 100 Å pore size) (both Thermo Fisher Scientific, Schwerte, Germany) with a linear gradient from 3-30% ACN with 0.1% formic acid for 30 min.

HT2 clone A5E proliferation assay

HT2 clone A5E cells (92021401, ECACC, Salisbury, UK) were maintained in T75 flasks in growth medium (RPMI-1640 containing 10% heat-inactivated FCS, 0.05 mM β-mercaptoethanol, 100 IU/ml murine IL2, penicillin G (100 U/ml) and streptomycin (100 mg/ml) at 37 °C and 5% CO_2.

For the proliferation assay, HT2 cells were seeded in a 96-well plate at 50,000 cells/well in growth medium without IL2, but supplemented with a dilution series of IL4 variants, ranging from 0.05 to 100 ng/mL, respectively. After stimulation for 20 h, 10 µl of WST-1 (Roche, Mannheim, Germany) per well were added and the cells were incubated for 2-4 h at 37 °C. The absorbance of the soluble formazan product was determined at 450 nm using a Spectramax 250 microplate reader (Molecular Devices, Sunnyvale, USA). Relative

proliferation is expressed in comparison to wild type IL4 (R&D Systems, Wiesbaden, Germany).

Macrophage isolation, polarization and qPCR

Mouse BMDCs were obtained by flushing the femurs, humeri, and tibiae of C57BL/6J mice with PBS. Cells were incubated in Red Blood Cell Lysis Solution (Miltenyi Biotec, Bergisch Gladbach, Germany) and washed with PBS. Cells were seeded in 6-well plates at 3.6 million cells/well in 2 ml WTM medium containing mM-CSF (45% F12 (Invitrogen, Karlsruhe, Germany), 45% DMEM (Invitrogen, Karlsruhe, Germany), 10% FCS (BioConcept, Allschwil, Switzerland), 40 ng/ml mM-CSF).

For in vitro stimulation of mouse macrophages 1.428 nM of each mIL4 variant was added to the cells on day 4 without removing the medium. On day 7, floating cells were removed, adherent cells were washed with PBS and harvested with 700 µl TRIzol reagent (Invitrogen, Karlsruhe, Germany) for RNA isolation according to the manufacturer's instructions.

cDNA was prepared using the SuperScript™ III First-Strand Synthesis System (Invitrogen, Karlsruhe, Germany). A QuantStudio 7 Flex System (Applied Biosystems) was used for quantitative PCR. The results are presented as relative quantification versus the basal condition using the comparative Ct method. Expression of all genes was measured using Taqman gene assays kits (Applied Biosystems) (Table SI 3).

Assessment of serum stability by western blot

IL4 S46Alk was labeled using NHS-biotin (H1759; Sigma-Aldrich, Schnelldorf, Germany) according to the manufacturer's instructions. In short, IL4 S46Alk (250 µg/ml) was mixed with a 50-fold excess of NHS-Biotin in DMF (100 mM) and incubated on ice for 2 h. Reaction was quenched with a 5-fold excess of Tris and subsequently used for PEGylation as described above. Biotinylated wild type IL4, IL4-PEG and IL4-PEG-folate were diluted to a final concentration of 30 nM with 10% (v/v) human serum (taken from a pool of healthy donors) in PBS and incubated at 37 °C. IL4 variants incubated without serum served as a control. Samples were inactivated after 0 h, 24 h and 48 h using cOmplete™ Protease Inhibitor Cocktail (Roche, Mannheim, Germany), 33 mM EDTA, 7 mM PMSF as well as 6x sample buffer for SDS-PAGE and heating to 95 °C for 5 min. Samples were analyzed by western blot using streptavidin-HRP conjugate (GE Healthcare Life Sciences, Freiburg, Germany) and

SuperSignal™ West Pico PLUS Chemiluminescent Substrate (Thermo Fisher Scientific, Schwerte, Germany).

PK study

All mice were used in accordance with Swiss Federal and Cantonal Authorities. Three female BALB/cJRj mice (10-12 weeks, 20-23 g) per group received an intravenous injection of 100 µg of the protein conjugates in a total volume of 100 µl. In time intervals of 10 min, 1 h, 3 h, 7 h, 24 h and 48 h blood samples were taken from the tail. Serum IL4 concentrations were determined by ELISA (#BMS613, Invitrogen, Karlsruhe, Germany) according to the manufacturer's instructions. Terminal half-lives were calculated with Microsoft Excel using the last three serum concentrations.

Imaging

Imaging experiments were performed as described elsewhere.[44] In short, female Balb/cByJ mice (6-8 weeks) were sensitized with methylated BSA and complete Freund's adjuvant on days 21 and 14. On day 0 the right knee was injected with mBSA (antigen-injected knee). Two days after intraarticular knee challenge, 100 µg of Cy5.5, Atto655-labeled IL4-PEG or Atto655-labeled IL4-PEG-folate in PBS was injected i.v. via the tail vein. Spectral fluorescence images were obtained after 0.5 h, 1 h, 2 h, 4 h, 24 h and 48 h using an in vivo imaging system (Maestro; CRi Inc.) To evaluate signal intensities, regions of interest were selected over the knee areas, and the mean fluorescence signal from those areas was determined.

Material

All chemicals were purchased from Sigma-Aldrich unless stated otherwise.

References

1. Vos, T. *et al.* Global, regional, and national incidence, prevalence, and years lived with disability for 310 diseases and injuries, 1990–2015: a systematic analysis for the Global Burden of Disease Study 2015. *Lancet* **388**, 1545–1602 (2016).
2. Weissmann, G. The pathogenesis of rheumatoid arthritis. *N. Engl. J. Med.* **365**, 2205–2219 (2011).
3. Mulherin, D., Fitzgerald, O. & Bresnihan, B. Synovial tissue macrophage populations and articular damage in rheumatoid arthritis. *Arthritis Rheum.* **39**, 115–124 (1996).
4. Kinne, R. W., Stuhlmüller, B. & Burmester, G. R. Cells of the synovium in rheumatoid arthritis. Macrophages. *Arthritis Res. Ther.* **9**, 1–16 (2007).
5. Antony, A. C. Folate receptors. *Annu. Rev. Nutr.* **16**, 501–521 (1996).
6. Joosten, L. A. B. *et al.* Role of interleukin-4 and interleukin-10 in murine collagen-induced arthritis: Protective effect of interleukin-4 and interleukin-10 treatment on cartilage destruction. *Arthritis Rheum.* **40**, 249–260 (1997).
7. Joosten, L. A. B. *et al.* Protection against cartilage and bone destruction by systemic interleukin-4 treatment in established murine type II collagen-induced arthritis. *Arthritis Res.* **1**, 81–91 (1999).
8. Van Lent, P. L. E. M., Holthuysen, A. E. M., Slöetjes, A., Lubberts, E. & Van Den Berg, W. B. Local overexpression of adeno-viral IL-4 protects cartilage from metallo proteinase-induced destruction during immune complex-mediated arthritis by preventing activation of pro-MMPs. *Osteoarthr. Cartil.* **10**, 234–243 (2002).
9. Lubberts, E. *et al.* IL-4 gene therapy for collagen arthritis suppresses synovial IL-17 and osteoprotegerin ligand and prevents bone erosion. *J. Clin. Invest.* **105**, 1697–1710 (2000).
10. Lubberts, E. *et al.* Adenoviral vector-mediated overexpression of IL-4 in the knee joint of mice with collagen-induced arthritis prevents cartilage destruction. *J Immunol* **163**, 4546–4556 (1999).
11. Hemmerle, T., Doll, F. & Neri, D. Antibody-based delivery of IL4 to the neovasculature cures mice with arthritis. *Proc. Natl. Acad. Sci. U. S. A.* **111**, 12008–12 (2014).
12. Luzina, I. G., Keegan, A. D., Heller, N. M. & Rook, G. A. W. Regulation of inflammation by interleukin-4 : a review of " alternatives ". **92**, 753–764 (2012).
13. Cawston, T. E. *et al.* Interleukin-4 blocks the release of collagen fragments from bovine nasal cartilage treated with cytokines. *Biochim. Biophys. Acta* **1314**, 226–232 (1996).
14. Whitehead, R. P. *et al.* Phase II trial of recombinant human interleukin-4 in patients with advanced renal cell carcinoma: a southwest oncology group study. *J. Immunother.* **25**, 352–358 (2002).
15. Lundin, J. *et al.* Interleukin 4 therapy for patients with chronic lymphocytic leukaemia: A phase I/II study. *Br. J. Haematol.* **112**, 155–160 (2001).
16. Ghoreschi, K. *et al.* Interleukin-4 therapy of psoriasis induces Th2 responses and improves human autoimmune disease. *Nat. Med.* **9**, 40–46 (2003).

17. Sosman, J. a, Fisher, S. G., Kefer, C., Fisher, R. I. & Ellis, T. M. A phase I trial of continuous infusion interleukin-4 (IL-4) alone and following interleukin-2 (IL-2) in cancer patients. *Ann. Oncol.* **5**, 447–52 (1994).

18. Turecek, P. L., Bossard, M. J., Schoetens, F. & Ivens, I. A. PEGylation of Biopharmaceuticals: A Review of Chemistry and Nonclinical Safety Information of Approved Drugs. *J. Pharm. Sci.* **105**, 460–475 (2016).

19. Lühmann, T. *et al.* Interleukin-4-Clicked Surfaces Drive M2 Macrophage Polarization. *ChemBioChem* **17**, 2123–2128 (2016).

20. Lühmann, T. *et al.* Site-Specific POxylation of Interleukin-4. *ACS Biomater. Sci. Eng.* acsbiomaterials.6b00578 (2017). doi:10.1021/acsbiomaterials.6b00578

21. Waterhouse, A. M., Procter, J. B., Martin, D. M. A., Clamp, M. & Barton, G. J. Jalview Version 2-A multiple sequence alignment editor and analysis workbench. *Bioinformatics* **25**, 1189–1191 (2009).

22. Pettersen, E. F. *et al.* UCSF Chimera - A visualization system for exploratory research and analysis. *J. Comput. Chem.* **25**, 1605–1612 (2004).

23. Lühmann, T. *et al.* Interleukin-4 clicked surfaces drive M2 macrophage polarization. *Chembiochem* (2016).

24. Carr, C., Aykent, S., Kimack, N. M. & Levine, A. D. Disulfide assignments in recombinant mouse and human interleukin 4. *Biochemistry* **30**, 1515–1523 (1991).

25. Mueller, T. D., Zhang, J. L., Sebald, W. & Duschl, A. Structure, binding, and antagonists in the IL-4/IL-13 receptor system. *Biochim. Biophys. Acta - Mol. Cell Res.* **1592**, 237–250 (2002).

26. Waterhouse, A. *et al.* SWISS-MODEL: Homology modelling of protein structures and complexes. *Nucleic Acids Res.* **46**, W296–W303 (2018).

27. Nguyen, D. P. *et al.* Genetic encoding and labeling of aliphatic azides and alkynes in recombinant proteins via a pyrrolysyl-tRNA synthetase/tRNACUA pair and click chemistry. *J. Am. Chem. Soc.* **131**, 8720–8721 (2009).

28. Malyala, P. & Singh, M. Endotoxin Limits in Formulations for Preclinical Research. *J. Pharm. Sci.* **97**, 2041–2044 (2008).

29. Prendiville, J. *et al.* Recombinant human interleukin-4 (rhu IL-4) administered by the intravenous and subcutaneous routes in patients with advanced cancer-A phase I toxicity study and pharmacokinetic analysis. *Eur. J. Cancer* **29**, 1700–1707 (1993).

30. Bachmann, K., Chupka, J., Erhardt, P. & White, D. Application of Simple Mathematical Expressions to Relate Half-Lives of Drugs in Mice to Those in Humans. *Drug Metab. Lett.* **1**, 127–129 (2008).

31. van den Berg, W. B., Joosten, L. A. B. & van Lent, P. L. E. M. Murine antigen-induced arthritis. in *Arthritis Research* 243–253 (Springer, 2007).

32. Richards, P. J., Williams, A. S., Goodfellow, R. M. & Williams, B. D. Liposomal clodronate eliminates synovial macrophages, reduces inflammation and ameliorates joint destruction in antigen-induced arthritis. *Rheumatology* **38**, 818–825 (1999).

33. Levick, R. Permeability of Rheumatoid and Specific Plasma Proteins. *Arthritis Rheum.* **24**, 1550–1560 (1981).

34. Kitagawa, S. & Johnston, R. B. Relationship between membrane potential changes and superoxide-releasing capacity in resident and activated mouse peritoneal macrophages. *J. Immunol.* **135**, 3417–3423 (1985).

35. Hansch, A. *et al.* Diagnosis of arthritis using near-infrared fluorochrome Cy5.5. *Invest. Radiol.* **39**, 626–632 (2004).

36. Johnson, W. J. *et al.* Macrophage activation in rat models of inflammation and arthritis: Systemic activation precedes arthritis induction and progression. *Arthritis Rheum.* **29**, 1122–1130 (1986).

37. Schwager, K. *et al.* Preclinical characterization of DEKAVIL (F8-IL10), a novel clinical-stage immunocytokine which inhibits the progression of collagen-induced arthritis. *Arthritis Res. Ther.* **11**, R142 (2009).

38. Tzeng, A., Kwan, B. H., Opel, C. F., Navaratna, T. & Wittrup, K. D. Antigen specificity can be irrelevant to immunocytokine efficacy and biodistribution. *Proc. Natl. Acad. Sci. U. S. A.* **112**, 3320–5 (2015).

39. Hansch, A. *et al.* Near-infrared imaging of flare-up arthritis with native fluorochrome Cy5.5 and albumin-bound Cy5.5. *J. Exp. Anim. Sci.* **43**, 129–139 (2006).

40. Gutmann, M. Functionalization of cells, extracellular matrix components and proteins for therapeutic application. (Julius-Maximilians-Universität Würzburg, 2018).

41. Eger, S., Scheffner, M., Marx, A. & Rubini, M. Synthesis of defined ubiquitin dimers. *J. Am. Chem. Soc.* **132**, 16337–16339 (2010).

42. Gallagher, S. R. One-dimensional SDS gel electrophoresis of proteins. *Curr. Protoc. Protein Sci.* **1**, (2012).

43. Lawrence, A.-M. & Besir, H. Staining of Proteins in Gels with Coomassie G-250 without Organic Solvent and Acetic Acid. *J. Vis. Exp.* 2–4 (2009). doi:10.3791/1350

44. Littlewood-Evans, A. *et al.* GPR91 senses extracellular succinate released from inflammatory macrophages and exacerbates rheumatoid arthritis. *J. Exp. Med.* **213**, 1655–1662 (2016).

Supporting information

Codon optimization FF

```
        10          20          30          40          50          60
ATGGCACACA TTCATGGTTG CGACAAGAAC CATCTGCGCG AAATCATCGG CATTCTGAAC

        70          80          90         100         110         120
GAGGTGACAG GCGAAGGCAC ACCTTGCACC GAAATGGATG TGCCGAACGT ACTGACTGCG

       130         140         150         160         170         180
ACGAAGAACA CCACGGAGAG CGAACTGGTC TGTCGTGCTT CCAAAGTTCT GCGCATCTTC

       190         200         210         220         230         240
TATCTGAAGC ATGGCAAGAC GCCGTGTCTG AAGAAGAACA GCAGCGTCCT GATGGAACTT

       250         260         270         280         290         300
CAGCGCCTGT TTCGCGCCTT TCGTTGTCTG GACAGTTCCA TCAGCTGCAC AATGAACGAG

       310         320         330         340         350         360
AGCAAGAGCA CAAGTCTGAA AGACTTTCTG GAGTCTCTGA AGTCCATCAT GCAGATGGAC

       370
TACTCTTAAT AA
```

Codon optimization FH

```
        10          20          30          40          50          60
ATGGCACATA  TTCATGGTTG  TGATAAAAAT  CATTTACGAG  AAATTATTGG  CATTCTGAAC

        70          80          90         100         110         120
GAAGTTACTG  GTGAAGGCAC  TCCATGTACA  GAAATGGACG  TTCCAAACGT  ACTGACTGCT

       130         140         150         160         170         180
ACTAAAAATA  CTACAGAATA  GGAACTAGTA  TGTCGAGCAT  CAAAAGTATT  ACGTATCTTT

       190         200         210         220         230         240
TATCTGAAAC  ACGGCAAAAC  ACCTTGTTTA  AAGAAAAACA  GTTCAGTTCT  GATGGAGCTT

       250         260         270         280         290         300
CAGCGTTTAT  TTCGAGCTTT  TCGATGTCTG  GATTCAAGTA  TTTCATGTAC  TATGAATGAA

       310         320         330         340         350         360
AGCAAATCAA  CTTCACTTAA  GGATTTTCTG  GAAAGTTTGA  AGAGTATTAT  GCAAATGGAT

       370
TACAGCTAAT AA
```

Fig. SI 1 Codon optimized wild type mIL4 DNA sequences “FF” and “FH”.

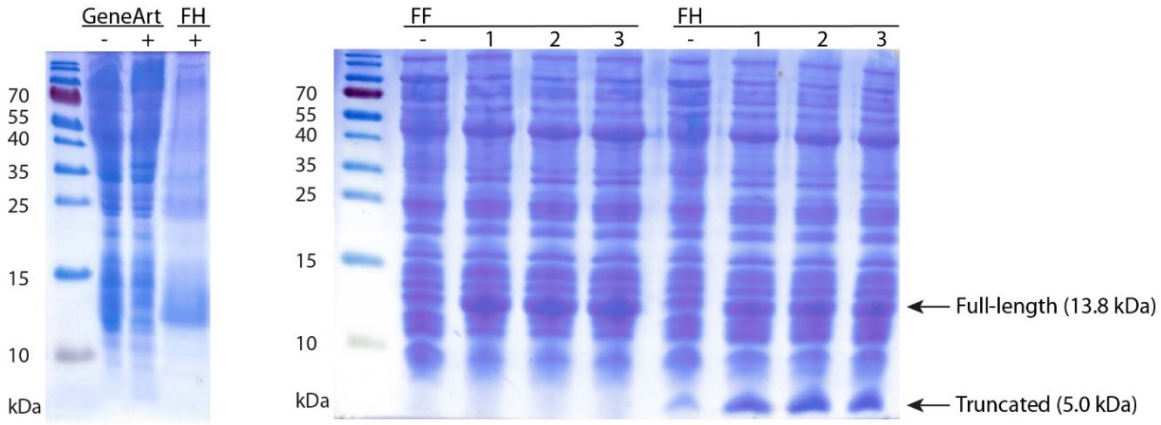

Fig. SI 2 Comparison of codon optimizations "FF" and "FH" of murine IL4 for expression in *E. coli*. FH was used for expression of wild type IL4, FF was used for expression of IL4 S46Alk (with codon for S46 mutated to amber stop codon "TAG"). Left: SDS-PAGE of inclusion bodies of wt mIL4 of codon optimizations GeneArt and "FH". "-" = uninduced, "+" = induced. Right: SDS-PAGE of whole-cell extracts of *E. coli* after expression of different codon optimizations "FF" and "FH" of mIL4 S46Alk. "-" = uninduced, 1-3 = clone number.

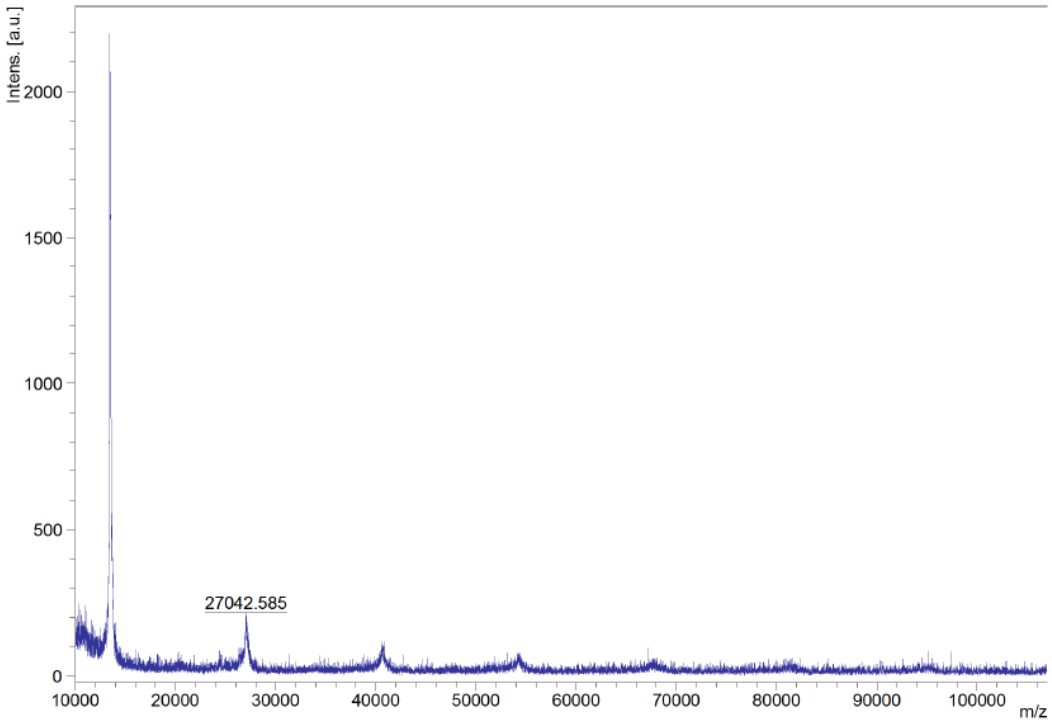

Fig. SI 3 MALDI-MS analysis of wt mIL4: observed average mass 13658.167 Da, calculated average mass 13622.801 Da.

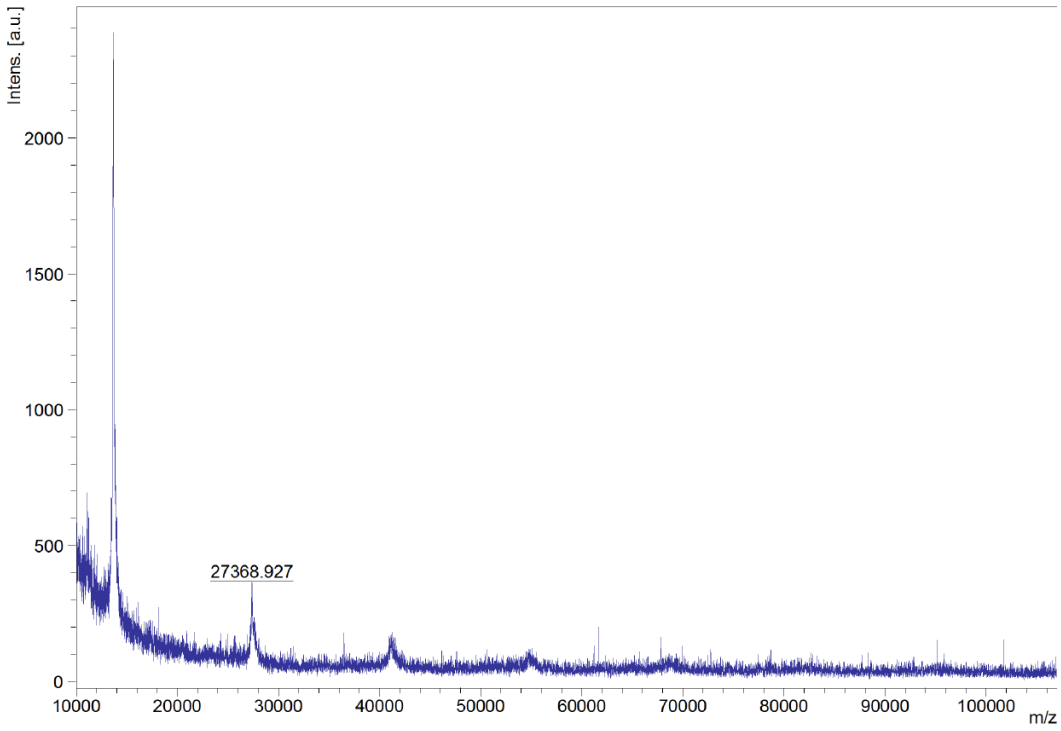

Fig. SI 4 MALDI-MS analysis of mIL4 S46Alk: observed average mass 13785.511 Da, calculated average mass 13777.983 Da.

Table SI 3 qPCR probes

Gene symbol	Gene name	Assay ID
HPRT	hypoxanthine guanine phosphoribosyl transferase	Mm00446968_m1
GAPDH	glyceraldehyde-3-phosphate dehydrogenase	Mm99999915_g1
Fizz1	resistin like alpha	Mm00445109_m1
beta actin	actin, beta	Mm02619580_g1
CD206	mannose receptor, C type 1	Mm01329362_m1
iNOS	nitric oxide synthase 2	Mm00440502_m1
Maoa	monoamine oxidase A	Mm00558004_m1
Chil3	chitinase-like 3	Mm00657889_mH
Arg1	arginase, liver	Mm00475988_m1
Trem2	triggering receptor expressed on myeloid cells 2	Mm04209424_g1

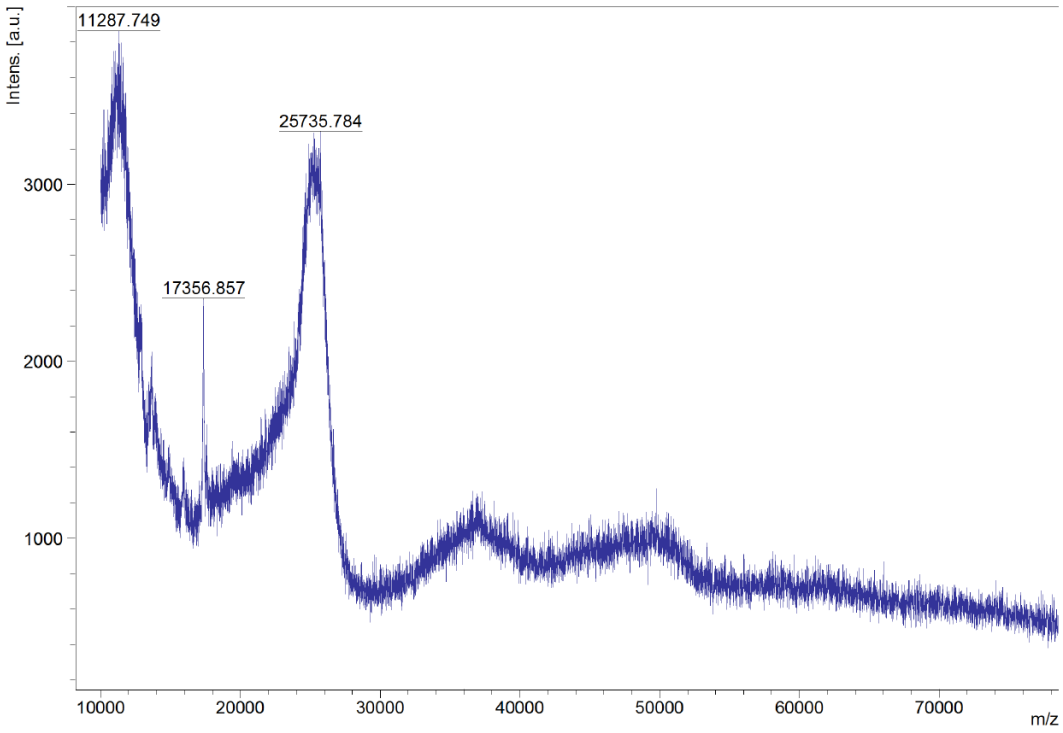

Fig. SI 5 MALDI-MS analysis of mIL4-PEG-folate: observed average mass 25735.784 Da, expected average mass >23777 Da.

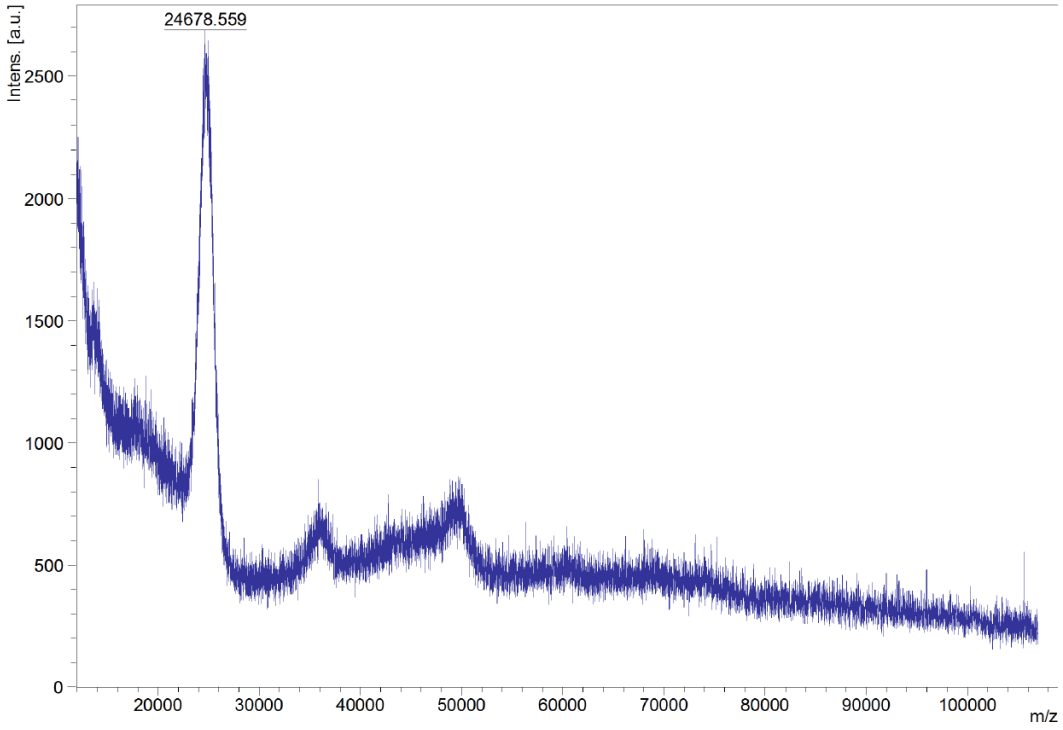

Fig. SI 6 MALDI-MS analysis of mIL4-PEG: observed average mass 24678.559 Da, expected average mass >23777 Da.

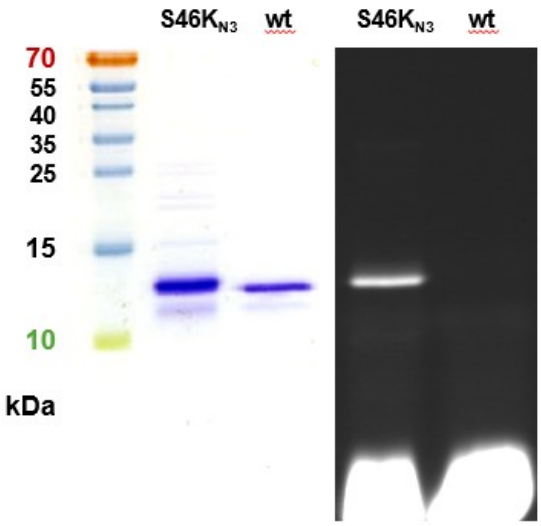

Fig. SI 7 SDS-PAGE of SPAAC between mIL4 S46Alk and DBCO-dye. wt mIL4 serves as negative control. Left panel: Coomassie staining. Right panel: Detection of fluorescence under UV light.

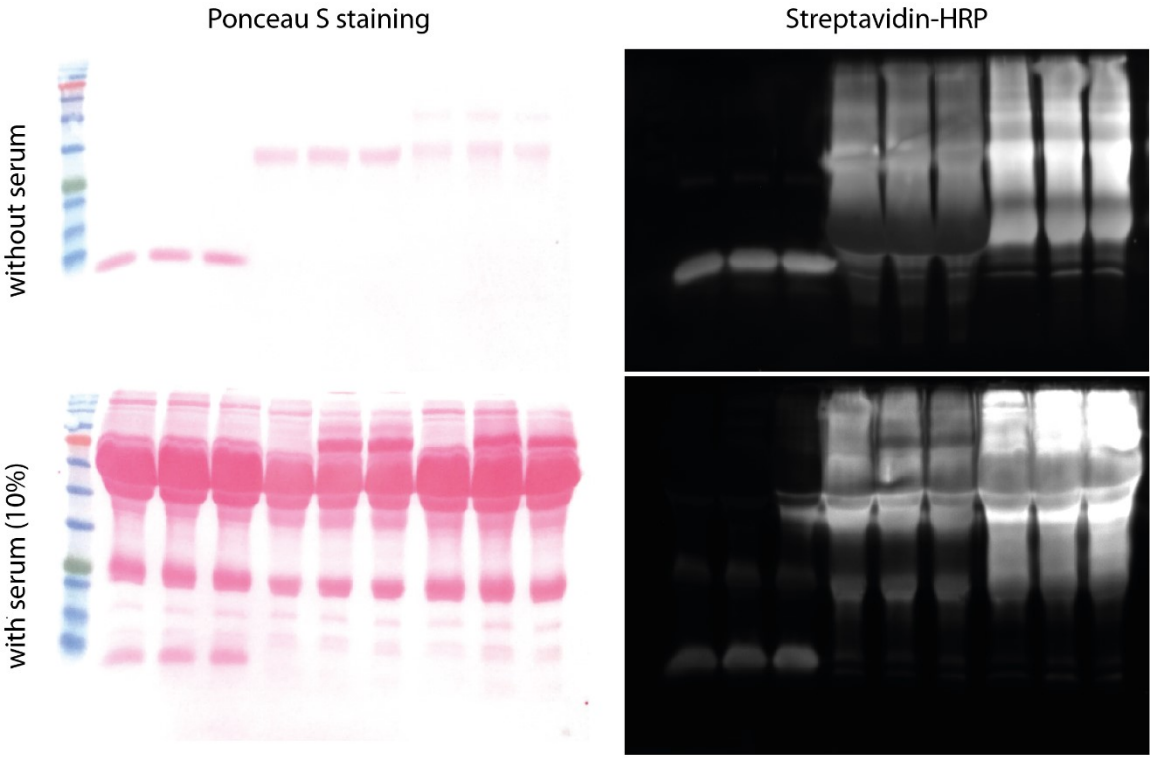

Marker	wt mIL4			mIL4-PEG			mIL4-PEG-Folate		
	0 h	24 h	48 h	0 h	24 h	48 h	0 h	24 h	48 h

Fig. SI 8 Assessment of serum stability by western blot. Top: Ponceau S staining and Streptavidin-HRP detection of western blots of biotinylated wt mIL4, mIL4-PEG and mIL4-PEG-folate incubated with and without serum, respectively. Bottom: Gel loading scheme.

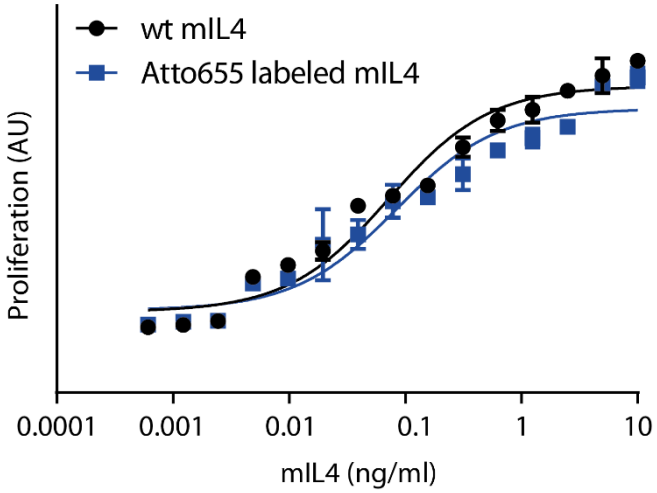

Fig. SI 9 HT2 clone A5E cell proliferation assay. EC_{50} values: wt IL4 0.266 nM, Atto655 labeled mIL4 0.031 nM.

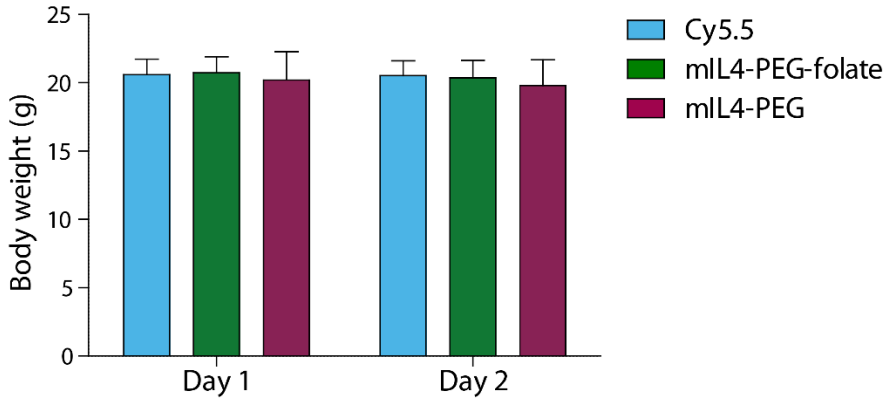

Fig. SI 10 Imaging study: body weight of mice

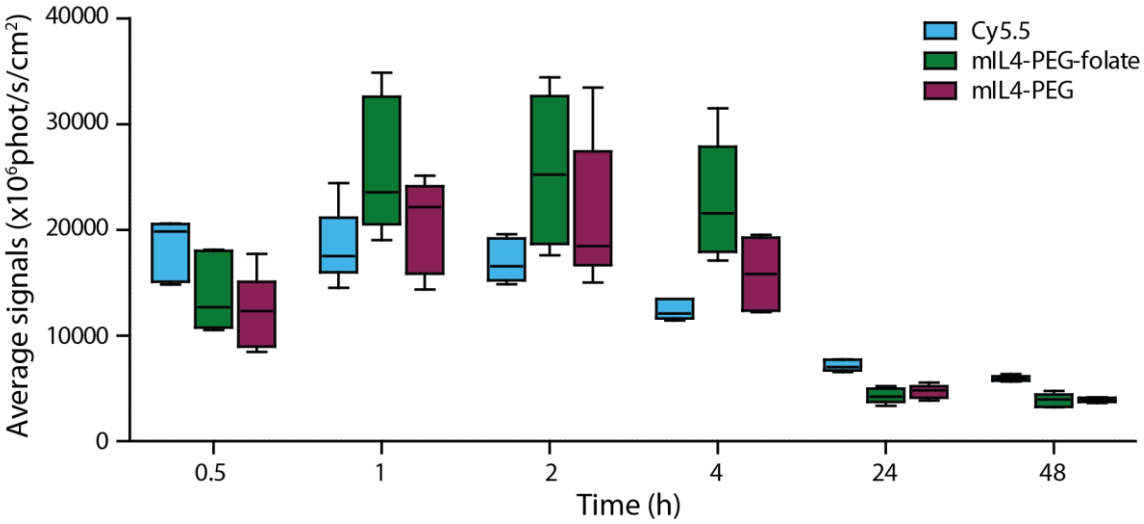

Fig. SI 11 NIR signals detected in liver.

Conclusion & Outlook

Cytokines play a central role in various inflammatory diseases, including rheumatoid arthritis, diabetes, or autoinflammatory syndromes and are therefore promising targets for new therapies. Different strategies that are already in use or currently being investigated include targeting of cytokine receptors via soluble antagonists (e.g. Anakinra, a recombinant version of the IL-1 receptor antagonist IL1RA) or antagonistic antibodies (e.g. Atrosab, a humanized monoclonal antibody against TNF receptor 1), as well as neutralization of cytokines via soluble decoy receptors (e.g. Etanercept, a fusion protein of soluble TNF receptor 2 linked to the Fc portion of an IgG1) or neutralizing antibodies (e.g. Adalimumab, a human monoclonal antibody against TNFα). Although most research focuses on suppressing the pro-inflammatory cytokine response, some studies deploy anti-inflammatory cytokines as therapeutics. For example, the immunocytokine Dekavil (fusion protein composed of the vascular targeting antibody F8 and the cytokine interleukin-10) has entered phase II clinical trials in combination with methotrexate for treatment of rheumatoid arthritis.[1] Pegilodecakin (Pegylated interleukin-10) is currently being tested in a phase 1/1b trial for treatment of multiple advanced solid tumors.[2]

Cytokines are challenging drugs from a pharmacological perspective: they are potent molecules with pleiotropic effects and have a short serum half-life due to their small size. Therefore, to achieve biologically active concentrations in the targeted tissue, they would need high systemic doses but this is limited by safety issues – overall, their therapeutic window typically prevents their therapeutic use.[3,4] This work is focused on increasing the therapeutic window of cytokines by different modes of delivery using interleukin-4 as a prototypical anti-inflammatory cytokine.

In **chapter 1**, the use of MMP-driven cytokine delivery systems is introduced, matching the complex progression of inflammatory diseases by linking MMP profiles to the disease phases of rheumatoid arthritis (RA) and myocardial infarction (MI). The characteristic temporal expression patterns of MMPs make them surrogate biomarkers for distinct disease phases and their high substrate efficiency can be used for the design of specifically cleaved peptide linkers that connect anti-inflammatory therapeutics, e.g. cytokines with a carrier or targeting moiety.[5] The protease-sensitive peptide linker mediates release of the cytokines in response to upregulation of MMPs during flares of inflammation. The reduced systemic exposure to therapeutic cytokines by local release could help to prevent side effects associated with anti-inflammatory cytokines, like vascular leak syndrome.[6] Moreover, this

actively sensing and self-dosing system could be helpful to treat patients in asymptomatic states as a preventive measure.

Chapter 2 discusses immobilized IL4 for local applications. In this first proof of concept study, the integration of unnatural amino acids into human IL4 via amber codon suppression in *E. coli* was established. An IL4 mutein was designed to have wild type activity by choosing an integration site distant from the receptor binding interface. Thorough in vitro characterization of the IL4 mutein was conducted using physicochemical and cell-based assays. Site-selective immobilization by two different types of click reactions on agarose particles was performed in order to maintain local concentrations of IL4 at the site of inflammation thereby reducing systemic side effects.

Chapter 3 returns to MMP-driven cytokine delivery systems, with IL4 variants being suitable for building bioresponsive drug depot. This system emulates nature's approach of storing cytokines and growth factors in the extracellular matrix (ECM) and releasing them during tissue remodeling processes as in inflammation and wound healing.[7] To allow storage in the ECM, IL4 was equipped with an 8-amino-acid recognition sequence for the transglutaminase FXIIIa, derived from the D domain of human IGF-1.[8] An interposed protease-sensitive peptide linker facilitated the release by MMPs. Human IL4 with an unnatural amino acid at position 42 (see chapter 2) was conjugated with this bifunctional peptide consisting of the protease-sensitive linker and the transglutaminase tag via bioorthogonal click chemistry. The IL4 conjugate was tested in a rabbit osteoarthritis model by intraarticular co-injection with FXIIIa into the knee. Compared to the control groups, the bioresponsive release of IL4 lead to a delayed deterioration of non-load bearing cartilage and protection of the anterior cruciate ligament. The study would benefit from additional experiments to evaluate the residence time of IL4 in the joint, since this is an aspect that could easily be optimized by using different peptide linker sequences. Furthermore, it is debatable if OA is the best model to test this IL4 delivery system, since OA is not exclusively inflammation-driven, but also a disease of "wear and tear". Unfortunately, the species selectivity of IL4 drastically reduces the amount of available animal models, apart from non-human primates.

To expand the number of available animal models, in **chapter 4** the approach was transferred to murine IL4, which in contrast to human IL4 is not negatively affected by C-terminal elongation. Murine IL4 was designed as C-terminal fusion protein with a flexible peptide spacer, the protease-sensitive peptide linker and the FXIIIa recognition sequence.

The fusion protein was successfully characterized in vitro for IL4 bioactivity, cleavage of the protease-sensitive linker by MMPs and immobilization on ECM by FXIIIa. Interestingly, the MMP cleavage rate of the protease sensitive linker is about 10-fold slower when part of the fusion protein than the sole linker produced by solid phase peptide synthesis. Further experiments with different protease sensitive linker and spacer sequences will allow to further control the release rate of the drug from the depot in the future.

Another approach, inspired by PEGylation as well as immunocytokines, was tested in **chapter 5**. Here, the aim was to increase the serum half-life of IL4 by PEGylation and additionally attach a targeting moiety to activated macrophages in the form of a folate group. The integration site of the unnatural amino acid was transferred from human to murine IL4 by sequence homology modelling. Initial expression problems were improved by optimizing the codon usage. In contrast to human IL4, the bioactivity of the murine IL4 is slightly affected by the integration of the unnatural amino acid. Murine IL4 S46Alk was conjugated with DBCO-PEG-folate using strain-promoted alkyne-azide cycloaddition. The serum stability of the bioconjugate was shown with in vitro experiments and an increased serum half-life was observed in a pharmacokinetics study in mice. The targeting of folate to activated macrophages and thereby sites of inflammation was tested in an antigen-induced arthritis (AIA) mouse model. It seems that IL4 mediates stronger targeting than the folate, as IL4-PEG, originally considered to be the negative control, showed superior targeting to the inflamed joint than IL4-PEG-folate. This phenomenon is known from immunocytokines, where in some cases cytokine – cytokine-receptor interactions rather than antibody–antigen targeting dictate immunocytokine localization.[9] Further studies should be conducted detailing the localization of PEGylated IL4 with and without folate in AIA mice and, if successful, this should be followed by an efficacy study. The long-term goal is to create a latent cytokine conjugate for i.v. application, which is inactive while circulating in the body and gets locally activated at the site of inflammation. Examples from the human body are proteolytic cytokine maturation of the interleukin-1 family or the latency of TGFβ, which is conferred by special binding proteins.[7,10] Our approach could be achieved by introducing MMP cleavable peptide sequences to release the active cytokine from a larger construct at sites of inflammation.

In conclusion, bioresponsive release of anti-inflammatory cytokines from a carrier is a promising therapeutic strategy for different local or subcutaneous applications as it expands administration intervals and is suited for preventive treatment. This work presents a platform technology which can be easily expanded to other cytokines, growth factors or

biologics as therapeutics or other proteases as biomarker and drug-releasing trigger. PEGylation or immobilization on the ECM represent only two possible options to prolong the serum half-life and facilitate targeting. Alternative strategies are fusion to antibodies, Fc fragments or other carriers, e.g. hydrogels. It is especially important to discriminate between disease conditions in which different MMPs are upregulated and activated, to tailor the protease-sensitive linkers accordingly. Ultimately, a combined treatment with a drug depot of multiple cytokines connected to multiple linkers that target different proteases might be the way to go. Complex diseases require complex modes of delivery.

References

1. Galeazzi, M. *et al.* A phase IB clinical trial with dekavil (F8-Il10), An immunoregulatory 'armed antibody' for the treatment of rheumatoid arthritis, used in combination with methotrexate. *Isr. Med. Assoc. J.* **16**, 666 (2014).

2. Naing, A. *et al.* PEGylated IL-10 (Pegilodecakin) Induces Systemic Immune Activation, CD8 + T Cell Invigoration and Polyclonal T Cell Expansion in Cancer Patients. *Cancer Cell* **34**, 775-791.e1-e3 (2018).

3. Whitehead, R. P. *et al.* Phase II trial of recombinant human interleukin-4 in patients with advanced renal cell carcinoma: a southwest oncology group study. *J. Immunother.* **25**, 352–358 (2002).

4. Lundin, J. *et al.* Interleukin 4 therapy for patients with chronic lymphocytic leukaemia: A phase I/II study. *Br. J. Haematol.* **112**, 155–160 (2001).

5. Parks, W. C., Wilson, C. L. & Lopez-Boado, Y. S. Matrix metalloproteinases as modulators of inflammation and innate immunity. *Nat. Rev. Immunol.* **4**, 617–629 (2004).

6. Sosman, J. a, Fisher, S. G., Kefer, C., Fisher, R. I. & Ellis, T. M. A phase I trial of continuous infusion interleukin-4 (IL-4) alone and following interleukin-2 (IL-2) in cancer patients. *Ann. Oncol.* **5**, 447–52 (1994).

7. Robertson, I. B. *et al.* Latent TGF-β-binding proteins. *Matrix Biol.* **47**, 44–53 (2015).

8. Braun, A. C., Gutmann, M., Mueller, T. D., Lühmann, T. & Meinel, L. Bioresponsive release of insulin-like growth factor-I from its PEGylated conjugate. *J. Control. Release* **279**, 17–28 (2018).

9. Tzeng, A., Kwan, B. H., Opel, C. F., Navaratna, T. & Wittrup, K. D. Antigen specificity can be irrelevant to immunocytokine efficacy and biodistribution. *Proc. Natl. Acad. Sci. U. S. A.* **112**, 3320–5 (2015).

10. Afonina, I. S., Müller, C., Martin, S. J. & Beyaert, R. Proteolytic Processing of Interleukin-1 Family Cytokines: Variations on a Common Theme. *Immunity* **42**, 991–1004 (2015).

Abbreviations

AA	Amino acid
ACL	Anterior cruciate ligament
ACN	Acetonitrile
AIA	Antigen-induced arthritis
Alk	(S)-2-amino-6-((2-azidoethoxy)carbonylamino)hexanoic acid
ANOVA	Analysis of variance
APTES	(3-Aminopropyl)triethoxysilane
AU	Arbitrary units
AUC	Area under the curve
BCA	Bicinchoninic acid
BCS	Bovine calf serum
BMDM	Bone marrow-derived macrophage
CD	Circular dichroism
CDM	Cell-derived matrices
cDNA	Complementary deoxyribonucleic acid
CuAAC	Copper (I)-catalyzed azide-alkyne cycloaddition
DBCO	Dibenzocyclooctyne
DDS	Drug delivery system
DMEM	Dulbecco's modified Eagle's medium
DMM	Destabilization of the medial meniscus
DNA	Deoxyribonucleic acid
EC_{50}	Half maximal effective concentration
ECM	Extracellular matrix
EDTA	Ethylenediaminetetraacetic acid
ELISA	Enzyme-linked immunosorbent assay
FACS	Fluorescent activated cell sorting
FBS	Fetal bovine serum
FCA	Freund's complete adjuvant
FCS	Fetal calf serum
FDA	Food and Drug Administration
h	Hour

HE	Hematoxylin & eosin
HPLC	High-performance liquid chromatography
HPRT	Hypoxanthine-guanine phosphoribosyltransferase
HRP	Horseradish peroxidase
IHC	Immunohistochemistry
IgG	Immunoglobulin G
IPTG	Isopropyl ß-D-1-thiogalactopyranosid
K_D	Dissociation constant
k_{off}	Off-rate constant
k_{on}	On-rate constant
LC-MS	Liquid chromatography - mass spectrometry
m/z	mass to charge ratio
MALDI-MS	Matrix-assisted laser desorption ionization mass spectrometry
mBSA	Methylated bovine serum albumin
MI	Myocardial infarction
min	Minute
MMP	Matrix metalloproteinase
Mϕ	Macrophage
mRNA	Messenger ribonucleic acid
MS	Mass spectrometry
MWCO	Molecular weight cut-off
NHS	N-Hydroxysuccinimide
NIR	Near-infrared
OA	Osteoarthritis
OARSI	Osteoarthritis Research Society International
OD	Optical density
PBDM	Peripheral blood-derived macrophage
PBS	Phosphate-buffered saline
PEG	Polyethylene glycol
Pen/Strep	Penicillin and streptomycin
PK	Pharmacokinetic
Plk	Propargyl-L-lysine
PMSF	Phenylmethylsulfonyl fluoride
PSL	Protease-sensitive linker

PylRS	Pyrrolysyl-tRNA synthetase
qPCR	quantitative polymerase chain reaction
RA	Rheumatoid arthritis
RNA	Ribonucleic acid
ROS	Reactive oxygen species
RP-HPLC	Reversed-phase high performance liquid chromatography
RPM	Rounds per minute
RT	Room temperature
RT-PCR	Real time polymerase chain reaction
SD	Standard deviation
SDS	Sodium dodecyl sulfate
SDS-PAGE	Sodium dodecyl sulfate polyacrylamide gel electrophoresis
SEC	Size exclusion chromatography
SEAP	Secreted embryonic alkaline phosphatase
SPAAC	Strain-promoted alkyne-azide cycloaddition
SPPS	Solid phase peptide synthesis
SPR	Surface plasmon resonance
SO	Safranin O
TB	Terrific broth
TBS	Tris-buffered saline
TBST	Tris-buffered saline + Tween
TFA	Trifluoracetic acid
TGase	Transglutaminase
THPTA	Tris(3-hydroxypropyltriazolylmethyl)amine
U	Unit
UAA	Unnatural amino acid
UV	Ultraviolet
WST-1	Water soluble tetrazolium
wt	Wild type

Acknowledgments

I am sincerely grateful to Prof. Dr. Dr. Lorenz Meinel for giving me the opportunity to join his group and work in an exciting field of research. His constant support, advice and comprehensive knowledge allowed me to constantly keep track in my projects and to always connect to the right people and get the equipment needed. Additionally, I would like to thank PD Dr. Tessa Lühmann for her supervision and helpful guidance, discussions and scientific input throughout this work.

I would like to express special thanks to several people from Novartis AG in Basel, Switzerland. Dr. Marie-Gabrielle Ludwig as a key coordinator allowed to drive this successful collaboration; Dr. Klaus Seuwen constantly supported this project; Dr. Amanda Littlewood-Evans, Dr. Janet Dawson and Dr. Bruno Tigani performed several in vivo studies that are key experiments of this work; Caterina Safina provided numerous critical qPCR experiments; Dr. Hilmar Ebersberg and his colleagues performed codon optimization of murine IL4 that only enabled to gain high quality material.

I am very much obliged to our collaboration partners at Zhejiang University in Hangzhou, China. Prof. Dr. Hongwei Ouyang along with Yejun Hu and Dr. Zongyou Pan performed very critical in vivo experiments. Additionally, I would like to thank them for their excellent hospitality during my visit in China.

I also received generous support and help by several colleagues from the University of Würzburg. I would like to express my thanks to Prof. Dr. Thomas Müller for his support in SPR measurements and providing expression plasmids as well as mIL4 cDNA. Thanks to Dr. Clemens Grimm who enabled access to laboratory equipment and thereby allowed to extend our capacities in recombinant protein expression.

I certainly take this opportunity to warmly thank all my dear colleagues of the Meinel group. I owe special thanks to Dr. Marcus Gutmann not only for his support in CLSM but also for discussions and activities in and outside the lab. I equally thank Katharina Güntzel for her professional support in HPLC measurements but also for being a splendid travel fellow in China. I also want to thank Martina Raschig for synthesizing an unnatural amino acid critical for this work.

Finally, I wish to thank my family for their support and encouragement throughout the last years and beyond.

Documentation of authorship

This section contains a list of the individual contribution for each author to the publication reprinted in this thesis. Unpublished manuscripts are handled, accordingly.

1	**V. Spieler, T. Lühmann, L. Meinel** Cytokine drug delivery in chronic systemic versus acute local inflammation. (2019) [unpublished]			
Author		**1**	**2**	**3**
Development of concept		×	×	×
Preparation of manuscript		×		×
Design of figures		×		
Correction of manuscript		×	×	×
Supervision of V.Spieler				×

2	**T. Lühmann, V. Spieler, V. Werner, M.-G. Ludwig, J. Fiebig, T. D. Müller, L. Meinel** Interleukin-4-Clicked Surfaces Drive M2 Macrophage Polarization. *ChemBioChem* 17, 2123–2128 (2016).						
Author		**1**	**2**	**3**	**4**	**5**	**6**	**7**
Chemical synthesis of propargyl-L-lysine			×					
Cloning of IL4 variants		×						
Expression & purification of IL4 variants			×					
Protein characterization by SDS-PAGE, RP-HPLC, CD spectroscopy, cell culture assays			×	×				
Protein characterization by dose-dependent qPCR					×			
Conjugation of IL4 with particles by CuAAC and SPAAC			×					
Microscopic characterization of conjugates			×					
Characterization of conjugate bioactivity, IL4 quantification by ELISA			×					
Expression, purification and biotinylation of the extracellular domain of human IL-4Rα, IL-13Rα1 and γc, SPR						×		
Statistical analysis			×					
Development of concept		×						×
Preparation of manuscript		×	×			×	×	
Correction of manuscript		×	×	×	×	×	×	×
Supervision of V.Spieler		×						×

3	**V. Spieler, Y. Hu, K. Güntzel, T. Lühmann, H. Ouyang, L. Meinel** Creating an inflammation-responsive cytokine depot by co-injection with FXIIIa. (2019) [unpublished]

Author	**1**	**2**	**3**	**4**	**5**	**6**
Peptide synthesis and purification	×					
Preparation of hIL4 K42Plk and conjugates	×					
Protein characterization by SDS-PAGE and cell culture assays	×					
Protein characterization by RP-HPLC			×			
MMP digest and RP-HPLC analysis	×		×			
Conjugation with fibronectin and western blot analysis	×					
Rabbit model of partial meniscectomy		×				
Macroscopic and histological assessment		×				
Immunohistochemistry		×				
Statistical analysis	×					
Development of concept	×			×	×	×
Preparation of manuscript	×					
Correction of manuscript	×			×		×
Supervision of V. Spieler				×		×

4	**V. Spieler, K. Güntzel, T. Lühmann, L. Meinel** Improved interleukin-4 fusion proteins for bioresponsive depot formation. (2019) [unpublished]

Author	**1**	**2**	**3**	**4**
Cloning of mIL4 fusion proteins	×			
Expression and purification of mIL4 fusion proteins	×			
Protein characterization by SDS-PAGE and cell culture assays	×			
Protein characterization by RP-HPLC		×		
MMP digest and RP-HPLC analysis	×	×		
Conjugation with cell-derived matrices	×			
Statistical analysis	×			
Development of concept	×		×	×
Preparation of manuscript	×			
Correction of manuscript	×		×	×
Supervision of V. Spieler			×	×

5	**V. Spieler, M.-G. Ludwig, A. Littlewood-Evans, J. Dawson, B. Tigani, M. Raschig, T. D. Müller, L. Meinel, T. Lühmann** IL4 conjugation with PEG-folate for improved targeting of activated macrophages. (2019) [unpublished]

Author	**1**	**2**	**3**	**4**	**5**	**6**	**7**	**8**	**9**
Cloning	×								
Synthesis of S)-2-amino-6-((2-azidoethoxy) carbonylamino)hexanoic acid						×			
Preparation of IL4 S46Alk	×								
Preparation of IL4 conjugates	×								
Fluorescent labeling of proteins	×								
Protein characterization by SDS-PAGE, RP-HPLC, cell culture assays	×								
Macrophage polarization, qPCR		×							
Analysis of serum stability by western blot	×								
Endotoxin removal and quantification	×								
Pharmacokinetics study		×	×	×	×				
Targeting study		×	×	×	×				
Statistical analysis	×								
Development of concept	×	×	×	×			×	×	×
Preparation of manuscript	×								
Correction of manuscript	×						×	×	×
Supervision of V. Spieler								×	×

Erklärung zu den Eigenanteilen des Doktoranden sowie der weiteren Doktoranden als Koautoren an Publikationen und Zweitpublikationsrechten bei einer kumulativen Dissertation.

Für alle in dieser kumulativen Dissertation verwendeten Manuskripte liegen die notwendigen Genehmigungen der Verlage (‚reprint permission') für die Zweitpublikation vor, außer das betreffende Kapitel ist noch gar nicht publiziert. Dieser Umstand wird einerseits durch die genaue Angabe der Literaturstelle der Erstpublikation auf der ersten Seite des betreffenden Kapitels deutlich gemacht oder die bisherige Nichtveröffentlichung durch den Vermerk „unpublished" oder „nicht veröffentlicht" gekennzeichnet.

Die Mitautoren der in dieser kumulativen Dissertation verwendeten Manuskripte sind sowohl über die Nutzung als auch über die oben angegebenen Eigenanteile informiert.

Die Anteile der Mitautoren an den Publikationen sind in den vorausgehenden Tabellen aufgeführt.

Prof. Dr. Dr. Lorenz Meinel	Unterschrift
Valerie Spieler	Unterschrift